Positron Emission Tomography (PET) Replacements with Hyperpolarisable *N*-Methoxybenzylphenethylamines (NBOMe's)

J Marron

PhD 2021

Positron Emission Tomography (PET) Replacements with Hyperpolarisable *N*-Methoxybenzylphenethylamines (NBOMe's)

JACK MARRON

A thesis submitted in partial fulfilment of the requirements of Manchester Metropolitan University for the degree of Doctor of Philosophy

Department of Natural Sciences
Faculty of Science and Engineering
Manchester Metropolitan University
John Dalton Building, Chester Street
Manchester M1 5GD

2021

Author's Declaration

I declare that none of the work detailed herein has been submitted for any other award at Manchester Metropolitan University or any other Institution."

"I declare that, except where specifically indicated, all the work presented in this report is my own, and I am the sole author of all parts. I understand that any evidence of plagiarism and/or the use of unacknowledged third part data will be dealt with as a very serious matter."

Signature  Date: 26-07-20

Acknowledgments

I would like to start with huge thanks to Dr. Oliver Sutcliffe, Dr. Ryan Mewis and Dr. David Williamson for providing the opportunity to continue studying after completion of undergraduate studies. Thanks for the continued supervision and continued support and guidance in and outside of studies. Their support of the last 4 years has pushed me through to completion, and without it, it would have been a struggle.

I would also like to thank all the past and present PhD and masters students within the labs over the years, especially those that were within the Sutcliffe research group. This includes the MChem students who worked within the synthetic laboratories, who have made it a pleasure to work alongside them. A final thanks to the MMU golf team who have provided support outside of university time for the last 4 years.

Thanks also to Oxford Instruments for financially funding the PhD and access to instrumentation. Special thanks to Dr. David Williamson for initial contact and continued support and advice on your visits to Manchester.

Thanks to all technical staff at MMU on both level 6 and level 7. Special thanks to Lee Harman for initial training and continued technical support with use of the GC-MS instrumentation. I would also like to thank Dr. Nicolas Gilbert for SIM training on the GC-MS.

Finally, I would to mention a big thanks to my family, friends and partner for their continued support throughout all my years of study at Manchester Metropolitan University.

This work is dedicated to my mum, who passed away on the 7th December 2014.

Abstract

N-methoxybenzylphenethylamines (NBOMe) were first synthesised and published in Ralf Heim's thesis in 2003,[1] detailing the selectivity of these compounds towards serotonin receptors (5-HT_{2A}). This thesis details the full synthesis of seven phenethylamines (10 – 93 % yield as their hydrochlorides) and their transformation into the corresponding NBOMe's (27 – 74 % yield as their hydrochlorides) with full characterisation to compare against literature. The synthesis of 21 novel derivatives (containing either a 3-pyridylmethyl-, 5-fluoro-3-pyridylmethyl- or 4-methoxy-3-pyridylmethyl- moiety) was achieved via reductive amination (3 – 18 % yield as their hydrochlorides), which were evaluated in Signal Amplification By Reversible Exchange (SABRE) Hyperpolarisation experiments in their free-base forms. A GC-MS method has be developed and achieves separation of eight NBOMe's in 11 minutes with Limits of Detection (LoD) and Quantification (LoQ) of 6.2 – 10.8 μg mL^{-1} and 18.8 – 32.6 μg mL^{-1} respectively. The developed method has been validated against simulated blotters impregnated with the NBOMe's and directly compared against ATR-FTIR and presumptive (Marquis and Lieberman) colour tests.

SABRE Hyperpolarisation was explored using the 3-pyridylmethyl-, 5-fluoro-3-pyridylmethyl- or 4-methoxy-3-pyridylmethyl-containing derivatives, and achieved ^{1}H and enhancements, via a low field (60 MHz) NMR, of 2x – 192x – where the best enhancement was observed in the 25B-NBOMe derivative where the 2-methoxybenzyl- group was replaced with a 4-methoxy-3-pyridylmethyl- moiety. These preliminary results indicate the potential for further development of these compounds as possible agents for medical imaging.

Contents

List of tables

List of schemes

List of figures

Abbreviations and acronyms

Micrograms	µg
2-(2,5-dimethoxy-4-bromo-phenyl)-*N*-[(5-fluoro-3-pyridyl)methyl]ethanamine	25B-NPF
2-(2,5-dimethoxy-4-bromo-phenyl)-*N*-[(4-methoxy-3-pyridyl)methyl]ethanamine	25B-NPOMe
2-(2,5-dimethoxy-4-bromo-phenyl)-*N*-(3-pyridylmethyl)ethanamine	25B-Npyr
2-(2,5-dimethoxy-4-chloro-phenyl)-*N*-[(5-fluoro-3-pyridyl)methyl]ethanamine	25C-NPF
2-(2,5-dimethoxy-4-chloro-phenyl)-*N*-[(4-methoxy-3-pyridyl)methyl]ethanamine	25C-NPOMe
2-(2,5-dimethoxy-4-chloro-phenyl)-*N*-(3-pyridylmethyl)ethanamine	25C-Npyr
2-(2,5-dimethoxy-4-methyl-phenyl)-*N*-[(5-fluoro-3-pyridyl)methyl]ethanamine	25D-NPF
2-(2,5-dimethoxy-4-methyl-phenyl)-*N*-[(4-methoxy-3-pyridyl)methyl]ethanamine	25D-NPOMe
2-(2,5-dimethoxy-4-methyl-phenyl)-*N*-(3-pyridylmethyl)ethanamine	25D-Npyr
2-(2,5-dimethoxy-4-ethyl-phenyl)-*N*-[(5-fluoro-3-pyridyl)methyl]ethanamine	25E-NPF
2-(2,5-dimethoxy-4-ethyl-phenyl)-*N*-[(4-methoxy-3-pyridyl)methyl]ethanamine	25E-NPOMe
2-(2,5-dimethoxy-4-ethyl-phenyl)-*N*-(3-pyridylmethyl)ethanamine	25E-Npyr
2-(2,5-dimethoxy-4-fluoro-phenyl)-*N*-[(5-fluoro-3-pyridyl)methyl]ethanamine	25F-NPF
2-(2,5-dimethoxy-4-fluoro-phenyl)-*N*-[(4-methoxy-3-pyridyl)methyl]ethanamine	25F-NPOMe
2-(2,5-dimethoxy-4-fluoro-phenyl)-*N*-(3-pyridylmethyl)ethanamine	25F-Npyr
2-(2,5-dimethoxy-4-iodo-phenyl)-*N*-[(5-fluoro-3-pyridyl)methyl]ethanamine	25I-NPF
2-(2,5-dimethoxy-4-iodo-phenyl)-*N*-[(4-methoxy-3-pyridyl)methyl]ethanamine	25I-NPOMe
2-(2,5-dimethoxy-4-iodo-phenyl)-*N*-(3-pyridylmethyl)ethanamine	25I-Npyr
2-(2,5-dimethoxy-4-nitro-phenyl)-*N*-[(5-fluoro-3-pyridyl)methyl]ethanamine	25N-NPF
2-(2,5-dimethoxy-4-nitro-phenyl)-*N*-[(4-methoxy-3-pyridyl)methyl]ethanamine	25N-NPOMe
2-(2,5-dimethoxy-4-nitro-phenyl)-*N*-(3-pyridylmethyl)ethanamine	25N-Npyr
2-(4-Bromo-2,5-dimethoxy-phenyl)ethanamine	2C-B
2-(4-Chloro-2,5-dimethoxy-phenyl)ethanamine	2C-C
2-(4-Methyl-2,5-dimethoxy-phenyl)ethanamine	2C-D
2-(4-Ethyl-2,5-dimethoxy-phenyl)ethanamine	2C-E
2-(4-Fluoro-2,5-dimethoxy-phenyl)ethanamine	2C-F
2,5-dimethoxyphenylethanamine	2C-H
2-(4-Iodo-2,5-dimethoxy-phenyl)ethanamine	2C-I
2-(4-Nitro-2,5-dimethoxy-phenyl)ethanamine	2C-N
5-Hydroxytryptamine	5-HT
Sodium Chloride (saturated)	Brine
Dichloromethane	DCM
Diethyl ether	Et_2O
Drug Enforcement Administration	DEA
Dimethyl sulfoxide	DMSO
Dynamic Nuclear Polarisation	DNP
Ethanol	EtOH
Gas Chromotography - Mass Spectroscopy	GC-MS

Hours	h
Hydrochloric acid	HCl
Head twitch response	HTR
Isopropyl alcohol	IPA
Lithium aluminium hydride	LAH
Limits Of Detection	LoD
Limit Of Quantification	LoQ
Methanol	MeOH
Magnesium sulfate	$MgSO_4$
Misuse of Drugs Act	MoDA
Magnetic resonance imaging	MRI
Mass Spectroscopy	MS
Sodium Hydroxide	NaOH
Sodium sulfate	$NaSO_4$
N-methoxybenzylphenethylamines	NBOMe
Nuclear Magnetic Resonance	NMR
N-fluoropyridylphenethylamines	NPF
N-methoxypyridylphenethylamines	NPOMe
N-pyridylphenethylamines	Npyr
Positron Emission Tomography	PET
*para*hydrogen-induced polarisation	PHIP
Retention factor	R_f
Relative Retention time	RR_f
Relative Standard Deviation	RSD
Retention time	Rt
Room temperature	RT
Spin amplification by reversible exchange	SABRE
Spin exchange optical pumping	SEOP
Single Ion Monitoring	SIM
Signal to noise	SINO
Street Sample	SS
Triethylamine	TEA
Trifluoroacetic acid	TFA
Tetrahydrofuran	THF
Thin Layer Chromotography	TLC

1 Chapter 1 - Introduction

1.1 Misuse of Drugs Act (1971)

In the United Kingdom (UK), the regulation of drugs and illegal substances is controlled through the Misuse of Drugs Act (1971), the Misuse of Drugs Regulations (2001) and their subsequent amendments, which makes new laws with respect to the dangerous or otherwise harmful drugs and related matters. The act repealed the whole of the Drugs (Prevention of Misuse) Act 1964, and the Dangerous Drugs Acts of 1965 and 1967.[2] The UK legislation before 1971 was fragmented and inflexible due to the constantly changing nature of drugs. For example, a drug, which may have never been abused previously, may become a popular drug of abuse in a very short time period. In this circumstance, it was difficult for the UK to bring such a drug under the restrictions of the original Dangerous Drugs Act unless it was recommended to, or appeared to be recommended to, by the United Nations Narcotics Commission.[2]

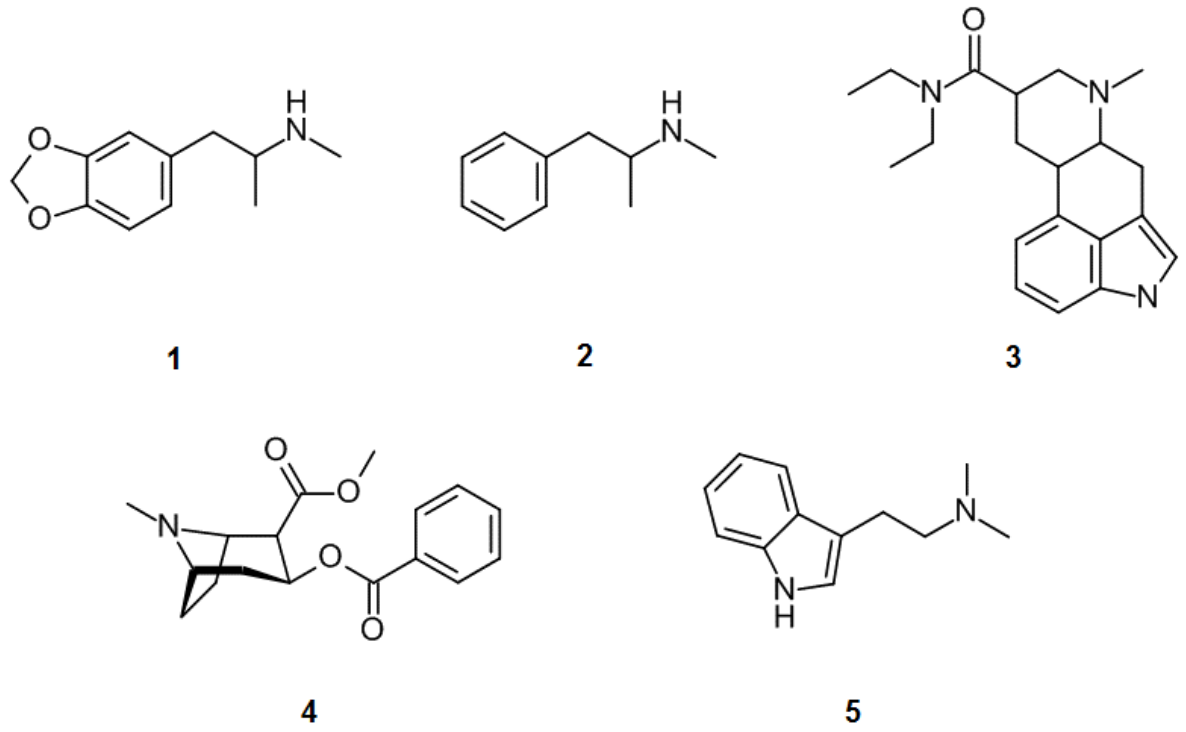

Figure 1 – Chemical structures of class A drugs; 3,4-methylenedioxymethamphetamine (MDMA, **1**), methamphetamine (**2**), lysergic acid diethylamide (LSD, **3**), cocaine (**4**), *N,N*-dimethyltryptamine (DMT, **5**)

Unless an appropriate license is held, it is now illegal for a person to possess a controlled drug, with or without intent to supply (with or without exchange in currency), including within a property. Such substances can be separated into different classes

(A, B, C) each with different penalties associated with them (Table 1). Class A, being the most dangerous, has the highest penalties (examples of class A's in Figure 1) and Class C the least, but one can possess a Class A drug as long as they have a prescription. However, administration of the drug is done under close scrutiny by a medical professional.

Substances can also be controlled by the controlled substances act, which is part of the Comprehensive Drug Abuse Prevention and Control Act (1970). The Drug Enforcement Administration (DEA) divided substances into schedules based on potential for abuse and addictiveness, as well as whether or not the substance has any legitimate medicinal uses.[3] There are three factors on which the substance is scheduled; the potential of abuse, accepted medical use (used as a treatment in the US), potential of addiction. Table 2 summarises the different schedules.[4]

Table 1 - Penalties associated for possession and supply of controlled drugs[4]

Offence	Court	Class A	Class B	Class C
Possession	Magistrates	6 months / £5000 fine	3 months / £2500 fine	3 months / £250 fine
	Crown	7 years / unlimited fines	5 years / unlimited fines	2 years / unlimited fines
Supply and intent to supply	Magistrates	6 months / £5000 fine	6 months / £5000 fine	3 months / £2000 fine
	Crown	Life / unlimited fine	14 years / unlimited fine	14 years / unlimited fine

There are some crossovers between class A substances and schedule 1 substances. Compounds such as LSD and DMT appearing on both lists. There are also differences with substances such as cocaine appearing as a class A drug but being placed into schedule 2, whereas cannabis is a class B schedule 1 drug. Some drugs of abuse (including the prior mentioned) have been listed in Table 3.

Table 2 – List of schedules for controlled substances

	Potential for abuse	Accepted medical use	Potential for addiction
Schedule 1	High	None	Not safe to use
Schedule 2	High	Yes (sometimes allowed with serious restrictions)	The drug can cause severe mental and physical addiction
Schedule 3	Medium	Yes	The drug can cause severe mental addiction and moderate physical addiction
Schedule 4	Moderate	Yes	The drug may cause moderate mental or physical addiction
Schedule 5	Lowest	Yes	The drug may cause mild mental or physical addiction

Table 3 – Exemplar list of drugs with their associated class and schedule regulations

	Class	Schedule
Amphetamine	B	2
Anabolic steroids	C	3
Benzodiazepines	C	4
Cannabis	B	1
DMT	A	1
Ecstasy	A	1
Heroin	A	2
Ketamine	B	3
LSD	A	1
Methadone	B	2
Morphine	A	2
NBOMe	A	1
Pyrovalerone	C	5
2C-series	A	1

The Misuse of Drugs Regulations (2001) were produced in order to allow the lawful production and possession of controlled substances for legitimate circumstances. This regulation covers the administration, possession, destruction and disposal of these substances.[5] The Misuse of Drugs Act (1971) was amended in 2005 to review the classification system of controlled substances and amendments were made to

schedule 1. Changes were also made to policing powers relating to drugs and sentencing punishments.[6]

Phenethylamine (**6**, Figure 2) has a basic structure that can elicit stimulant and/or hallucinogenic properties, which can be differentiated as catecholamines (**7**), amphetamines (**8**), synthetic cathinones (**9**), and many other drugs.[7] These are typically composed of a benzyl ring with a terminal amine separated by an ethyl chain. However, the 2C series (**10**) possess dimethoxy groups in the two and five position, with the lipophilicity of the group in the four position can alter its pharmacological and clinical effects, creating a vast array of derivatives.[8] These can include halogens, alkyl, thiol and nitro groups but the most popular within the recreational scene is with bromine, 2,5-dimethoxy-4-bromophenethylamine (2C-B). This drug first appeared on the illicit market scene in 1980[9] and then gained increasing popularity in the 1990's, when it was sold in so-called smart shops.[10] All of the 2C family (**11**) is currently legislated in the Class A category meaning they are illegal to produce, supply or possess.

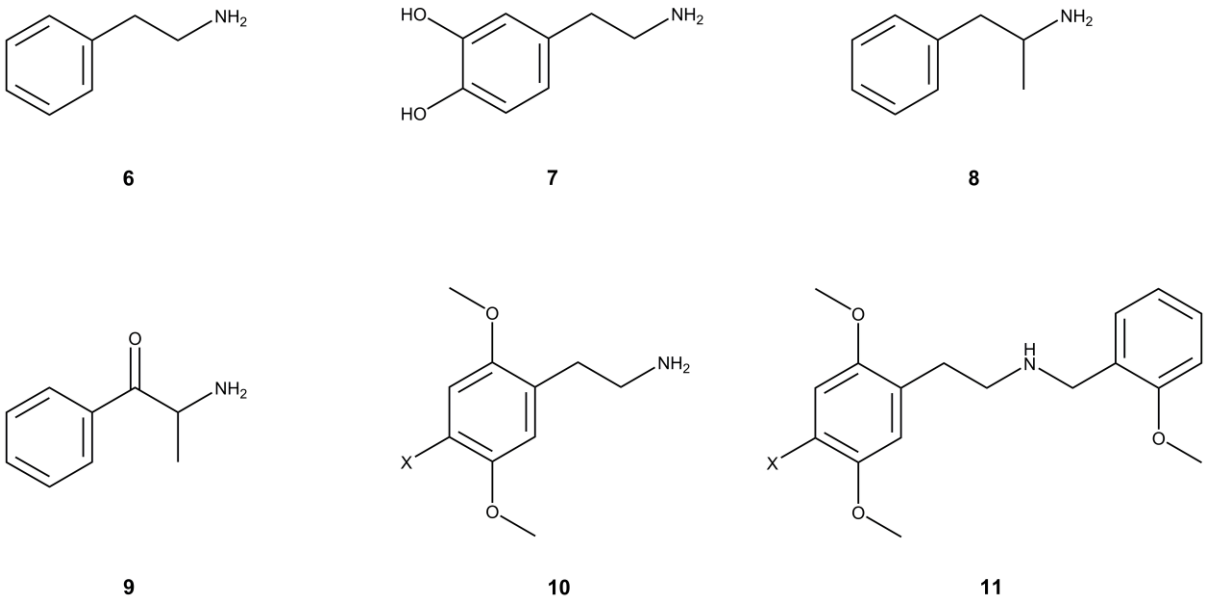

Figure 2 - Chemical structures of phenethylamine (**6**), dopamine (**7**), amphetamine (**8**), cathinone (**9**), "2C-series" (**10**, X = halogen, alkyl, thiol, nitro) and NBOMe series (**11**, X = halogen, alkyl, thiol, nitro)

The 2C family is the parent for the *N*-methoxybenzyl (NBOMe, **11**) analogues, which fall into the phenethylamine "catch-all" clause meaning they are also Class A drugs. This class of drugs were first synthesised in 2003 by Ralf Heim as part of his PhD

thesis,[1] and deemed a hazard to public health and safety later on.[11] The Drug Enforcement Administration placed 25I-NBOMe, 25B-NBOMe and 25C-NBOMe into Schedule 1 of the Controlled Substances Act on 10 October 2013.[12] The nature of the drug is to mimic LSD as it stimulates the 5-HT_{2A} receptor, therefore blotter papers containing 2-(4-iodo-2,5-dimethoxyphenyl)-*N*-[(2-methoxyphenyl)methyl] ethanamine (25I-NBOMe) appeared on the designer drug market beginning 2011[13] and since then numerous derivatives have been seized including: 2-(2,5-dimethoxy-4-methylphenyl)-*N*-(2-methoxybenzyl)ethanamine (25D-NBOMe, **11a**, X = Me), 2-(4-ethyl-2,5-dimethoxyphenyl)-*N*-(2- methoxybenzyl)ethanamine (25E-NBOMe, **11b**, X = Et) and *N*-(2-methoxybenzyl)-2,5-dimethoxy-4-chlorophenethylamine (25C-NBOMe, **11c**, X = Cl).[14,15,16]

1.2 *N*-Methoxybenzylphenethylamines (NBOMe)

Ralf Heim first synthesised the *N*-methoxybenzyl phenethylamine (NBOMe) series of psychoactive substances and determined them to be potent serotonin (5-HT) agonists. This was previously known due to the 2C series also showing agonistic properties towards this receptor, which bind the 5-HT receptor to cause a response. Specifically, this compound targets the 5-HT_{2A} receptor that appears to play a key role in a number of disease states. These disease states include addiction,[17] schizophrenia,[18] obsessive compulsive disorder,[19,20] depression,[21,22] pain,[23] inflammation,[24] migraine,[25] and cluster headaches,[26] and in the manifestation of mystical/religious-type experiences as well as in altered states of consciousness.[18, 27]

Initially, *N*-substituted phenethylamines were thought to be inferior compared to the parent phenethylamines because early studies involving *N*-alkylation with simple substituents (e.g. methyl, ethyl, propyl) produced compounds with significantly diminished activity.[28] Therefore, it was surprising when Heim discovered that *N*-benzyl, and specifically *N*-(2-methoxy)benzyl, substitution dramatically improved both binding affinity and functional activity and *in vivo* 5-HT_{2A} activation compared to simple phenethylamines such as 4-iodo-2,5-dimethoxyphenethylamine (2C-I).[1, 29]

1.2.1 NBOMe Synthesis

NBOMe's are synthesised with a reductive amination (Scheme 1) of a 2C series compound to form a potent hallucinogen with high abuse potential,[30] powerful psychoactive properties and stimulating effects (Scheme 2).[31]

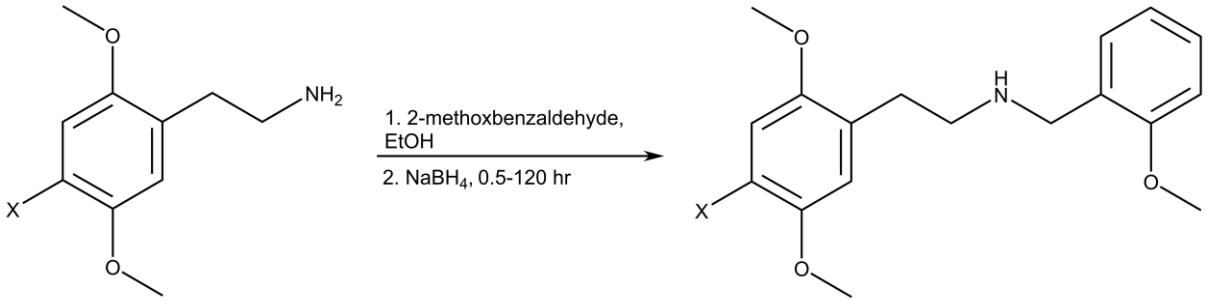

10 **11**

Scheme 1 - General reaction scheme of NBOMe synthesis (X=F, Cl, Br, I), (1 eq. triethylamine (TEA) required if phenethylamine is a hydrochloride salt)

In 2003, preliminary explorations led to the conclusion that *N*-2-methoxybenzyl substitution, not only of phenylethylamines but also phenylisopropylamines, tryptamines and 3-(2-aminoethyl)-(1H,3H) quinazoline-2,4-diones related to the typical 5-HT_2 receptor antagonist ketanserin (**12**, Figure 3), results in particularly high affinities for 5-HT_{2A} receptors. [1] The pharmacophore shown in Figure 4 highlights the similarities of functional groups.

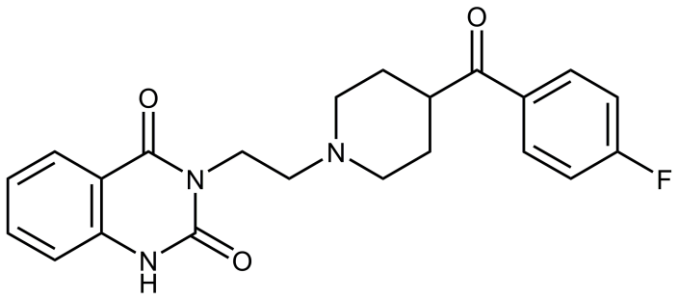

12

Figure 3 - Chemical structure of the 5-HT_2 receptor antagonist Ketanserin (**12**)

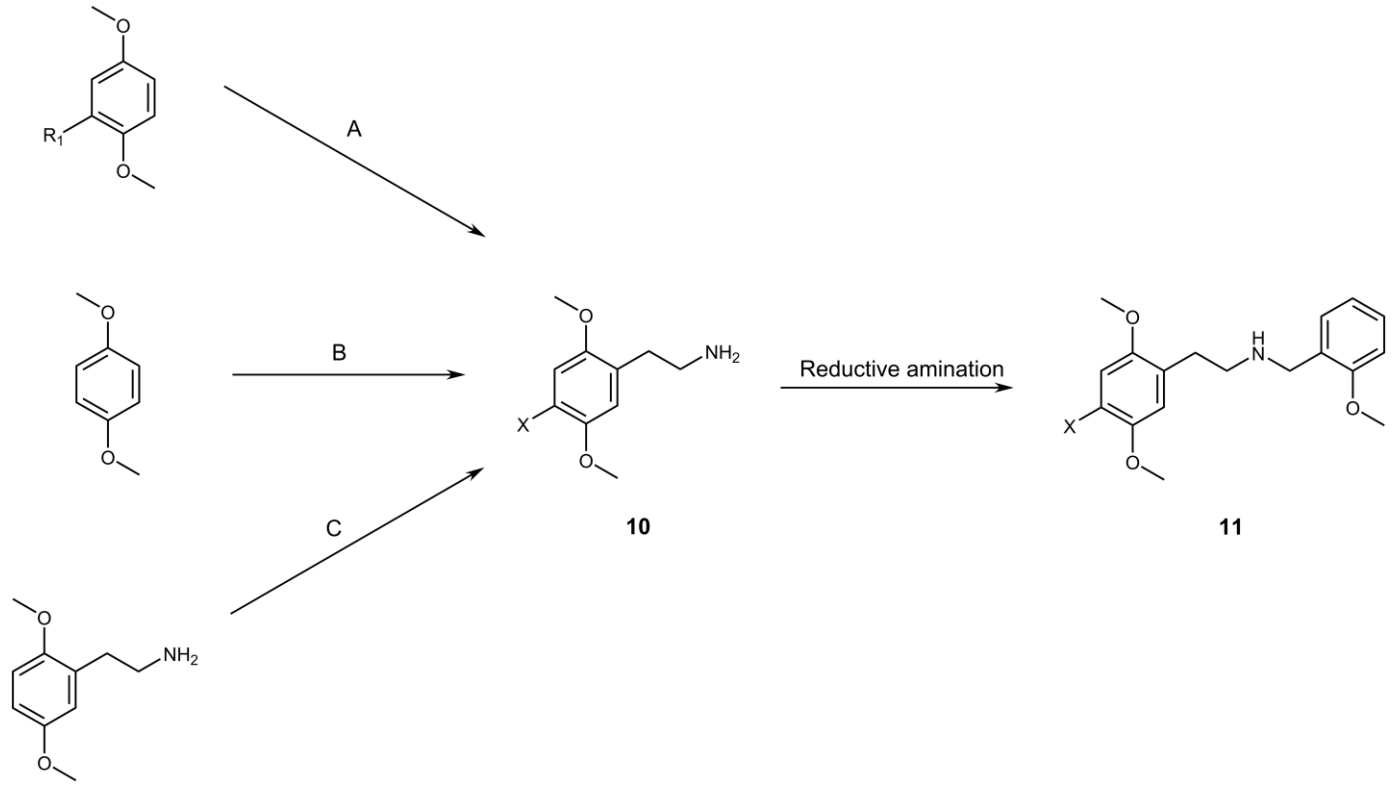

Scheme 2 - General reaction scheme for final compound synthesis (R_1 = Me, Cl, F; X = F, Cl, Br, I, Me, Et, NO_2). A) Synthetic route of **31,** HMTA, TFA, reflux, 15 h, 55 %; b) nitromethane, ammonium acetate, AcOH, reflux, 4 h, 34 %; c) $LiAH_4$, THF, RT, 3 h, 34%; synthetic route of **34,** $POCl_3$, *N*-methylformanilide, RT, 2 h, 97 %; b) nitromethane, ammonium acetate, acetic acid, reflux, 3 h, 66 %; c) $LiAH_4$, THF, RT, 3 h, 14 %; B) Synthetic route of **41,** acetyl chloride, aluminium chloride, DCM, RT, 1 h, 83%; (b) KOH, triethylene glycol, hydrazine hydrate (40 %), 150°C, 4 h, 85%; (c) iodomethane, KOH, DMSO, 40°C, 1 h, 95 – 99%; (d) tin (IV) chloride, dichloromethyl methyl ether, anhydrous DCM, 0°C – RT, 1 h, 83%; (e) nitromethane, ammonium acetate, 100°C, 4 h, 29%; (f) $LiAH_4$, anhydrous THF, RT, 3 h, 50%; C) Synthetic route of **28,** Br_2, AcOH, RT, 5 min, 49%; synthetic route of **47** a) phthalic anhydride, reflux, 6 h, 72 %; b) iodine monochloride, AcOH, 40 °C, 1 h, 76 %; c) hydrazine hydrate, IPA, reflux, 12 h, 10 %; synthetic route of **48,** HNO_3, AcOH, 0 °C, 1 h, 66%

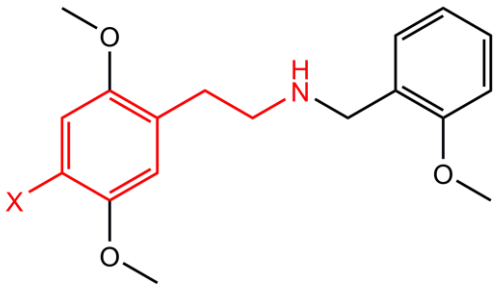

11

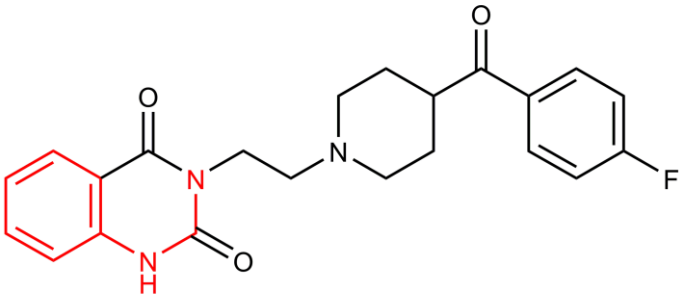

12

Figure 4 - Pharmacophore of both **11** and **12** highlighted in red

In NBOMe's, substitution patterns at the *ortho* position of the benzyl group showed similar potencies with an oxygen, however, the range of substituents remains unknown. It is difficult to rationalize the molecular basis of receptor affinity and functional potency and efficacy of this interesting family of drugs even though a π-π stacking interaction and a hydrogen bond, both involving the benzyl moiety, have been invoked as partial explanations.[32, 33, 34] Also, the pharmacological study of an expanded set of analogues is likely to reveal the causes of their suspected toxicity and uncover new substances with therapeutic potential.[35]

A part that is not well recognised in medicinal chemistry is the halogen bonding associated with the protein backbone. These can be as strong as hydrogen bonding, whilst also having an almost neutral net enthalpy change. The strength of the bonding is due to the electronegativity associated with the halogen in use. A recent example of compounds that may merit analysis in this context are cytotoxic oxadiazoles in which replacement of a methyl group by a chlorine or bromine atom results in an at least fourfold increase in potency which is greater for bromine than for chlorine.[36] The

presence of bromine could potentially lead to increasing 5-HT_{2A} receptor affinity thus increasing the potency and the ability to study the differences in their actions. 25B-NBOMe derivatives were the primary focus of Tiraoegui as the affinities associated with 5-HT_{2A} was higher than most 25X related compounds (X = F, Cl, I, Me, NO_2) with Et being an exception.[37]

Tiraoegui *et al.*[35] investigated reductive amination (Scheme 3) with aryl-brominated compounds, as these derivatives of NBOMe's have not been described (tryptamine derivatives also included) in literature. An "indirect" procedure was used by reacting the amine and aldehyde to generate the imine. After being left to stir overnight, addition of sodium borohydride ($NaBH_4$) was the reducing agent used *in situ* in methanol to form the substituted NBOMe derivatives. The two examples of halogenated 2-oxygenated NBOMe derivatives are 2-(4-bromo- 2,5-dimethoxyphenyl)-*N*-(4-bromo-2-methoxyphenylmethyl)ethanamine (**13a**) and 2-(4-bromo- 2,5-dimethoxyphenyl)-*N*-(5-bromo-2-methoxyphenylmethyl)ethanamine (**13b**), which exhibited submicromolar affinities (against the antagonist [^{3}H] ketanserin) for human 5- HT_{2A} receptors with pKi values of 7.17 and 7.63 respectively. This is two orders of magnitude less than 25B-NBOMe.[33]

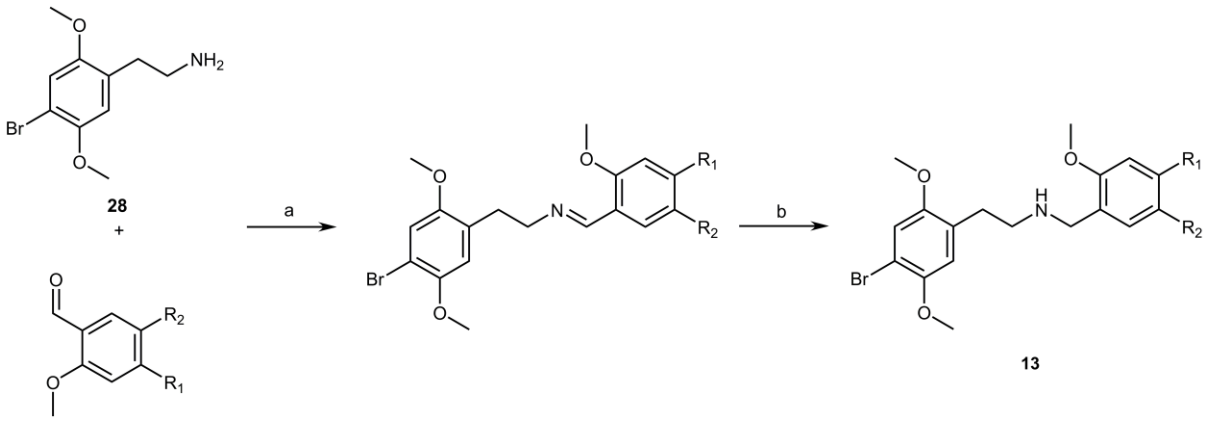

Scheme 3 – Preparation of 2-aryl-*N*-substituted benzylethanamines. a) MeOH, 12 h; b) $NaBH_4$ 24 h; **13a** R_1 = Br, R_2 = H; **13b** R_1 = H, R_2 = Br

1.2.2 Structure-Activity relationship between NBOMe derivatives and the 5-HT receptor family

Data suggests that drugs of the 2C-class interact effectively with serotonin receptors, most of which act as 5-HT_{2A} receptor agonists. Typically, a 2C-class substance carries a lipophilic substituent in the *para*-position (relative to the side chain), which contributes to further enhance 5-HT_{2A} affinity and partial agonistic action.[38] The most active compounds identified to date possess an ether, alkylthio, alkyl, or halogen group at this position and their potency increases in the aforementioned sequence.[39, 40] The results retrieved from SAR studies suggest that *N*-substitution of common phenethylamines with short alkyl substituents (methyl or ethyl groups) considerably decreases the binding affinity for serotonin receptors compared to the unmodified compounds (Figure 5).

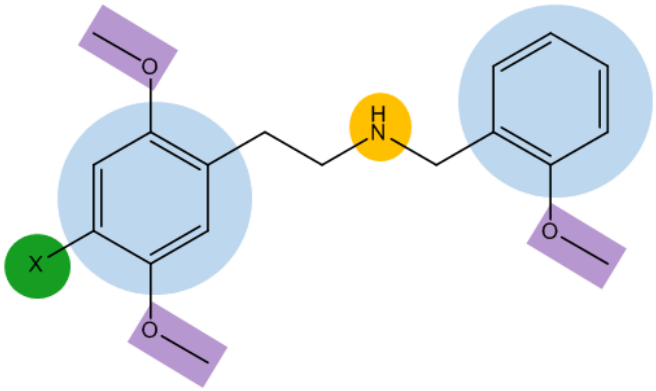

Figure 5 – SAR diagram of an NBOMe; green indicates halogen bonding when X = Br, Cl, F, I; blue indicates π-π stacking; purple indicates H bond acceptor groups and yellow indicates H bond donor/acceptor group

However, the addition of an *N*-benzyl moiety increases the affinity and potency. Braden *et al.*[41] illustrated this by performing a radio ligand binding assay which monitors the drugs ability to displace either [^{125}I]4-iodo-2,5-dimethoxyphenylisopropylamine (DOI) and [^{3}H]ketanserin in different membranes. By adding an *N*-benzyl group to 2,5-dimethoxy-b-phenethylamine (2C-H), the binding affinity increased 13-times.[41] The addition of an *N*-(2-methoxy) benzyl, or *N*-(2-hydroxy) benzyl, group to 2C-H led to 190- and 82-fold increases in affinity, respectively. Moreover, the latter substances displayed high selectivity (> 1000-fold)

for 5-HT_{2A} receptors over 5-HT_{1A} and moderate selectivity (up to 35-fold) for 5-HT_{2A} over 5-HT_{2C}.

Heim[1] was the first to investigate the pharmacological properties of the NBOMe series. 25C-NBOMe acts as a potent 5-HT_{2A} receptor's partial agonist. ^{11}C radiolabelled form of 25C-NBOMe has been studied as a potential ligand to map the distribution of 5-HT_{2A} receptors in the brain by positron emission tomography (PET).[42] This drug has a nanomolar affinity to the 5-HT_{2A} receptor displaying an agonistic binding affinity of 2.89 ± 1.05 nM *in vitro*,[43] thus it has been characterized as "superpotent" by Braden *et al*.[32] It is pharmacologically active even at considerably small submilligram doses.[15]

Moreover, Halberstadt and Geyer[29] studied the effects of 25I-NBOMe on the head twitch response (HTR) that is induced by activation of 5- HT_{2A} receptor in rats and mice and is widely used as a behavioural proxy for hallucinogen effects in humans. 25I-NBOMe displayed 14-fold higher potency than 2C-I. The findings suggest that phenethylamine hallucinogens induce the HTR by activating 5-HT_{2A} receptors and that 25I-NBOMe is a highly potent derivative of 2C-I, which is in accordance to previous *in vitro* findings suggesting that *N*-benzyl substitution increases 5-HT_{2A} affinity.

25I-NBOMe is active from 50 – 250 µg but dosing ranges from 500 – 800 µg for insufflation and has a 6 h duration.[29] However, what all the NBOMe's have in common is that if the dosing is not correct, fatalities can occur.[44] This is primarily due to the user not knowing what substance they are taking, they can be passed on as research chemicals, herbal remedies, bath salts, etc., without proper labelling as to what the product contains along with concentrations of substances encased. The effects of 25I-NBOMe intoxication can lead to tachycardia, hypertension, agitation and aggression, visual and auditory hallucinations, seizures, hyperpyrexia, clonus, elevated white blood cell count and metabolic acidosis.[44]

The docking process involves the prediction of a ligand conformation and orientation within a target's binding/active site. Subsequent calculations calculate structural factors that determine the correct positioning within the active site.[45] Multiple steps are

taken with each step increasing the degree of complexity,[46] due to the complex issues involved with biological recognition and the ability to simulate these on a computer.

There are currently seven 5-HT family receptor types with 14 known subtypes integrated within. 13 of these belong to the G protein-coupled receptor (GPCR), with 5-HT_3 classified an ion channel.[47, 48, 49] Among the seven subclasses (5- HT_{1-7}) of serotonin receptors, 5-HT_{1A}, 5-HT_{1B}, 5-HT_{2A}, and 5-HT_3 are especially well known for their association with addictive substances, such as cocaine, amphetamine, methamphetamine, MDMA (ecstasy), morphine/heroin, cannabis, alcohol, and nicotine.[50]

Wang *et al.*[51] reported the crystal structures of the human 5- HT_{1B} receptor bound to its agonists ergotamine (ERG) and dihydroergotamine. Their structures revealed that these ligands shared similar binding modes in 5-HT_{1B}, occupying the orthosteric pocket and an extended binding pocket close to the extracellular loops. They also compared the structure with the 5-HT_{2B} receptor and found that the 5-HT_{1B} receptor displayed a 3 Å outward shift at the intracellular end of 6th trans-member helices (TM6), resulting in a more open extended pocket that may explain the subtype selectivity. To investigate the structural basis for biased signalling, Wacker *et al.*[52] reported the crystal structure of the human 5-HT_{2B} receptor bound to ERG (Protein Data Bank (PDB) entry: 4IB4, resolution: 2.7 Å) and compared it with the 5-HT_{1B}/ERG structure. These crystal structures provide a comprehensive structural basis for understanding the receptor‑ligand interactions of the 5-HT family subtypes.

Wang *et al.*[53] researched molecular docking, molecular dynamics simulation and systems pharmacology analysis with the serotonin receptor family. Previous models, protocols and parameters were used for these studies[54-57] to view the binding pockets of all of the receptor groups. Through molecular docking and simulations, commonalities between each subtype was identified and the uniqueness of the residues which contribute to the selectivity of each receptor. Table 4 shows the key residues involved within the 5-HT_2 family biding pockets, with the bold residues playing being the grantor between the selectivity.

Table 4 – Key residues involved in the binding pocket of 5-HT_2 receptors

No.	Location	5-HT_{2A}	5-HT_{2B}	5-HT_{2C}
1	3 x 32	Asp155	Asp135	Asp134
2	3 x 33	Val156	Val136	Val135
3	3 x 36	Ser159	Ser139	Ser138
4	5 x 39	Phe234	Phe217	Phe214
5	5 x 40	Val235	**Met218**	Val215
6	5 x 43	Gly238	Gly221	Gly218
7	5 x 46	**Ser242**	Ala225	Ala222
8	6 x 48	Trp336	Trp337	Trp324
9	6 x 51	Phe339	Phe340	Phe327
10	6 x 52	Phe340	Phe341	Phe328
11	6 x 55	Asn343	Asn344	Asn331
12	7 x 35	Asn363	**Glu363**	Asn351
13	7 x 38	Val366	Val366	Val354
14	7 x 42	Tyr370	Tyr370	Tyr358

1.2.3 NBOMe Metabolism

The study of the metabolism of 2C-B (**28**, Scheme 4) has been extensively researched using rat and mice models, as well as human urine. The studies showed the major metabolic pathway to be deamination (Phase I, **14a**) followed by oxidation of the aldehyde to the corresponding carboxylic acid (Phase II, **14b**). The minor metabolic pathway 2C-B is *O*-demethylation (Phase I, **15a**) of the parent compound, followed by acetylation (Phase II, **15b**).[58]

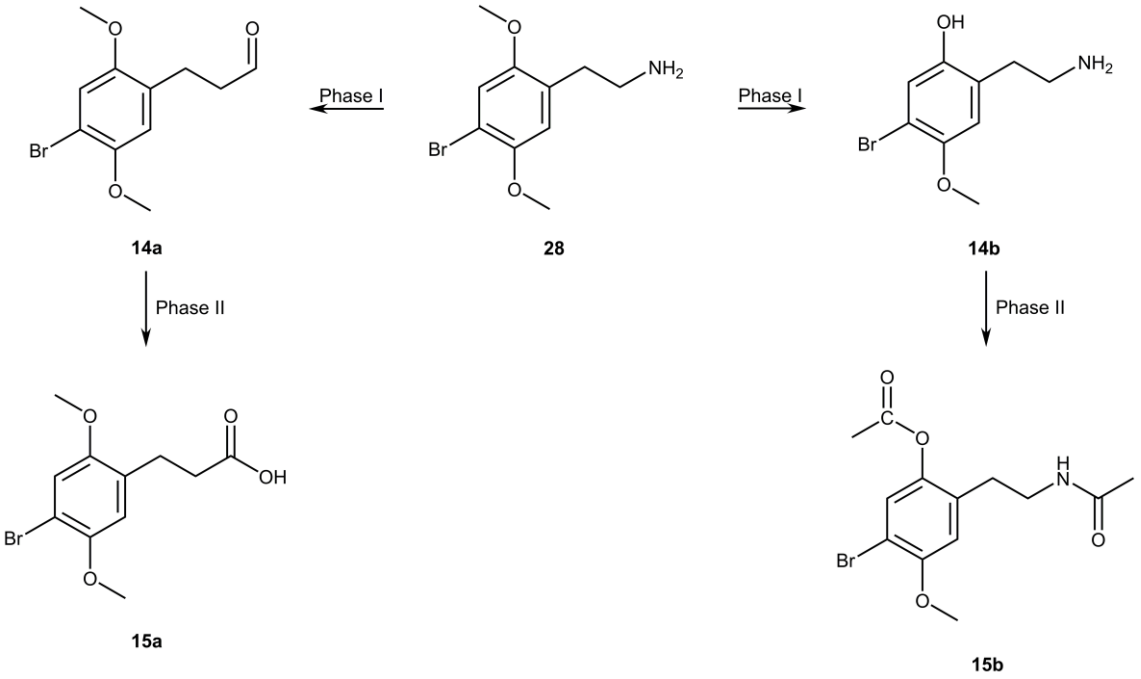

Scheme 4 – Major and minor metabolic pathways processes of 2C-B

When looking at the metabolism of the NBOMe compounds, a precise mechanism of action is difficult due to an increased number metabolic routes. For 25B-NBOMe, Boumrah *et al.*[59] identified 21 Phase I and II metabolites only *in vitro* after incubation with human liver microsomes and cofactors for CYPs and glucuronyl transferases. Caspar *et al.*[30] have identified 35 Phase I and 31 Phase II metabolites present in human and rat urine, due to several being combined metabolic reactions or isomers of previous ones.

Caspar *et al.*[60] previously studied the metabolism process of 25I-NBOMe. A total of 68 metabolites found, 37 of those being phase I and 30 being phase II. In summary, O-demethylation seemed to be the main metabolic pathway and *N*-demethoxybenzylation only a minor one in humans and rats.[60]

All phase II pathways could be proposed for both species with the exception of the *N*-acetylation, which was observed only in rats after the high dose. Again, the relative abundance also of the different conjugates varied between the species, but this was only a rough estimation as already discussed above.[60]

1.2.4 NBOMe Prevalence

Despite NBOMe's being synthesised in 2003, recreational use of these drugs did not occur until 2010 and case reports followed in 2013 after David Nichol's research on the drug in 2008. This included creating a radio-labelled form of 25I-NBOMe for use as a high affinity, traceable 5- HT_{2A} ligand, applicable to positron emission tomography and other research purposes.[61] However, by 2010, 25I-NBOMe began to appear on the internet.[62] Recreational users then went online to post their experiences on EROWID, an online psychoactive drug and plant library, which defined NBOMe's as "the defining psychedelics of 2013".

25I-NBOMe, described as the prototype, is part of the expanded class of NBOMe's with the defining group being the addition of 2-methoxybenzyl moiety to the backbone of the phenethylamine. This addition increases the affinity by up to 16 times compared to its counterpart, 2C-I.

Laskowski *et al.*[63] showcases an example of the prevalence of NBOMe's with two case studies, both being teenagers, who claimed to ingest 25I-NBOMe. The patient in the first case study self-administered a "25I-NBOMe" blotter, followed by a seizure within 30 minutes. After being taken to the emergency department (ED), a second seizure occurred minutes after being admitted which was resolved with lorazepam. Serum and urine obtained (7 and 9 hours post admission respectively) contained 25C-NBOMe at >0.025 ng mL^{-1} and 1 ng mL^{-1} respectively. 25I-NBOMe was not detected. The patient in the second case study, again, self-administered "25I-NBOMe" as a blotter and admitted to the ED 6 hours after ingestion. Two seizures registered whilst being in the hospital, both treated with lorazepam. Serum specimens were obtained upon arrival and 4 hours post-arrival containing 25B-NBOMe at 1.2 ng mL^{-1} and 0.51 ng mL^{-1} respectively. Again, 25I-NBOMe was not detected.[63]

Several other case studies of NBOMe ingestion have been noted by Al-Imam[64] who summarises 13 intoxication and fatality incidents between 2013 and 2015. The 11 males and 2 females, largely from the USA, included in this study were aged between 15 – 31 years old. Outcomes from ingestion included death, intoxication and potential suicide. In most of the cases of death (9 cases), 6 of these were due to 25I-NBOMe.

This led to the analysis of NBOMe's becoming vital in the knowledge of thresholds and how to treat patients who had ingested this class of drugs.

1.2.5 NBOMe Analysis

Analysis of NBOMe's can be determined on the nature that they are presented in, which is often as blotters. Poklis *et al.*[11] have reported a work on the analysis of blotters. The authors performed their analysis with direct analysis in real time mass spectrometry (DART-MS) followed by confirmation and quantification with high-performance liquid chromatography triple quadrupole mass spectrometry (HPLC-MS-MS). The advantages of the DART-MS technique are that it requires no solvent, extractions or solvent preparation. The authors reported that by holding the blotter paper into the direct gas stream, using forceps, a spectrum was yielded within seconds. They then combined this with the HPLC-MS-MS analysis to become the first to compare concentrations of the blotter to the advertised amount. They found the vendor's blotter paper 25C-NBOMe had been correctly labelled with the drug, containing 102% of the labelled dose and 3.3% NBOMe derivative impurities. The 25I-NBOMe blotter was determined to be correctly labelled with the drug, containing 108% of the labelled dose and 8.0% NBOMe derivative impurities. The 25B-NBOMe blotter was also determined to be correctly labelled with the drug, containing 300% of the labelled dose and 2.2% NBOMe derivative impurities.[11]

Elbardisy *et al.*[65] used high-performance liquid chromatography-photodiode array detection (HPLC-DAD) and high-performance liquid chromatography-amperometric detection (HPLC-AD). The photodiode array detection technique is used to determine the purity of an analyte during HPLC separation. It works similarly to a variable wavelength detector (VWD). However, this method has its advantage over conventional UV detectors due to its speed of scanning. Multiple scans occur during the array of diodes whereas VWD does one scan. This electrochemical approach was the first presentation of both photodiode array and amperometric detection for the simultaneous qualitative and quantitative analysis for NBOMe's in a single run. The limit of detection (LOD) is low enough to target analytes within a seized blotter with both detection methods (HPLC-DAD 4.56 – 6.65 μg mL^{-1} and HPLC-AD 9.65 – 17.98 μg mL^{-1}).

Duffau *et al*[66] used a combination of high-performance thin-layer chromatography (HPTLC) and gas chromatography mass spectrometry (GC-MS). HPTLC is an

enhanced form of TLC, that increases the resolution to acquire more accurate quantitative measurements. 25C-NBOMe blotters were analysed from a seized batch, with the results varying from 701 to 1943.5 µg per blotter. The results here indicate the dangers associated with this derivative and its dosage, with intoxication and fatalities occurring with >1000 µg doses sublingually.[67] They found that 8 of the 15 blotters exceeded 1000 µg increasing the risk of acute intoxication because of its high potency. The LOD and LOQ associated with HPTLC is 7.1 and 21.63 µg respectively.

Aside from HPLC based methods, blotter analysis can be performed via attenuated total reflection Fourier transform infrared (ATR-FTIR)[68] and ultra-performance liquid chromatography (UPLC).[69]

However, as mentioned on page 35, NBOMe ingestion requires biological analysis. Moreira *et al.*[70] have detailed the variation in the value obtained by different methodologies due to the concentration found in biological matrices being generally very low (0.025 – 500 ng mL^{-1}). Therefore, this requires a different extraction process and highly sensitive analytical techniques.

Biological samples described for the identification and quantification of NBOMe compounds included whole blood,[71, 72] plasma,[71, 73] serum,[74, 75] and urine.[71, 76] For post-mortem, matrices included fluids,[77, 78] tissues,[79, 80] heart blood,[69, 81] peripheral whole blood,[77, 79] vitreous humor,[13, 77] liver[59, 77] and stomach contents ,[77, 79] with a focus on urine[77, 79] and serum[31, 82] samples. The required volume of these biological samples for the analytical techniques employed for identification of new psychoactive substance (NPS) ranged from 0.5 to 1 mL.[67, 71]

The two main extraction methods found by Moreira *et al.* included liquid-liquid extraction (LLE) and solid-phase extraction (SPE). [70] For assays using LLE, the linear range varied between 0.1 to 500 ng mL^{-1} whereas the SPE linear range varied between 25 pg mL^{-1} to 100 ng mL^{-1}. The analytical techniques employed were gas chromatography with mass-spectrometry (GC-MS), high performance liquid chromatography coupled to positive ion-mode electrospray mass-spectrometry (ESI(+)-LC-MS/MS), and quantum time of flight (QTOF).

LLE methods are considered simpler but a time consuming process. However, due to its ease of handling, availability of materials, and low cost, it is still a widely used method. Rose *et al.*[74] reported the identification of 25I-NBOMe using 1.0 mL of serum sample. This analyte was extracted with 2 mL hexane: ethyl acetate (1: 1, v/v). Thus, 0.76 ng mL^{-1} of analyte was determined in the sample. Walterscheid *et al.*[81] reported two cases of death following ingestion of the same analyte, which was confirmed by analysis of biological samples (heart blood and urine). In this assay, 0.5 mL of samples were analyzed using 2 mL of ethyl acetate and 0.2 mL of saturated alkaline sodium borate buffer (pH 12). The residue was suspended in 1 mL of 7 mM ammonia prepared with 10% acetonitrile buffer. Aliquots of the analyzed samples confirmed the presence of 25I-NBOMe (7.5 ng mL^{-1}) in both cases.

SPE methods are thought to be more advantageous than LLE, as lower volumes of solvent are required, extracts are cleaner and usually faster.[83] To enhance the efficiency of SPE cartridges, a pre-treatment of the sample is desired. The most commonly used pre-treatment is denaturation of serum proteins with organic solvents (acetonitrile, acetone, ethanol and methanol), acids (10% w/v trichloroacetic, 6% w/v perchloric and 5% w/v metaphosphoric) or salts and metal ions (5% w/v copper sulfate and 6% w/v sodium tungstate). Generally, this pre-treatment is always applied before traditional extraction techniques (LLE and SPE) in search of a method that is fast, simple and inexpensive.[84] Poklis *et al.*[82] developed a method to determine two NBOMe in serum samples. The method was applied in samples of two patients who were admitted having used 25I-NBOMe. In this case, 2780 pg mL^{-1} of 25I-NBOMe was found in the samples. Hill *et al.*[73] described seven cases of analytically confirmed toxicity due to the recreational use of the same analyte, and biological samples were analysed for all seven cases. Next, Poklis *et al.*[77] reported a case detection of the same analyte in different biological samples. For post-mortem specimens, the results between the procedures were in good agreement and demonstrated a lack of matrix effects and ease of extraction of 25I-NBOMe from tissue matrices. Toxicology findings for fluids based upon blood or urine calibrators were as follows: 405 pg mL^{-1} in peripheral blood, 410 pg mL^{-1} in heart blood, 2.86 ng mL^{-1} in urine, and 99 pg mL^{-1} in vitreous humor. Poklis *et al.*[76] also developed a method for the simultaneous

determination and quantification of nine NBOMe in urine samples. The method detected the presence of NBOMe derivatives in four specimens from emergency room patients. It was determined that one specimen contained only 25B-NBOMe at 1.7 ng mL^{-1}, while another contained only 25I-NBOMe at 1.0 ng mL^{-1}. A further specimen from another patient contained 2.3 ng mL^{-1} of 25I-NBOMe and <1.0 mg mL^{-1} of 2C-NBOMe, and the other contained 1.2 ng mL^{-1} of 25I-NBOMe and <1.0 ng mL^{-1} of 25H-NBOMe.

1.3 Hyperpolarisation Techniques

The use of techniques to enhance nuclear spin polarization (P) to order unity (i.e. 100%) results in corresponding gains in NMR sensitivity by 4–8 orders of magnitude.[85] This process of significant polarization enhancement—well above that achieved at thermal equilibrium—is termed hyperpolarization. Hyperpolarization of solids, liquids, and gases[86] has been demonstrated via a number of techniques including Brute Force Polarization (BFP),[87] Spin Exchange Optical Pumping (SEOP),[88] Dynamic Nuclear Polarization (DNP),[89] Chemically-Induced Dynamic Nuclear Polarization (CIDNP)[90] photo-CIDNP,[91] Parahydrogen Induced Polarization (PHIP),[92] and Signal Amplification By Reversible Exchange (SABRE).[93]

1.3.1 SABRE Hyperpolarisation

Signal amplification by reversible exchange (SABRE) is a non-hydrogenative polarisation technique that enhances the sensitivity of an NMR experiment by increasing the signal intensity. Although NMR, and by extension, MRI, are thought to be intrinsically insensitive techniques, polarisation techniques such as SABRE can vastly overcome this. Insensitivity arises due to the distribution of nuclear spins being almost equal and this means that only a very small fraction of spins actively contribute in terms of producing a signal.

The source of polarisation in SABRE is *para*hydrogen, a spin isomer of dihydrogen. *Para*hydrogen is a nuclear singlet (total spin of zero), and is, therefore, NMR silent. However, by breaking the symmetry of *para*hydrogen, the polarised state can be accessed. In the right conditions, this polarisation can be transferred to other molecules.

Transfer of polarisation in SABRE occurs through the *J*-coupling from a *para*-hydrogen-derived hydride ligand to spin-½ nuclei of those associated with the analyte molecule (Figure 6).[94] A metal “catalyst” is used to facilitate polarisation transfer. These catalysts, which are typically iridium centred, catalyse the transfer of polarisation and not chemical change, as unlike PHIP, SABRE does not lead to the chemical modification of the substrate. As polarisation transfer occurs through

the *J*-coupling, coupling is maximised for analyte molecules *trans* to *para*hydrogen-derived hydrides, whereas polarisation transfer to molecules that are *cis* is negligible.

The analyte molecule is required to have a ligation point for which to ligate to the metal catalysts. Nitrogen heterocyclic molecules have been extensively explored in the literature.[95-100] **24 - 26** all possess a pyridyl motif and so, theoretically, could be potentially SABRE active. Pyridine is the most studied *N*-heterocycle for SABRE. Using this technique, it may be possible to successfully image the binding of NBOMe derivatives, such as **24 - 26** to 5-HT receptors. This may offer an alternative technique to PET imaging.

SABRE was first reported in 2009 by Duckett and co-workers when it was demonstrated that PHIP could occur without the incorporation of *para*hydrogen into the analyte.[101] By using an iridium-based catalyst, spin polarisation was transferred at low magnetic field ligands (typically 0.5 to 150 G (0.5 to 150 x10^{-4} T)) to ^{15}N-labelled pyridine. ^{15}N-labelled pyridine, therefore, became the first compound to demonstrate that SABRE did not chemically change the analyte and that a catalyst was required to facilitate transfer of spin magnetisation. This initial observation was sufficient to demonstrate the applicability of this technique to both NMR and MRI, and it led to the phrase SABRE being coined to describe this technique.[102] In a second publication, a range of *N*-heterocyclic ligands, such as nicotine and 3-fluoropyridine, were polarised by SABRE in CD_3OD. The polarisation transfer was evident by inspection of the resulting polarised ^{1}H, ^{13}C, ^{19}F and ^{31}P NMR spectra that were recorded relative to their normal Boltzmann distribution. In terms of signal gain, the enhancement of the ^{1}H spins of pyridine increased by 550-fold (Polarization (P) = 0.4%) following polarisation transfer at 2 × 10^{-2} T. In this instance, the spin transfer catalyst $[Ir(H)_2(PCy_3)(pyridine)_3][BF_4]$ was used.[94]

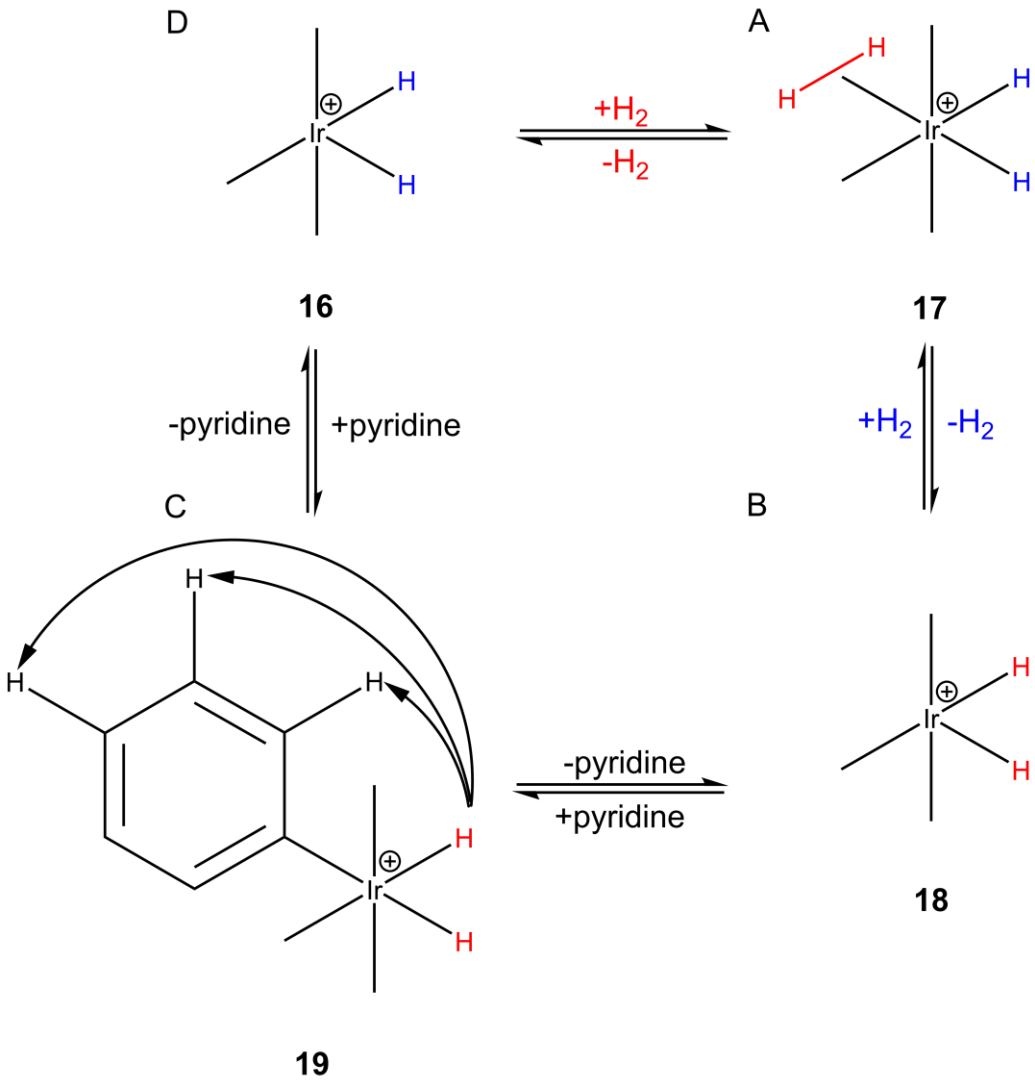

Figure 6 - Catalytic cycle of *para*hydrogen (red) binding to an iridium based catalyst via oxidative addition (A) followed by reductive elimination of *ortho*hydrogen (blue) from the complex (B) and lastly pyridine substrate binding to the iridium complex (C), which can then dissociate after polarisation transfer so the process can start again.

Richardson *et al.*[103] have since shown, in 2018, that SABRE has progressed and an enhancement for pyridine increased greatly. The polarisation performed via high field NMR (9.4 T, 400 MHz) yielded *ortho*-proton enhancement values of 1610-fold and low field NMR (1 T, 43 MHz) yielded an *ortho* enhancement of 17100-fold using $[Ir(IMes)(H)_2(py)_3]Cl$ as the catalyst (py = pyridine).[103]

1.4 Positron Emission Tomography (PET)

Molecular imaging involves the *in vivo* examination of molecular and cellular processes through the application of a number of imaging techniques, including positron emission tomography (PET),[104] single-photon emission computed tomography (SPECT),[105] magnetic resonance imaging (MRI)[106] and optical imaging.[107]

Of all the tomographic molecular imaging modalities, PET imaging offers more translational possibilities than any other modality due to its combination of sensitivity and quantitative accuracy. PET is a non-invasive imaging modality that provides physiological information through the injection of radioactive compounds (radiotracers), detection of radiation, and reconstruction of the distribution of the radiotracer.[104]. The radioisotopes frequently used include ^{18}F, ^{11}C, ^{15}O, ^{13}N, ^{82}Rb, ^{64}Cu and ^{68}Ga, with ^{18}F and ^{11}C being the most popular due to their longer half life time (109.77 and 20.33 min respectively) and can also be used in drug compounds as they have no pharmacological effect.[108]

The evolution of this technique has become a standard component of diagnosis and staging in oncology, along with specific neurological and cardiovascular indications. It is known that the NBOMe series has a high binding affinity with the serotonin receptors (5-HT) so by altering the structure of the molecule it can be used as a PET agent for studies on neuropsychiatric disorders.[109] To further enhance binding, classical receptor binding assays have demonstrated that 5-HT_{2A} receptors exists in two affinity states, agonistic and antagonistic.[110] NBOMe related compounds (Figure 7), Cimbi-5 (**20**) and Cimbi-36 (**21**), have agonistic binding properties to the 5-HT_{2A} receptor.[111] [^{18}F] Altanserin[112] (**22**) and [^{11}C]MDL 100907[113] (**23**), have been found not to be displaced by elevated levels of endogenous serotonin (5-HT) as they are antagonists,[114] so it would not be suitable for PET imaging studies. By changing the substituted benzaldehyde to a substituted nicotinaldehyde (Figure 8), a potential new range of compounds (NPyr **24**, NPF **25** and NPOMe **26**) can be approached with a different analytical technique (hyperpolarisation).

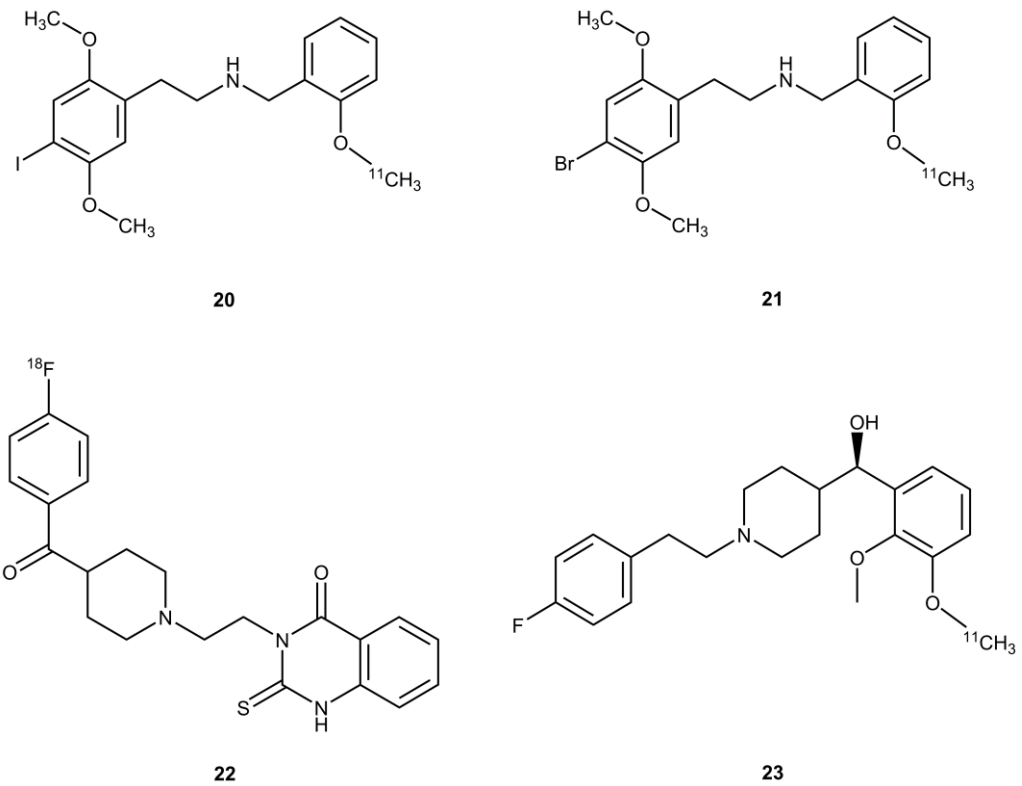

Figure 7 – Previous radio ligands involved with 5-HT_{2A} studies

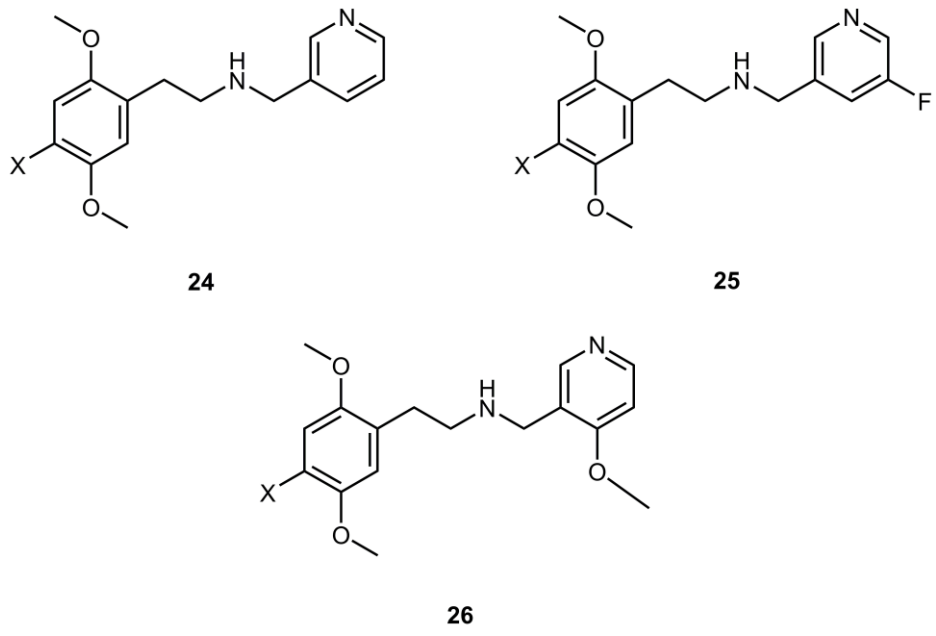

Figure 8 – Proposed structures to replace PET imaging compounds (X=F, Cl, Br, I, Me, Et, NO_2)

5-Hydroxytryptamine (serotonin, 5-HT) receptors are scattered throughout the body as they mediate a wide range of physiological processes. These receptors are found in the central and peripheral nervous system (CNS/PNS), as well as in a number of

non-neuronal tissues in the gut, cardiovascular system and blood. Dysfunction of these has been implicated in cardiovascular and digestive disorders as well as numerous psychiatric disorders.[115] Pharmacological manipulation of the 5-HT system is believed to have therapeutic potential, and is therefore the subject of intense research.[116] The 5-HT receptor branches off into seven different subtypes, with evidence showing there are at least 14 mammalian subtypes in existence.[117] All the 5-HT receptors are G protein-coupled receptors (GPCRs), with the exception of the 5-HT_3 receptor (ligand-gated ion channel).[117,118] The 5-HT_2 family has three known subtypes: 2A, 2B and 2C. The transmembrane domains of the 5-HT_{2A} and 5-HT_{2C} receptors share an 80% sequence identity and possess similar pharmacological profiles.[119]

NBOMe's are known to be potent partial agonists for the 5-HT_{2A} receptor, which is comprised of 471 amino acids and is widely distributed in peripheral and central tissues.[115] This receptor plays a physiological role in working memory,[120] the regulation of cognitive states and associative learning.[121] Peripheral 5-HT_{2a} receptors mediate diverse processes such as vasoconstriction and platelet aggregation.[122] Various other responses have been observed and these are highlighted in Figure 9.

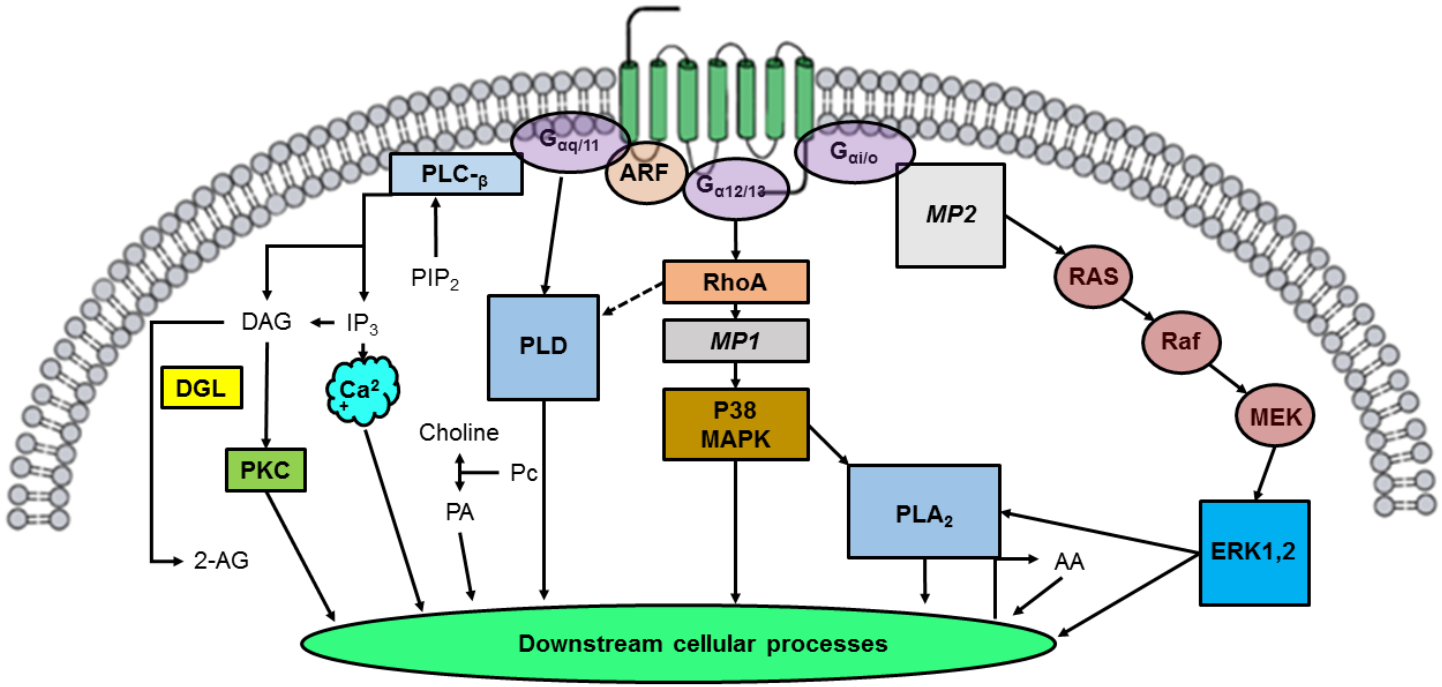

Figure 9 - Graphical representation of the known 5-HT_{2A} signalling pathways. The 5-HT_{2A} receptor couples to various downstream effectors enabling diverse cellular responses following receptor activation. Some of the mediating proteins (MP) are omitted for clarity. Mediating proteins (MP1) in the $G\alpha_{12/13}$-hoAMKK4. p38 pathway most probably are PKN, MEKK, MKK3/6 and Shc, Grb2 and SOS are the proteins mediating (MP2) the Ras-Raf-MEK1,2-ERK1,2 pathway. Receptor regulatory pathways (e.g. phosphorylation; internalization; desensitization) following agonist activation, are not shown. Note: the localization of proteins and messengers in this Figure does not represent their localization in a functional cell.[123]

By incorporating radionuclei (e.g. [^{11}C]) within the NBOMe structure, these molecules have been employed as radiotracers to visualise the release patterns of serotonin receptors using PET MRI. This also includes diseases that arise from these faulty receptors, including depression, anxiety, obsessive-compulsive disorders (OCD) and schizophrenia. The radiosynthesis and the use of these molecules have been investigated.[43]

PET studies of 5-HT$_2$ receptors have shown that agonist PET tracers are more displaceable by elevated levels of endogenous dopamine compared to antagonist tracers.[124, 125] PET imaging allows for the quantification of neuroreceptors, and with the appropriate radioligand, neurotransmitter release can be detected as receptor binding will be inversely correlated to extracellular levels of neurotransmitters such as has been shown for the dopamine system.[126] Therefore, PET imaging has the potential to measure serotonin levels in the human brain safely. A radioligand has not yet been fully developed that is sensitive enough to detect the change in serotonin levels. Ettrup *et al.* has since developed and validated a series of NBOMe's as agonist PET radioligands for the selective mapping and quantification of 5-HT$_{2A}$ receptors *in vivo,*[111, 43] with [^{11}C]Cimbi-36 (Scheme 5, **21**) having the strongest PET tracer properties when scanned in a pig brain. When looking at the other results such as whole body distribution and head twitch response (HTR), it was found that the lungs had the highest uptake in rats, whereas in pigs it was the excretory organs (bladder, gall bladder and kidneys) (Figure 10).[127] The *in vivo* pharmacological effects showed that the HTR in mice was most comparable to saline, with a prominent HTR with Cimbi-36 at a higher dose of 0.5 mg/kg. This suggests, for humans, doses between 300 – 600 µg will yield hallucinogenic effects. However, the doses generally given in PET scanning are in the low µg range (*ca*. 1 µg for a 70 kg human).

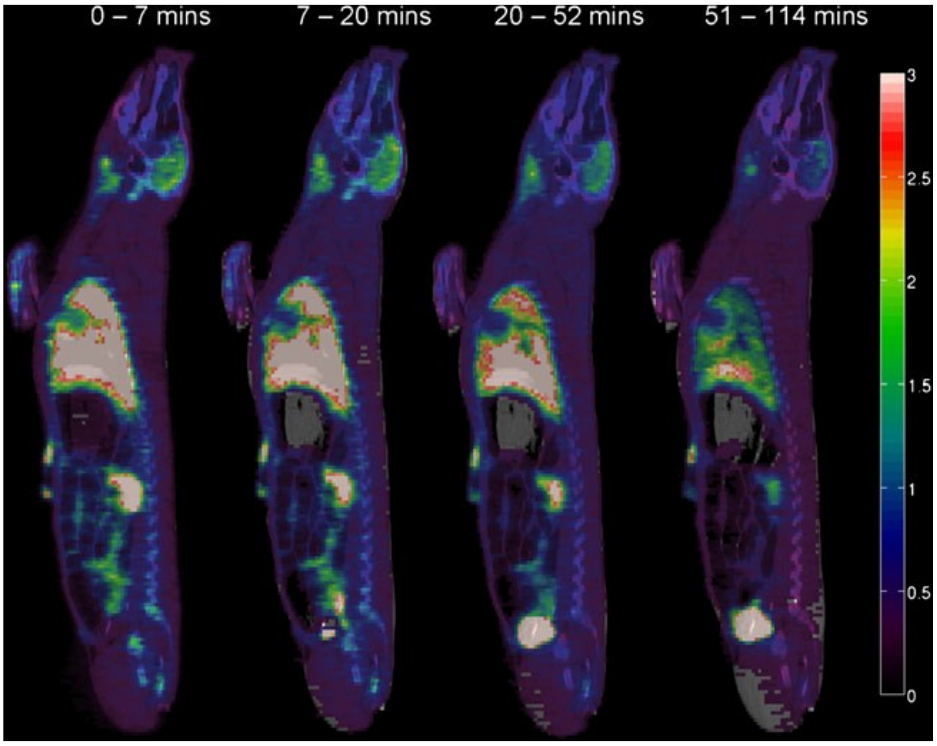

Figure 10 - Ettrup *et al.* imaging data of the sagittal whole body PET images of [^{11}C]Cimbi-36 distribution in a pig. Images are averaged over the indicated time interval and are overlaid on to the corresponding section in the CT image. Images are scaled to standardised uptake values (SUVs) as given by the colour bar. PET images are threshold so that voxels with SUV values lower than 0.2 % of the maximal volumetric pixel (voxel) value are not shown.[127]

Ettrup and co-workers then looked at how Cimbi-36 binds to the human brain. Twenty-nine healthy males participated in this study with the results being that Cimbi-36 successfully labelled the 5-HT$_{2A}$ receptor. However, as these compounds are comprised of labelled [^{11}C] (Scheme 5), they only have a half-life of 20 minutes. Therefore implementing these PET tracers will have to be done in a time efficient manner to ensure that appropriate images can still be acquired.

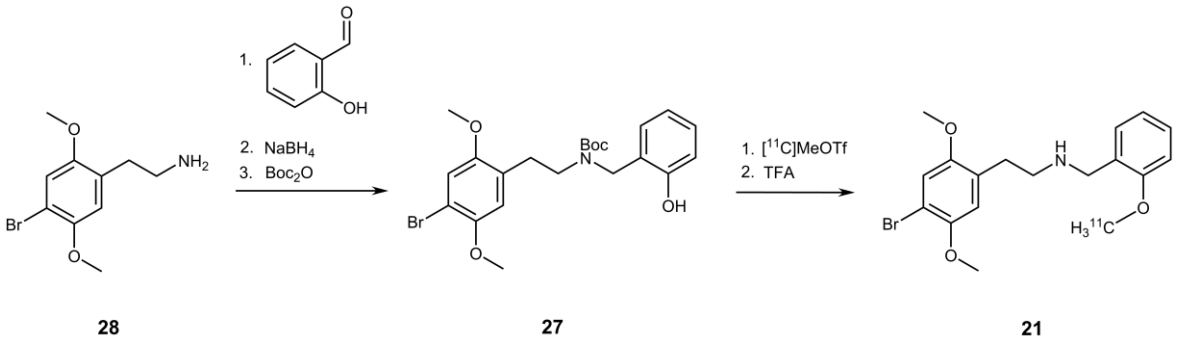

Scheme 5 - Chemical synthesis of the precursor and PET tracer [^{11}C]Cimbi-36[43]

1.5 Aims and Objectives

Since the introduction of misuse of drugs act, illicit drug suppliers and clandestine labs have been looking at ways to avoid detection and alter structures of controlled substances. An example of this would be to include fluorine into the molecule, as research has indicated that this enhances biological activity and increased chemical and metabolic stability.[128] This has also lead to the suppliers mixing drugs, so the "research chemicals" being sold by these vendors are not necessarily what it says they are, with the dosing also being potentially wrong. However, NBOMe studies have looked at the positive aspects of this illicit drug by altering them to radio labelled compounds to be used in PET imaging. The aim of this project, outlined in Scheme 6, is to synthesise NBOMe compounds as reference standards for street sample analysis including GC-MS validation and presumptive testing of impregnated blotters. This is complemented by the synthesis of 21 novel compounds, which could potentially replace PET imaging agents, with polarisable pyridyl tethers such that they could be hyperpolarised via SABRE.

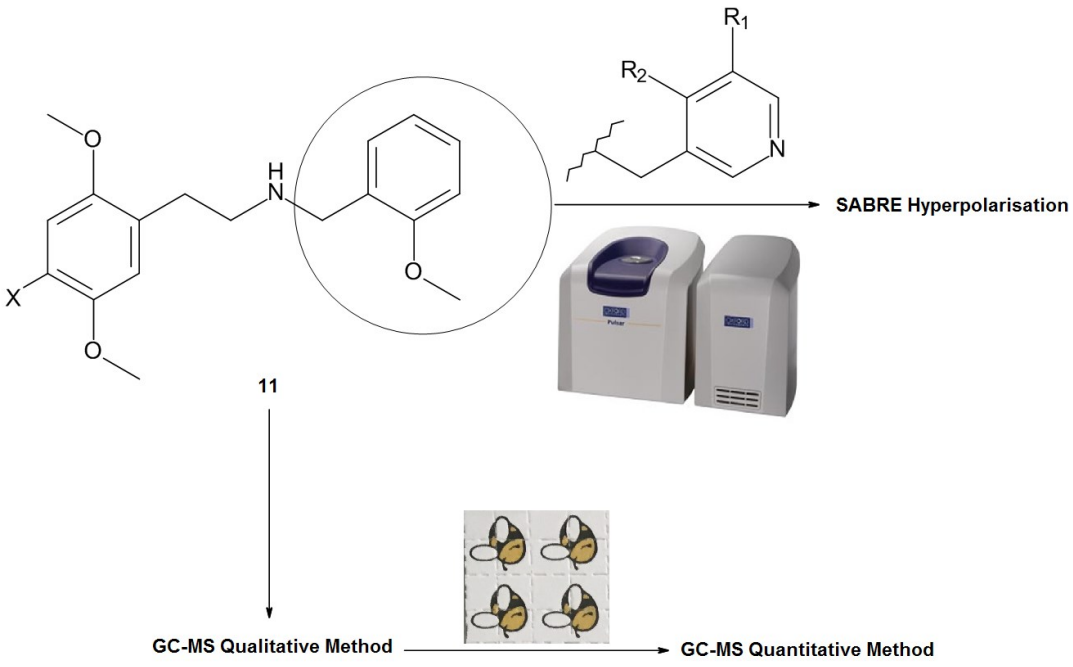

Scheme 6 – Objectives for the research presented; X = F, Cl, Br, I, Me, Et, NO_2; 25X-NPyr (**24**) – R_1 = R_2 = H; 25X-NPF (**25**) – R_1 = F, R_2 = H; 25X-NPOMe (**26**) – R_1 = H, R_2 = OMe

2 Chapter 2 - Experimental

2.1 Apparatus Used

All chemicals were obtained from Sigma Aldrich (Gillingham, UK), Fluorochem (Hadfield, UK) or Tokyo Chemical Industry (Oxford, UK) and used without further purification. ^{1}H- and ^{13}C-NMR spectra were acquired on a JEOL ECS 400 (JEOL, Hertfordshire, UK) NMR spectrometer operating at a proton resonance frequency of 400 MHz and carbon resonance frequency of 101 MHz. ^{1}H-NMR analysis performed on a Pulsar (Oxford Instruments, Abingdon, UK) NMR spectrometer, operating at a resonance frequency of 60 MHz, was acquired in 1 scan using a filter file of 2000 Hz and a relaxation delay of 0.01 seconds. Infrared spectra were obtained in the range 4000 – 400 cm^{-1} using a ThermoScientific Nicolet iS10ATR-FTIR instrument (ThermoScientific, Rochester, USA). GC-MS spectra were recorded on an Agilent 7890B gas chromatograph with split-splitless injection (sample volume: 0.5 µL), split ratio of 50:1 and a HP-5MS column (30 m × 0.25 mm, 0.25 µm film thickness). Helium (He) was used as the carrier gas at a flow rate of 1.2 mL min^{-1}. The GC was coupled to an Agilent 5977 MSD (EI, 70 eV, TIC mode scanning *m/z* 50 – 500) and injector port was set at 265 °C, the transfer line at 300 °C. The following temperature program was used: 50°C, ramped by a rate of 30°C min^{-1} to 320°C and held for 3 min. Thin-Layer Chromatography (TLC) was carried out on aluminium-backed SiO_2 plates (Merck, Darmstadt, Germany) and spots were visualised using ultra-violet light (254 nm).

2.2 Presumptive Test Reagents

Presumptive tests reagents were prepared according to the United Nations recommended guidelines.[129] The following standard presumptive tests applied in this study: (i) Marquis; (ii) Liebermann. Sample solutions were prepared at 10 mg mL^{-1} by dissolving the reference standards in distilled water. Negative control samples (distilled water) were used in all tests in order to indicate clearly when a positive result occurred.

Marquis Test: 1% formaldehyde (37% aqueous solution) in concentrated sulfuric acid (10 mL). 5 drops of test sample in distilled water (10 mg mL^{-1}) was placed into a dimple well of a white spotting tile and 5 drops of the test reagent added. Any

immediate colour change or other noticeable effect occurring was noted and observations were made again after a 5 minute period.

Liebermann test: Potassium nitrite (2 g) in concentrated sulfuric acid (20 mL). 5 drops of test sample in distilled water (10 mg mL^{-1}) was placed into a dimple well of a white spotting tile and 5 drops of the test reagent added. Any immediate colour change or other noticeable effect occurring was noted and observations were made again after a 30 minute period.

2.3 Developed GC-MS method for NBOMe separation

A method was created (stated in apparatus used) for the separation of NBOMe analogues by GC-MS. A SIM detection mode was used for the increased sensitivity when identifying each NBOMe, with the SIM ions being *m/z* = 91.1, 121.1 and 151.1.

2.4 Reference standard preparation for GC-MS

All compounds were prepared as 1 mg mL^{-1} solutions for initial GC-MS screening. 3-4 mg of each reference material dissolved in MeOH to the matching volume (3 – 4 mL) in 5 mL volumetric flasks.

2.5 NBOMe calibration standards for GC-MS

5 mg of each NBOMe was weighed and diluted to 5 mL with MeOH to give a 1 mg mL^{-1} solution. This solution was then further diluted with MeOH (10 mL) to give a 100 µg mL^{-1} solution. This was diluted further with MeOH (0.3 – 0.6 mL) and 0.75 mL eicosane (25 µg mL^{-1} in MeOH) to give calibration standards containing 10 µg mL^{-1}, 15 µg mL^{-1}, 20 µg mL^{-1}, 25 µg mL^{-1} and 30 µg mL^{-1}.

2.6 Blotter preparation

Pre-perforated blotting paper (1/4” x 1/4”) (Amazon, Zane Kesey, UK) were prepared and analysed by the following techniques; 0.2 mL of 300 ug mL^{-1} 25B-NBOMe, 500 ug mL^{-1}, 25C-NBOMe and 800 ug mL^{-1} 25I-NBOMe in MeOH was dripped evenly onto a 3 x 3 (3/4” x 3/4") block of papers (plain and patterned) and left to dry. For the extraction, 1 mL MeOH was added to 1 blotter per vial and ultra-

sonicated for 15 mins, the solution was pipetted into a separate vial and the blotter was re-extracted with 1 mL MeOH. This process was repeated 3 times and the MeOH collections concentrated *in vacuo*. Appropriate dilutions was applied so the concentrations are in the calibration range with eicosane (12.5 ug mL^{-1}) being the internal standard.

2.7 Sample Preparation for SABRE experiments

5 mM of an iridium based catalyst [Ir(COD)(IMes)Cl] (COD = cyclooctadiene, IMes = 1,3-*bis*(2,4,6-trimethylphenyl)imidazole-2-ylidene)[130] (**85**) was used with 4 mol eq. of the selected substrate (catalyst synthesised by a PhD colleague, Thomas Robertson, Dr Ryan Mewis research group). The solvent used was methanol-d_4 and the total volume used was 0.6 mL in each sample. NMR samples were prepared in 5 mm diameter NMR tubes fitted with Youngs caps, samples were degassed on a high-vacuum line *via* three 'cool'-pump-thaw cycles (using a acetone/CO_2 slush bath). *Para*hydrogen, at a pressure of 3.0 atmospheres, was then admitted to the NMR tube. *Para*hydrogen was produced by cooling hydrogen gas to 77 K over charcoal.

Preparation for SABRE experiments followed A. M. Olaru *et al*.[131]. NMR samples were prepared containing 5 mM catalyst precursor in 0.6 mL of methanol-d_4. Arrays of NMR measurements were collected using either 4 equivalents of substrate to 5 mM of iridium in 0.6 mL MeOD (leading to samples containing 1- and 17-fold excesses of ligand relative to iridium, respectively). After adding *p*-H_2 at 3 bar pressure, ^{1}H NMR spectra were recorded using π/2 excitation pulses immediately after shaking the sample in a magnetic field of 65 G.

2.8 Compound data

Synthesis of 2-(4-bromo-2,5-dimethoxy-phenyl)ethanamine (28)

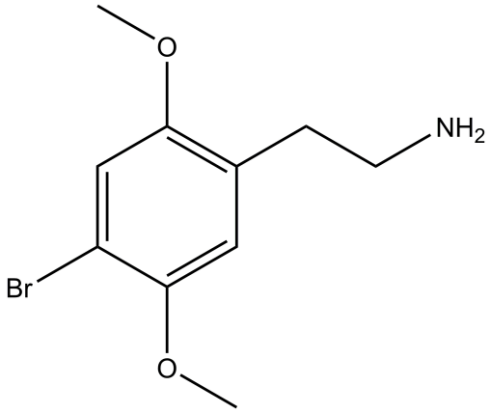

2,5-Dimethoxyphenethylamine (2C-H) (4.96 g, 27.7 mmol) was added to glacial acetic acid (40 mL). To this solution was added bromine (4.4 g, 27.7 mmol) in glacial acetic acid (8 mL) slowly. The solution was then left to stir at RT for 5 min. A yellow solid spontaneously formed exothermically and was left to cool down to room temperature before filtering. The filtrate was dissolved in aqueous NaOH (25% w/v), extracted with DCM (3 x 100 mL) and dried *in vacuo* to obtain a white oil. The oil was dissolved in a mixture of water (50 mL), acetic acid (6.7 mL), and conc. HCl (12 M, 20 mL) to obtain the hydrochloride salt. The precipitate was collected via filtration. This was then washed sequentially with water (60 mL), Et_2O (150 mL) and acetone (60 mL) to obtain a pure white powder (3.51 g, 49 %); Mp. 236-238°C; ^{1}H NMR (400 MHz, CD_3OD) δ 7.18 (s, 1 H), 6.97 (s, 1 H), 3.84 (s, 3 H), 3.82 (s, 3 H), 3.14 (t, *J*=7.22 Hz, 2 H), 2.95 (t, *J*=7.22 Hz, 2 H); ^{13}C NMR (101 MHz, CD_3OD) δ 153.5, 151.8, 126.4, 117.2, 116.4, 111.4, 57.5, 56.7, 40.7, 29.8. GC-MS 6.856 min, m/z=230. Data corresponds to the spectroscopic assignments reported by Kanamori *et al*[132]

Synthesis of 4-chloro-2,5-dimethoxy-benzaldehyde (29)

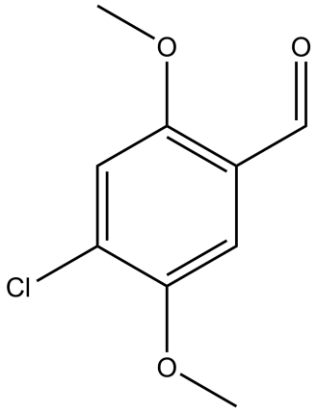

The approach of Wright *et al*[133] was used with an argon-flushed system to suspend hexamethylenetetramine (1.40 g, 10 mmol) in 1-chloro-2,5-dimethoxybenzene (1.26 g, 7.32 mmol) to which was added TFA (25 mL) dropwise with stirring until the solution was yellow. This was heated to reflux for 15 h with the brown solution poured onto ice (25 g) and $NaHCO_3$ added in slowly until a yellow solid formed and the solution is basic. The solid was filtered and washed with water then dissolved in Et_2O. The organic solution washed with water, brine, dried with $MgSO_4$ and dried *in vacuo* to obtain a crude yellow/brown product. The aldehyde was recrystallized with high b.p petroleum ether (80-100ºC) and the yellow powder filtered yielding (0.80 g, 55 %); Mp. 158-161 ˚C; ^1H NMR (400 MHz, $CDCl_3$) δ 10.39 (s, 1 H), 7.38 (s, 1 H), 7.07 (s, 1 H), 3.90 (s, 6 H); GC-MS 6.061 min, m/z = 200 (M^+). Data corresponds to the spectroscopic assignments reported by Bloomer *et al.*[134]

Synthesis of 1-chloro-2,5-dimethoxy-4-[(E)-2-nitrovinyl]benzene (30)

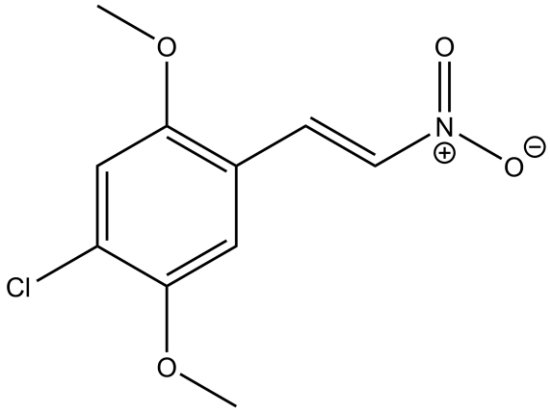

29 (8.80 g, 36.2 mmol), nitromethane (3.31 g, 54.3 mmol) and ammonium acetate (6.98 g, 90.5 mmol) were added to acetic acid (60 mL). The solution was then stirred to reflux for 4 hr. After cooling, water was added until a yellow/orange solid formed, which was then left to stir for a further 10 min in an ice bath. This was filtered and washed with water as a yellow/orange solid. The nitrostyrene was recrystallized with IPA and filtered to yield a yellow powder (2.99 g, 34 %); Mp. 158-160˚C; ^{1}H NMR (400 MHz, $CDCl_3$) δ 8.08 (d, *J*=13.74 Hz, 1 H), 7.87 (d, *J*=13.74 Hz, 1 H), 7.03 (s, 1 H), 6.98 (s, 1 H), 3.91 (s, 3 H), 3.92 (s, 3 H;. ^{13}C NMR (101 MHz, $CDCl_3$) δ 153.725, 149.272, 138.479, 134.494, 127.610, 117.856, 114.690, 113.956, 56.739, 56.615, 56.567, 56.501, 56.262. GC-MS 7.685 min, m/z 243

Synthesis of 2-(4-chloro-2,5-dimethoxy-phenyl)ethanamine (31)

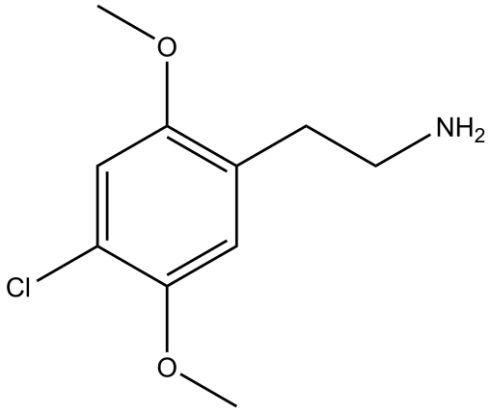

In an argon-flushed system, lithium aluminium hydride (0.5 g, 13 mmol) was suspended in anhydrous THF (50 mL) and the solution was stirred thoroughly. **30** (0.61 g, 2.5 mmol) dissolved in THF (10 mL) was added in slowly and stirred for 3 h at RT prior to heating to reflux for 15 min. The remaining LAH was decomposed by water (5 mL) followed by aqueous NaOH (15%, 5 mL) in an ice bath to precipitate out the basic insoluble components. The solution was then filtered and the filtrate washed with THF (3 x 40 mL). The organic solution was concentrated *in vacuo* and 2M HCl (20 mL) was added. This solution was washed with DCM (3 x 20 mL) and the aqueous layer then neutralised with aqueous NaOH. This was extracted with DCM (5 x 20 mL), dried with $MgSO_4$ and concentrated *in vacuo*. The amber oil was dissolved with IPA (10 mL), neutralised with conc. HCl (12 M) and upon addition of anhydrous ether crystals formed. The salt was recrystallized with IPA and filtered yielding a white powder (0.27 g, 50%); Mp. 240-242°C; ^{1}H NMR (400 MHz, CD_3OD) δ 7.04 (s, 1 H), 6.98 (s, 1 H), 3.82 (s, 3 H), 3.84 (s, 3 H), 3.14 (t, *J*=7.33 Hz, 2 H), 2.95 (t, *J*=7.33 Hz, 2 H). ^{13}C NMR (101 MHz, CD_3OD) δ 153.22, 150.70, 125.60, 122.73, 116.71, 114.34, 57.45, 56.73, 40.77, 29.73. GC-MS 6.526 min, m/z 186

Synthesis of 2,5-dimethoxy-4-methyl-benzaldehyde (32)

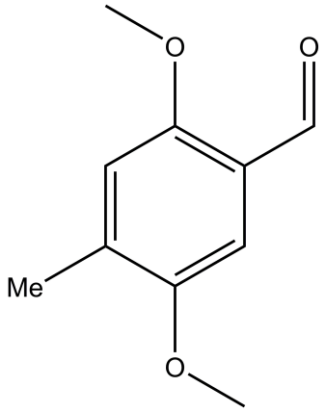

Phosphorus(V)oxychloride (20 mL, 0.8 mol) and *N*-methylformanilide (22.5 mL, 0.15 mol) was stirred at room temperature for 1 h until the solution went orange indicating the formation of the Vilsmeier complex. 2,5-dimethoxytoluene (7.15 mL, 0.05 mol) was added and heated to 70°C for 2 h. The heat source was removed and allowed to cool to room temperature. The flask was reheated, poured into ice water (1 L) and stirred for 10 mins. The solution was filtered and the crude aldehyde collected as a red solid. This was suspended in boiling petroleum ether (50 mL) and decanted; this process was repeated twice. The solution was left to crystallize and filtered to obtain 2,5-dimethoxy-4-methylbenzaldehyde as a white powder (8.86 g, 97%); ^{1}H NMR (400 MHz, CD_2Cl_2) δ 10.4 (s, 1 H), 7.2 (s, 1 H), 6.8 (s, 1 H), 3.9 (s, 3 H), 3.8 (s, 3 H), 2.3 (s, 3 H). Data corresponds to the spectroscopic assignments reported by Miyawaki *et al*[135]

Synthesis of 2,5-dimethoxy-1-methyl-4-[(E)-2-nitrovinyl]benzene (33)

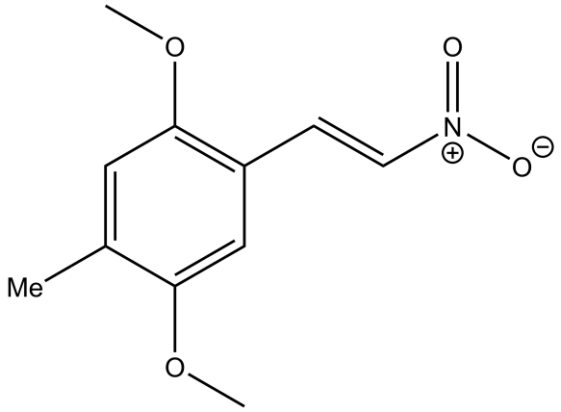

32 (8.86 g, 50 mmol), nitromethane (75 mmol) and ammonium acetate (9.64 g, 125 mmol) were added to acetic acid (90 mL). The solution was then heated to reflux, with stirring, for 4 hr. After cooling, water was added until a yellow/orange solid formed, which was then left to stir for a further 10 min in an ice bath. This was filtered and washed with water (20 mL) to afford a yellow/orange solid. The nitrostyrene was recrystallized with IPA and filtered yielding a yellow powder (7.38 g, 66%); ^{1}H NMR (400 MHz, $CDCl_3$) δ 8.1 (d, J=13.74 Hz, 1 H), 7.9 (d, J=13.28 Hz, 1 H), 6.8 (s, 1 H), 6.8 (s, 1 H), 3.9 (s, 3 H), 3.8 (s, 3 H), 2.3 (s, 3 H).

Synthesis of 2-(2,5-dimethoxy-4-methyl-phenyl)ethanamine (34)

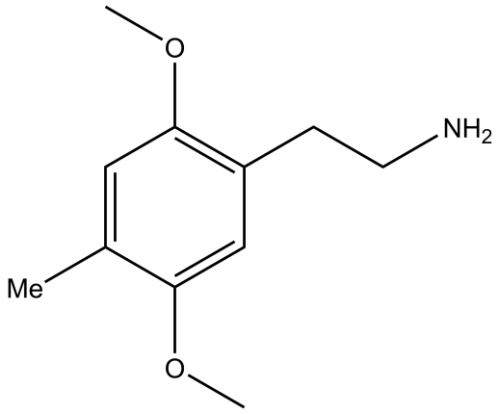

In an argon-flushed system, lithium aluminium hydride (6.73 g, 0.18 mol) was suspended in anhydrous THF (200 mL) and the solution was stirred thoroughly. **33** (7.38 g, 0.03 mmol) was dissolved in THF (40 mL) and was added in slowly, this was stirred for 3 h at RT then refluxed for 15 min. The remaining LAH was decomposed by water followed by NaOH (15%, 10 mL) to precipitate out the basic insolubilities, this was then filtered and the filtrate washed with THF (3 x 40 mL). The organic solution was concentrated *in vacuo* and HCl (2 M, 20 mL) was added. This was washed with DCM (3 x 20 mL) and the aqueous layer then neutralised with aqueous NaOH. This was extracted with DCM (5 x 20 mL), dried with $MgSO_4$ and concentrated *in vacuo*. The amber oil was dissolved with IPA (10 mL), neutralised with conc. HCl (12 M) and upon addition of anhydrous ether (10 mL) crystals formed. The salt was recrystallized with IPA and filtered yielding a white powder (0.92 g, 14%); ^{1}H NMR (400 MHz, CD_3OD) δ 6.7 - 6.7 (m, 1 H), 6.7 (s, 1 H), 3.8 (dd, J=3.89, 1.60 Hz, 6 H), 2.8 (d, J=6.87 Hz, 2 H), 2.7 (d, J=6.87 Hz, 2 H), 2.2 (s, 3 H); ^{13}C NMR (101 MHz, CD_3OD) δ 153.1, 152.8, 126.9, 126.3, 115.0, 114.4, 56.5, 55.0, 43.1, 35.1, 16.4.

Synthesis of 2,5-dimethoxyacetophenone (35)

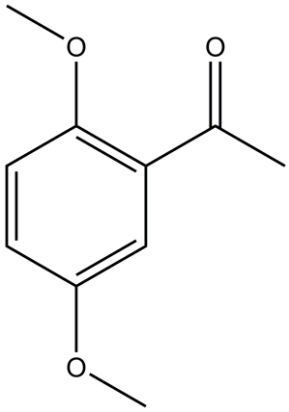

1,4-dimethoxybenzene (24.7g, 0.18 mol) was dissolved in DCM (50 mL) and added slowly to a stirred solution of acetyl chloride (22 g, 0.23 mol), aluminium chloride (30.6 g, 0.23 mol) and DCM (70 mL) with external cooling. This was stirred for 1 h at RT then poured into H_2O (200 mL) and extracted with DCM (4 x 50 mL). The organic layer washed with 5% NaOH (3 x 50 mL) and concentrated *in vacuo* to afford a red oil, 2,5-dimethoxyacetophenone (26.86 g, 83%); ^{1}H NMR (400 MHz, $CDCl_3$) δ 7.3 (d, J=3.21 Hz, 1 H), 7.0 (dd, J=8.93, 3.21 Hz, 1 H), 6.9 (d, J=8.93 Hz, 1 H), 3.9 (s, 3 H), 3.8 (s, 3 H), 2.6 (s, 3 H). Data corresponds to the spectroscopic assignments reported by Shagari *et a.l*[136]

2-hydroxy-5-methoxyacetophenone (36)

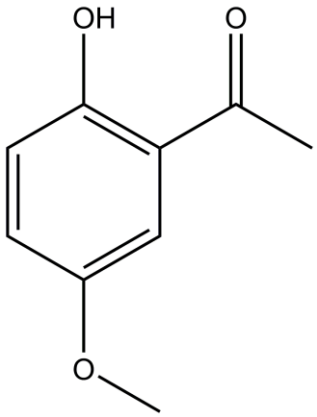

After acidification of the spent aqueous phase (HCl, 2 M) and extraction with DCM (3 x 40 mL), the organic solution washed with saturated $NaHCO_3$ and concentrated *in vacuo*. 2-hydroxy-5-methoxyacetophenone was produced as yellow crystals and recrystallized with MeOH, dried and filtered yielding (2.68 g, 9%); ^1H NMR (400 MHz, $CDCl_3$) δ 11.9 (s, 1 H) , 7.2 (d, *J*=3.21 Hz, 1 H), 7.1 (dd, *J*=8.93 3.21 Hz, 1 H), 6.9 (d, *J*=8.93 Hz, 1 H), 3.8 (s, 3 H), 2.6 (s, 3 H). Data corresponds to the spectroscopic assignments reported by Saito *et al.*[137] Iodomethane (1.5 mol eq.) was added dropwise to a solution of **36** (1 mol eq.), KOH (10 mol eq.) and DMSO (50 mL). The solution was stirred for 1 h at 40°C. The mixture was then neutralised with sat. NH_4Cl and extracted with DCM (4 x 25 mL). The organic phase was washed with water (8 x 40 mL), dried with Na_2SO_4 and concentrated *in vacuo*. No further purification was required as **35** was synthesised as a red oil yielding 2.31 g (0.013 mol, 80%)

Synthesis of 2-ethyl-1,4-dimethoxybenzene (37)

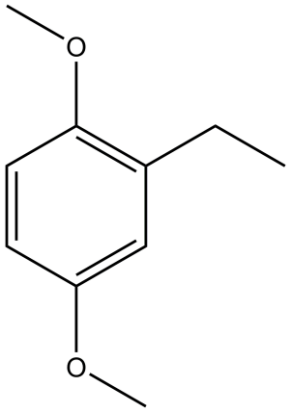

With a Dean-Stark set up, **35** (28.86 g, 0.15 mol), KOH (18.3 g, 0.33 mol), triethylene glycol (125 mL) and 40% hydrazine hydrate (32 mL) was heated to 150°C until no more water was produced, whereupon the solution was maintained at reflux for a further 3 h. After cooling, the reaction mixture and distillate was poured into water (1 L) and extracted with DCM (4 x 50 mL), dried with $NaSO_4$ and concentrated *in vacuo* to afford a deep red oil. This was purified *via* column chromatography (EtOAc-hexane; 1:9 v/v) and concentrated *in vacuo* to obtain 2-ethyl-1,4-dimethoxybenzene as a deep red oil (3.0007 g, 12%); ^{1}H NMR (400 MHz, $CDCl_3$) δ ppm 6.8 (d, J=9.16 Hz, 2 H), 6.7 (dd, J=3.20 Hz, 1 H), 3.8 (s, 3 H), 3.8 (s, 3 H), 2.6 (q, J=7.33 Hz, 2 H), 1.1 - 1.3 (m, 3 H). Data corresponds to the spectroscopic assignments reported by Roberts *et al*[138]

2-ethyl-4-methoxyphenol (38)

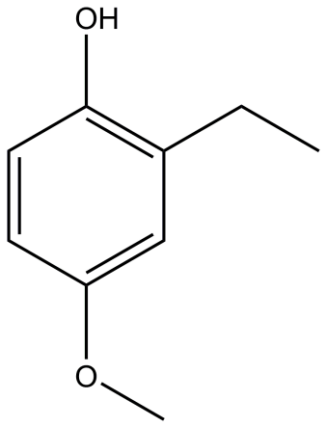

Acidification of the previous aqueous phase with conc. HCl (2 M) was extracted with DCM (4 x 50 mL) and concentrated *in vacuo* to a deep red residue. This was distilled at 115 – 120 °C at 6 mm/Hg to obtain a light red oil that was 2-ethyl-4-methoxyphenol (19.38 g, 87%); ^{1}H NMR (400 MHz, $CDCl_3$) δ 6.7 (dd, *J*=4.81, 2.98 Hz, 1 H), 6.7 (dd, *J*=4.58, 2.75 Hz, 1 H), 6.6 (dd, *J*=5.95, 2.70 Hz, 1 H), 5.2 (br. s, 1 H), 3.8 (s, 3 H), 2.6 (dq, *J*=12.80, 9.60 Hz, 2 H), 1.2 (dt, *J*=23.81, 7.33 Hz, 3 H). Data corresponds to the spectroscopic assignments reported by Wang *et al.*[139] Iodomethane (1.5 mol eq.) was added dropwise to a solution of **38** (1 mol eq.), KOH (10 mol eq.) and DMSO (50 mL). The solution was stirred for 1 h at 40°C. The mixture was then neutralised with sat. NH_4Cl and extracted with DCM (4 x 25 mL). The organic phase was washed with water (8 x 40 mL), dried with Na_2SO_4 and concentrated *in vacuo*. No further purification was required for **37** and was synthesised as a deep red oil yielding 17.57 g (0.11 mol, 85 %)

Synthesis of 4-ethyl-2,5-dimethoxy-benzaldehyde (39)

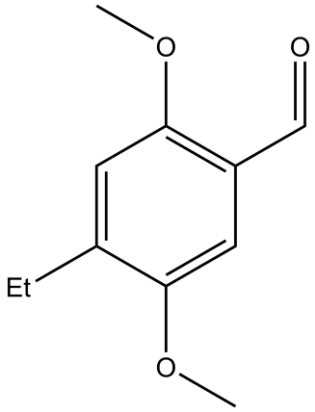

37 (20.57 g, 0.124 mmol) and tin (IV) chloride (64.6 g, 0.248 mol) were dissolved in anhydrous DCM (80 mL) and cooled to 0 °C. Dichloromethyl methyl ether (15.68 g, 0.136 mol) was dropped in slowly overtime and left to stir until it reached room temperature. The solution was quenched in ice (100 g) with conc. HCl (12 M, 40 mL) and stirred o/n. The organic layer was separated and washed (2 x 40 mL) with 10% HCl, 1 M NaOH, water and brine and concentrated *in vacuo* to a white powder (20.2 g, 83%) with no further purification; ^{1}H NMR (400 MHz, $CDCl_3$) δ ppm 10.4 (s, 1 H), 7.3 (s, 1 H), 6.8 (s, 1 H), 3.9 (s, 3 H), 3.8 (s, 3 H), 2.7 (q, J=7.63 Hz, 2 H), 1.2 (t, J=7.56 Hz, 3 H). Data corresponds to the spectroscopic assignments reported by Shulgin *et al*[140]

Synthesis of 1-ethyl-2,5-dimethoxy-4-[(E)-2-nitrovinyl]benzene (40)

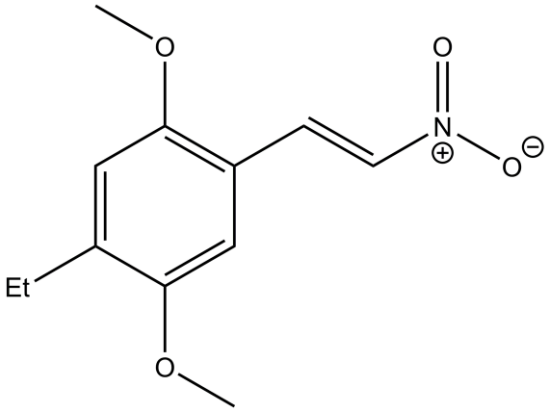

39 (20.2 g, 0.104 mol), nitromethane (63.8 g, 1.04 mol) and ammonium acetate (2.67 g, 0.035 mol) was heated to reflux, with stirring, for 4 hr. After cooling, this was concentrated *in vacuo* to afford the crude nitrostyrene. After recrystallisation with IPA, this was filtered yielding a yellow powder (7 g, 29%); ^{1}H NMR (400 MHz, $CDCl_3$) δ 8.1 (d, J=13.74 Hz, 1 H), 7.9 (d, J=13.74 Hz, 1 H), 6.9 (s, 1 H), 6.8 (s, 1 H), 3.9 (s, 3 H), 3.8 (s, 3 H), 2.7 (q, J=7.33 Hz, 2 H), 1.2 (t, J=7.33 Hz, 3 H); ^{13}C NMR (101 MHz, $CDCl_3$) δ ppm 154.2, 151.4, 139.6, 137.4, 135.7, 116.4, 112.7, 112.6, 55.9, 55.9, 23.9, 13.9.

Synthesis of 2-(4-ethyl-2,5-dimethoxy-phenyl)ethanamine (41)

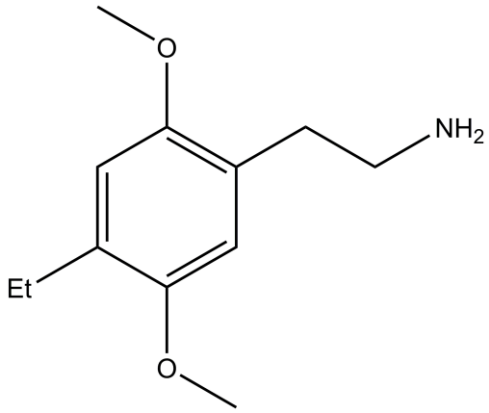

In an argon-flushed system, lithium aluminium hydride (5.8 g, 0.15 mol) was suspended in anhydrous THF (200 mL) and the solution was stirred thoroughly. **40** (7 g, 0.03 mol) was dissolved in THF (40 mL) was added in slowly, and this was stirred for 3 h at RT then refluxed for 15 min. The remaining LAH was decomposed by water followed by NaOH (15 %, 10 mL) to precipitate out the basic insolubilities, this was then filtered and the filtrate being washed with THF (3 x 40 mL). The organic solution was concentrated *in vacuo* and HCl (2 M, 20 mL) was added. This was washed with DCM (3 x 20 mL) and the aq. layer then neutralised with aqueous NaOH. This was extracted with DCM (5 x 20 mL), dried with $MgSO_4$ and concentrated *in vacuo*. The amber oil was dissolved with IPA (10 mL), neutralised with conc. HCl (12 M) and upon addition of anhydrous ether crystals formed. The amber oil was dissolved with IPA (10 mL), neutralised with conc. HCl (12 M) and upon addition of anhydrous ether crystals formed. The salt was filtered and washed with ether yielding a white powder (3.21 g, 50 %); ^{1}H NMR (400 MHz, CD_3OD) δ 6.8 (s, 1 H), 6.8 (s, 1 H), 3.8 (s, 3 H), 3.8 (s, 3 H), 3.1 - 3.2 (m, 2 H), 2.9 - 3.0 (m, 2 H), 2.6 (q, J=7.33 Hz, 2 H), 1.2 (t, J=7.56 Hz, 3 H); ^{13}C NMR (101 MHz, CD3OD) δ 153.0, 152.9, 134.0, 123.6, 114.7, 113.6, 56.6, 56.4, 41.2, 30.0, 24.6, 15.1; GC-MS 6.159 min, m/z = 209.1

Synthesis of 4-fluoro-2,5-dimethoxy-benzaldehyde (42)

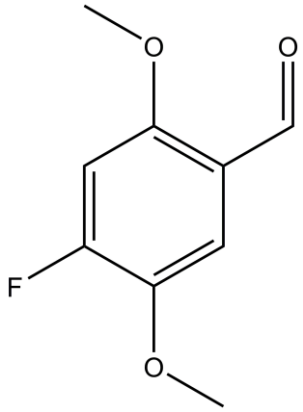

1-Fluoro-2,5-dimethoxybenzene (4.07 g, 26 mmol) and tin (IV) chloride (13.4 g, 51 mmol) were dissolved in anhydrous DCM (25 mL) and cooled to 0 °C. Dichloromethyl methyl ether (2.64 g, 23 mmol) was dropped in slowly overtime and left to stir until it reached room temperature. The solution was quenched in ice (50 g) with conc. HCl (12 M, 10 mL) and stirred o/n. The organic layer was separated and washed (2 x 10 mL) with 10% HCl, 1 M NaOH, water and brine and concentrated *in vacuo* to a white powder. This was recrystallized with EtOH and filtered yielding a white powder (1.39 g, 30 %); Mp. 99 °C; ^{1}H NMR (400 MHz, $CDCl_3$) δ 10.37 (s, 1 H), 7.45 (d, *J*=9.62 Hz, 1 H), 6.79 (d, *J*=12.36 Hz, 1 H), 3.89 (d, *J*=0.92 Hz, 6 H); GC-MS 5.368 min, m/z 184. Data corresponds to the spectroscopic assignments reported by Glennon *et al.*[141]

Synthesis of 1-fluoro-2,5-dimethoxy-4-[(E)-2-nitrovinyl]benzene (43)

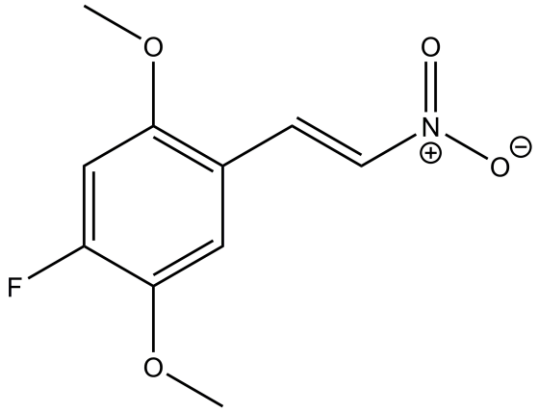

42 (3.57 g, 15.7 mmol), nitromethane (1.78 g, 23.6 mmol) and ammonium acetate (3.75 g, 39.3 mmol) were added with acetic acid (25 mL) which was stirred to reflux for 4 hr. After cooling, water was added until a yellow/orange solid formed, which was then left to stir for a further 10 min in an ice bath. This was filtered and washed with water as a yellow/orange solid. This was recrystallized with IPA and filtered yielding a yellow powder (2.10 g, 47%). Mp. 159-161 ˚C; ^{1}H NMR (400 MHz, $CDCl_3$) δ 8.10 (d, *J*=13.74 Hz, 1 H), 7.83 (d, *J*=13.74 Hz, 1 H), 7.04 (d, *J*=9.16 Hz, 1 H), 6.79 (d, *J*=12.36 Hz, 1 H), 3.90 (s, 3 H), 3.91 (s, 3 H). 154.6 (d, *J*=8.63 Hz); ^{13}C NMR (101 MHz, $CDCl_3$) δ 56.3, 57.0, 101.2 (d, *J*=23.96 Hz), 114.5 (d, *J*=3.83 Hz), 116.7 (d, *J*=3.83 Hz), 134.5, 137.7, 141.8 (d, *J*=11.50 Hz), 155.5 (d, *J*=255.91 Hz), 154.6 (d, *J*=8.63 Hz); GC-MS 7.065 min, m/z 227

Synthesis of 2-(4-fluoro-2,5-dimethoxy-phenyl)ethanamine (44)

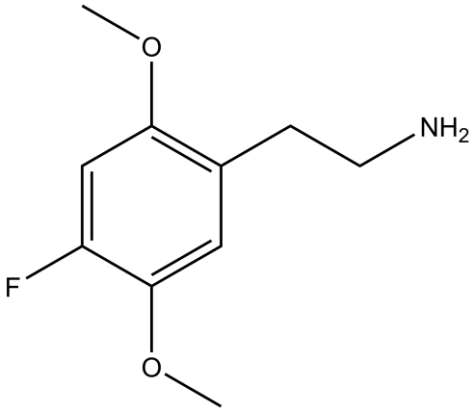

In an argon-flushed system, lithium aluminium hydride (2 g, 6 mmol) was suspended in anhydrous THF (100 mL) and the solution was stirred thoroughly. **43** (2 g, 8.84 mmol) was dissolved in THF (50 mL) and was added in slowly, this was stirred for 3 h at RT then refluxed for 15 min. The remaining LAH was decomposed by water followed by NaOH (15%, 2 mL) to precipitate out the basic insolubilities, this was then filtered and the filtrate being washed with THF (3 x 40 mL). The organic solution was concentrated *in vacuo* and 2M HCl (20 mL) was added. This was washed with DCM (3 x 20 mL) and the aq layer then neutralised with aqueous NaOH. This was extracted with DCM (5 x 20 mL), dried with $MgSO_4$ and concentrated *in vacuo*. The amber oil was dissolved with IPA (10 mL), neutralised with conc. HCl (12 M) and upon addition of anhydrous ether crystals formed. The salt was recrystallized with IPA and filtered yielding a white powder (1.63 g, 93%); Mp. 180-182 ˚C; ^{1}H NMR (400 MHz, CD_3OD) δ 6.99 (d, *J*=9.16 Hz, 1 H), 6.86 (d, *J*=13.28 Hz, 1 H), 3.81 (s, 3 H), 3.83 (s, 3 H), 3.08 - 3.16 (m, 2 H), 2.89 - 2.97 (m, 2 H); ^{13}C NMR (101 MHz, CD_3OD) δ 153.3, 153.5 (d, J=244.41 Hz), 142.7, 121.3 (d, J=3.83 Hz), 118.3 (d, J=2.87 Hz), 101.8 (d, J=23.00 Hz), 57.8, 56.7, 40.9, 29.5.

Synthesis of 2-[2-(2,5-dimethoxyphenyl)ethyl]isoindoline-1,3-dione (45)

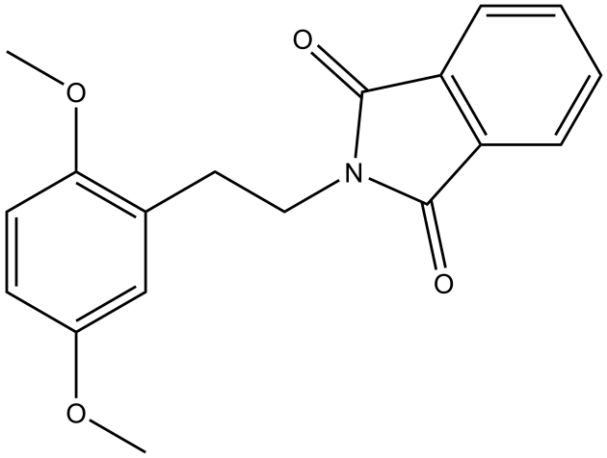

With a Dean-Stark set up, phthalic anhydride (11.105 g, 75 mmol) was suspended in an excess of toluene and heated to reflux until there was no more water evolution. 2,5-dimethoxyphenethylamine (10.87 g, 62.5 mmol) was added dropwise and left to reflux for 3 hr. This was concentrated *in vacuo* to a yellow oil that spontaneously crystallized to a yellow solid. The pthalimide was further recrystallized with IPA and filtered yielding a white powder (14.00 g, 72%); Mp. 110 ˚C; ^{1}H NMR (400 MHz, $CDCl_3$) δ 8.03 (dd, *J*=5.50, 3.21 Hz, 1 H), 7.92 (dd, *J*=5.72, 2.98 Hz, 1 H), 7.78 - 7.85 (m, 2 H), 7.65 - 7.73 (m, 2 H), 6.66 - 6.76 (m, 3 H), 3.95 (t, *J*=7.10 Hz, 2 H), 3.67 (s, 3 H), 3.71 (s, 3 H), 2.98 (t, *J*=7.10 Hz, 2 H); ^{13}C NMR (101 MHz, CD_3Cl) δ 168.2, 153.2, 152.0, 133.7, 132.1, 127.6, 123.0, 116.6, 112.2, 111.0, 55.7, 55.6, 37.8, 29.7; GC-MS 9.062 min, m/z 311

Synthesis of 2-[2-(4-iodo-2,5-dimethoxy-phenyl)ethyl]isoindoline-1,3-dione (46)

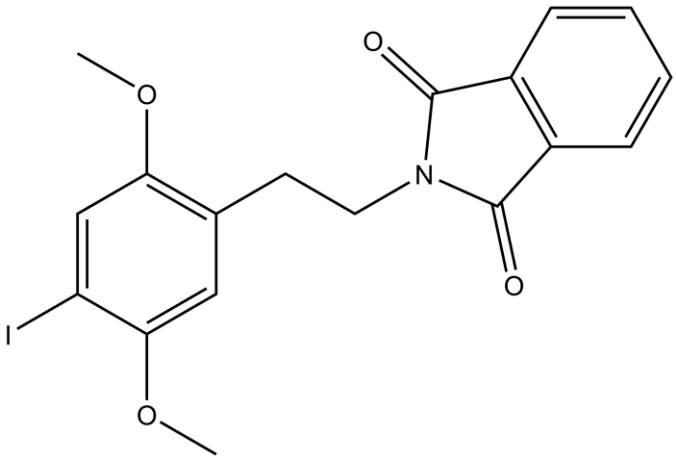

To a solution of **45** (12.76g, 41 mmol) in glacial acetic acid (120 mL), 1 M iodine monochloride in acetic acid (61.69 mL, 61.6 mmol) was added dropwise and stirred for 1 hr at 40 ˚C. The solution was poured into water (1500 mL) and extracted with DCM (4 x 75 mL) with the organic layers being collected. The organic solution washed with sodium dithionite (2 g) in water (150 mL), with the colour changing from red to yellow, and concentrated *in vacuo* to obtain a brown solid. The iodated pthalimide was recrystallized with IPA and filtered yielding a white powder (13.53 g, 76 %); Mp. 147-149˚C; ^{1}H NMR (400 MHz, $CDCl_3$) δ 7.78 - 7.86 (m, 2 H), 7.66 - 7.75 (m, 2 H), 6.65 - 6.77 (m, 3 H), 3.91 - 4.02 (m, 2 H), 3.66 - 3.75 (m, 6 H), 2.98 (t, *J*=7.10 Hz, 2 H).

Synthesis of 2-(4-iodo-2,5-dimethoxy-phenyl)ethanamine (47)

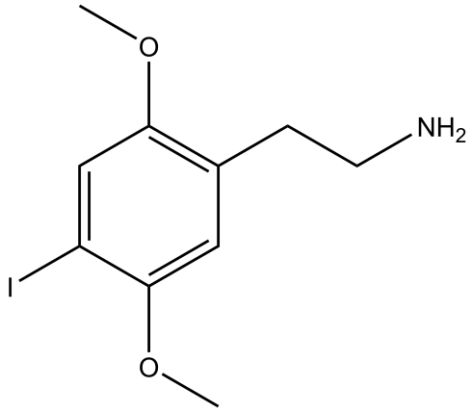

IPA was heated to reflux temperature with **46** (12.2 g, 28 mmol), treated with hydrazine hydrate (6 mL, 190 mmol) and refluxed o/n. The solution was left to cool, and the solids removed by filtration, washed with EtOH (2 x 20 mL) and the combined filtrate concentrated *in vacuo*. The oily residue treated with conc. HCl (12 M) produced white crystals. The salt was recrystallized in water (3 mL), filtered, washed with IPA and further washed with Et_2O to produce a pure white/pink powder and filtered yielding (0.85 g, 10%); Mp. 240-242°C; ^{1}H NMR (400 MHz, CD_3OD) δ 7.35 (s, 1 H), 6.86 (s, 1 H), 3.81 (s, 3 H), 3.82 (s, 3 H), 3.14 (t, *J*=7.33 Hz, 2 H), 2.94 (t, *J*=7.33 Hz, 2 H); ^{13}C NMR (101 MHz, CD_3OD) δ 154.46, 153.79, 127.33, 123.17, 115.07, 85.00, 57.64, 56.74, 40.71, 30.04; GC-MS 7.210 min, m/z 278.

Synthesis of 2-(2,5-dimethoxy-4-nitro-phenyl)ethanamine (48)

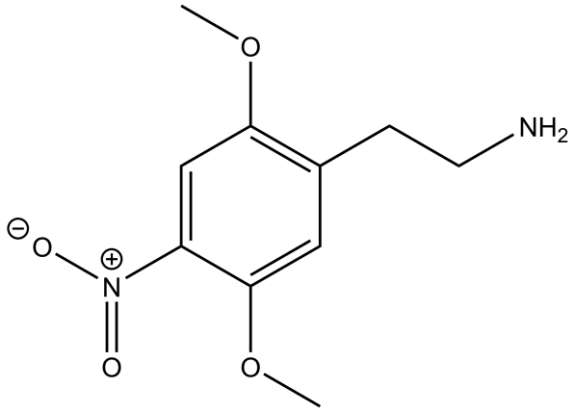

To cooled glacial acetic acid (60 mL), 2,5-dimethoxyphenethylamine (2.905 g, 15.95 mmol) and nitric acid (10 mL) was stirred with external cooling for 1 hr. The solution was poured into water (200 mL), followed by the addition of NaOH (6 M, 300 mL) and extracted with DCM (6 x 100 mL). The organic solution was washed with water (3 x 200 mL), brine (3 x 200 mL), dried with $NaSO_4$ and concentrated *in vacuo* to a deep red oil. The free base crystallised (2.3961 g, 66%) and no further purification required. ^{1}H NMR (400 MHz, $CDCl_3$) δ 7.4 (s, 1 H), 6.9 (s, 1 H), 3.9 (s, 3 H), 3.8 (s, 3 H), 3.0 (t, J=6.87 Hz, 2 H), 2.8 (t, J=6.87 Hz, 2 H), 1.5 (br. s., 3 H); ^{13}C NMR (101 MHz, $CDCl_3$) δ 150.9, 147.6, 136.6, 116.3, 107.5, 57.1, 56.0, 41.7, 35.1; GC-MS 7.253 min, M/Z 226.

General procedure A - for the synthesis of secondary amines

Adapting Hansen's synthesis of NBOMe's, Et_3N (1.0 eq.) was added to a suspension of phenethylamine hydrochloride (1.0 mmol) and aldehyde (1.1 mmol) in 10 mL EtOH. The reaction was stirred until the imine formation was complete according to TLC. $NaBH_4$ (2.0 mmol) was added slowly and the reaction stirred for a further 30 mins. The reaction mixture was concentrated *in vacuo* and the residue portioned between DCM and water (30 mL, 1:1). The organic layer was isolated and the aqueos layer extracted twice more with DCM (2 x 15 mL). The combined layers were dried over $MgSO_4$, filtered and concentrated *in vacuo* to an amber residue. The residue was purified by flash chromatography (DCM/MeOH/NH_3 98:2:0.04). The purified free base was then dissolved in EtOH (2 mL) followed by ethanolic HCl (1 M, 2 mL) and the solution then further diluted with EtOH until crystals formed. The crystals were collected by filtration and dried under reduced pressure.

2-(4-bromo-2,5-dimethoxy-phenyl)-*N*-[(2-methoxyphenyl)methyl]ethanamine (49)

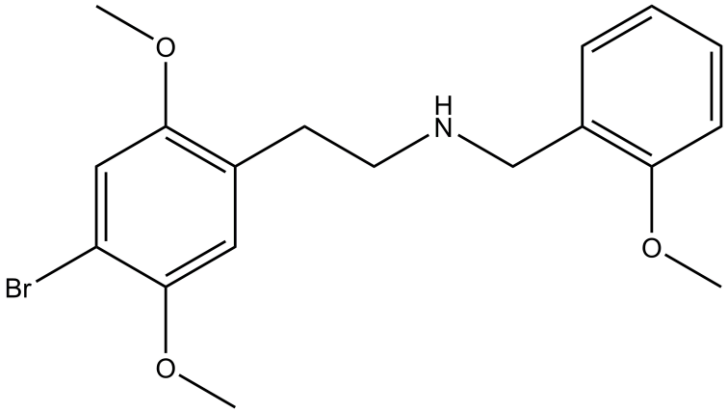

Using general procedure A, the target compound was obtained with **28** (0.26 g, 1 mmol) and 2-methoxybenzaldehyde (0.15 g, 1.1 mmol). The salt was filtered yielding a white powder (0.18 g, 47%); Mp. 178-180 ˚C; ^{1}H NMR (400 MHz, CD_3OD) δ 7.43 - 7.49 (m, 1 H), 7.39 (dd, *J*=7.56, 1.60 Hz, 1 H), 7.17 (s, 1 H), 7.09 (d, *J*=8.24 Hz, 1 H), 7.00 - 7.06 (m, 1 H), 6.98 (s, 1 H), 4.25 (s, 2 H), 3.89 (s, 3 H), 3.83 (s, 3 H), 3.79 (s, 3 H), 3.18 - 3.26 (m, 2 H), 2.99 - 3.07 (m, 2 H); ^{13}C NMR (101 MHz, CD_3OD) δ 157.5, 151.5, 149.4, 131.5, 130.7, 125.5, 120.3, 119.7, 115.9, 114.9, 111.1, 108.9, 56.6, 56.2, 55.6, 45.7, 44.7, 26.3. GC-MS 9.506 min, m/z 121. Data corresponds to the spectroscopic assignments reported by M. Hansen *et al.*[142]

2-(4-chloro-2,5-dimethoxy-phenyl)-*N*-[(2-methoxyphenyl)methyl]ethanamine (50)

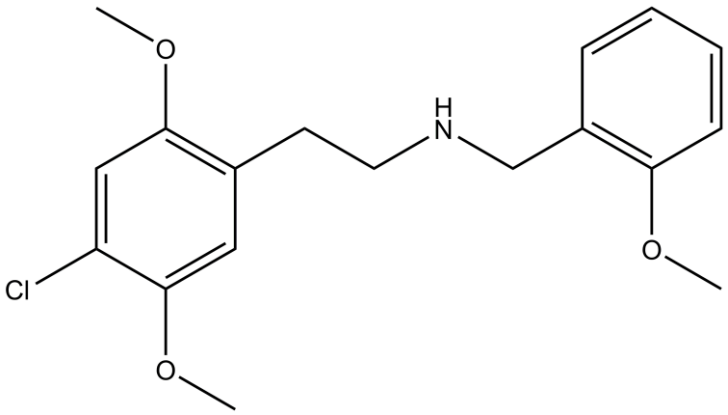

Using general procedure A, the target compound was obtained with **31** (0.22g g, 1 mmol) and 2-methoxybenzaldehyde (0.15 g, 1.1 mmol). The salt was filtered yielding a white powder (0.09 g, 26%); Mp. 180-181 ˚C; ^{1}H NMR (400 MHz, CD_3OD) δ 7.43 - 7.49 (m, 1 H), 7.37 - 7.41 (m, 1 H), 7.10 (d, *J*=8.24 Hz, 1 H), 7.00 – 7.05 (m, 1 H), 7.04 (s, 1 H) 6.98 (s, 1 H), 4.25 (s, 2 H), 3.89 (s, 3 H), 3.84 (s, 3 H), 3.79 (s, 3 H), 3.19 - 3.26 (m, 2 H), 3.00 - 3.06 (m, 2 H); ^{13}C NMR (101 MHz, CD_3OD) δ ppm 159.5, 153.1, 150.8, 132.9, 125.3, 122.9, 122.2, 120.4, 116.7, 114.5, 112.2, 57.5, 56.8, 56.4, 48.1, 48.1, 28.3, 24.4; GC-MS 9.225 min, m/z 321. Data corresponds to the spectroscopic assignments reported by M. Hansen *et al*[142]

2-(2,5-dimethoxy-4-methyl-phenyl)-*N*-[(2-methoxyphenyl)methyl]ethanamine (51)

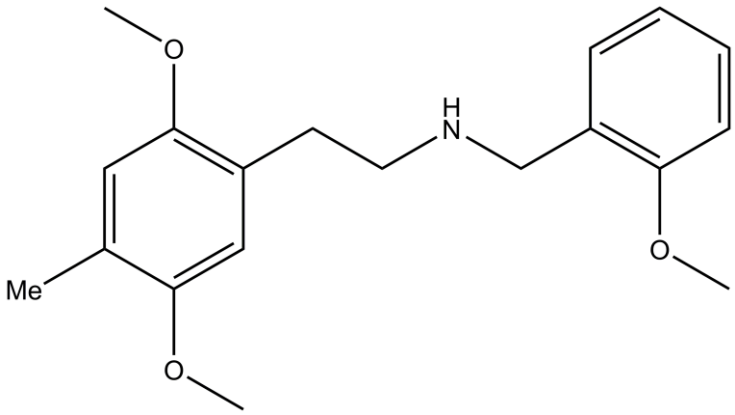

Using general procedure A, the target compound was obtained with **34** (0.2 g, 1 mmol) and 2-methoxybenzaldehyde (0.15 g, 1.1 mmol). The salt was filtered yielding a white powder (0.14 g, 44%); ^{1}H NMR (400 MHz, CD_3OD) δ 7.2 - 7.3 (m, 1 H), 7.2 (dd, J=7.33, 1.37 Hz, 1 H), 6.9 - 7.0 (m, 2 H), 6.7 (s, 1 H), 6.7 (s, 1 H), 3.8 (s, 2 H), 3.7 (s, 3 H), 3.7 (s, 3 H), 3.7 (s, 3 H), 2.8 (t, J=3.89 Hz, 4 H), 2.2 (s, 3 H); ^{13}C NMR (101 MHz, CD_3OD) δ 159.3, 153.1, 152.8, 131.8, 130.6, 126.7, 126.5, 125.9, 121.6, 115.0, 114.2, 111.6, 56.5, 56.5, 55.8, 49.2, 30.6, 16.4. Data corresponds to the spectroscopic assignments reported by Hansen *et al*[142]

2-(4-ethyl-2,5-dimethoxy-phenyl)-*N*-[(2-methoxyphenyl)methyl]ethanamine (52)

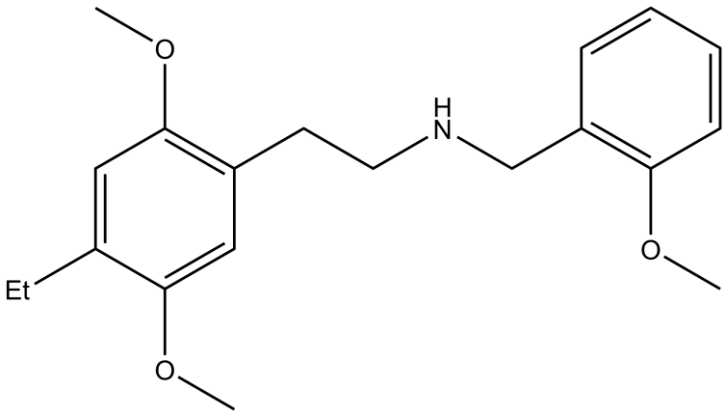

Using general procedure A, the target compound was obtained with **41** (0.42 g, 2 mmol) and 2-methoxybenzaldehyde (0.3 g, 2.2 mmol). The salt was filtered yielding a white powder (0.31 g, 47%); ^{1}H NMR (400 MHz, CD_3OD) δ 9.4 (br. s., 2 H), 7.4 (dd, J=7.56, 1.60 Hz, 1 H), 7.3 (td, J=7.90, 1.60 Hz, 1 H), 7.0 (t, J=7.33 Hz, 1 H), 6.8 (d, J=8.24 Hz, 1 H), 6.7 (s, 1 H), 6.7 (s, 1 H), 4.1 (t, J=5.27 Hz, 2 H), 3.7 (s, 3 H), 3.7 (s, 3 H), 3.6 (s, 3 H), 3.0 - 3.2 (m, 4 H), 2.5 - 2.6 (m, 2 H), 1.2 (t, J=7.33 Hz, 3 H); ^{13}C NMR (101 MHz, CD_3OD) δ 159.3, 153.0, 152.7, 133.0, 131.7, 130.6, 126.6, 126.1, 121.6, 114.5, 113.6, 111.6, 56.6, 56.5, 55.9, 49.8, 49.2, 30.6, 24.6, 15.2. Data corresponds to the spectroscopic assignments reported by Hansen *et al*[142]

2-(4-fluoro-2,5-dimethoxy-phenyl)-*N*-[(2-methoxyphenyl)methyl]ethanamine (53)

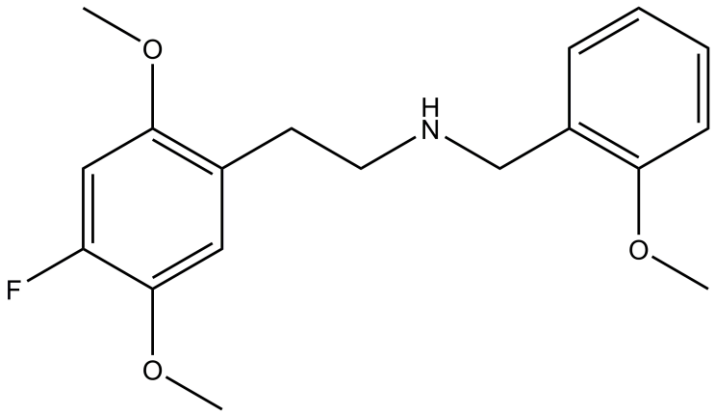

Using general procedure A, the target compound was obtained with **44** (0.21 g, 1.0 mmol) and 2-methoxybenzaldehyde (0.15 g, 1.1 mmol). The salt was filtered yielding a white powder (0.11 g, 64%); Mp. 141-144°C; ^{1}H NMR (400 MHz, CD_3OD) δ 7.46 (ddd, *J*=8.36, 7.44, 1.60 Hz, 1 H), 7.38 (dd, *J*=7.33, 1.83 Hz, 1 H), 7.11 (d, *J*=8.24 Hz, 1 H), 6.97 - 7.07 (m, 2 H), 6.87 (d, *J*=12.82 Hz, 1 H), 4.24 (s, 2 H), 3.90 (s, 3 H), 3.83 (s, 3 H), 3.78 (s, 3 H), 3.17 - 3.24 (m, 2 H), 2.97 - 3.03 (m, 2 H); ^{13}C NMR (101 MHz, CD_3OD) δ 158.0, 151.7, 141.3, 131.4, 120.7, 119.6, 118.9, 116.8, 110.7, 100.6, 100.3, 56.4, 55.3, 54.9, 46.7, 46.6, 26.5, 22.9; GC-MS 8.692 min, m/z 121. Data corresponds to the spectroscopic assignments reported by Hansen *et al*[142]

2-(4-iodo-2,5-dimethoxy-phenyl)-*N*-[(2-methoxyphenyl)methyl]ethanamine (54)

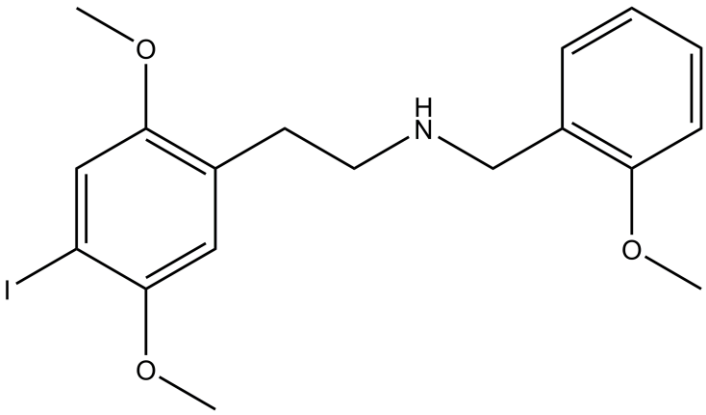

Using general procedure A, the target compound was obtained with **47** (0.31 g, 1 mmol) and 2-methoxybenzaldehyde (0.15 g, 1.1 mmol). The salt was filtered yielding a white powder (0.26 g, 61%); Mp. 161-163 ˚C; ^{1}H NMR (400 MHz, CD_3OD) δ 7.43 - 7.49 (m, 1 H), 7.39 (dd, *J*=7.56, 1.60 Hz, 1 H), 7.34 (s, 1 H), 7.09 (d, *J*=8.24 Hz, 1 H), 7.00 - 7.05 (m, 1 H), 6.87 (s, 1 H), 4.24 (s, 2 H), 3.89 (s, 3 H), 3.82 (s, 3 H), 3.78 (s, 3 H), 3.19 - 3.26 (m, 2 H), 2.99 - 3.05 (m, 2 H); ^{13}C NMR (101 MHz, CD_3OD) δ 157.7, 152.5, 151.9, 132.0, 131.1, 125.9, 121.5, 120.9, 118.3, 114.0, 110.4, 83.8, 57.1, 55.8, 55.5, 46.4, 44.9, 28.0; GC-MS 9.851 min, m/z 121. Data corresponds to the spectroscopic assignments reported by Hansen *et al*[142]

2-(2,5-dimethoxy-4-nitro-phenyl)-*N*-[(2-methoxyphenyl)methyl]ethanamine (55)

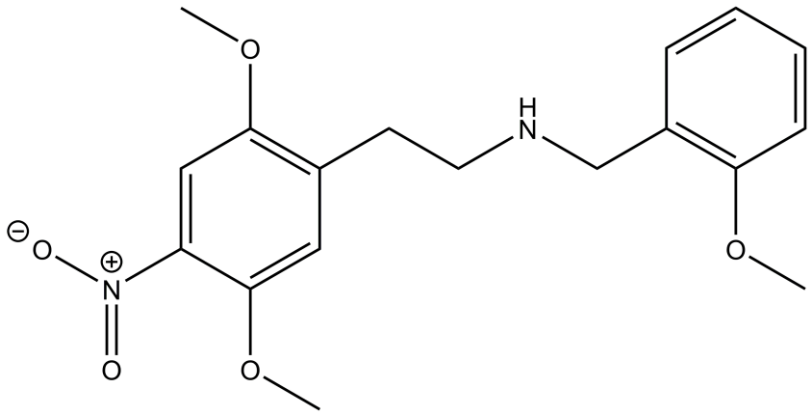

Using general procedure A, the target compound was obtained with **48** (0.47 g, 2 mmol) and 2-methoxybenzaldehyde (0.31 g, 2.2 mmol). The salt was filtered yielding a white powder (0.39 g, 74%); ^{1}H NMR (400 MHz, CD_3OD) δ 7.4 (s, 1 H), 7.2 (t, J=8.01 Hz, 1 H), 7.2 (d, J=7.33 Hz, 1 H), 7.0 (s, 1 H), 6.9 - 6.9 (m, 2 H), 3.9 (s, 3 H), 3.8 (s, 3 H), 3.7 (s, 5 H), 2.8 - 2.9 (m, 2 H), 2.8 - 2.8 (m, 2 H); ^{13}C NMR (101 MHz, CD_3OD) δ 159.5, 152.3, 148.5, 140.1, 133.1, 132.9, 122.2, 120.4, 118.2, 112.2, 108.7, 57.9, 56.9, 56.3, 48.1, 47.6, 28.5.

2-(4-bromo-2,5-dimethoxy-phenyl)-*N*-(3-pyridylmethyl)ethanamine (56)

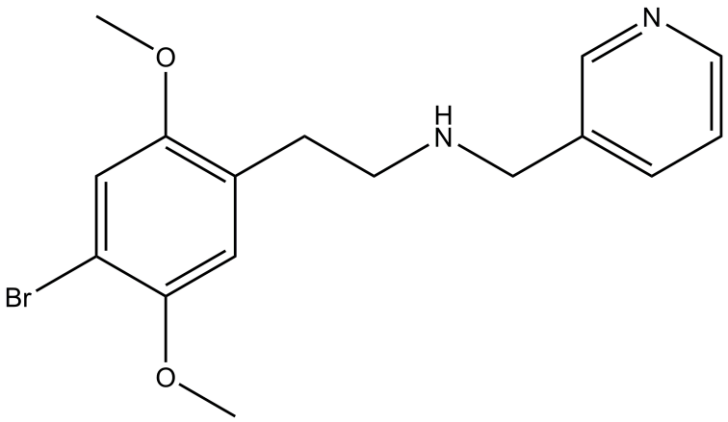

Using general procedure A, the target compound was obtained with **28** (0.26 g, 1 mmol) and nicotinaldehyde (0.10 mL, 1.1 mmol). The salt was filtered yielding a white powder (0.01 g, 3%); ^{1}H NMR (400 MHz, CD_3OD) δ 9.2 (s, 1 H), 9.0 (d, J=5.50 Hz, 1 H), 8.9 (d, J=8.24 Hz, 1 H), 8.2 (dd, J=8.24, 5.95 Hz, 1 H), 7.2 (s, 1 H), 7.1 (s, 1 H), 4.6 (s, 2 H), 3.8 (s, 3 H), 3.8 (s, 3 H), 3.3 - 3.4 (m, 2 H), 3.1 - 3.1 (m, 2 H); ^{13}C NMR (101 MHz, CD_3OD) δ 153.5, 151.6, 150.4, 149.0, 138.7, 137.1, 129.6, 125.4, 117.0, 116.2, 110.3, 62.6, 57.4, 56.7, 51.3, 49.8, 31.5

2-(4-chloro-2,5-dimethoxy-phenyl)-*N*-(3-pyridylmethyl)ethanamine (57)

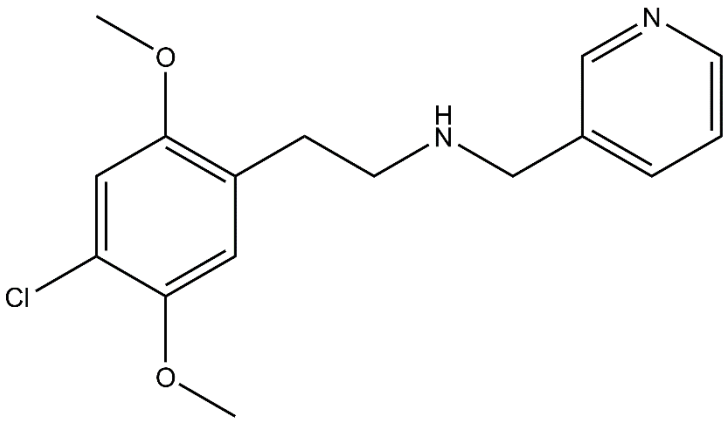

Using general procedure A, the target compound was obtained with **31** (0.32 g, 2 mmol) and nicotinaldehyde (0.2 mL, 2.2 mmol). The salt was filtered yielding a white powder (0.2024 g, 44%); ^{1}H NMR (400 MHz, CD_3OD) δ 9.2 (s, 1 H), 9.0 (d, J=5.95 Hz, 1 H), 8.8 - 8.9 (m, 2 H), 8.2 (dd, J=8.01, 5.72 Hz, 1 H), 7.1 (s, 1 H), 7.0 (s, 1 H), 4.6 (s, 2 H), 3.8 (s, 3 H), 3.8 (s, 3 H), 3.3 - 3.4 (m, 2 H), 3.1 - 3.1 (m, 2 H); ^{13}C NMR (101 MHz, CD_3OD) δ 153.02, 150.33, 145.86, 145.49, 144.81, 128.43, 128.30, 125.02, 122.52, 116.60, 114.22, 61.06, 57.47, 56.76, 48.77, 48.59, 28.36; GC-MS 9.167, m/z 121.

2-(2,5-dimethoxy-4-methyl-phenyl)-*N*-(3-pyridylmethyl)ethanamine (58)

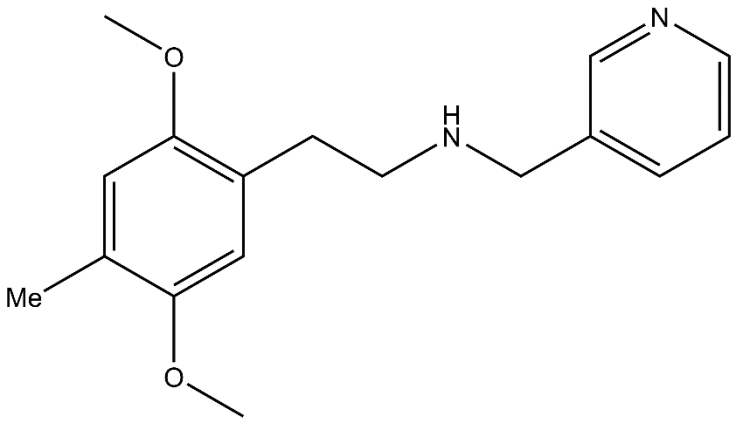

Using general procedure A, the target compound was obtained with **34** (0.2 g, 1 mmol) and nicotinaldehyde (0.1 mL, 1.1 mmol). The salt was filtered yielding a white powder (0.2 g, 69%); ^{1}H NMR (400 MHz, CD_3OD) δ 9.1 (br. s., 1 H), 9.0 (d, *J*=4.58 Hz, 1 H), 8.8 (d, *J*=7.78 Hz, 1 H), 8.2 (t, *J*=6.64 Hz, 1 H), 6.8 (s, 1 H), 6.8 (s, 1 H), 4.5 (s, 2 H), 3.8 (s, 3 H), 3.8 (s, 3 H), 3.4 (t, *J*=7.56 Hz, 2 H), 3.1 (t, *J*=7.56 Hz, 2 H), 2.2 (s, 3 H); ^{13}C NMR (101 MHz, CD_3OD) δ 153.4, 152.7, 149.5, 145.1, 144.3, 133.4, 129.0, 127.9, 123.0, 115.1, 114.4, 56.7, 56.6, 49.5, 48.6, 28.8, 16.5

2-(4-ethyl-2,5-dimethoxy-phenyl)-*N*-(3-pyridylmethyl)ethanamine (59)

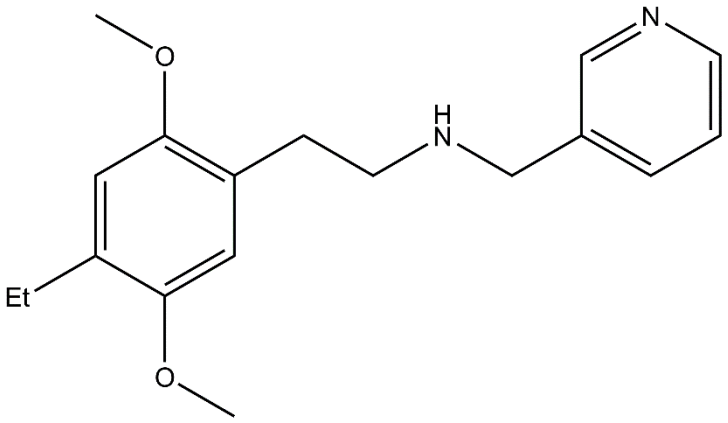

Using general procedure A, the target compound was obtained with **41** (0.31 g, 1.5 mmol) and nicotinaldehyde (0.15 mL, 1.65 mmol). The salt was filtered yielding a white powder (0.22 g, 49%); ^{1}H NMR (400 MHz, CD_3OD) δ 9.1 (s, 1 H), 9.0 (d, *J*=5.50 Hz, 1 H), 8.9 (d, *J*=8.24 Hz, 1 H), 8.2 (dd, *J*=8.24, 5.95 Hz, 1 H), 6.9 (s, 1 H), 6.8 (s, 1 H), 4.6 (s, 2 H), 3.8 (s, 3 H), 3.8 (s, 3 H), 3.4 (t, *J*=7.56 Hz, 2 H), 3.0 - 3.1 (m, 2 H), 2.6 (q, *J*=7.33 Hz, 2 H), 1.2 (t, *J*=7.56 Hz, 3 H); ^{13}C NMR (101 MHz, CD_3OD) δ 152.9, 149.6, 145.0, 144.2, 134.2, 133.5, 129.0, 123.1, 114.7, 113.7, 56.7, 56.6, 49.5, 28.8, 24.6, 15.1

2-(4-fluoro-2,5-dimethoxy-phenyl)-*N*-(3-pyridylmethyl)ethanamine (60)

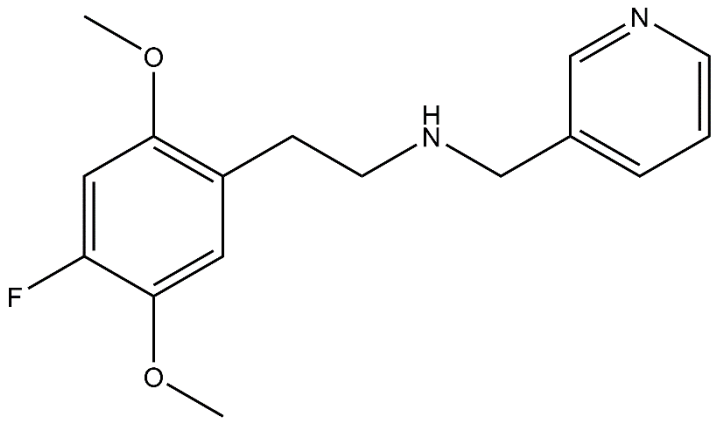

Using general procedure A, the target compound was obtained with **44** (0.4 g, 2 mmol) and nicotinaldehyde (0.2 mL, 2.2 mmol). The salt was filtered yielding a white powder (0.1597 g, 28%); ^{1}H NMR (400 MHz, CD_3OD) δ 9.2 (s, 1 H), 9.0 (d, *J*=5.50 Hz, 1 H), 8.9 (d, *J*=8.24 Hz, 1 H), 8.2 (dd, *J*=8.01, 5.72 Hz, 1 H), 7.1 (d, *J*=9.16 Hz, 1 H), 6.9 (d, *J*=12.82 Hz, 1 H), 4.6 (s, 2 H), 3.8 (s, 3 H), 3.8 (s, 3 H), 3.3 - 3.4 (m, 2 H), 3.0 - 3.1 (m, 2 H); ^{13}C NMR (101 MHz, CD_3OD) δ 153.3 (d, *J*=8.63 Hz), 153.4 (d, *J*=244.41 Hz), 149.9, 144.9, 144.0, 142.7, 142.6, 142.7 (d, *J*=10.54 Hz), 133.5, 129.0, 120.8 (d, *J*=3.83 Hz), 118.3, 118.3, 118.3 (d, *J*=2.88 Hz), 101.9 (d, *J*=23.00 Hz), 61.2, 57.9, 56.8, 48.5, 28.3; GC-MS 8.427, m/z 121.

2-(4-iodo-2,5-dimethoxy-phenyl)-*N*-(3-pyridylmethyl)ethanamine (61)

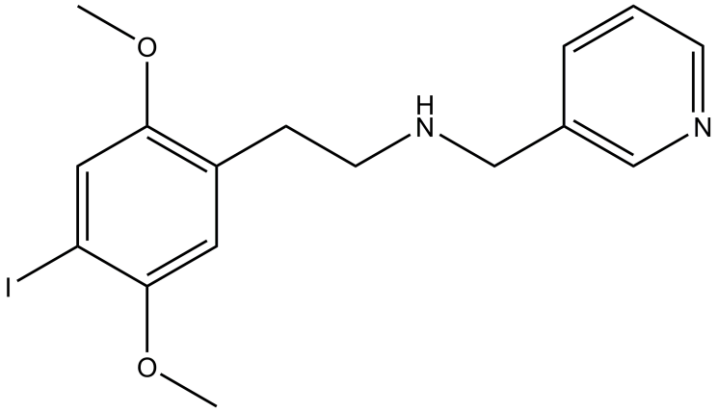

Using general procedure A, the target compound was obtained with **47** (0.64 g, 1.5 mmol) and nicotinaldehyde (0.15 mL, 1.65 mmol). The salt was filtered yielding a white powder (0.48 g, 81%); ^{1}H NMR (400 MHz, CD_3OD) δ 9.0 (s, 1 H), 8.8 (d, J=4.58 Hz, 1 H), 8.5 (d, J=8.24 Hz, 1 H), 7.9 (dd, J=8.24, 5.50 Hz, 1 H), 7.3 (s, 1 H), 6.9 (s, 1 H), 4.5 (s, 2 H), 3.8 (s, 3 H), 3.8 (s, 3 H), 3.4 (t, J=8.24 Hz, 2 H), 3.1 (t, J=7.33 Hz, 2 H); ^{13}C NMR (101 MHz, CD_3OD) δ 154.4, 153.7, 147.7, 147.1, 145.8, 131.8, 127.7, 126.9, 123.2, 115.1, 85.1, 57.7, 56.8, 49.0, 28.8; GC-MS 9.660 min, m/z 121;p Mp. 208-211 ˚C;

2-(2,5-dimethoxy-4-nitro-phenyl)-*N*-(3-pyridylmethyl)ethanamine (62)

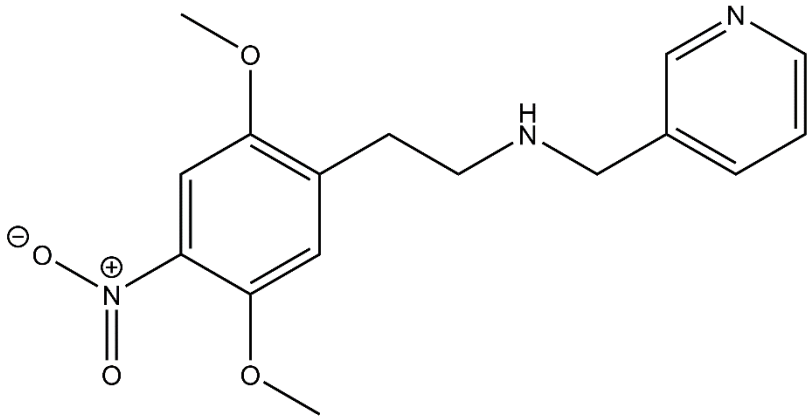

Using general procedure A, the target compound was obtained with **48** (0.45 g, 2 mmol) and nicotinaldehyde (0.2 mL, 2.2 mmol). The salt was filtered yielding a white powder (0.29 g, 46%); ^{1}H NMR (400 MHz, CD_3OD) δ 8.5 (d, *J*=2.29 Hz, 1 H), 8.4 (dd, *J*=5.04, 1.37 Hz, 1 H), 7.8 (dt, *J*=8.13, 1.89 Hz, 1 H), 7.4 - 7.5 (m, 2 H), 7.1 (s, 1 H), 4.7 (s, 1 H), 3.9 (s, 3 H), 3.8 (s, 2 H), 3.8 (s, 3 H), 2.9 (ddd, *J*=8.24, 6.41, 1.83 Hz, 2 H), 2.8 (ddd, *J*=8.36, 6.53, 2.06 Hz, 2 H); ^{13}C NMR (101 MHz, CD_3OD) δ 152.3, 151.2, 150.8, 148.5, 141.0, 140.1, 132.9, 129.7, 126.1, 118.2, 108.7, 61.4, 57.8, 56.9, 48.1, 28.8

2-(4-bromo-2,5-dimethoxy-phenyl)-*N*-[(5-fluoro-3-pyridyl)methyl]ethanamine (25B-NPF) (63)

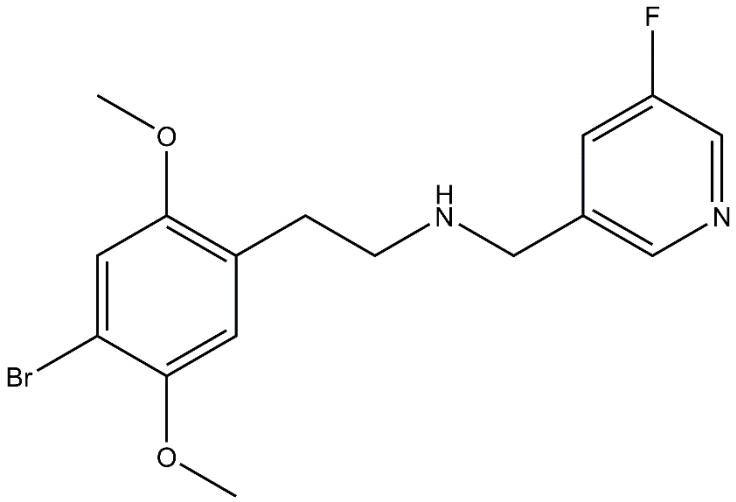

Using general procedure A, the target compound was obtained with **28** (0.52 g, 2 mmol) and 5-flouronicotinaldehyde (0.28 g, 2.2 mmol). The salt was filtered yielding a white powder (0.3022 g, 41%); ^{1}H NMR (400 MHz, CD_3OD) δ 8.9 - 9.0 (m, 3 H), 8.8 (s, 1 H), 8.5 - 8.6 (m, 2 H), 7.2 (s, 1 H), 7.0 (s, 1 H), 4.9 (s, 1 H), 4.5 (s, 2 H), 3.8 (s, 3 H), 3.8 (s, 3 H), 3.3 - 3.4 (m, 2 H), 3.1 - 3.1 (m, 2 H); ^{13}C NMR (101 MHz, CD_3OD) δ 162.0 (d, J=253.99 Hz), 153.4, 151.8, 144.3 (d, J=3.83 Hz), 138.0, 136.5 (d, J=29.71 Hz), 133.1 (d, J=19.17 Hz), 125.8, 117.3, 116.4, 61.0, 57.5, 56.8, 48.8, 28.7

2-(4-chloro-2,5-dimethoxy-phenyl)-*N*-[(5-fluoro-3-pyridyl)methyl]ethanamine (64)

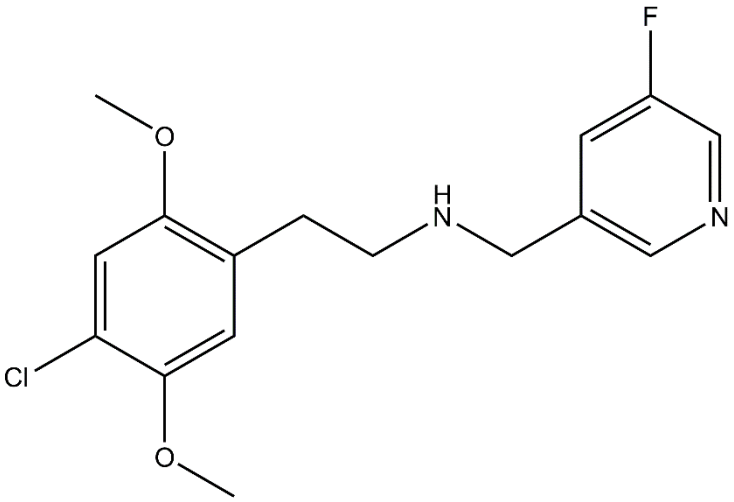

Using general procedure A, the target compound was obtained with **31** (0.33 g, 1.5 mmol) and 5-flouronicotinaldehyde (0.2127 g, 1.65 mmol). The salt was filtered yielding a white powder (0.1744 g, 36%); ^{1}H NMR (400 MHz, CD_3OD) δ 9.0 (s, 1 H), 8.9 (s, 1 H), 8.5 (d, J=8.24 Hz, 1 H), 7.1 (s, 1 H), 7.0 (s, 1 H), 4.5 (s, 2 H), 3.8 (s, 3 H), 3.8 (s, 3 H), 3.3 - 3.4 (m, 2 H), 3.0 - 3.1 (m, 2 H); ^{13}C NMR (101 MHz, CD_3OD) δ 161.4 (d, J=254.95 Hz), 153.3, 150.5, 146.7 (d, J=3.83 Hz), 137.2 (d, J=24.92 Hz), 128.9, 124.8 (d, J=18.21 Hz), 123.2 (d, J=18.21 Hz), 121.6, 116.5, 114.1, 61.8, 57.4, 56.6, 50.7, 31.5; GC-MS , m/z 324

2-(2,5-dimethoxy-4-methyl-phenyl)-*N*-[(5-fluoro-3-pyridyl)methyl]ethanamine (65)

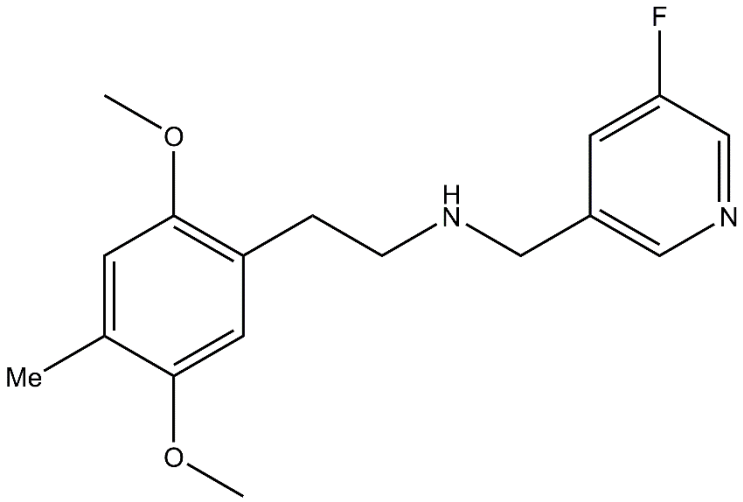

Using general procedure A, the target compound was obtained with **34** (0.2 g, 1 mmol) and 5-flouronicotinaldehyde (0.14 g, 1.1 mmol). The salt was filtered yielding a white powder (0.19 g, 61 %); ^{1}H NMR (400 MHz, CD_3OD) δ 9.0 (br. s., 1 H), 8.9 (s, 1 H), 8.5 (d, *J*=8.70 Hz, 1 H), 6.8 (s, 1 H), 6.8 (s, 1 H), 4.5 (s, 2 H), 3.8 (s, 3 H), 3.8 (s, 3 H), 3.3 (t, *J*=1.00 Hz, 2 H), 3.0 - 3.1 (m, 2 H), 2.2 (s, 3 H); ^{13}C NMR (101 MHz, CD_3OD) δ 161.0 (d, *J*=254.95 Hz), 153.1, 152.7, 146.8 (d, *J*=3.83 Hz), 138.7, 137.5 (d, *J*=24.92 Hz), 126.6, 126.5, 125.0 (d, *J*=18.21 Hz), 115.0, 114.2, 56.5, 56.5, 50.5, 50.0, 31.3, 16.4

2-(4-ethyl-2,5-dimethoxy-phenyl)-*N*-[(5-fluoro-3-pyridyl)methyl]ethanamine (66)

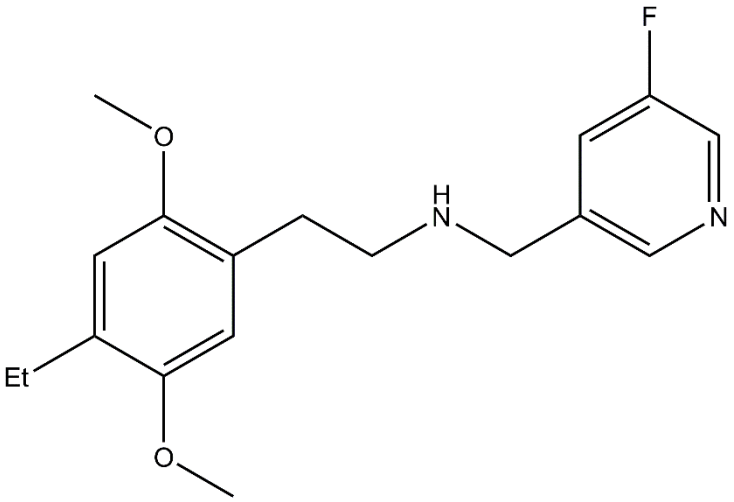

Using general procedure A, the target compound was obtained with **41** (0.31, 1.5 mmol) and 5-flouronicotinaldehyde (0.21 g, 1.65 mmol). The salt was filtered yielding a white powder (0.12 g, 25 %); ^{1}H NMR (400 MHz, CD_3OD) δ 9.0 (s, 1 H), 8.9 (s, 1 H), 8.5 (d, *J*=8.24 Hz, 1 H), 6.9 (s, 1 H), 6.8 (s, 1 H), 4.5 (s, 2 H), 3.8 (s, 3 H), 3.8 (s, 3 H), 3.3 - 3.4 (m, 2 H), 3.0 - 3.1 (m, 2 H), 2.6 (q, *J*=7.48 Hz, 2 H), 1.2 (t, *J*=7.56 Hz, 3 H); ^{13}C NMR (101 MHz, CD_3OD) δ 161.4 (d, *J*=256.87 Hz), 152.9, 144.5 (d, *J*=3.83 Hz), 136.7 (d, *J*=29.71 Hz), 134.2, 133.7, 133.6, 132.6 (d, *J*=19.17 Hz), 123.1, 114.7, 113.7, 56.7, 56.5, 48.5, 28.7, 24.6, 15.1

2-(4-fluoro-2,5-dimethoxy-phenyl)-*N*-[(5-fluoro-3-pyridyl)methyl]ethanamine (67)

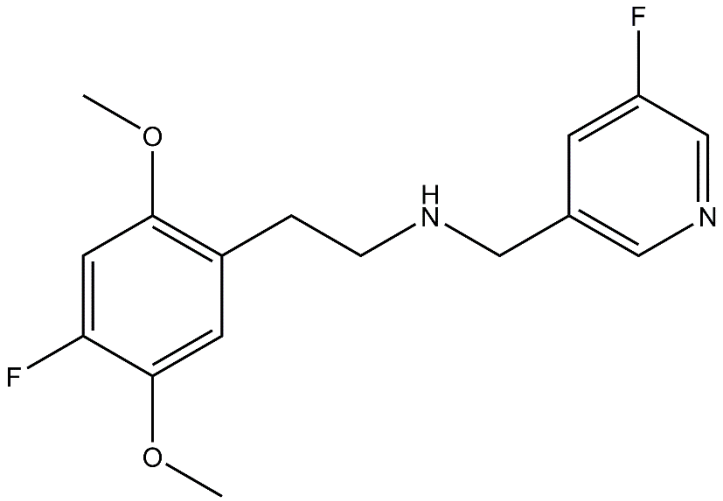

Using general procedure A, the target compound was obtained with **44** (0.28 g, 2 mmol) and 5-flouronicotinaldehyde (0.28 g, 2.2 mmol). The salt was filtered yielding a white powder (0.16 g, 27%); ^{1}H NMR (400 MHz, CD_3OD) δ 9.0 (br. s, 1 H), 9.0 (s, 1 H), 8.6 (d, *J*=8.24 Hz, 1 H), 7.1 (d, *J*=9.62 Hz, 1 H), 6.9 (d, *J*=12.82 Hz, 1 H), 4.5 (s, 2 H), 3.8 - 3.8 (m, 3 H), 3.8 (s, 3 H), 3.3 - 3.4 (m, 2 H), 3.0 - 3.1 (m, 2 H); ^{13}C NMR (101 MHz, CD_3OD) δ 161.5 (d, *J*=253.04 Hz), 153.2 (d, *J*=8.63 Hz), 153.4 (d, *J*=245.37 Hz), 143.9 (d, *J*=3.83 Hz), 142.7 (d, *J*=10.54 Hz), 136.0 (d, *J*=33.55 Hz), 134.0 (d, *J*=19.17 Hz), 132.8 (d, *J*=19.17 Hz), 120.8 (d, *J*=3.83 Hz), 118.3 (d, *J*=2.88 Hz), 102.0 (d, *J*=23.00 Hz), 57.8, 56.8, 48.4, 28.3

2-(4-iodo-2,5-dimethoxy-phenyl)-*N*-[(5-fluoro-3-pyridyl)methyl]ethanamine (68)

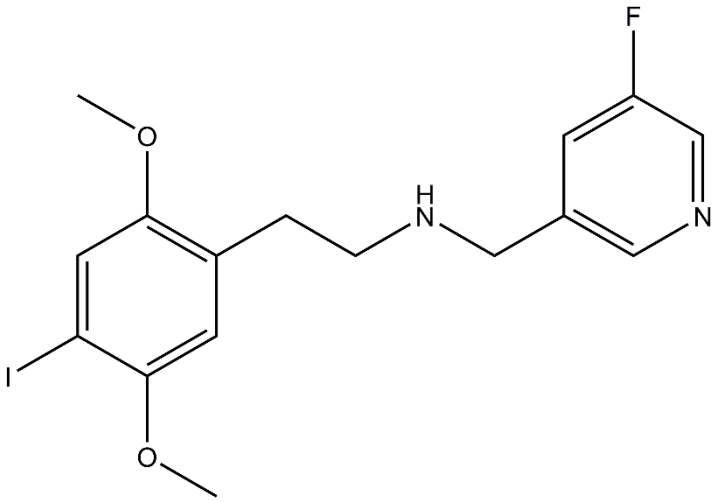

Using general procedure A, the target compound was obtained with **47** (0.80 g, 2 mmol) and 5-flouronicotinaldehyde (0.28 g, 2.2 mmol). The salt was filtered yielding a white powder (0.3841 g, 46%); ^{1}H NMR (400 MHz, CD_3OD) δ 8.9 (s, 1 H), 8.8 (d, J=6.87 Hz, 1 H), 7.8 (d, J=6.87 Hz, 1 H), 7.3 (s, 1 H), 7.0 (s, 1 H), 4.4 (s, 2 H), 4.3 (s, 3 H), 3.8 (s, 6 H), 3.4 (t, J=7.56 Hz, 2 H), 3.1 (t, J=6.41 Hz, 2 H); ^{13}C NMR (101 MHz, CD_3OD) δ 161.4 (d, J=261.66 Hz), 154.5, 153.7, 145.0 (d, J=3.83 Hz), 137.2 (d, J=29.71 Hz), 133.2, 131.9 (d, J=19.17 Hz), 126.8, 123.2, 115.1, 85.1, 57.7, 56.8, 48.8, 48.6, 28.9

2-(2,5-dimethoxy-4-nitro-phenyl)-*N*-[(5-fluoro-3-pyridyl)methyl]ethanamine (69)

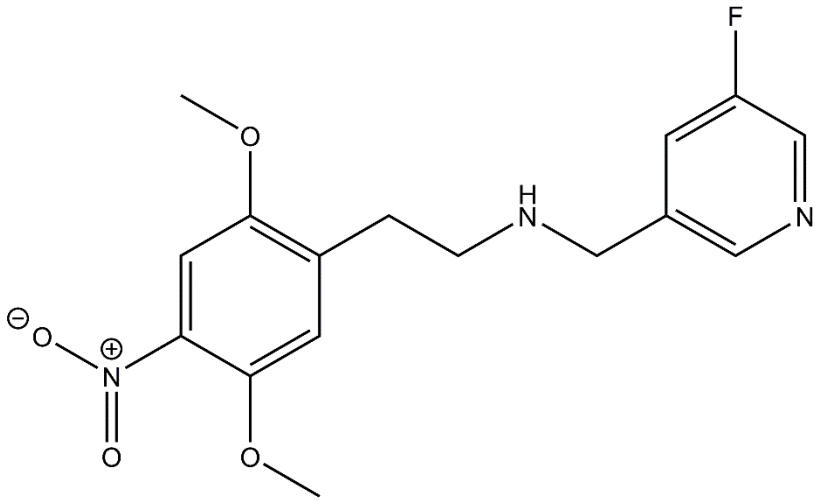

Using general procedure A, the target compound was obtained with **48** (0.45 g, 2 mmol) and 5-flouronicotinaldehyde (0.28 g, 2.2 mmol). The salt was filtered yielding a white powder (0.41 g, 61%); ^{1}H NMR (400 MHz, CD_3OD) δ 8.9 (br. s, 1 H), 8.8 (s, 1 H), 8.3 (d, *J*=8.24 Hz, 1 H), 7.5 (s, 1 H), 7.3 (s, 1 H), 4.5 (s, 2 H), 3.9 (s, 3 H), 3.9 (s, 3 H), 3.4 (t, *J*=7.56 Hz, 2 H), 3.1 - 3.2 (m, 2 H); ^{13}C NMR (101 MHz, CD_3OD) δ 161.4 (d, *J*=255.91 Hz), 152.4, 148.6, 146.7 (d, *J*=3.83 Hz), 145.0, 139.1, 137.4 (d, *J*=23.96 Hz), 137.1, 124.9 (d, *J*=18.21 Hz), 117.8, 108.4, 57.7, 56.7, 50.6, 40.5, 31.7**.**

2-(4-bromo-2,5-dimethoxy-phenyl)-*N*-[(4-methoxy-3-pyridyl)methyl]ethanamine (70)

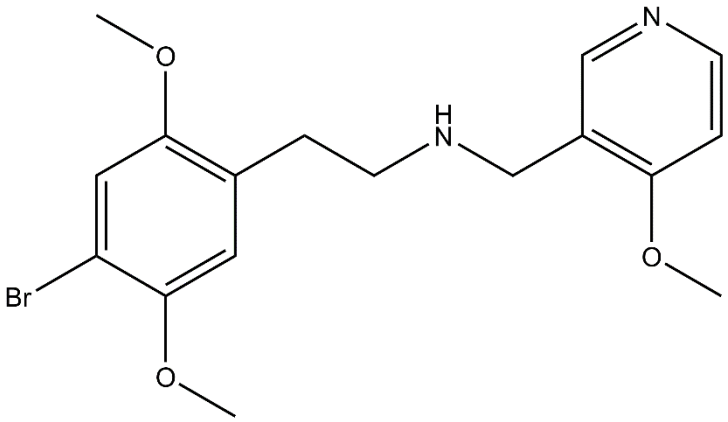

Using general procedure A, the target compound was obtained with **28** (0.52 g, 2 mmol) and 4-methoxypyridine-3-carbaldehyde (0.30 g, 2.2 mmol). The salt was filtered yielding a white powder (0.5067 g, 67%); ^{1}H NMR (400 MHz, CD_3OD) δ 8.9 (s, 1 H), 8.9 (d, J=6.87 Hz, 1 H), 7.8 (d, J=7.33 Hz, 1 H), 7.2 (s, 1 H), 7.0 (s, 1 H), 4.4 (s, 2 H), 4.3 (s, 3 H), 3.8 (s, 3 H), 3.8 (s, 3 H), 3.3 - 3.4 (m, 2 H), 3.0 - 3.2 (m, 2 H); ^{13}C NMR (101 MHz, CD_3OD) δ 172.7, 153.4, 151.8, 146.5, 144.8, 125.9, 121.2, 117.3, 116.5, 111.6, 111.4, 59.6, 57.6, 56.9, 49.0, 44.2, 28.5, 24.4

2-(4-chloro-2,5-dimethoxy-phenyl)-*N*-[(4-methoxy-3-pyridyl)methyl]ethanamine (71)

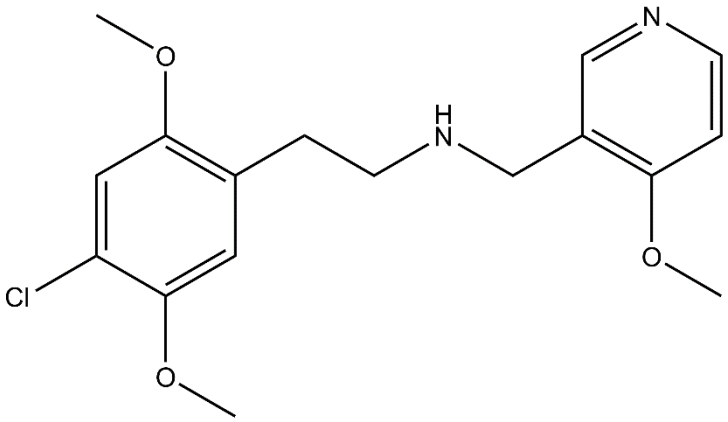

Using general procedure A, the target compound was obtained with **31** (0.32 g, 1.5 mmol) and 4-methoxypyridine-3-carbaldehyde (0.23 g, 1.65 mmol). The salt was filtered yielding a white powder (0.1697 g, 34%); ^{1}H NMR (400 MHz, CD_3OD) δ 8.9 (s, 1 H), 8.9 (dd, J=6.87, 1.37 Hz, 1 H), 7.8 (d, J=7.33 Hz, 1 H), 7.1 (s, 1 H), 7.1 (s, 1 H), 4.4 (s, 2 H), 4.3 (s, 3 H), 3.9 (s, 3 H), 3.8 (s, 3 H), 3.4 (dd, J=8.93, 6.64 Hz, 2 H), 3.1 - 3.1 (m, 2 H); ^{13}C NMR (101 MHz, CD_3OD) δ 172.6, 153.2, 150.8, 146.6, 144.9, 125.1, 121.2, 116.7, 114.5, 111.4, 59.6, 57.5, 56.8, 44.2, 28.4

2-(2,5-dimethoxy-4-methyl-phenyl)-*N*-[(4-methoxy-3-pyridyl)methyl]ethanamine (72)

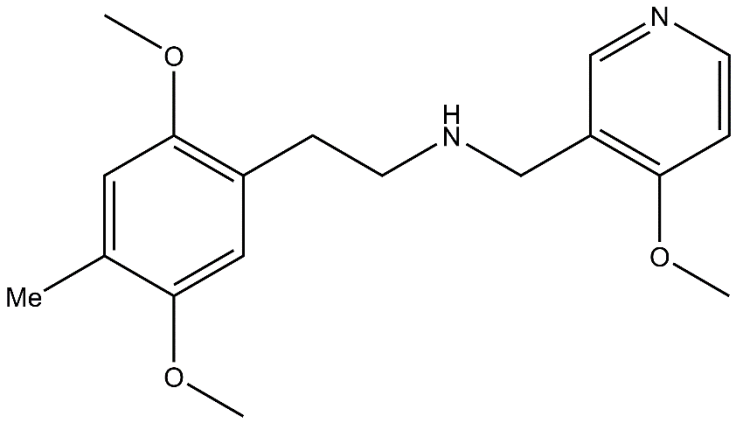

Using general procedure A, the target compound was obtained with **34** (0.2 g, 1.1 mmol) and 4-methoxypyridine-3-carbaldehyde (0.15 g, 1.1 mmol). The salt was filtered yielding a white powder (0.17 g, 53%); ^{1}H NMR (400 MHz, CD_3OD) δ 8.9 (s, 1 H), 8.9 (dd, *J*=1.00 Hz, 1 H), 7.8 (d, *J*=6.87 Hz, 1 H), 6.8 (s, 1 H), 6.8 (s, 1 H), 4.4 (s, 2 H), 4.3 (s, 3 H), 3.8 (s, 3 H), 3.8 (s, 3 H), 3.3 - 3.4 (m, 2 H), 3.0 - 3.1 (m, 2 H), 2.2 (s, 3 H); ^{13}C NMR (101 MHz, CD_3OD) δ 166.3, 153.1, 152.8, 151.9, 151.1, 126.7, 126.0, 115.0, 114.2, 108.1, 56.5, 56.5, 56.4, 56.3, 49.5, 46.7, 30.8, 16.4

2-(4-ethyl-2,5-dimethoxy-phenyl)-*N*-[(4-methoxy-3-pyridyl)methyl]ethanamine (73)

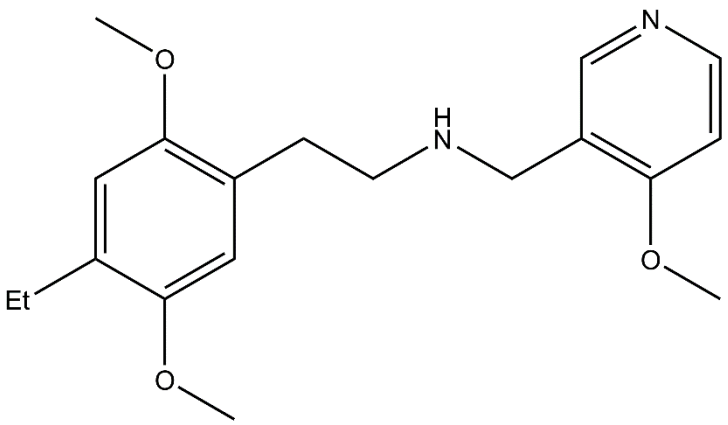

Using general procedure A, the target compound was obtained with **41** (0.31 g, 1.5 mmol) and 4-methoxypyridine-3-carbaldehyde (0.23 g, 1.65 mmol). The salt was filtered yielding a white powder (0.17 g, 34 %); ^{1}H NMR (400 MHz, CD_3OD) δ 8.9 (s, 1 H), 8.9 (d, *J*=6.87 Hz, 1 H), 7.8 (d, *J*=6.87 Hz, 1 H), 6.9 (s, 1 H), 6.8 (s, 1 H), 4.4 (s, 2 H), 4.3 (s, 3 H), 3.8 (s, 3 H), 3.8 (s, 3 H), 3.3 (t, *J*=1.00 Hz, 2 H), 3.1 (t, *J*=7.79 Hz, 2 H), 2.6 (q, *J*=7.63 Hz, 2 H), 1.2 (t, *J*=7.56 Hz, 3 H); ^{13}C NMR (101 MHz, CD_3OD) δ 172.7, 152.9, 152.9, 146.5, 144.8, 134.2, 123.1, 121.2, 114.7, 113.7, 111.4, 59.6, 56.7, 56.6, 44.2, 28.5, 24.6, 15.1

2-(4-fluoro-2,5-dimethoxy-phenyl)-*N*-[(4-methoxy-3-pyridyl)methyl]ethanamine (74)

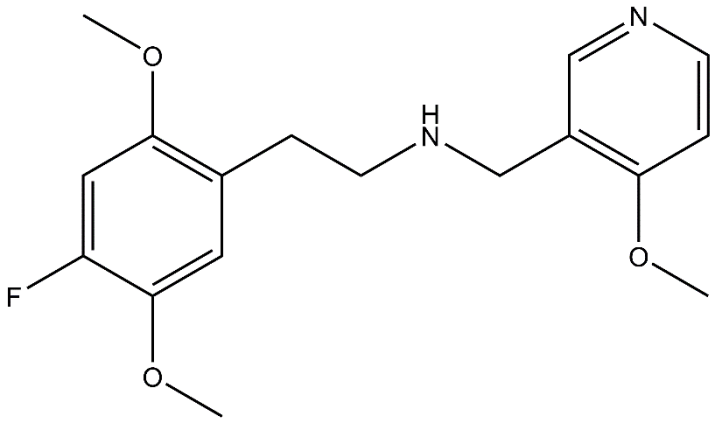

Using general procedure A, the target compound was obtained with **44** (0.4 g, 2 mmol) and 4-methoxypyridine-3-carbaldehyde (0.3 g, 1.65 mmol). The salt was filtered yielding a white powder (0.19 g, 31%); ^{1}H NMR (400 MHz, CD_3OD) δ 8.9 (s, 1 H), 8.9 (d, *J*=6.87 Hz, 1 H), 7.8 (d, *J*=7.33 Hz, 1 H), 7.1 (d, *J*=9.16 Hz, 1 H), 6.9 (d, *J*=13.28 Hz, 1 H), 4.4 (s, 2 H), 4.3 (s, 3 H), 3.8 (s, 3 H), 3.8 (s, 3 H), 3.3 (d, *J*=7.79 Hz, 2 H), 3.0 - 3.1 (m, 2 H); ^{13}C NMR (101 MHz, CD_3OD) δ 172.7, 153.3, 146.6, 144.8, 142.8, 121.2, 120.8, 118.3, 111.4, 102.1, 101.8, 59.6, 57.9, 56.8, 49.4, 44.2, 28.1

2-(4-iodo-2,5-dimethoxy-phenyl)-*N*-[(4-methoxy-3-pyridyl)methyl]ethanamine (75)

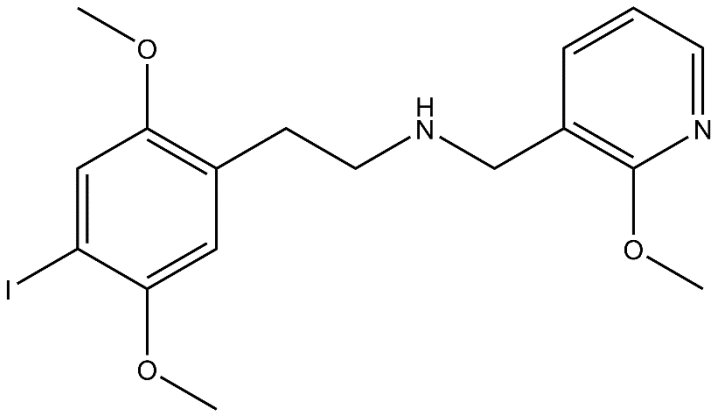

Using general procedure A, the target compound was obtained with **47** (0.39 g, 1 mmol) and 4-methoxypyridine-3-carbaldehyde (0.15 g, 1.1 mmol). The salt was filtered yielding a white powder (0.3022 g, 71%); ^{1}H NMR (400 MHz, $(CD_3)_2SO$) δ 9.9 (br. s., 2 H), 9.0 (s, 1 H), 8.9 (d, J=6.41 Hz, 1 H), 7.7 (d, J=6.87 Hz, 1 H), 7.3 (s, 1 H), 6.9 (s, 1 H), 4.3 (br. s., 2 H), 4.1 (s, 3 H), 3.8 (s, 3 H), 3.8 (s, 3 H), 3.4 - 3.6 (m, 3 H), 3.2 (br. s., 2 H), 2.9 - 3.0 (m, 2 H); ^{13}C NMR (101 MHz, $(CD_3)_2SO$) δ 169.6, 152.0, 151.8, 144.6, 143.5, 126.2, 121.4, 119.5, 113.8, 109.8, 84.0, 58.3, 56.9, 56.3, 46.1, 41.5, 26.4

2-(2,5-dimethoxy-4-nitro-phenyl)-*N*-[(4-methoxy-3-pyridyl)methyl]ethanamine (76)

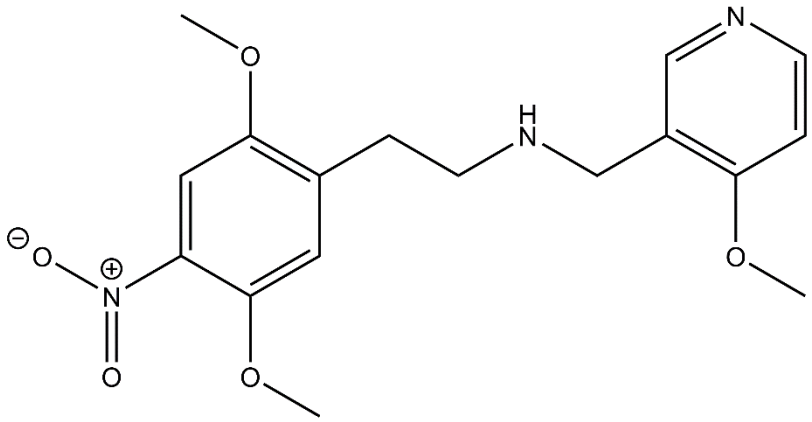

Using general procedure A, the target compound was obtained with **48** (0.45 g, 2 mmol) and 4-methoxypyridine-3-carbaldehyde (0.30 g, 2.2 mmol). The salt was filtered yielding a white powder (0.32 g, 47%); ^{1}H NMR (400 MHz, CD_3OD) δ 8.9 (s, 1 H), 8.9 (d, *J*=6.87 Hz, 1 H), 7.8 (d, *J*=6.87 Hz, 1 H), 7.5 (s, 1 H), 7.3 (s, 1 H), 4.5 (s, 2 H), 4.3 (s, 3 H), 3.9 (s, 3 H), 3.9 (s, 3 H), 3.4 - 3.5 (m, 2 H), 3.2 - 3.2 (m, 2 H) ^{13}C NMR (101 MHz, CD_3OD) δ 172.1, 151.7, 147.8, 145.8, 144.2, 139.5, 132.3, 120.5, 117.7, 110.8, 108.1, 59.0, 57.3, 56.3, 43.6, 27.9

3 Chapter 3 – Synthesis

3.1 Introduction

To synthesise the NBOMe and the PET imaging replacement compounds, a variety of reactions were required to get to the substituted phenethylamines, which would then be used as the starting material for the reductive alkylation step. Shulgin's book PIHKAL (Phenethylamines I have known and loved)[143] was used for the phenethylamine synthesis steps but some have been modified to maximise efficiency (Scheme 7). For example, the Hansen *et al.*[37] method was used to synthesise the NBOMe's, NPyr's, NPF's and NPOMe's.

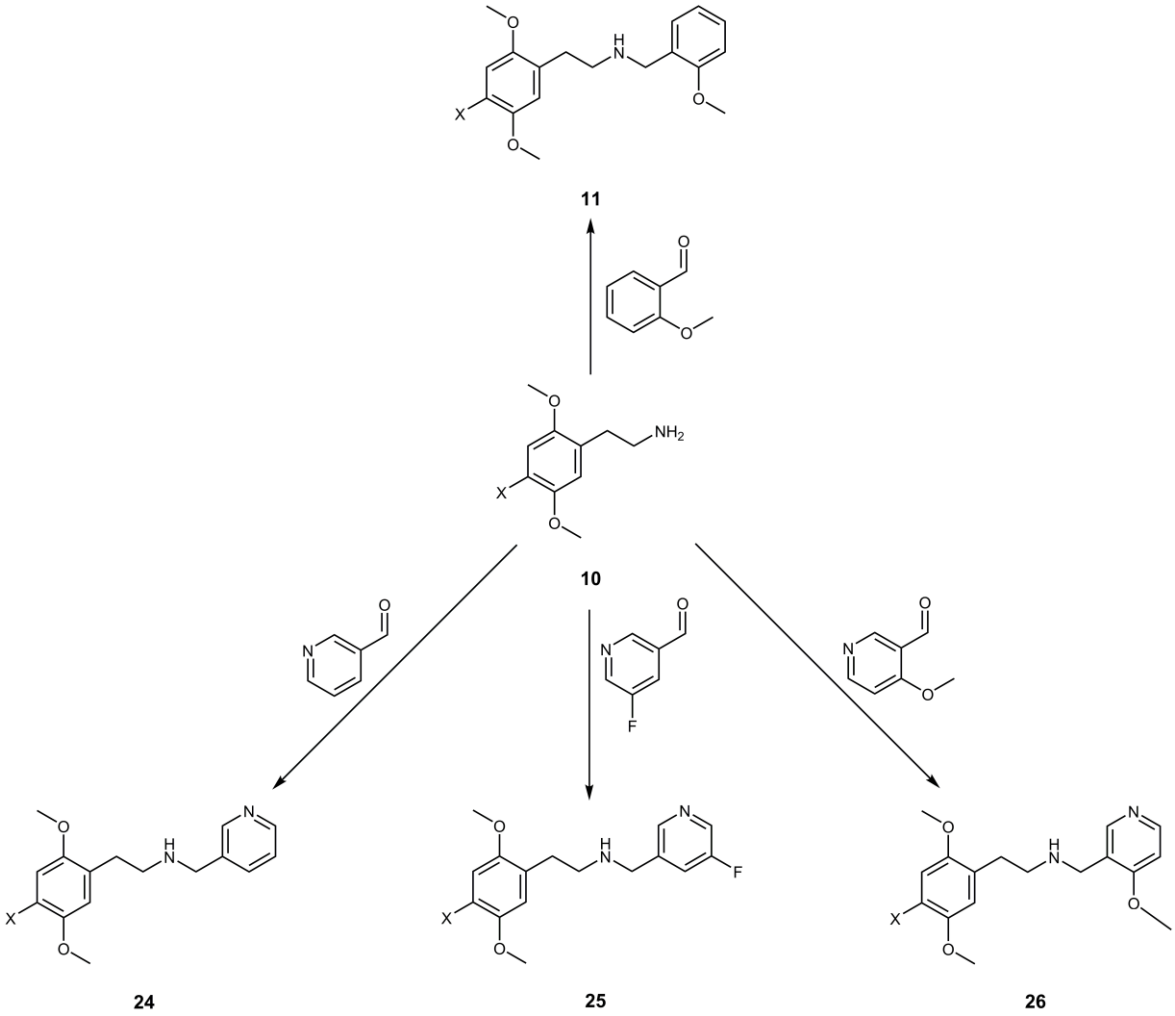

Scheme 7 - Reaction scheme for NBOMe compounds (**11**) and novel compounds **24**, **25**, and **26** using general method A (R1 = Me, Cl, F; X = F, Cl, Br, I, Me, Et, NO_2).

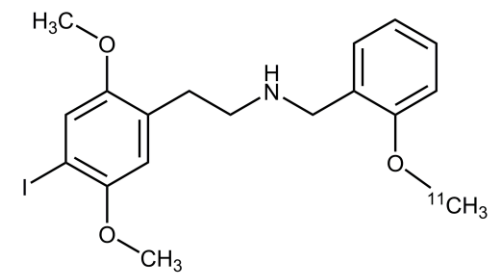

20

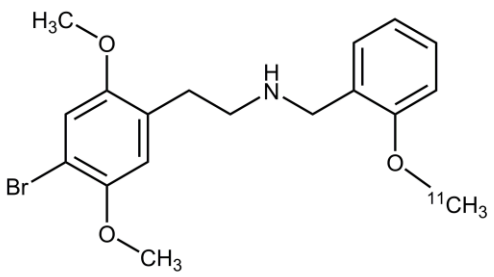

21

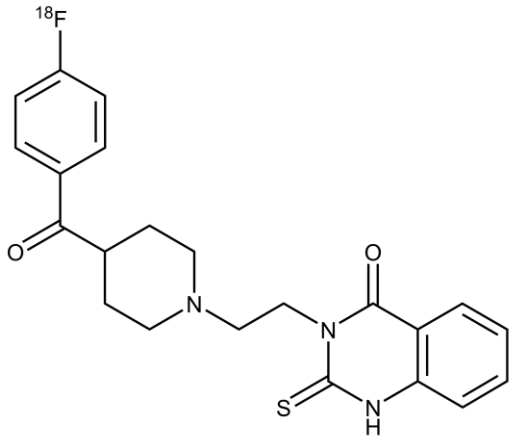

22

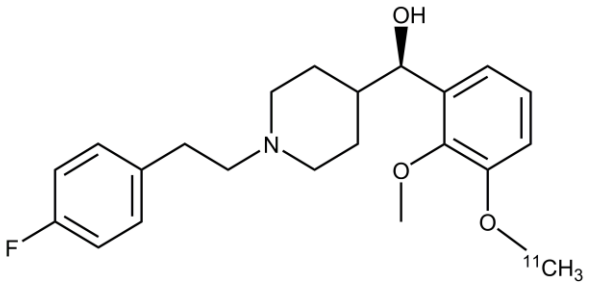

23

Figure 11 - Structures of NBOMe's (**11**, X = F, Cl, Br, I, Me, Et, NO_2), PET imaging agents (cimbi-5, **20**;cimbi-36, **21**) and NPOMe's (**26**, X = F, Cl, Br, I, Me, Et, NO_2)

The NPOMe's were the primary focus of this project as the similarity in structure with the NBOMe's and cimbi-5/36 (Figure 11) shows the real potential of replacing the imaging agents with a more stable drug. With positive biological assay results, this series of drugs would be a step in the right direction for mapping out $5HT_{2a}$ related diseases.

3.2 Synthesis of 2-(4-bromo-2,5-dimethoxy-phenyl)ethanamine (2C-B, 28)

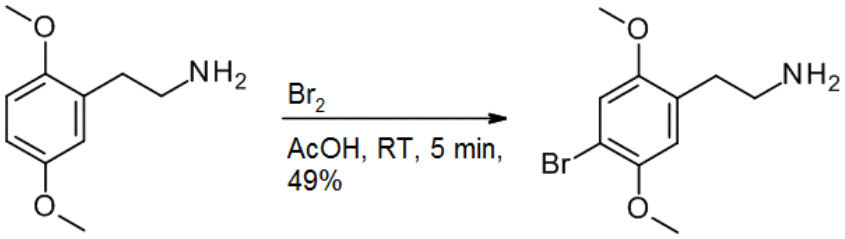

28

Scheme 8 - Synthetic scheme for the synthesis of 2C-B (**28**)

The synthesis of **28** (Scheme 8) was achieved using a one-step reaction as 2,5-dimethoxyphenethylamine (Scheme 9) was commercially available, so a bromination step was the easiest route. It was also noted that there was no recrystallization required as it was found that washing with ether (Figure 12) and cold acetone (Figure 13) purified the compound. Washing the powder with cold acetone decolourised the powder from an off white to white, furthermore, when left overnight this led to the formation of crystals. The crystals were further washed with cold acetone and characterised; the ^{1}H NMR spectrum of these crystals matched that of the powder obtained. When comparing the data to Kanamori *et al,*[132] two singlet peaks in the ^{1}H NMR aromatic region confirmed the bromination was successful and along with the GC-MS data possessing one peak (RT – 6.856 min), these data indicated a clean synthesis of 2C-B.

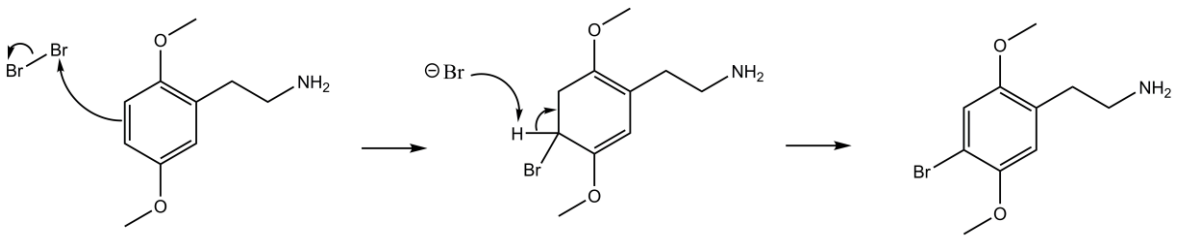

28

Scheme 9 – Reaction mechanism of the bromination of 2,5-dimethoxyphenethylamine

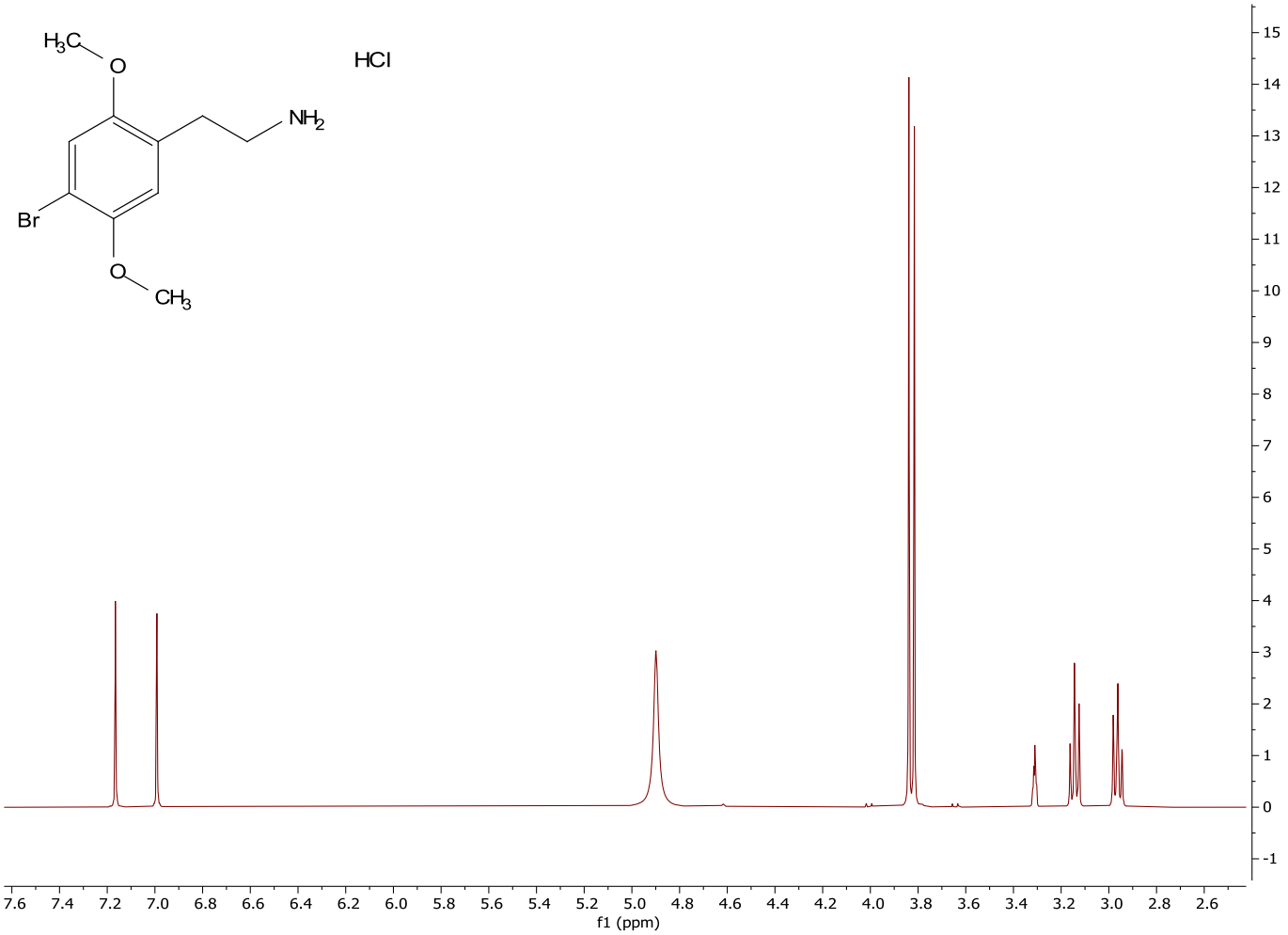

Figure 12 - ^{1}H NMR (CD_3OD, 400 MHz) spectra of **28.HCl** (30 mg mL^{-1}) after washing with H_2O and Et_2O

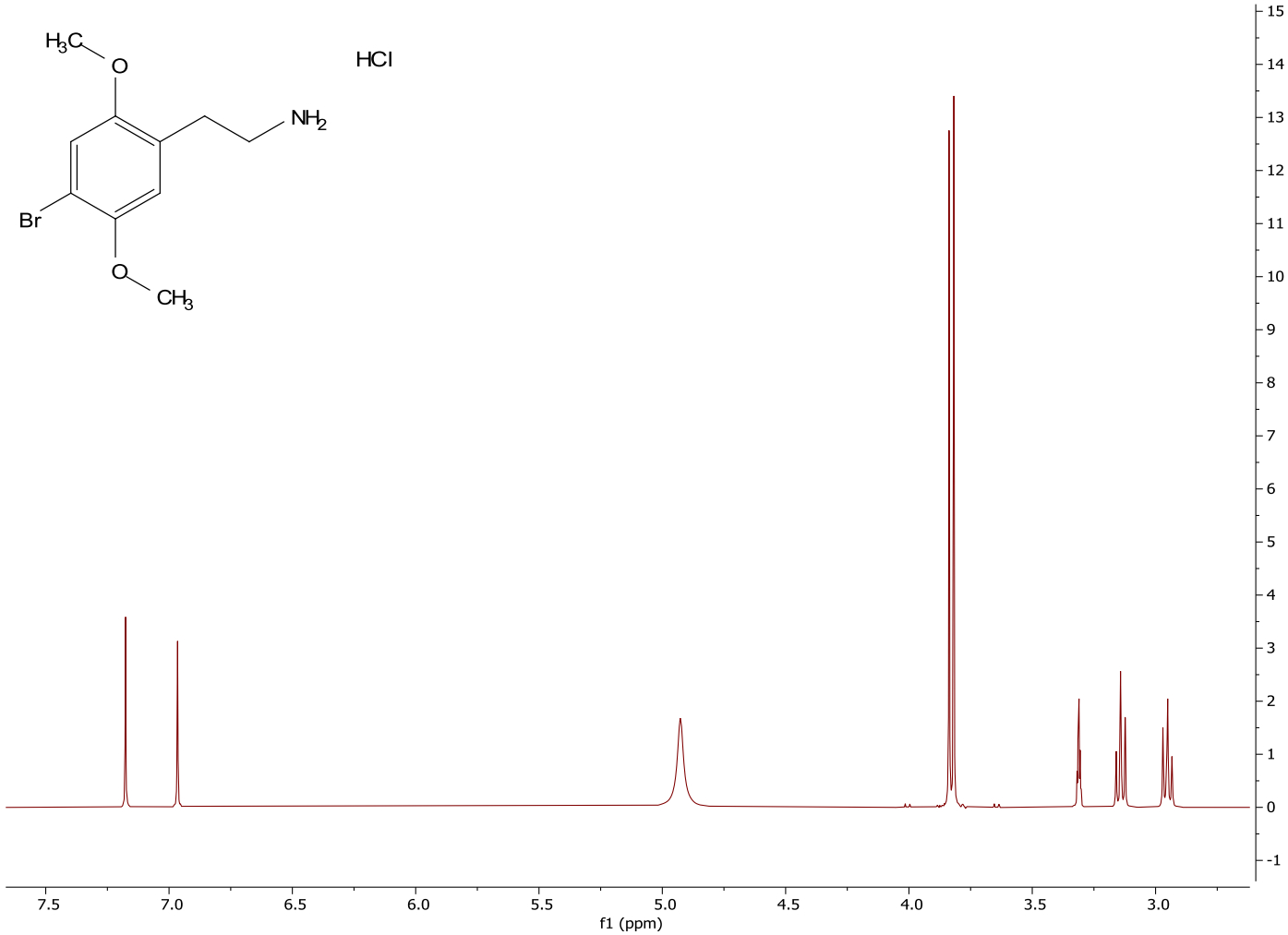

Figure 13 - ^{1}H NMR (CD_3OD, 400 MHz) spectrum of **28.HCl** (30 mg mL^{-1}) after washing with H_2O, Et_2O and acetone

3.3 Synthesis of 2-(4-chloro-2,5-dimethoxy-phenyl)ethanamine (2C-C, 31)

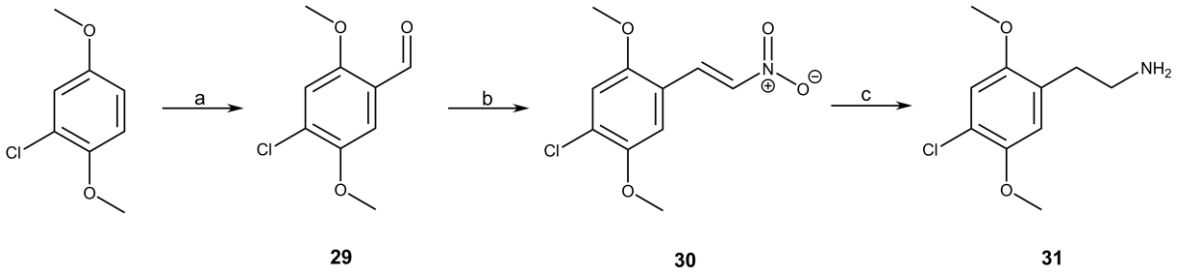

Scheme 10 - Synthetic scheme of 2C-C (**31**); a) HMTA, TFA, reflux, 15 h, 55 %; b) nitromethane, ammonium acetate, AcOH, reflux, 4 h, 34 %; c) $LiAH_4$, THF, RT, 3 h, 50 %

Following Shulgin's methodology (Scheme 10), the Duff formylation was utilised for the synthesis of **29**. Other formylating methods have been applied within the synthesis of other compounds (Rieche, Vilsmeier-Haack) but due to the inductive effect being larger than the mesomeric effects, these were not attempted. These mesomeric effects decrease the π-electron density within the ring making substitution reactions difficult. Therefore, a Duff formylation was utilised with hexamethylenetetramine (HMTA) and TFA being used as the formylating group. The proposed mechanism for the Duff formylation is shown in Scheme 11.

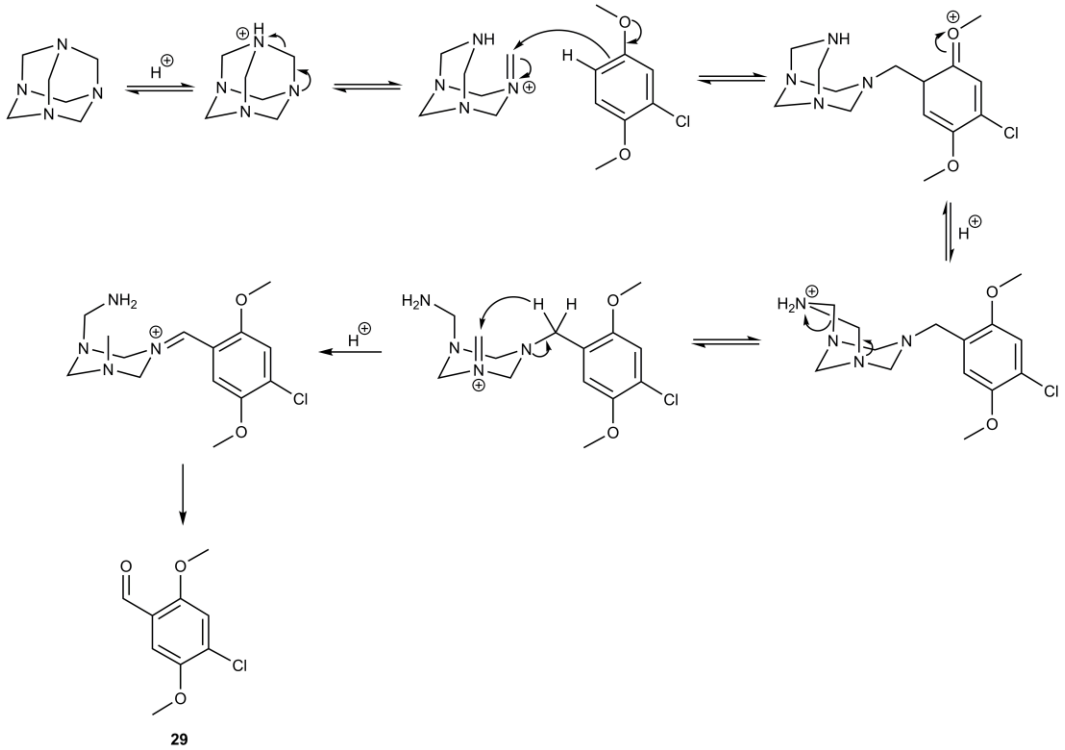

Scheme 11 - Proposed mechanism of Duff formylation

After comparison with the spectral data from Bloomer *et al.*[134] the aldehyde peak was found at 10.39 ppm whereas Bloomer reported it at 10.32 ppm. The difference of 0.07 ppm was found throughout the data but peak shapes and integration values all matched the previously reported data.

The Henry (nitro-aldol) reaction was utilised for five aldehydes (methyl, ethyl, fluoro, chloro and iodo derivatives) to be synthesised (Scheme 12). These compounds have not been produced before and so no data is available to compare to. Therefore, it is the first documented synthesis of all the substituted *beta*-nitrostyrenes.

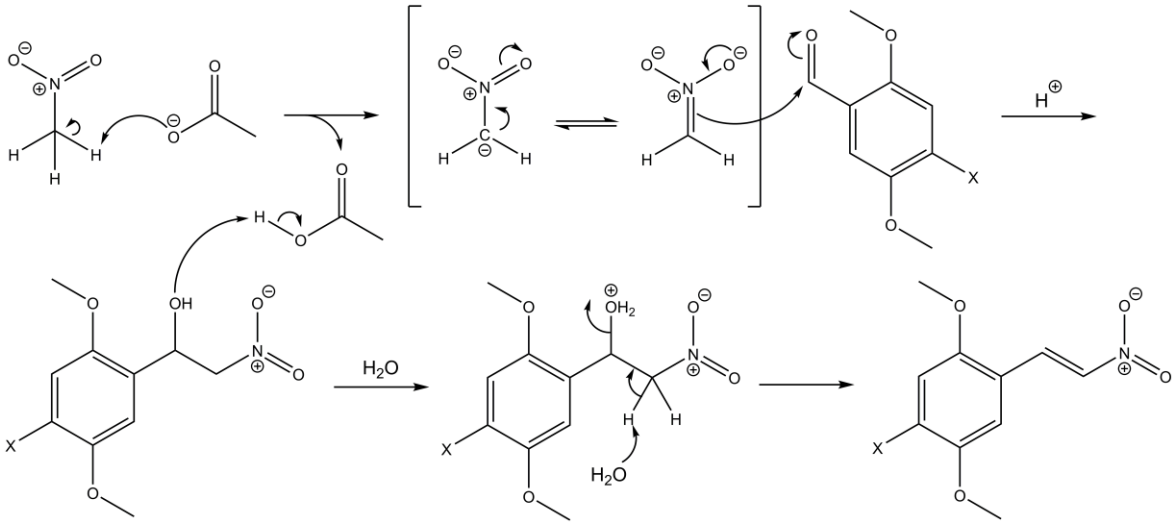

Scheme 12 - Proposed reaction mechanism of the Henry reaction followed by dehydration (X = Me, Et, Cl, F)

When looking at the ^{1}H NMR data for the β-nitrostryrenes (**30** shown in Figure 14), the dehydration step leaves these compounds in the *trans*-formation. This is shown by the *J*-couplings from the vicinal hydrogens being 14 Hz (between 11 – 18 Hz and typically 16 Hz) whereas vicinal *cis*-coupling would be in the region of 6 – 14 Hz and would typically be 10 Hz. This trend occurred during the synthesis of all the nitrostyrenes.

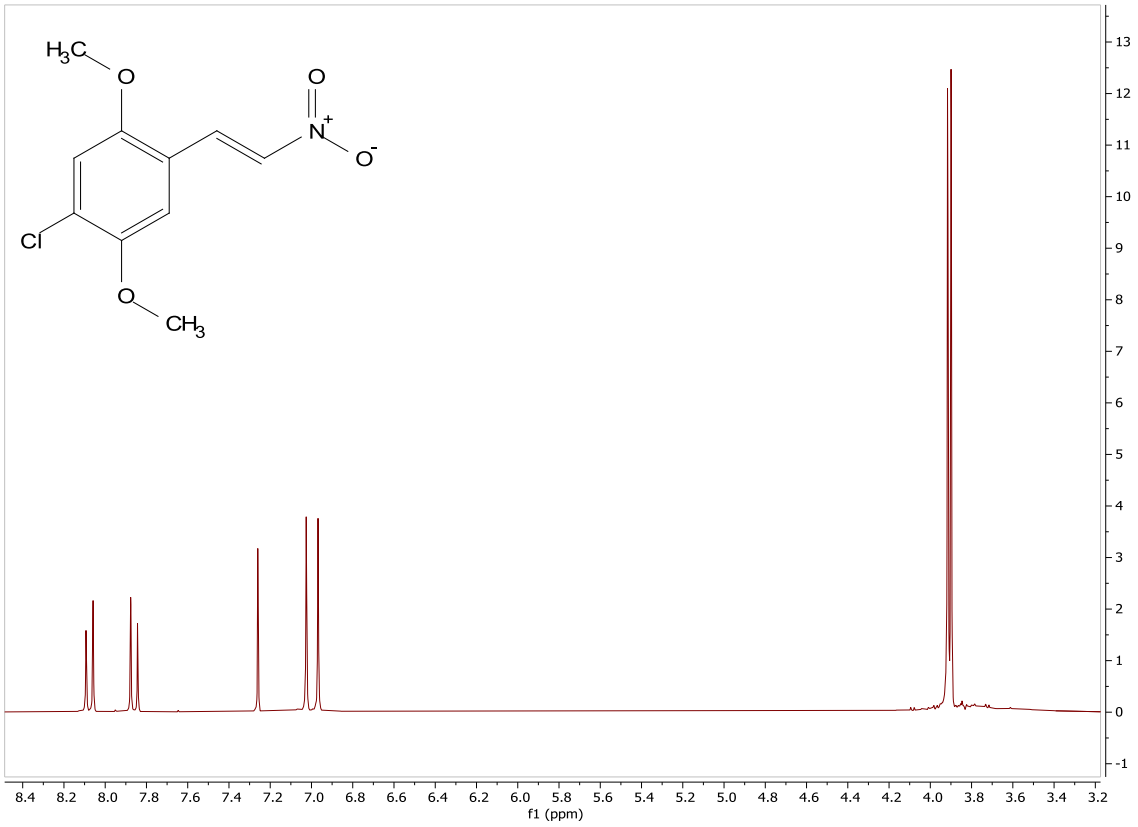

Figure 14 - ^{1}H NMR spectrum of **30**

The Shulgin method of lithium aluminium hydride (LAH) reductions had to be modified to maximise the yields, as to start with the LAH was stirred in anhydrous ether and cooled, to which was slowly added nitrostyrene dissolved in THF, followed by stirring at RT overnight and subsequent 15 min reflux. After forming the aluminium salts, this was filtered and washed with THF and concentred *in vacuo*. The oil was dissolved in IPA, acidified with 5 drops of conc. HCl (12 M) and anhydrous ether added to precipitate the phenethylamine as the salt. What was found is that this method was not reliable as the phenethylamine would not precipitate. This was modified by stirring the LAH with THF at RT and after the concentrating the TH*F in vacuo,* an acid base work up was used to purify and isolate the phenethylamine free-base. After concentration of the organic phase, the same HCl salt formation method was used which precipitated out the salts with no impurities. Despite being in harsh conditions, this method reduced both the alkene and nitro group effectively to the phenethylamine target (Figure 15). The alkene

peaks at 8.08 and 7.87 ppm both shifted upfield to 3.14 and 2.95 ppm indicating methylene peaks are present (triplet splitting pattern with a *J*-coupling of 7.33 Hz).

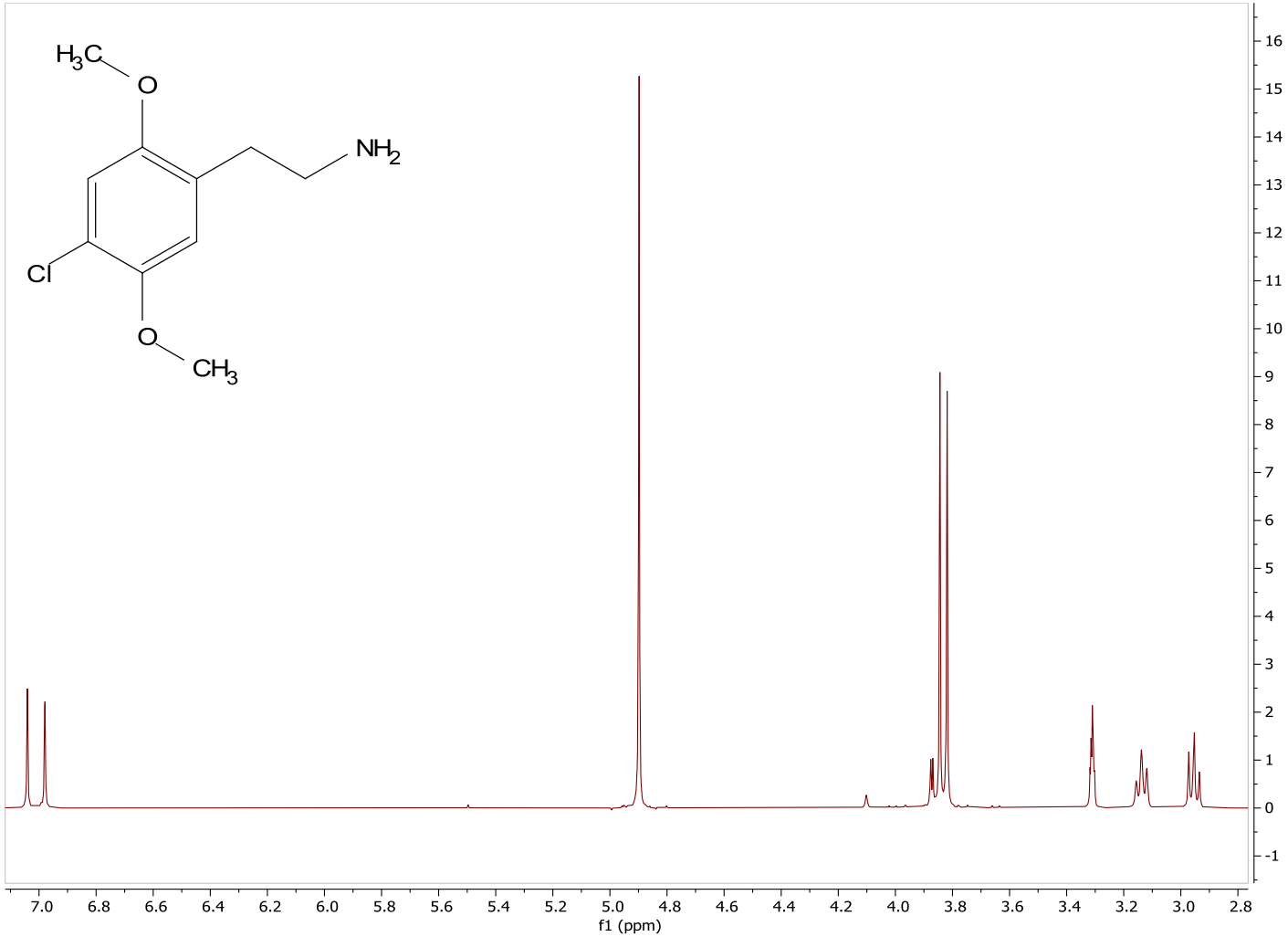

Figure 15 - ^{1}H NMR (CD_3OD, 400 MHz) spectrum of **31.HCl**

3.4 Synthesis of 2-(2,5-dimethoxy-4-methyl-phenyl)ethanamine (2C-D, 34)

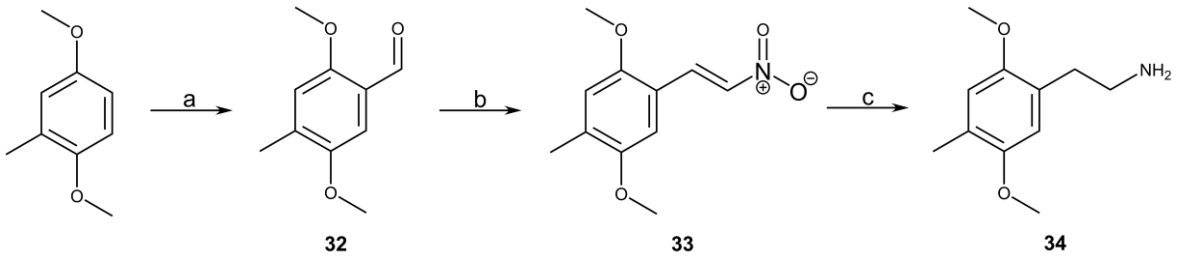

Scheme 13 – Synthetic scheme of 2C-D (**34**); a) $POCl_3$, *N*-methylformanilide, RT, 2 h, 97 %; b) nitromethane, ammonium acetate, acetic acid, reflux, 3 h, 66 %; c) LAH, THF, RT, 3 h, 14 %

34 was prepared via a three-step synthetic strategy (Scheme 13), which employed a sequential Vilsmeier-Haack reaction (Scheme 14, Scheme 15), Henry reaction (Scheme 12) followed by a LAH reduction. With the Vilsmeier-Haack reaction, the first step was to form the Vilsmeier reagent *in situ* (Scheme 14) before proceeding to the second step.

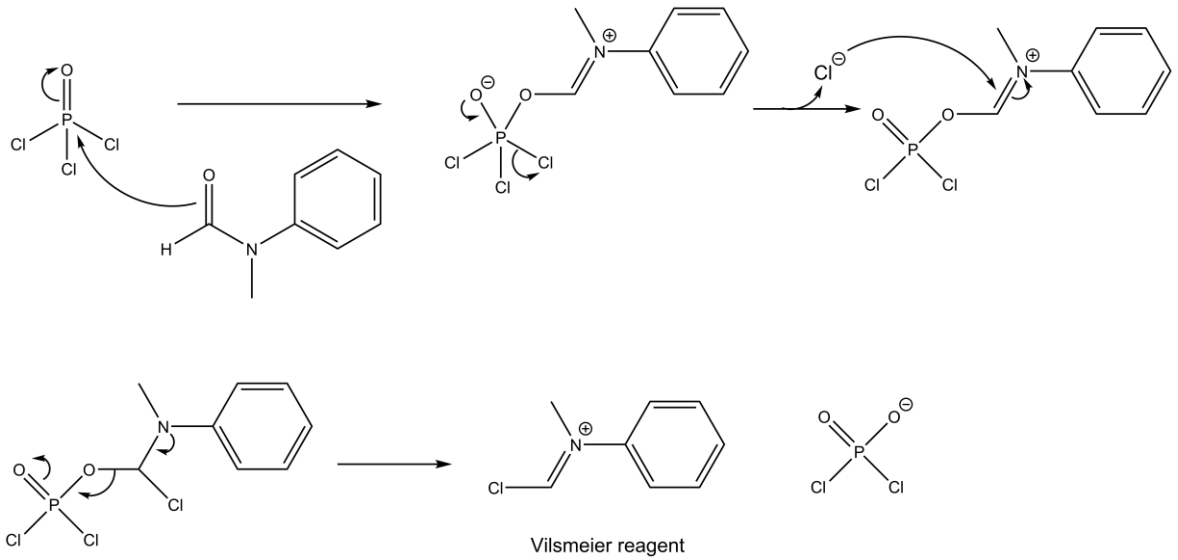

Scheme 14 - Reaction mechanism of the formation of the Vilsmeier reagent

The second step had to be monitored carefully as leaving to stir for too long would lead to the solution solidifying when cooled, and would not turn back to a solution when reheated. Taking off the heat source to cool down was necessary due to the reaction being exothermic as well as the evolution of HCl gas (Scheme 14).

Comparison of the data with Miyawaki *et al.*[135] indicate five peaks being present in the ^{1}H NMR corresponding to the five groups of protons (Figure 16).

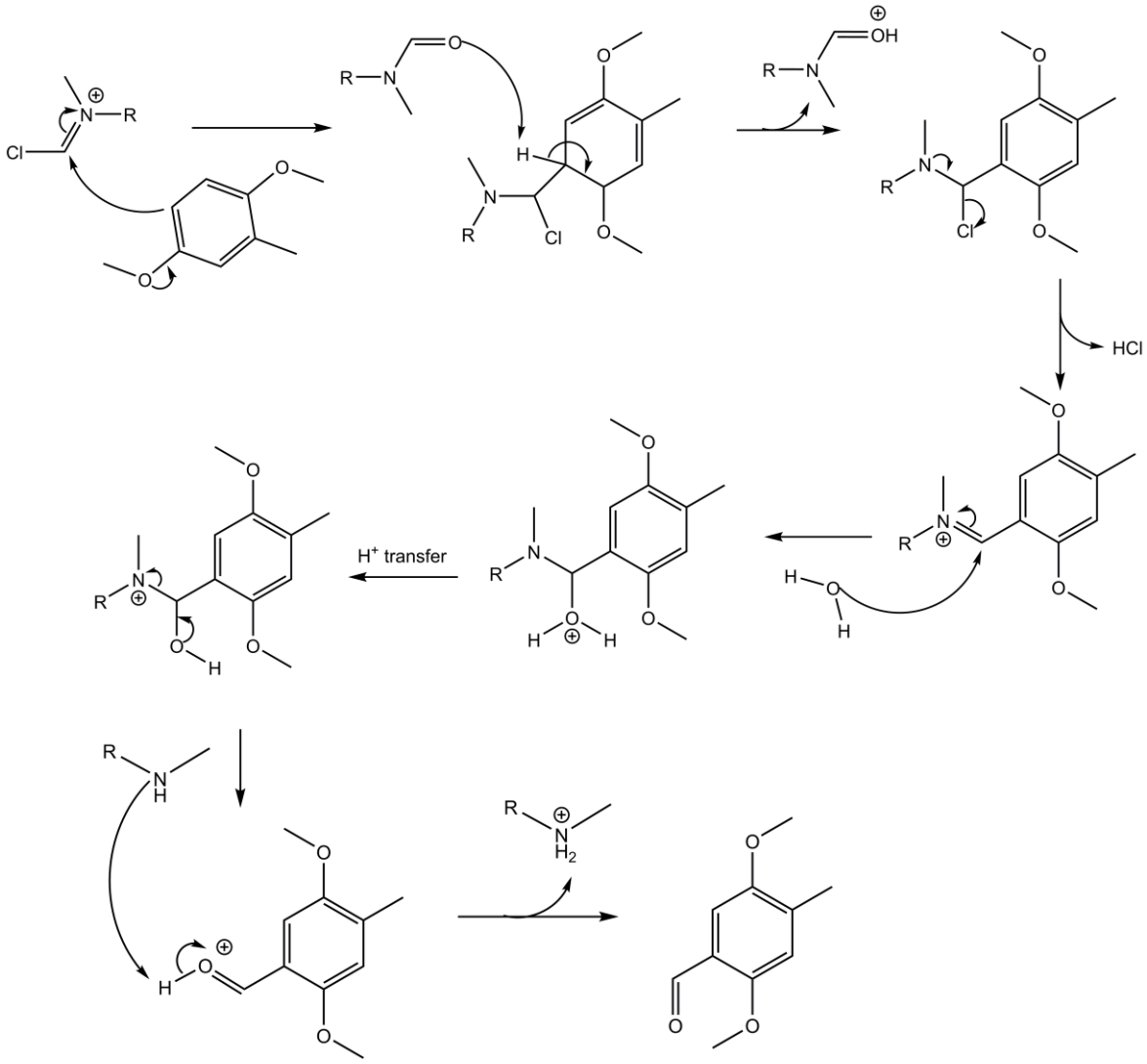

32

Scheme 15 - Reaction mechanism of the Vilsmeier reagent with 2,5-dimethoxytoluene (R = phenyl)

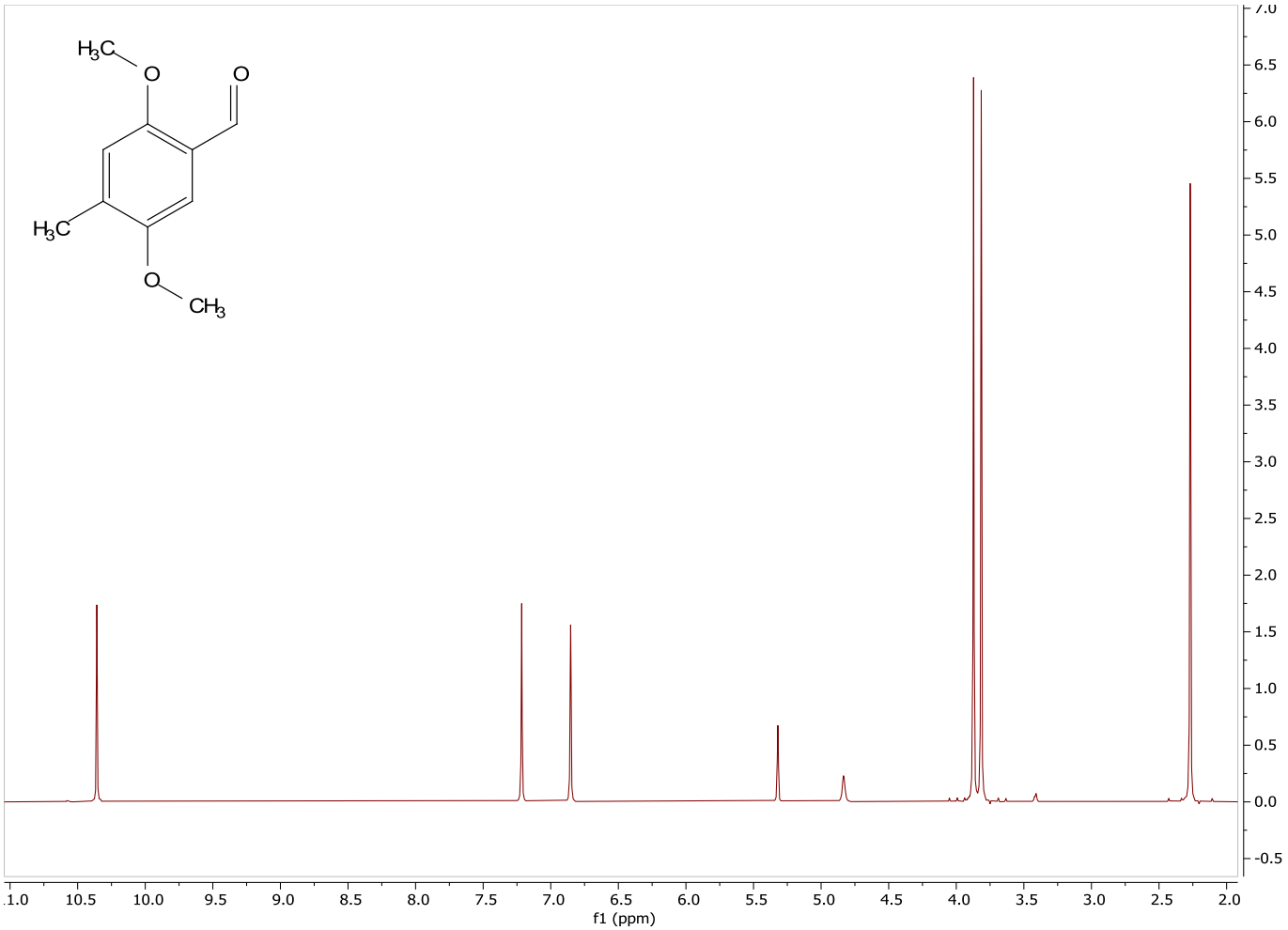

Figure 16 - ^{1}H NMR (CD_2Cl_2, 400 MHz) spectrum of **32**

3.5 Synthesis of 2-(4-ethyl-2,5-dimethoxy-phenyl)ethanamine (2C-E, 34)

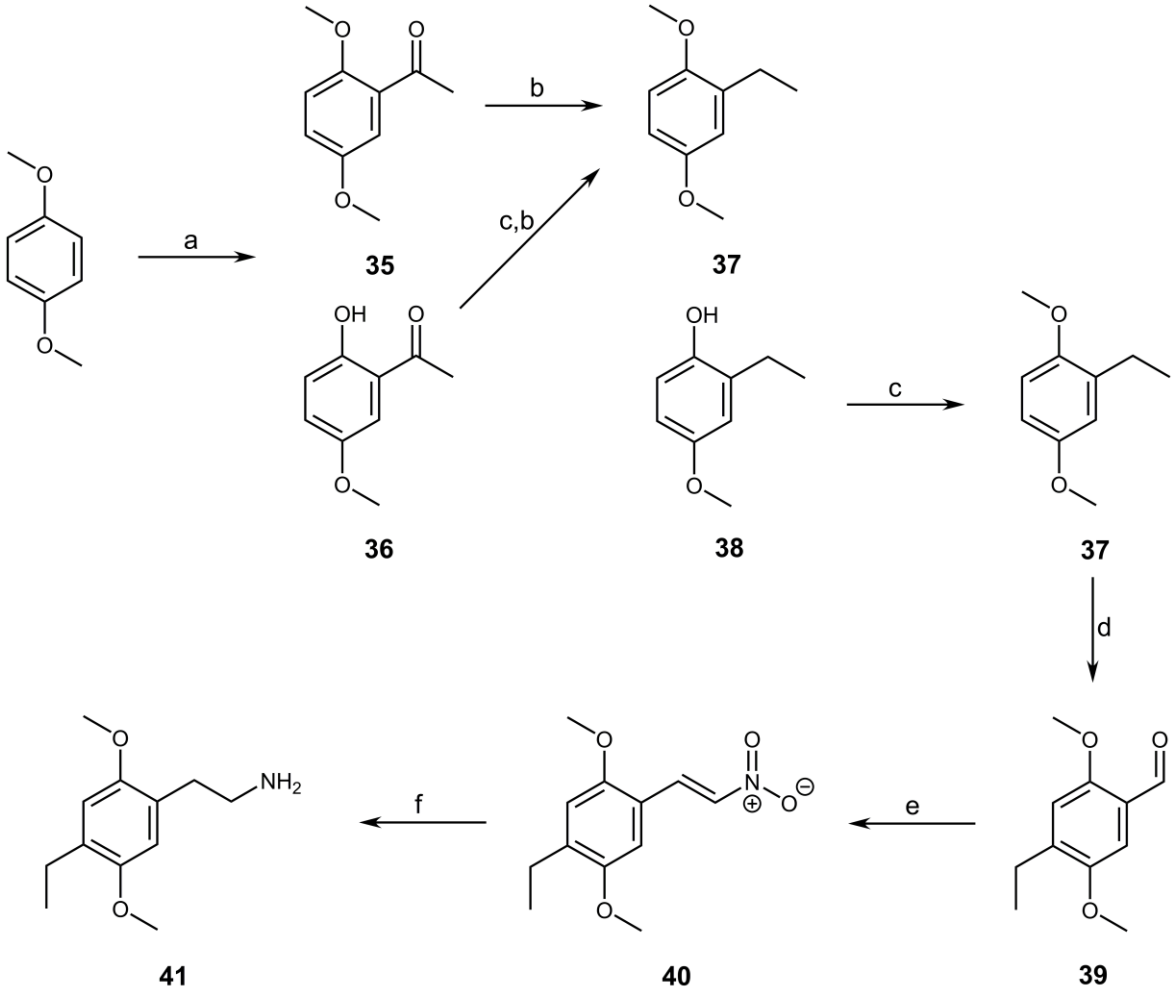

Scheme 16 - Synthetic route of 2C-E (**34**); (a) acetyl chloride, aluminium chloride, DCM, RT, 1 h, 83%; (b) KOH, triethylene glycol, hydrazine hydrate (40 %), 150°C, 4 h, 85%; (c) iodomethane, KOH, DMSO, 40°C, 1 h, 95 – 99%; (d) tin (IV) chloride, dichloromethyl methyl ether, anhydrous DCM, 0°C – RT, 1 h, 83%; (e) nitromethane, ammonium acetate, 100°C, 4 h, 29%; (f) LAH, anhydrous THF, RT, 3 h, 50%.

For the synthesis of **41**, a five step route was employed (Scheme 16). The first three reactions were performed on a smaller scale to monitor the yields as typically when performing nitro-aldol reactions the yields are 50% or less and the LAH yield is less than 20%. So, to maximise the amount of phenethylamine, 25 g of starting material (1,4-dimethoxybenzene) was used to result in 3 g of **41**. During the small-scale synthesis, it was noted in the acylation that a hydroxylated side product was made (Figure 17) which was seen after purification of the desired compound (**35**) by distillation (ratio of **35** to **36,** 7:1).

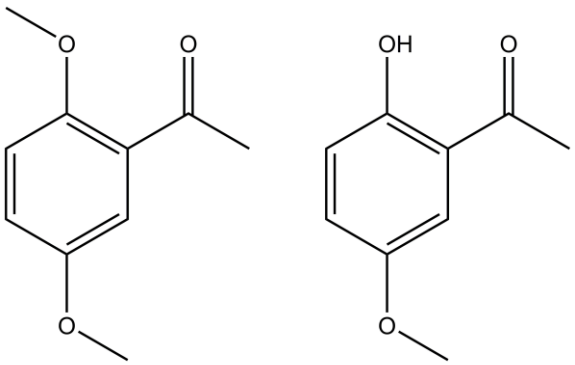

35 **36**

Figure 17 - Products after the Friedel-Crafts acylation; 2,5-dimethoxyacetophenone (**35**) and 2-hydroxy-5-methoxyacetophenone (**36**)

The hydroxylated compound was then methylated with iodomethane to produce **35** to be used in the Wolff-Kishner reduction. For the Wollf-Kishner reduction (Scheme 17), a Dean-Stark set up was used following the Huang-Minlon[144] modification as this would remove water and excess hydrazine from the reaction vessel, allowing the reaction to reach a temperature of 200˚C. After extraction with DCM, the organic phase yielded 15% of 1-ethyl-2,5-dimethoxybenzene. Following Shulgin's method,[143] it states that acidification of the aqueous phase followed by extraction with DCM would leave 2-ethyl-5-methoxyphenol (**38**, 87 %) which was then methylated with iodomethane to produce **37** (85 %).

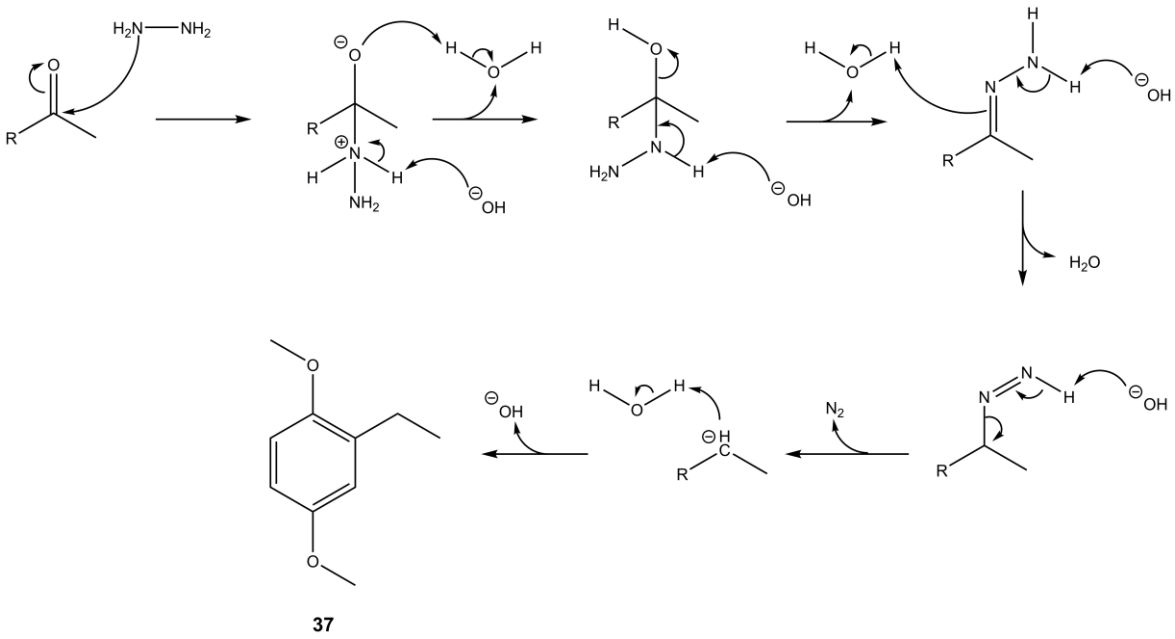

37

Scheme 17 - Reaction mechanism of the Wolff-Kishner reduction (R = 2,5-dimethoxybenzene)

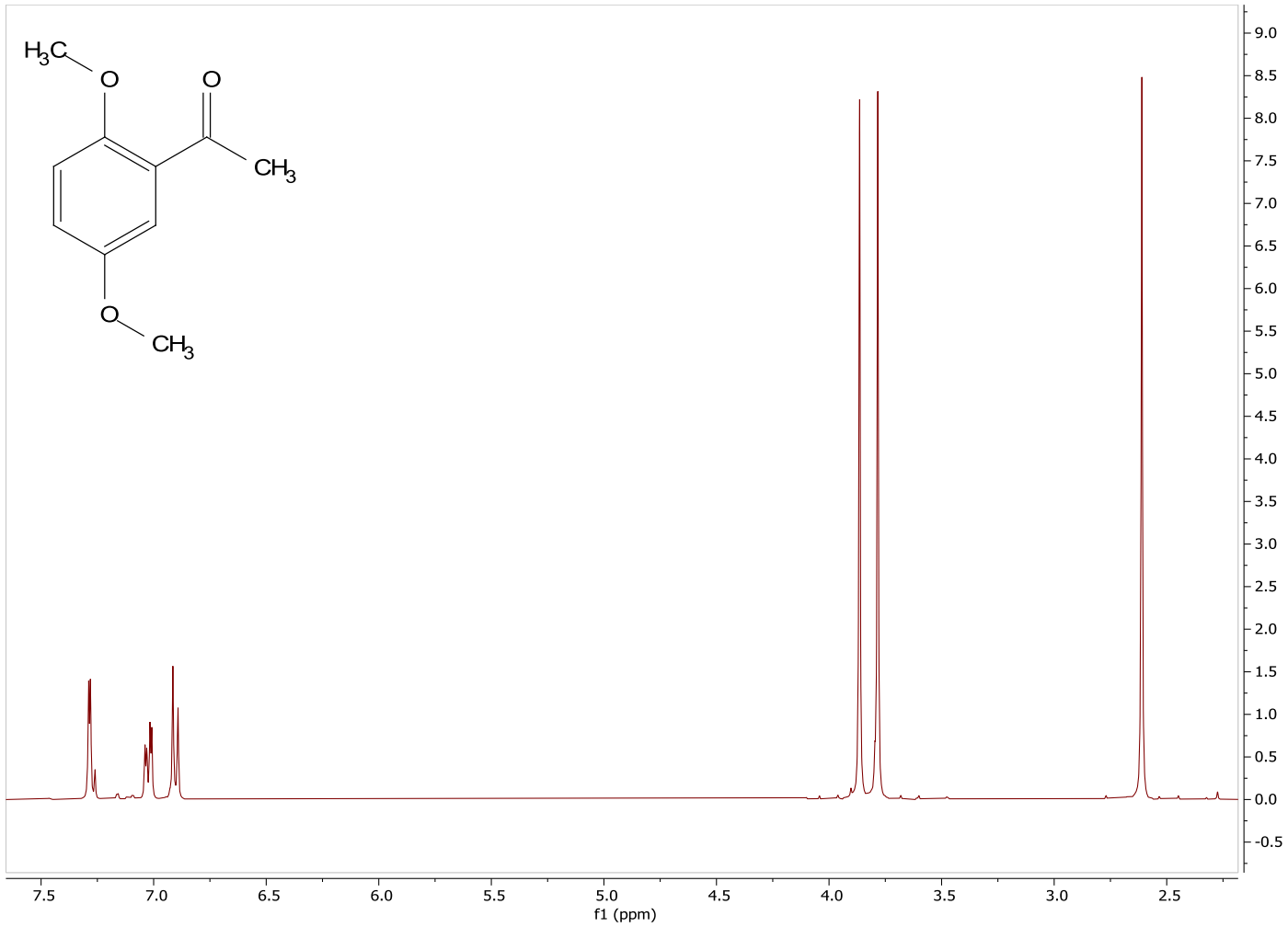

Figure 18 - ^{1}H NMR ($CDCl_3$, 400 MHz) spectrum of **35**

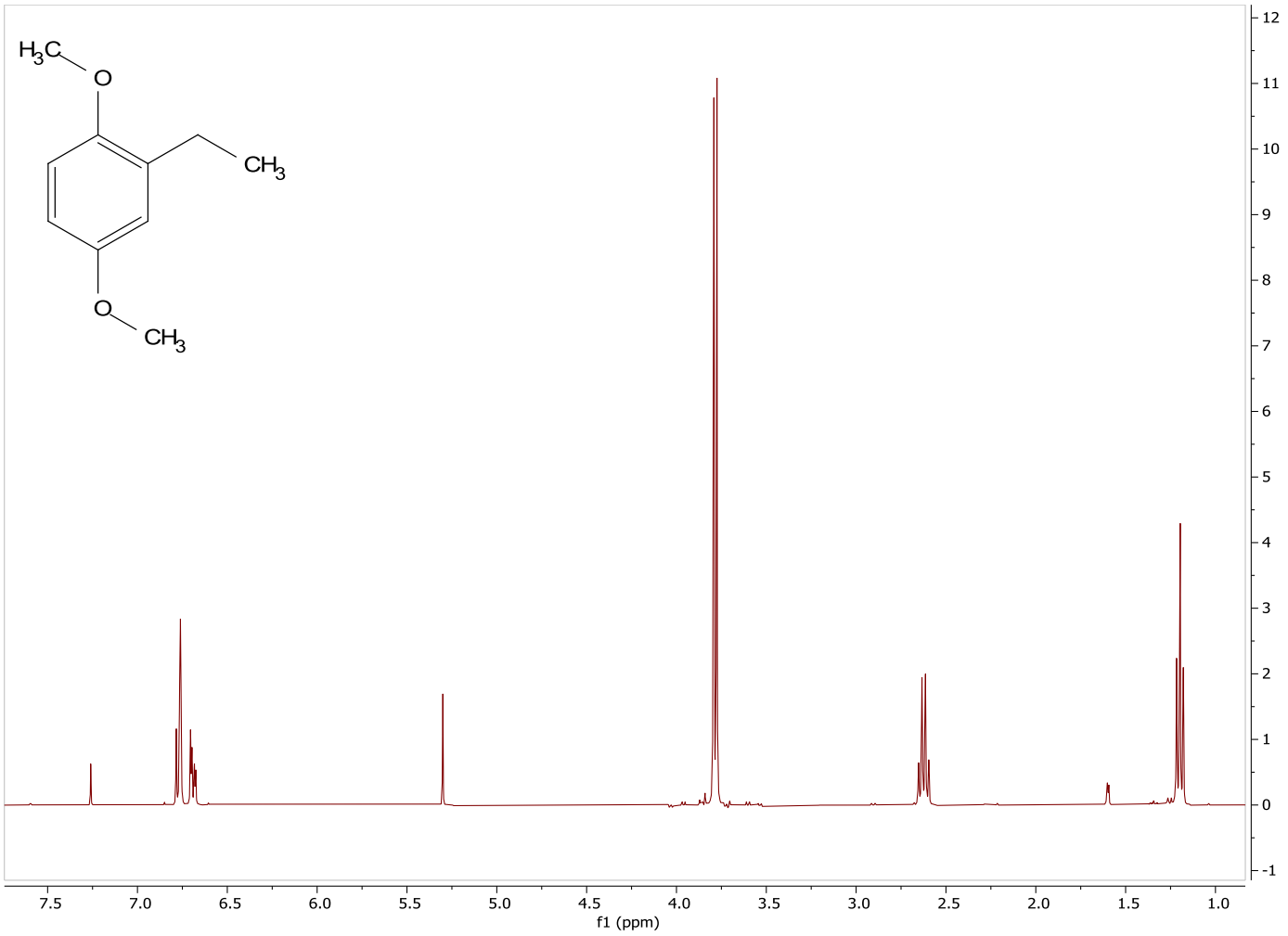

Figure 19 - ^{1}H NMR ($CDCl_3$, 400 MHz) spectrum of **37**

This series of compounds were synthesised following Shulgin methodology[143] with two purification methods used. Vacuum distillation was employed as the purification method of **35** due to high amount of crude product at the end of the reaction. As shown in Figure 18, the aromatic region of **35** shows two doublets and a doublet of doublets. Theoretically, there should be a singlet and two doublets. When looking at the *J*-coupling values of these peaks (Table 5), *ortho* H-H *J*-couplings occur between 6 – 9 Hz, *meta J*-coupling between 2 – 3 Hz and *para J*-coupling between 0 – 1 Hz. As the *J* values fit into this criteria, assigning hydrogens can be achieved without further NMR studies.

Table 5 - Aromatic ^{1}H NMR chemical shifts of **35**

Chemical shift (ppm)	Splitting pattern	*J*-coupling (Hz)
6.9	Doublet	8.93
7.0	Doublet of doublets	8.93, 3.21
7.3	Doublet	3.21

Figure 19 shows a clean sample of **37**, with two aliphatic peaks and two aromatic peaks. The aliphatic peaks show a triplet and a quartet, indicating the removal of the carbonyl was successful. In the aromatic region, there are two peaks with the *J*-couplings shown in Table 6.

Table 6 - Aromatic ^{1}H NMR chemical shifts of **37**

Chemical shift (ppm)	Splitting pattern	*J*-coupling (Hz)
6.7	Doublet of doublets	8.7, 3.2
6.8	doublet	9.2

3.6 Synthesis of 2-(4-fluoro-2,5-dimethoxy-phenyl)ethanamine (2C-F, 44)

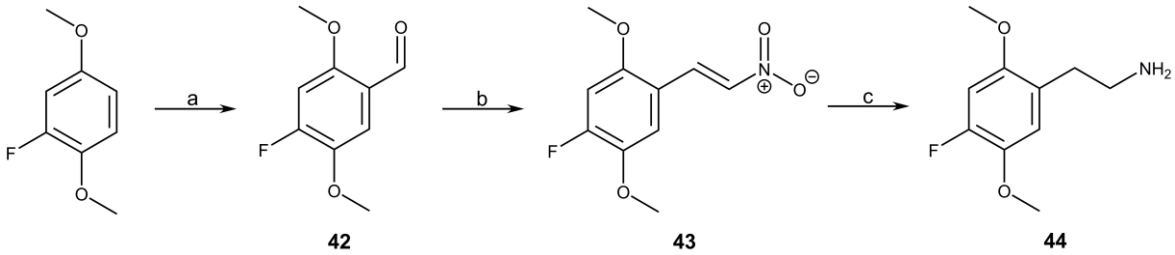

Scheme 18 - Synthetic scheme of 2C-F (**44**); a) nitromethane, ammonium acetate, AcOH, reflux, 3 h, 47 %; b) LAH, anhydrous THF, RT, 3 h, 93 %

For the synthesis of **44** (Scheme 18), the Reiche formylation was utilised as a one pot synthesis to add an aldehyde group, by using stannic chloride as a Lewis base in a Friedel-Craft's style alkylation reaction (mechanism shown in Scheme 19). This binds to a chlorine from dichloromethyl methyl ether to form the intermediate 1-[chloro(methoxy)methyl]-4-fluoro-2,5-dimethoxybenzene. Performing an acid base work up removed the methoxy group as MeOH and the chlorine ion as HCl, as well as removing the catalyst in the first acidic wash, to obtain a crude solid of 4-fluoro-2,5-dimethoxybenzaldehyde. Following a recrystallization with EtOH, this was filtered and dried to give a white powder. Analysis of the ^{1}H NMR spectrum, Figure 20, showed the reaction was successful with an aldehyde, two aromatic and two aliphatic peaks present.

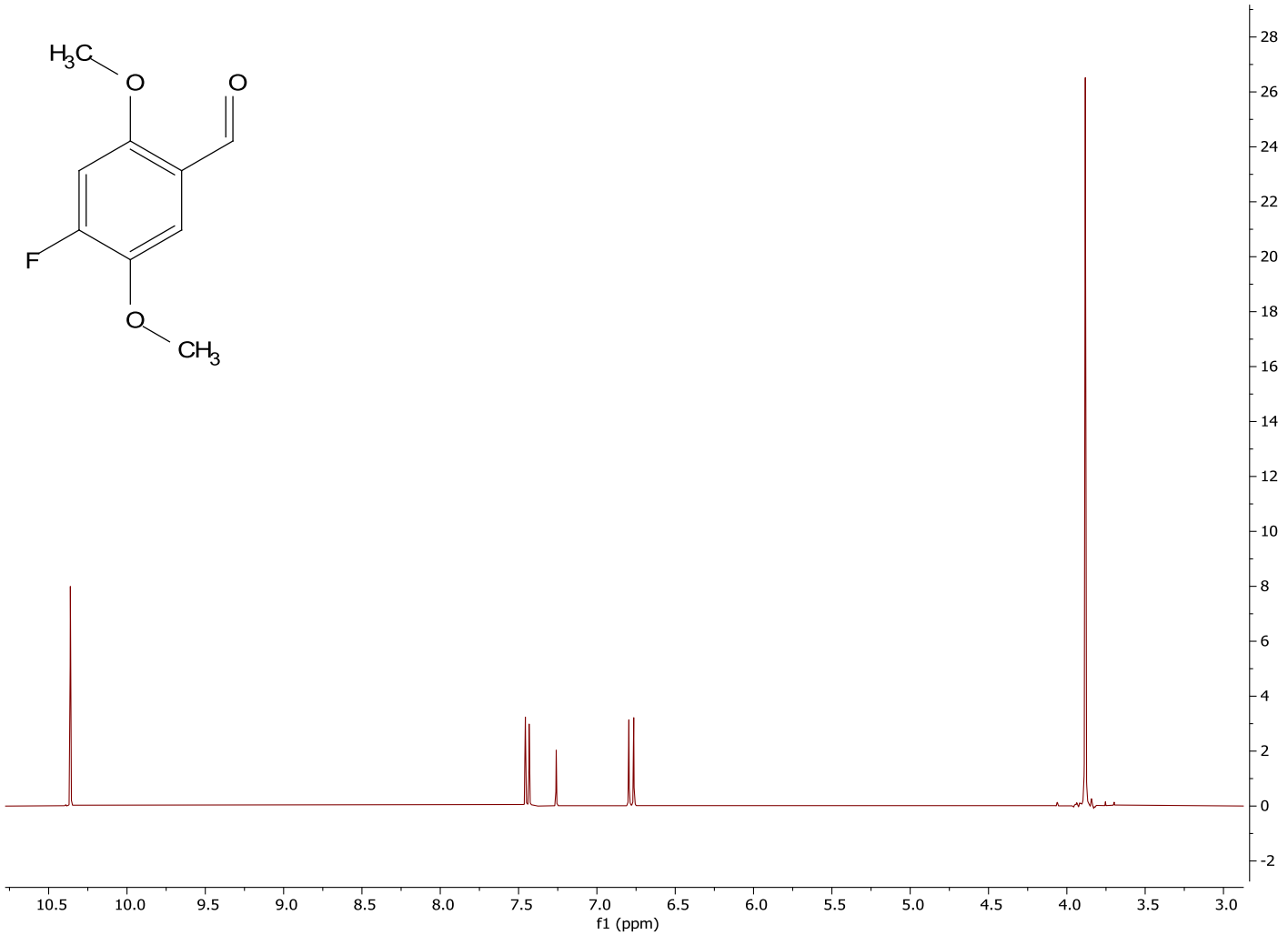

Figure 20 - ^{1}H NMR ($CDCl_3$, 400 MHz) spectrum of **42**

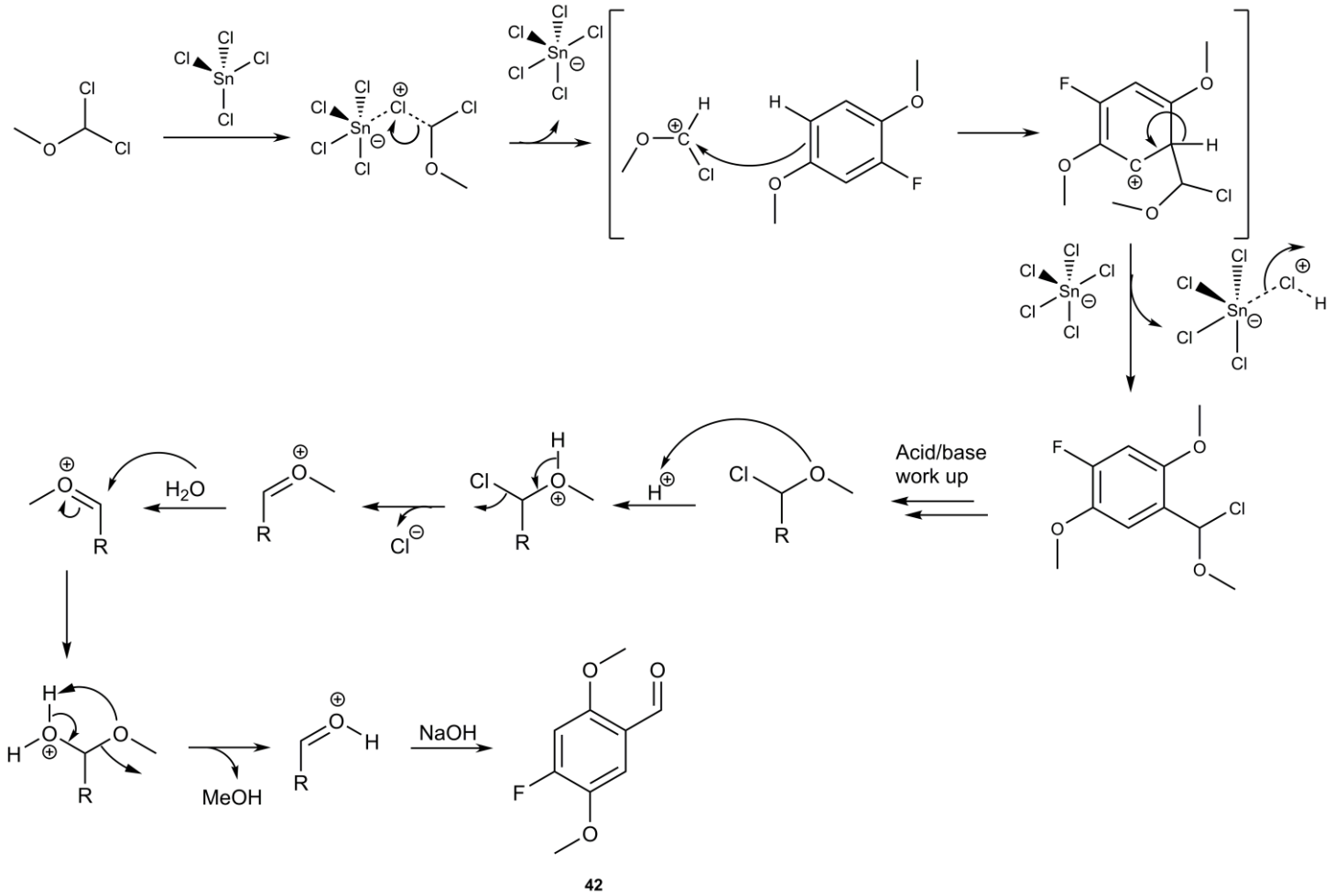

Scheme 19 - Reiche formylation mechanism with 1,4-dimethoxy-2-fluorobenzene and dichloromethyl methyl ether (R = 2,5-dimethoxy-4-fluorobenzene)

3.7 Synthesis of 2-(4-iodo-2,5-dimethoxy-phenyl)ethanamine (2C-I, 47)

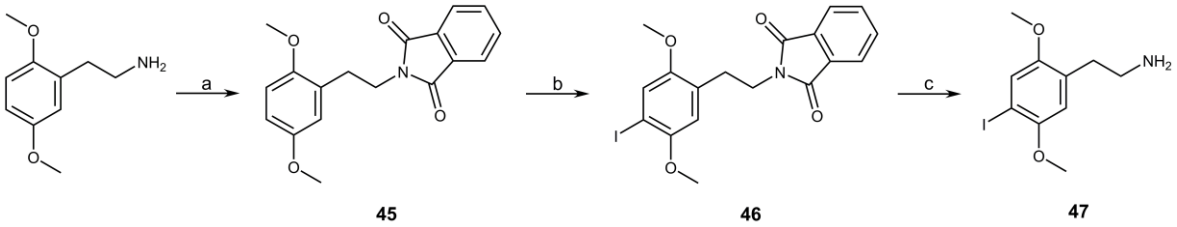

Scheme 20 - Synthetic route for 2C-I (**47**); a) phthalic anhydride, reflux, 6 h, 72 %; b) iodine monochloride, AcOH, 40 °C, 1 h, 76 %; c) hydrazine hydrate, IPA, reflux, 12 h, 10 %

This synthesis started with iodinating 2,5-dimethoxybenzaldehyde so it could follow a similar reaction scheme of 2C-F and 2C-C. This was due to one of the reagents Shulgin used being difficult to obtain (iodine monochloride, 1 M in AcOH). The method of Kaliyaperumal *et al.*[145] was utilised to obtain 4-iodo-2,5-dimethoxybenzaldehyde and followed this with the Henry reaction. However, this was unsuccessful. Baker *et al*.[146] have discussed the effect of halogens in the *m*- and *p*-positions on a substituted phenyl ring undergoing substitution reactions. The polar effects that were observed from the halogen substituents originated from tautomeric (electron-releasing) and inductive (electron-attracting) mechanisms. With *p*-halogens in benzaldehyde, the inductive electron attraction gives a fractional positive charge in the benzene ring displacing the carbonyl side chain. Fluorine exhibited an electron releasing effect meaning it must have a large mesomeric effect to overcome and reverse the polarisation of the inductive effect, allowing substitution reactions to occur. Whereas the other halogens exhibited an electron-attracting effect decreasing in the order I > Br > Cl, making it difficult for substitution of the carbonyl group to occur. Therefore, alternative routes to synthesise **47** were investigated. The synthetic route found to synthesise **47** was to protect 2,5-dimethoxyphenethylamine with phthalic anhydride, iodinate and then deprotect the phthalimide.

Proceeding with the protection route (Scheme 20), Shulgin performed this on a 12 g scale due to the final step (phthalimide deprotection) having a low yield (10%). The ^{1}H NMR spectrum of **47** (Figure 21) in the aromatic area shows two peaks with

integration values of one each; the aliphatic region has the two methoxy peaks as well as the two methylene peaks (H_2O peak at 4.91 ppm from CD_3OD, Table 7).

Table 7 - Assigned peaks for **47.HCl**

Atom	Exp. Shift (ppm)	Splitting Pattern	*J* coupling constant (Hz)
8	2.94	triplet	7.33
7	3.14	triplet	7.33
11	3.81	singlet	
13	3.82	singlet	
3	6.86	singlet	
6	7.35	singlet	

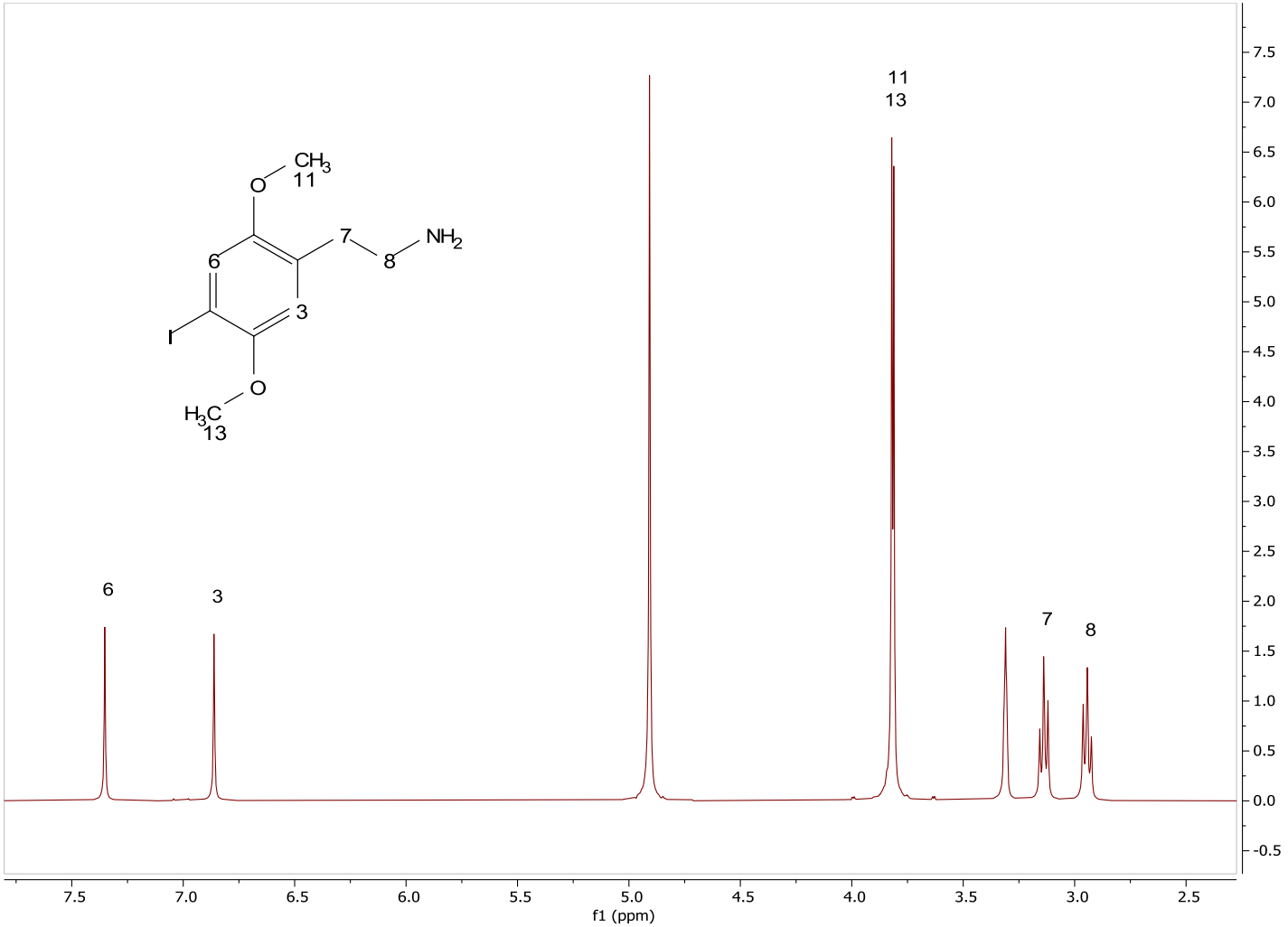

Figure 21 - ^{1}H NMR (400 MHz, CD_3OD) spectrum of **47.HCl**

3.8 Synthesis of 2-(2,5-dimethoxy-4-nitro-phenyl)ethanamine (2C-N, 48)

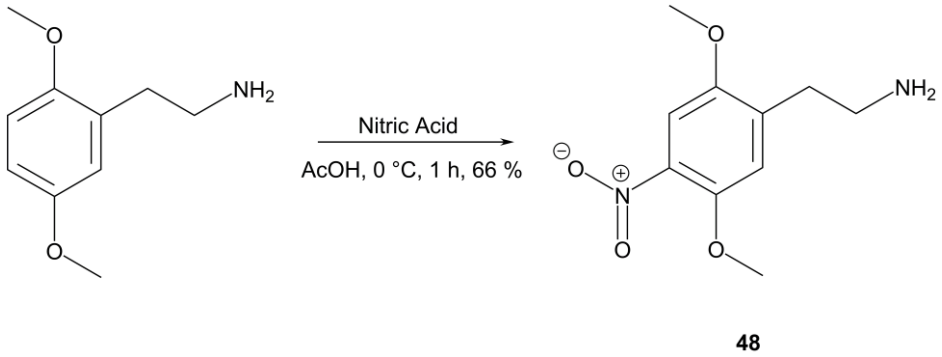

48

Scheme 21 – Synthetic scheme of 2C-N (**48**)

Synthesizing this compound was performed by a nitro addition using nitric acid (16 M) with 2,5-dimethoxyphenethylamine, Scheme 21, with the mechanism shown in Scheme 22. Direct nitration was successful in the presence of AcOH in which the free base crystallised. Upon ^{1}H NMR, Figure 22, no further purification was required and was not converted to the hydrochloride salt due to the ease of use.

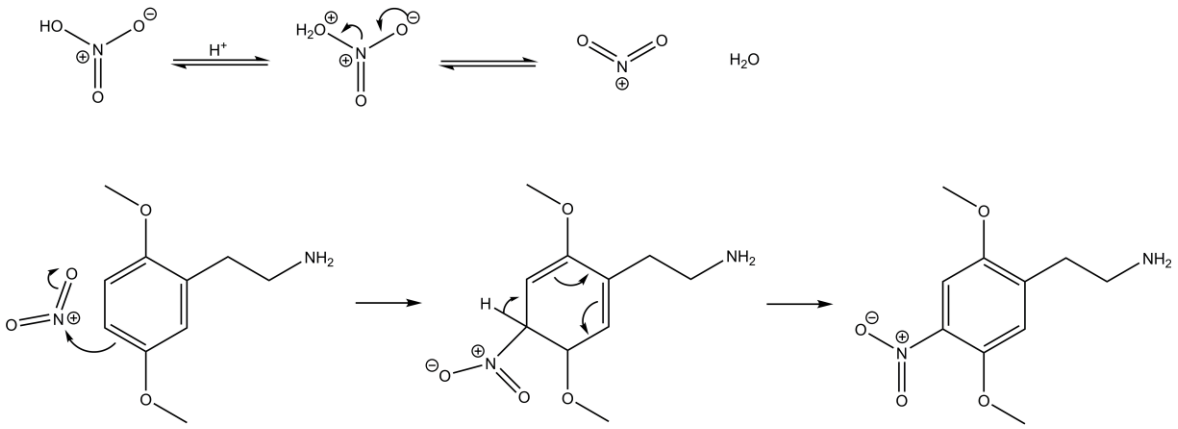

48

Scheme 22 - Reaction mechanism for the nitro addition of **48**

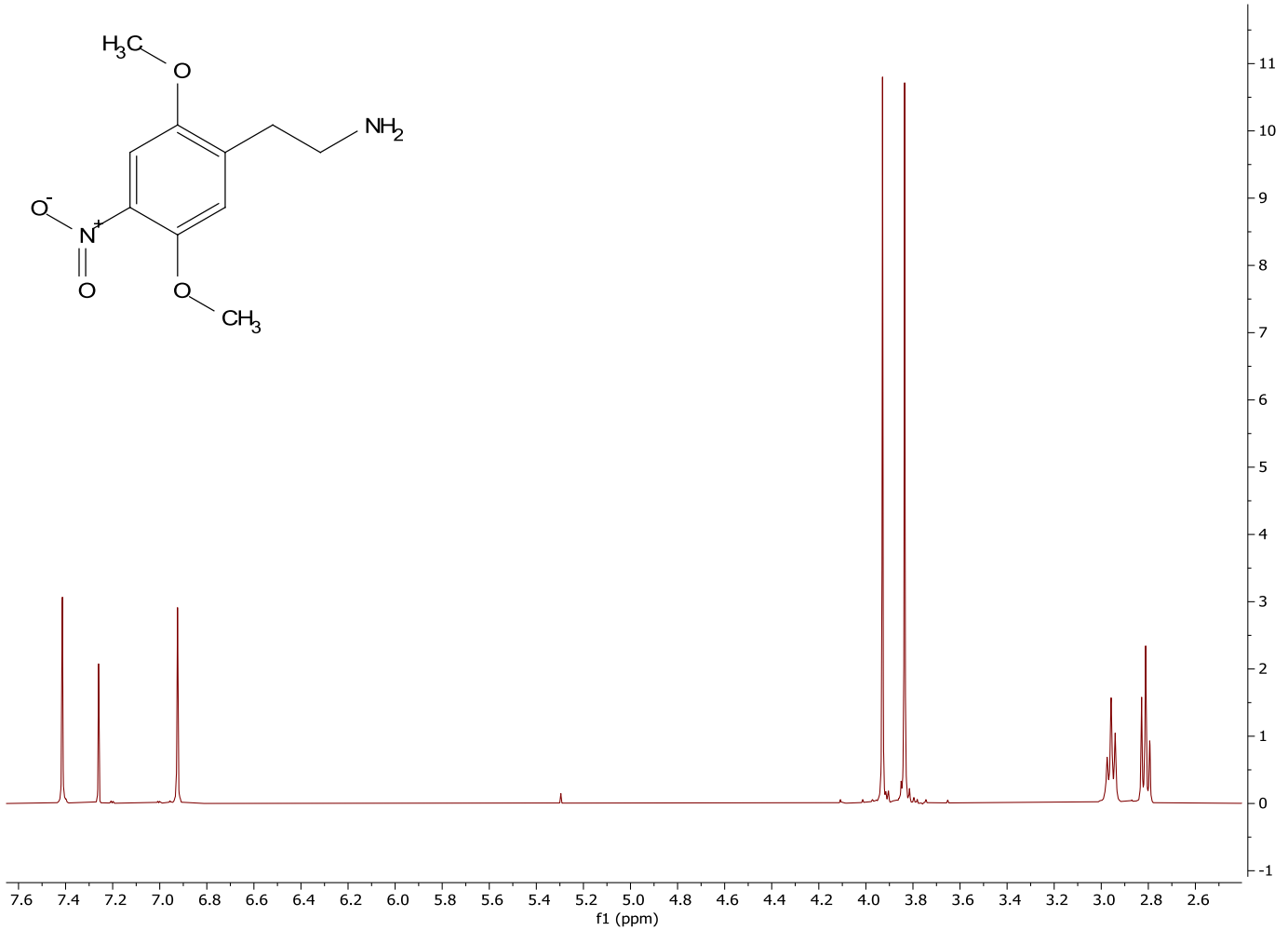

Figure 22 – ^{1}H NMR (400 MHz, $CDCl_3$) of **48.HCl**

3.9 Synthesis of *N*-methoxybenzylphenethylamines (NBOMe's, 49-55)

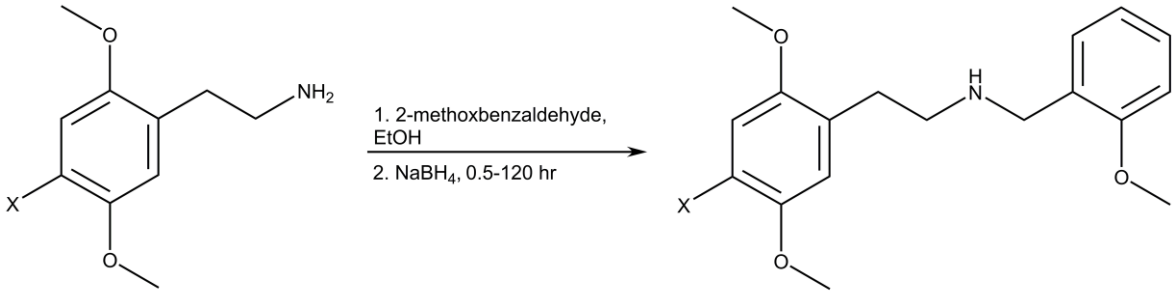

10 **11**

Scheme 23 - Reaction scheme for the synthesis of NBOMe compounds (X = F, Cl, Br, I, Me, Et, NO_2)

The approach of Hansen *et al*.[37] for NBOMe synthesis (Scheme 23) involved forming an imine between the free bases of the hydrochloride and an aldehyde (2-methoxybenzaldehyde or nicotinaldehyde), followed by reduction with $NaBH_4$ (Scheme 24). Repeating this method found that yields obtained compared to Hansen's did not match, for instance with 25C-NBOMe, a 25 % yield was obtained compared to the literature value of 86 %. Whilst performing the column chromatography step, the MeOH concentration in the eluent could increase due to the impurities running off the column quickly as well as decreasing the time for the product to come off. Once the product peak started eluting, a ninhyrdrin solution was used to spot test as it turned the peak a deep purple indicating a secondary amine is present.

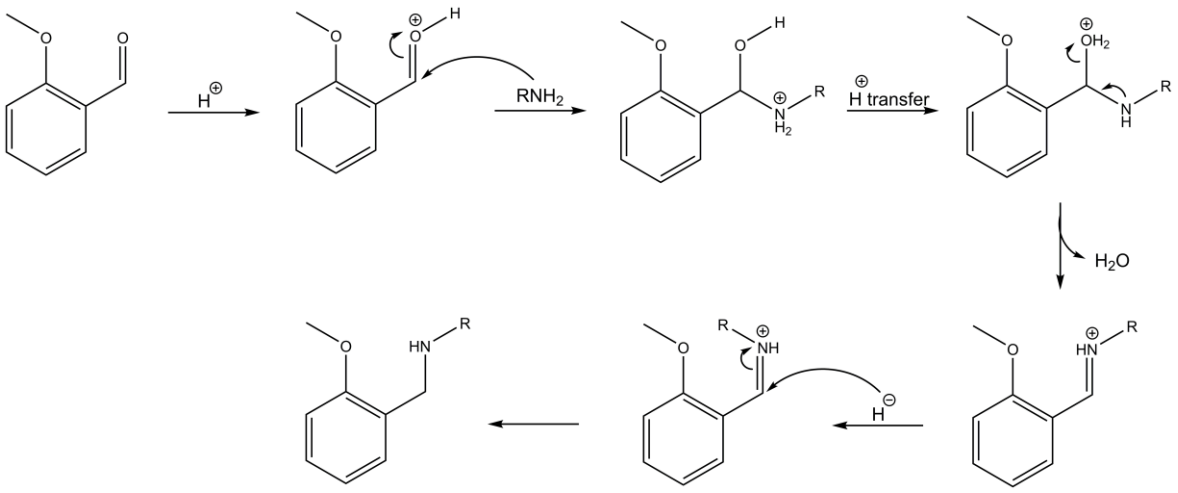

Scheme 24 - Reaction mechanism of a reductive alkylation (RNH_2 = phenethylamine)

The approach of Hansen *et al*.[142] used to suspend the phenethylamine hydrochloride (1 mmol) in EtOH (10 mL) and TEA (1 mmol eq.) with stirring for 5-10 min. After forming the free base, aldehyde (1.1 mmol eq.) was added and left to stir for 0.5 – 120 hr and the reaction was monitored *via* TLC (same as FCC eluent). Sodium borohydride (2 mmol) was added slowly and stirred for 1 hr and then concentrated *in vacuo*. The amber oil was partitioned between DCM and water with the organic layer being extracted, and the aqueous layer extracted further with DCM, dried with $MgSO_4$ and concentrated *in vacuo*. An amber oil was purified *via* column chromatography (DCM-MeOH-NH_3, 98:2:0.04 v/v) with the desired product being on the baseline, which was showed by staining the plate with a ninhydrin solution. After concentrating, the purified free-base was dissolved in EtOH (2 mL) followed by EtOH.HCl (1 M, 2 mL) and finally diluting with Et_2O (50 mL) until crystals formed. The crystals was filtered and dried to obtain pure powders.

When assigning the peaks (Figure 23, Table 8), comparison of **54** made it clear which peaks belonged to each group as the methoxy and methylene groups are both singlets and the aromatic protons are either doublets or triplets. This is consistent with all of the phenethylamine's and their corresponding NBOMe's. However, the fluorine derivatives differentiate from the rest of the halogenated spectra as the aromatic regions of both show doublets instead of singlets for atoms 3 and 6. ^{19}Fluorine has a spin-½ and is 100 % abundant allowing for proton-fluorine

coupling to occur. Thus, the multiplicity of some peaks increased (coupling constant *J*=12 Hz).

Distinguishing between NBOMe derivatives is possible in street samples as fluorine exhibits doublets with hydrogens 3 and 6, whereas increasing the mass of the remaining halogens increases the distance (ppm) between hydrogens 3 and 6. 25C-NBOMe has a difference of 6 ppm, 25B-NBOMe 19 ppm and 25I-NBOMe 47 ppm. However, a more robust method was utilised to distinguish between NBOMe derivatives by using GC-MS (page 52).

All NBOMe derivatives formulated corresponded with the spectral data reported by Hansen *et al*.[142]

Table 8 - Assigned peaks for **54.HCl**

Atom	Chemical Shift (ppm)	Splitting Pattern	*J* coupling constant (Hz)
8	3.02	Triplet	8.24
7	3.22	Triplet	7.33
18	3.78	Singlet	
20	3.82	Singlet	
23	3.89	Singlet	
10	4.24	Singlet	
3	6.87	Singlet	
14	7.03	Triplet of doublets	7.79, 0.92
13	7.09	Doublet	8.24
6	7.34	Singlet	
15	7.39	Doublet	7.56
16	7.46	Triplet of doublets	8.70, 1.83

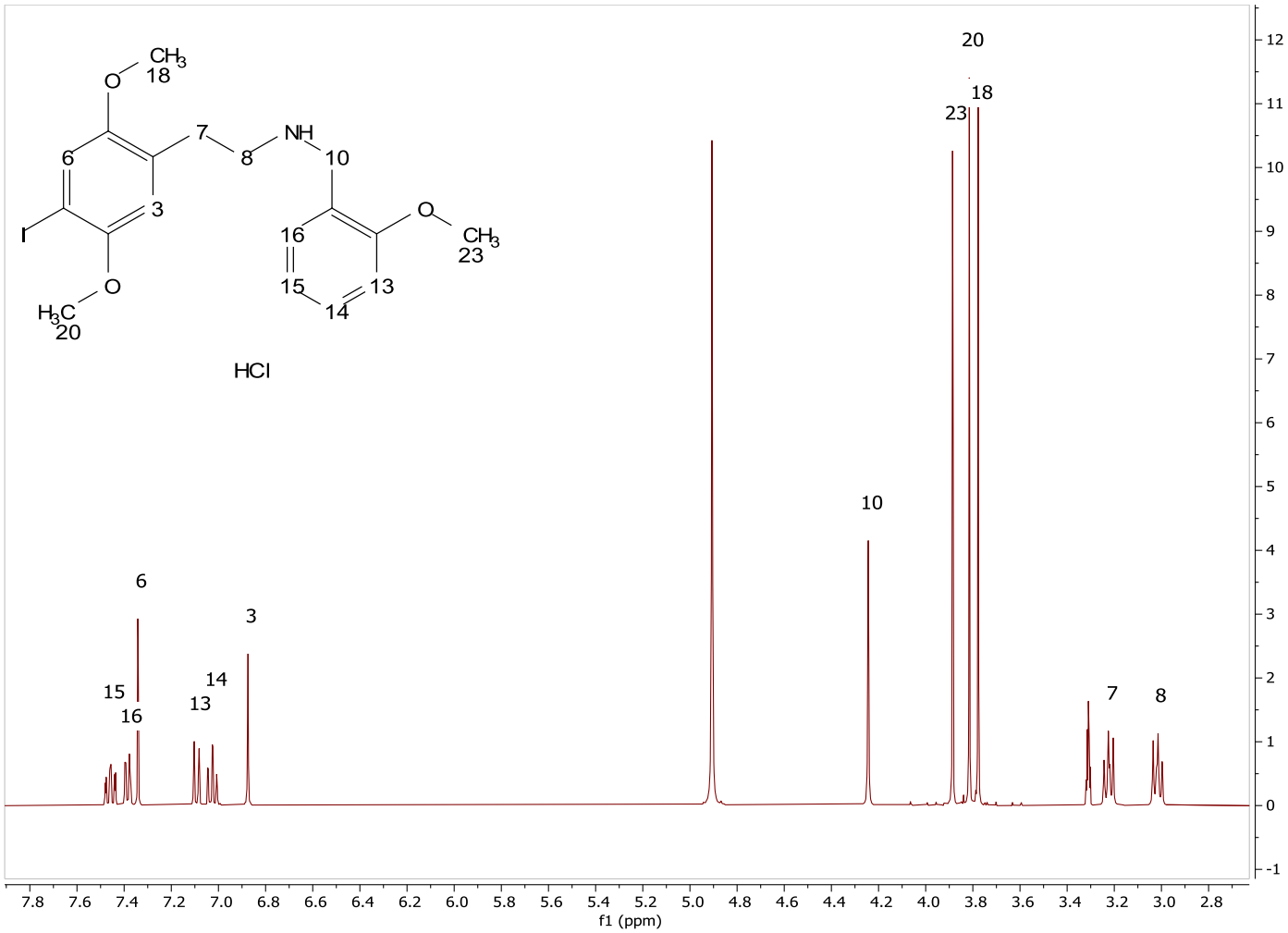

Figure 23 - ^{1}H NMR (400 MHz, CD_3OD) spectrum of **54.HCl**

3.10 Synthesis of *N*-pyridyls (NPyr's, 56-62)

Following the method of reductive amination outlined by Hansen *et al.*[37] it was possible to synthesise hyperpolarisable molecules (Scheme 25). The aldehyde being used must contain a pyridine moiety and not have any substituents *ortho* to the nitrogen (due to steric hindrance preventing binding to the catalyst used for polarisation transfer). The first synthesis attempt used 4-pyridinecarboxaldehyde as this fits the polarising criteria, but the reaction was unsuccessful; TLCs taken during the imine formation step showed no indication of product formation. An alternative route looked at nicotinaldehyde, as again this would fit the criteria for SABRE derived polarisation. The synthesis used **28** as a starting reagent and was successful, affording **56** in 3 % yield. When looking at the properties of these compounds and their ability to polarise, it became possible that PET imaging compounds could be replaced. Seven isomers were synthesised to see if the molecular size and electronics of these compounds would alter their ability to polarise. To obtain the hydrochloride salt, twice the amount of ethanolic HCl was used due to there being two nitrogen regions.

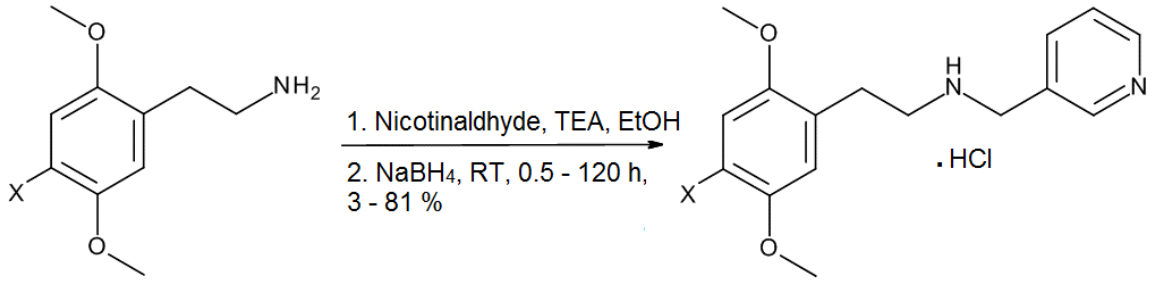

10 **24**

Scheme 25 - Reaction scheme for the synthesis of NPyr compounds (X = F, Cl, Br, I, Me, Et, NO_2)

Upon inspection of the data for this series of compounds, a lot of similarities were observed. This includes when running the ^{1}H NMR for the free base of these compounds. One difference that was observed with **61** between the free-base and the HCl salt was the ethylene side chain. As seen in Figure 24 and Table 9, two triplets (peaks 7 and 8) changed to a multiplet (Figure 25). The N-H peak is also observed (circa 4.66 ppm) within the free-base ^{1}H NMR spectrum and this was consistent between all of the compounds formulated in this series.

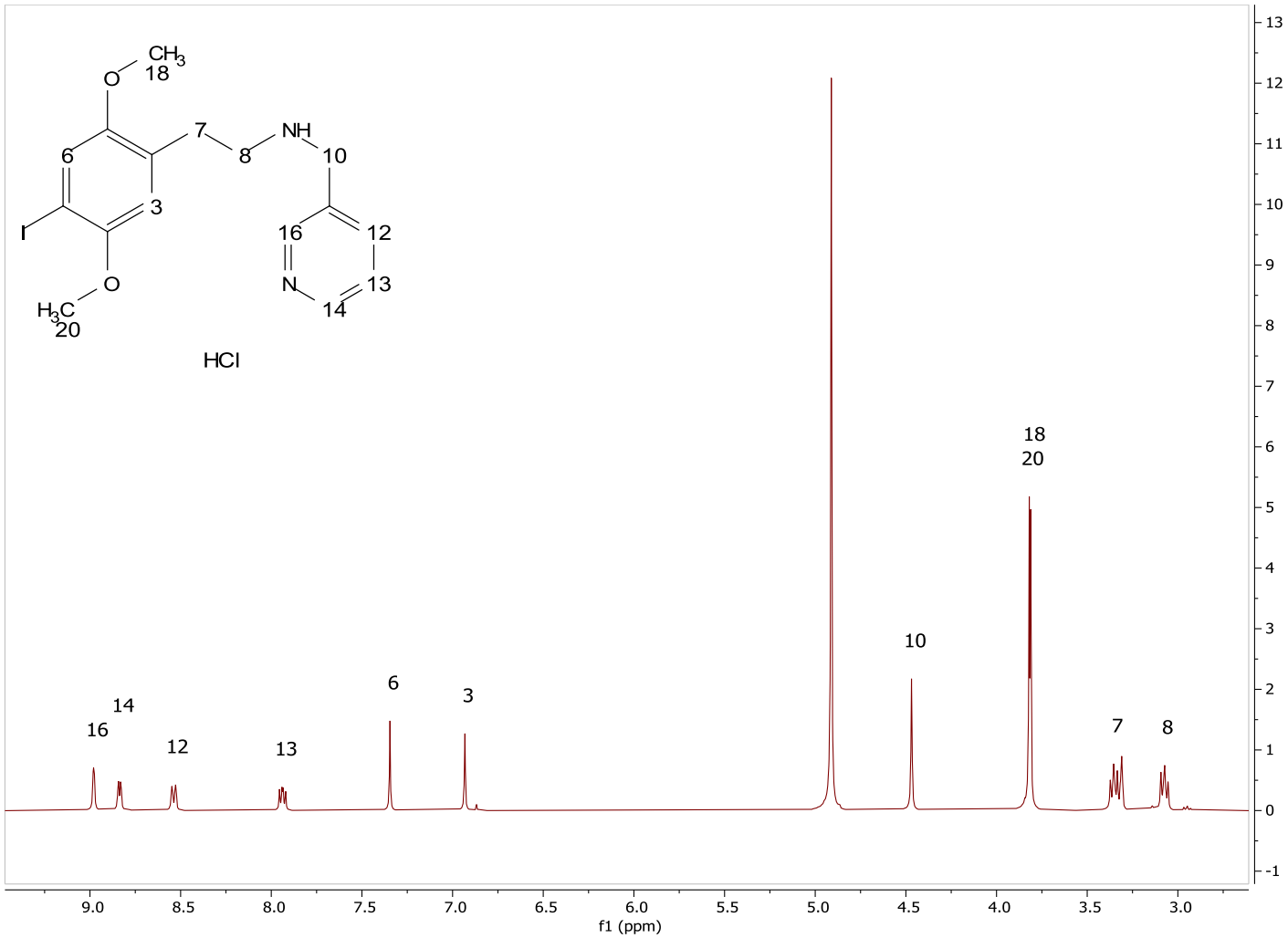

Figure 24 - ^{1}H NMR (CD_3OD, 400 MHz) spectrum of **61.HCl**

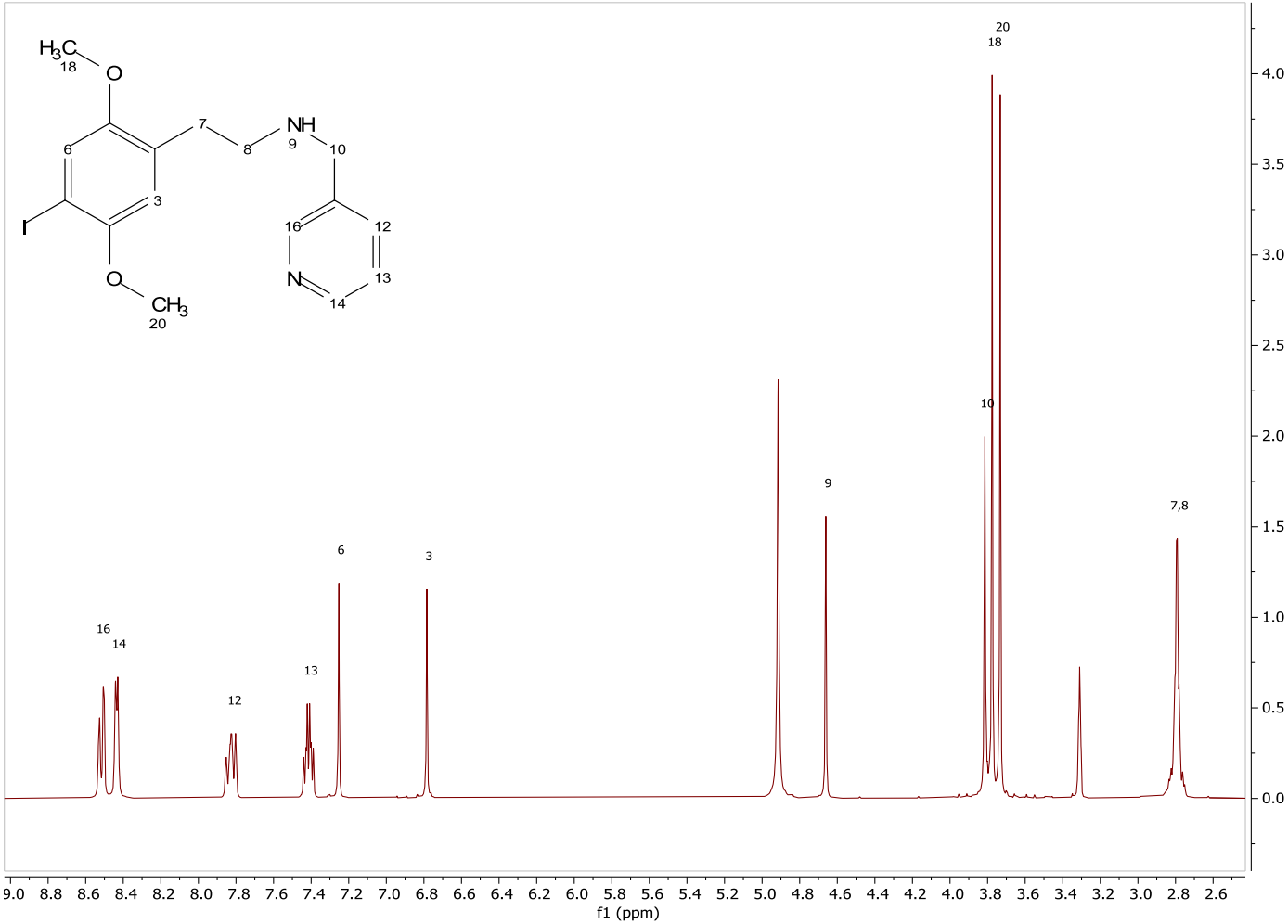

Figure 25 - ^{1}H NMR (CD_3OD, 400 MHz) spectrum of **61**

Table 9 - Assigned peaks for **61.HCl** from the ^{1}H NMR spectrum

Atom	Chemical shift (ppm)	Splitting pattern	*J* coupling constant (Hz)
8	3.07	Triplet	7.33
7	3.35	Triplet	8.24
18	3.81	Singlet	
20	3.82	Singlet	
10	4.47	Singlet	
3	6.93	Singlet	
6	7.35	Singlet	
13	7.94	Doublet of doublets	4.58, 8.24
12	8.54	Doublet	8.24
14	8.84	Doublet	4.58
16	8.98	Singlet	

3.11 Synthesis of *N*-fluoropyridyl derivatives (NPF's, 63-69)

Following the reductive amination reported by Hansen *et al.*[37], this series of compounds used 5-fluoronicotinaldehyde as the starting reagent (Scheme 26). Again, it possesses a polarisable tether group (pyridyl) and allows for ^{19}F NMR SABRE to be employed. Olaru *et al.*[131] discuss the scope of fluorinated containing ligands in medical applications as contrasting agents for MRI by increasing their signal intensity using SABRE. The advantage of these fluorine-containing compounds is that there is no fluorine present in biological tissue, so there is no background signals when performing MRI. Their MRI results showed the increase in intensity after being polarised to be 75-fold, which shows the potential in this technique to be looked at in clinical investigations and molecular imaging. Therefore, this range of compounds were synthesised as they could have great potential to be used in molecular imaging.

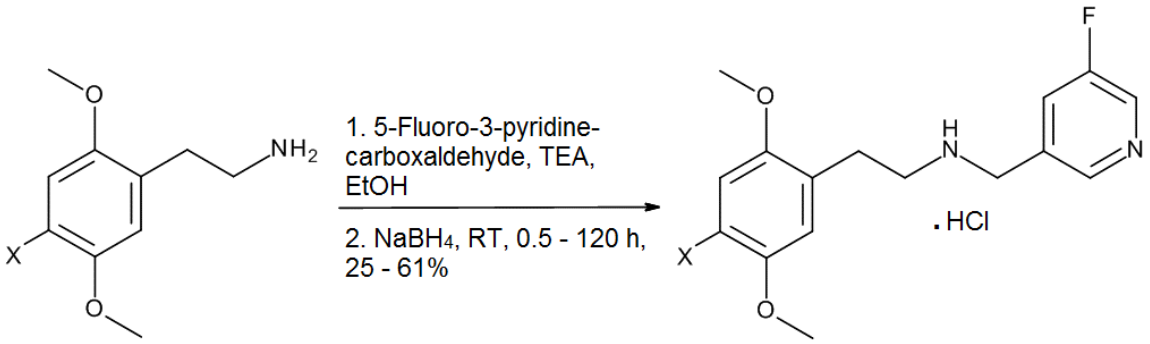

10 25

Scheme 26 - Reaction scheme for the synthesis of NPF compounds (X = F, Cl, Br, I, Me, Et, NO_2).

The range of NPF compounds exhibited the same splitting patterns in both ^{1}H and ^{13}C NMR spectra. When looking at the aromatic region of 25I-NPF (Figure 26, Table 10), the protons on the pyridyl show a doublet ($^{3}J_{HH}$ = 9 Hz) and two singlets. Hydrogen 14 experiences the effect of deshielding from the adjacent nitrogen.

The carbon NMR of **68** (Figure 27, Table 11) show five *J*-coupling constants which is consistent with ^{13}C-^{19}F coupling values and six singlets (Figure 28). The shift observed from C5 (85.1 ppm) is constant throughout the iodinated compounds due to the shielding effect moving it further upfield. By increasing the electronegativity of C5, this shifts it further downfield.

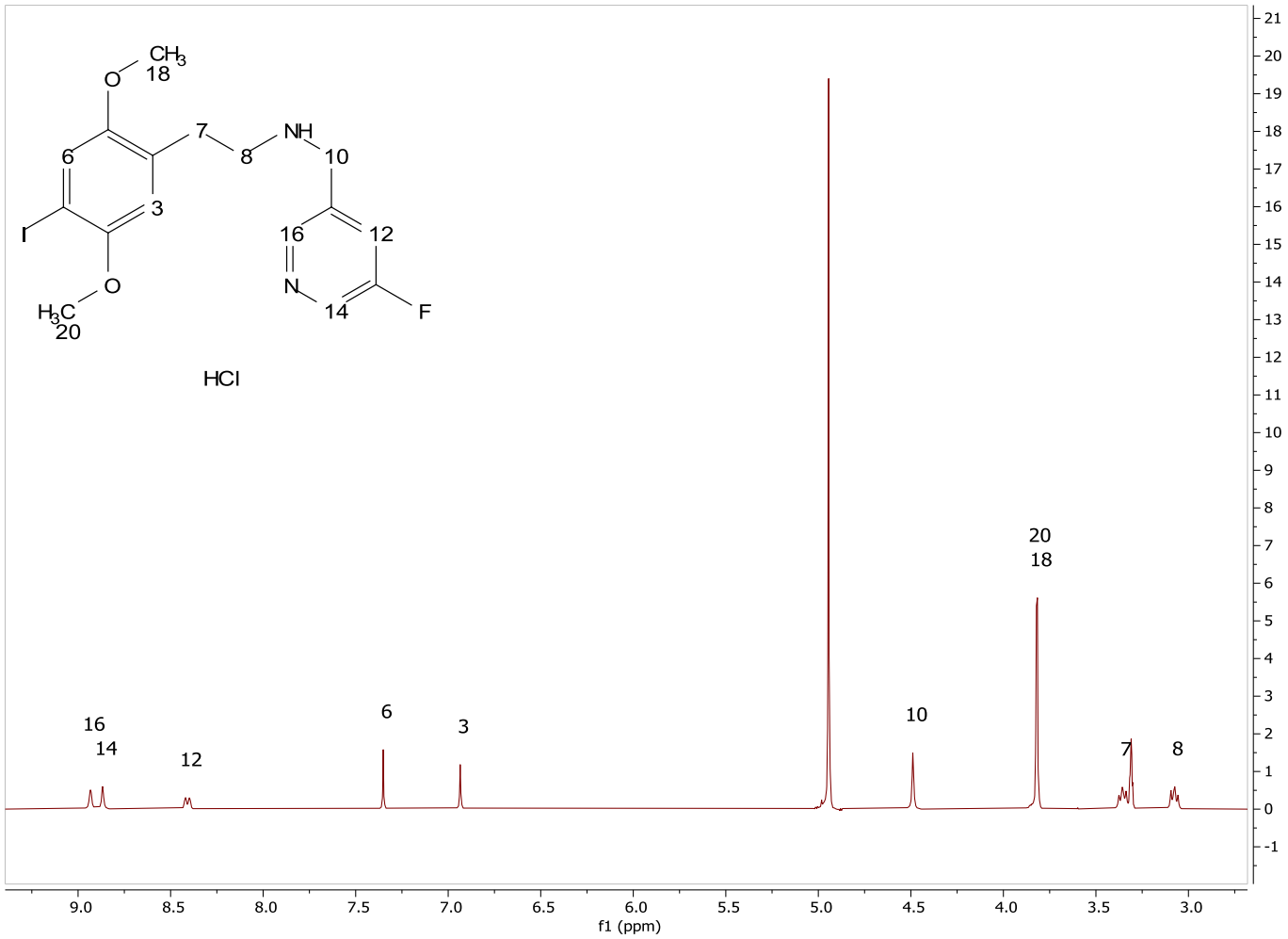

Figure 26 - ^{1}H NMR (CD_3OD, 400 MHz) spectrum of **68.HCl**

Table 10 - Assigned peaks for **68.HCl** for the ^{1}H NMR data

Atom	Chemical Shift (ppm)	Splitting pattern	*J* coupling constant (Hz)
8	3.08	Triplet	7.33
7	3.36	Triplet	8.24
18	3.82	Singlet	
20	3.82	Singlet	
10	4.49	Singlet	
3	6.94	Singlet	
6	7.35	Singlet	
14	8.41	Doublet	8.59
12	8.87	Singlet	
16	8.93	Singlet	

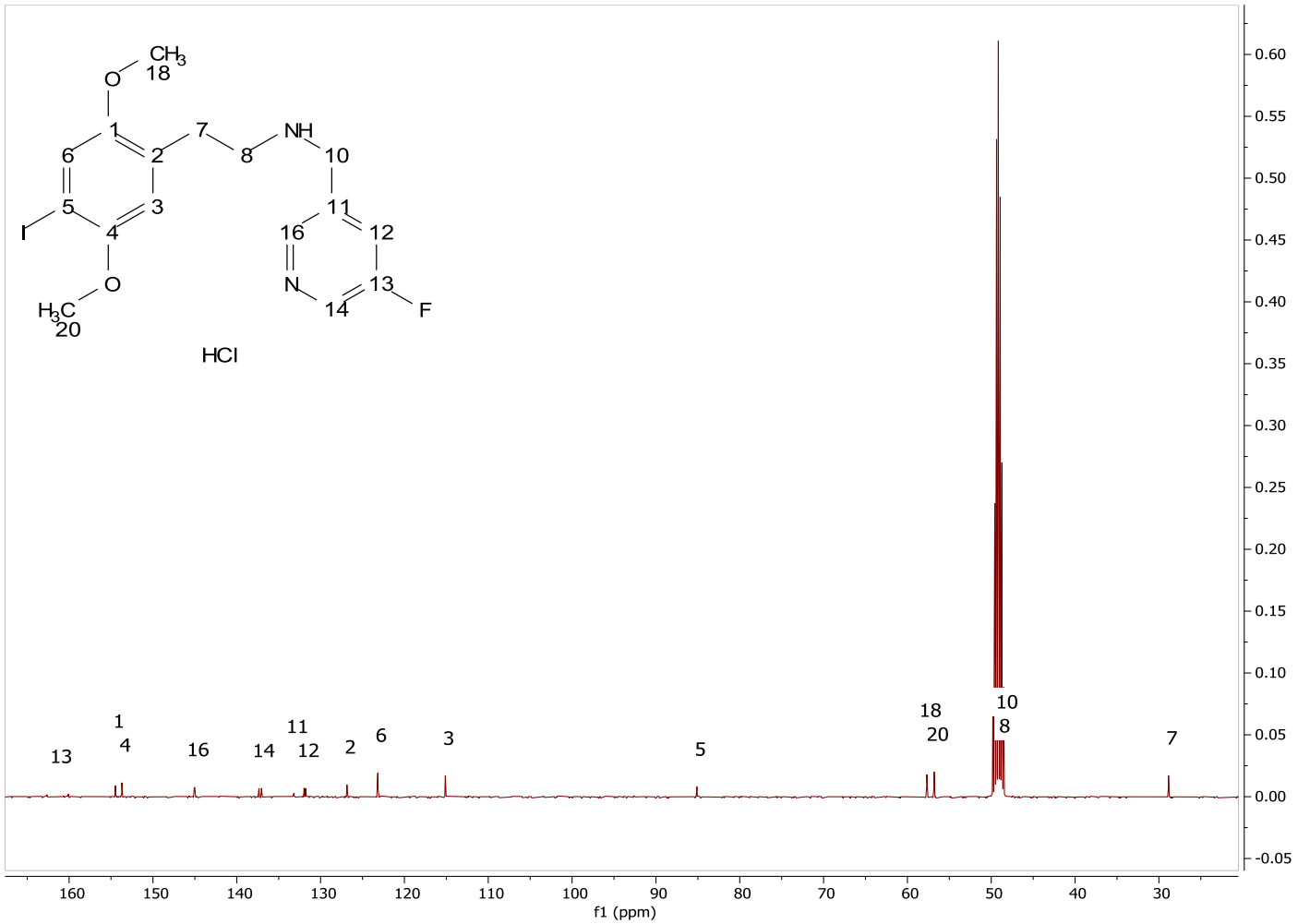

Figure 27 - ^{13}C NMR (CD_3OD, 101 MHz) spectrum of **68.HCl**

Table 11 - Assigned peaks for **68.HCl** for the ^{13}C NMR data

Atom	Chemical Shift (ppm)	Splitting pattern	*J* coupling constant (Hz)
7	28.9	Singlet	-
10	48.5	Singlet	-
8	48.8	Singlet	-
20	56.8	Singlet	-
18	57.7	Singlet	-
5	85.1	Singlet	-
3	115.1	Singlet	-
6	123.2	Singlet	-
2	126.9	Singlet	-
12	131.9	Doublet	19.3
11	133.2	Doublet	5.4
14	137.2	Doublet	29.7
16	145.0	Doublet	4.1
4	153.7	Singlet	-
1	154.5	Singlet	-
13	161.4	Doublet	257

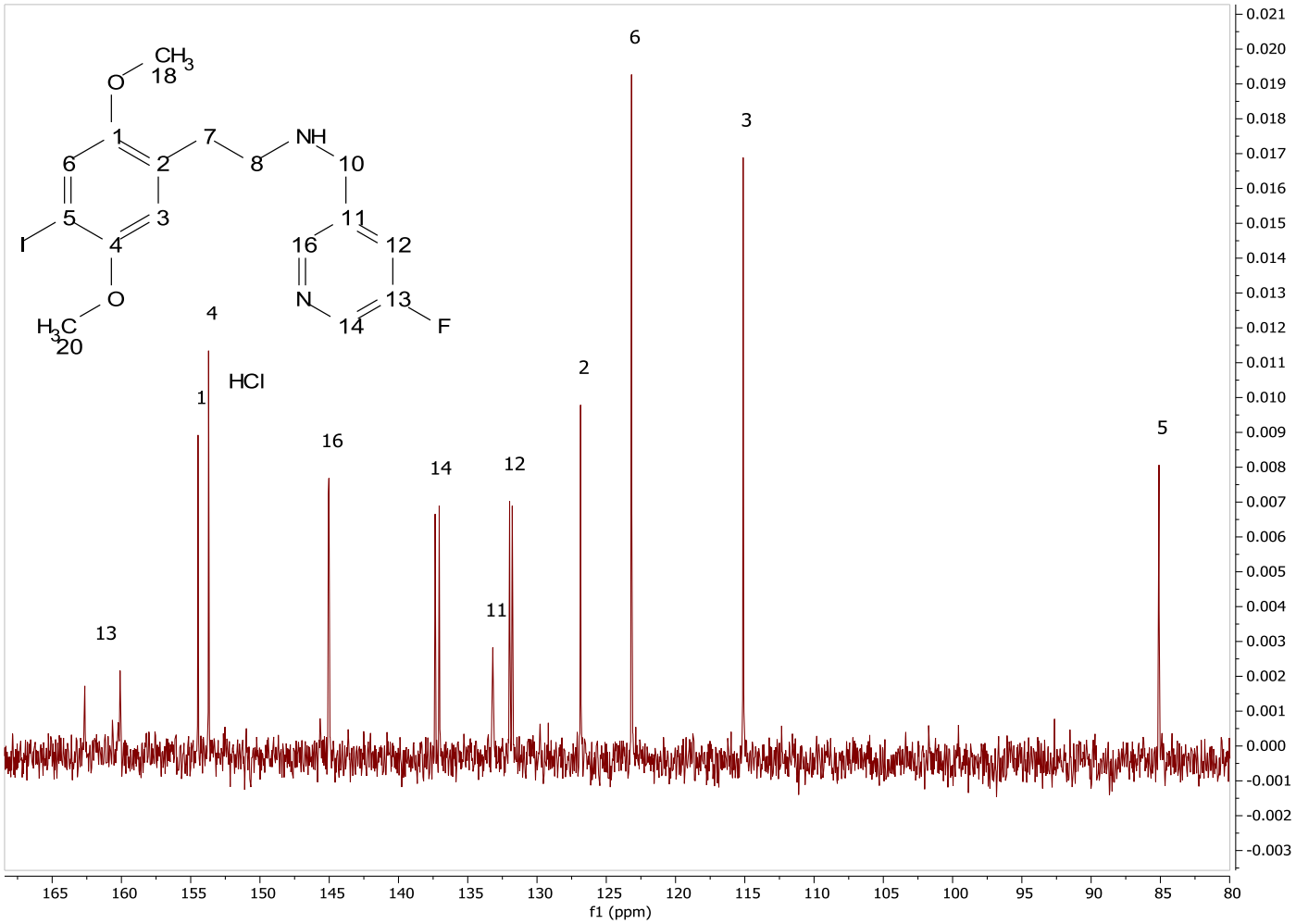

Figure 28 - ^{13}C NMR (CD_3OD, 101 MHz) spectrum of the aromatic region of **68.HCl**

3.12 Synthesis of *N*-methoxypyridyls (NPOMe's, 70-76)

The final series of compounds synthesised using Hansen's methodology was the NPOMe's (Scheme 27). This was our primary focus due to their resemblance to NBOMe's, which would allow comparison to the PET imaging counterparts.

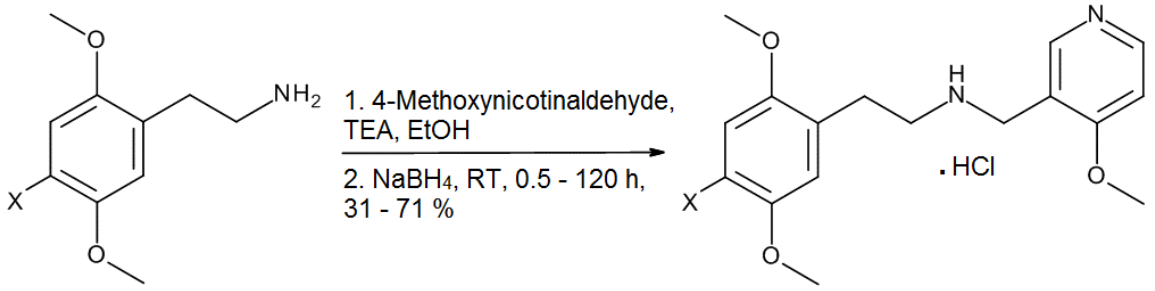

10 **26**

Scheme 27 - Reaction scheme for the synthesis of NPOMe compounds (X = F, Cl, Br, I, Me, Et, NO_2)

The ^{1}H NMR of **75** shows three aromatic peaks and five aliphatic peaks as shown in Figure 29 (Table 12). This was consistent throughout the NPOMe derivatives apart from 25F-NPOMe, where hydrogens six and three appear as doublets due to the fluorine coupling.

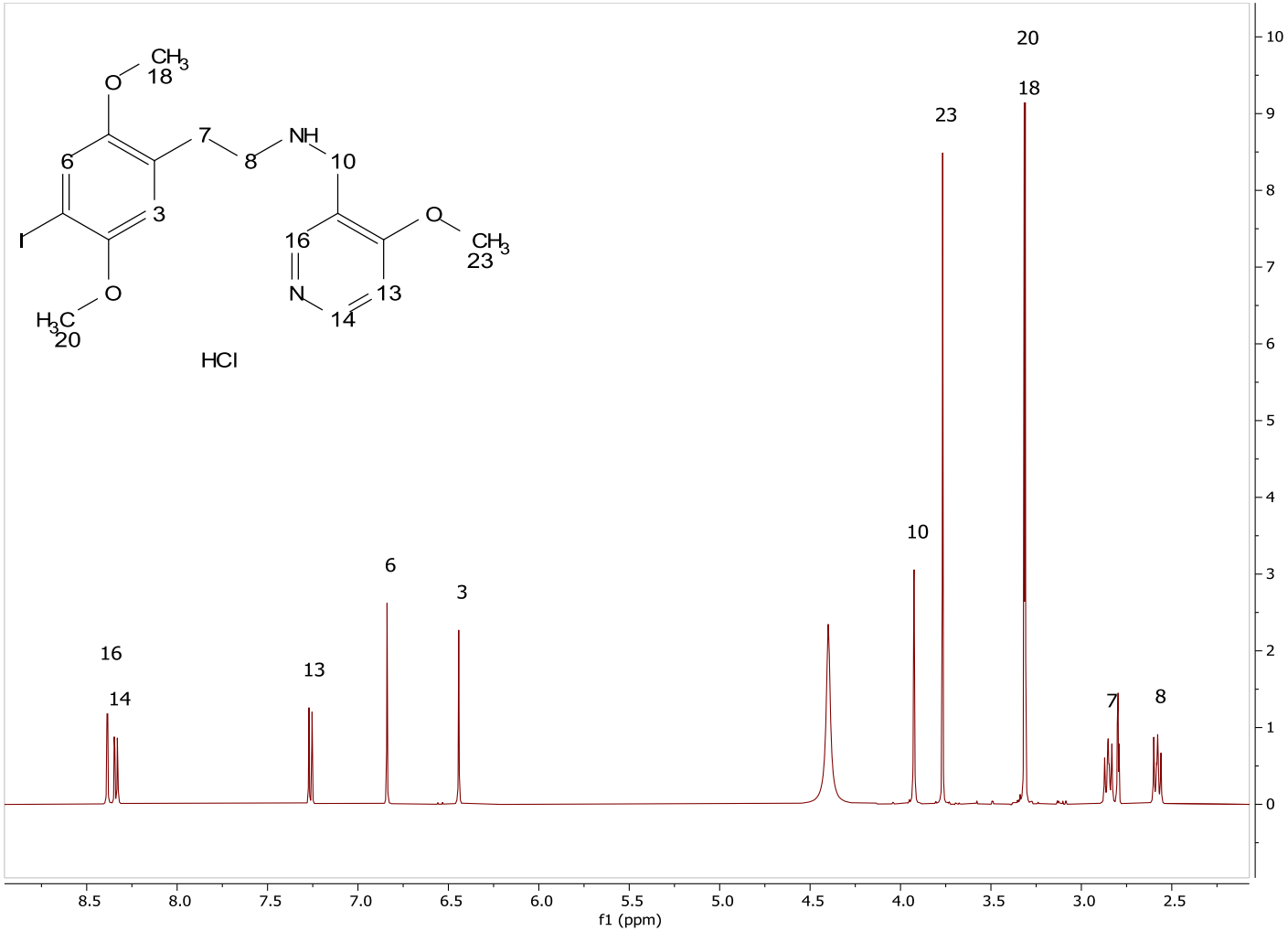

Figure 29 - ^{1}H NMR (CD_3OD, 400 MHz) spectrum of **75.HCl**

Table 12 - Assigned peaks for **75.HCl** for the ^{1}H NMR data

Atom	Chemical Shift (ppm)	Splitting Pattern	*J* coupling constant (Hz)
8	3.09	Triplet	6.4
7	3.36	Triplet	7.6
18	3.82	Singlet	
20	3.83	Singlet	
23	4.28	Singlet	
10	4.44	Singlet	
3	6.96	Singlet	
6	7.35	Singlet	
13	7.78	Doublet	6.9
14	8.85	Doublet	6.9
16	8.90	Singlet	

3.13 GC-MS

Comparing **47** and **54**, the mass spectra are very different as the fragments seen in **47** are not all seen in **54** (peak at m/z=207 is background noise). This can be seen in the fragmentation pathways in Figure 30 and Figure 31. The GC-MS mass spectra of **47** are shown in Figure 32a and was compared to the spectrum of **54** (c - GC-MS chromatogram from Cayman Chemicals).

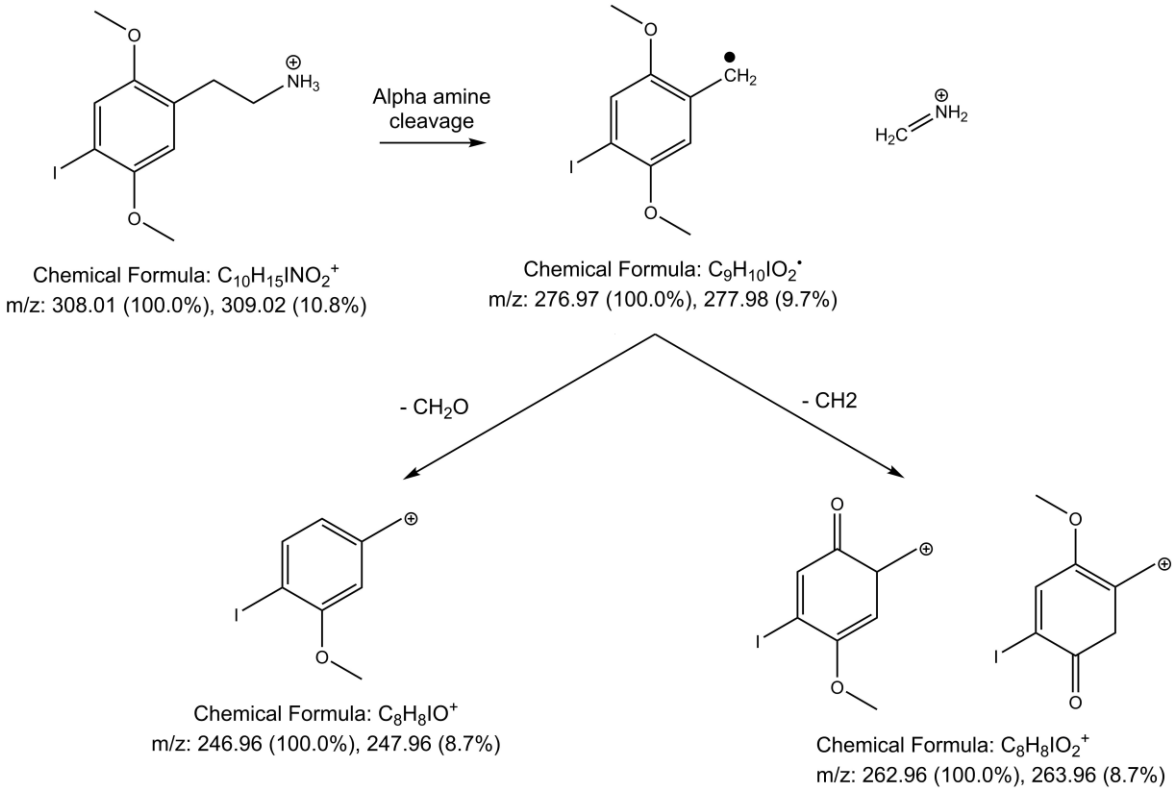

Figure 30 – GC-MS fragmentation pathway of **47**

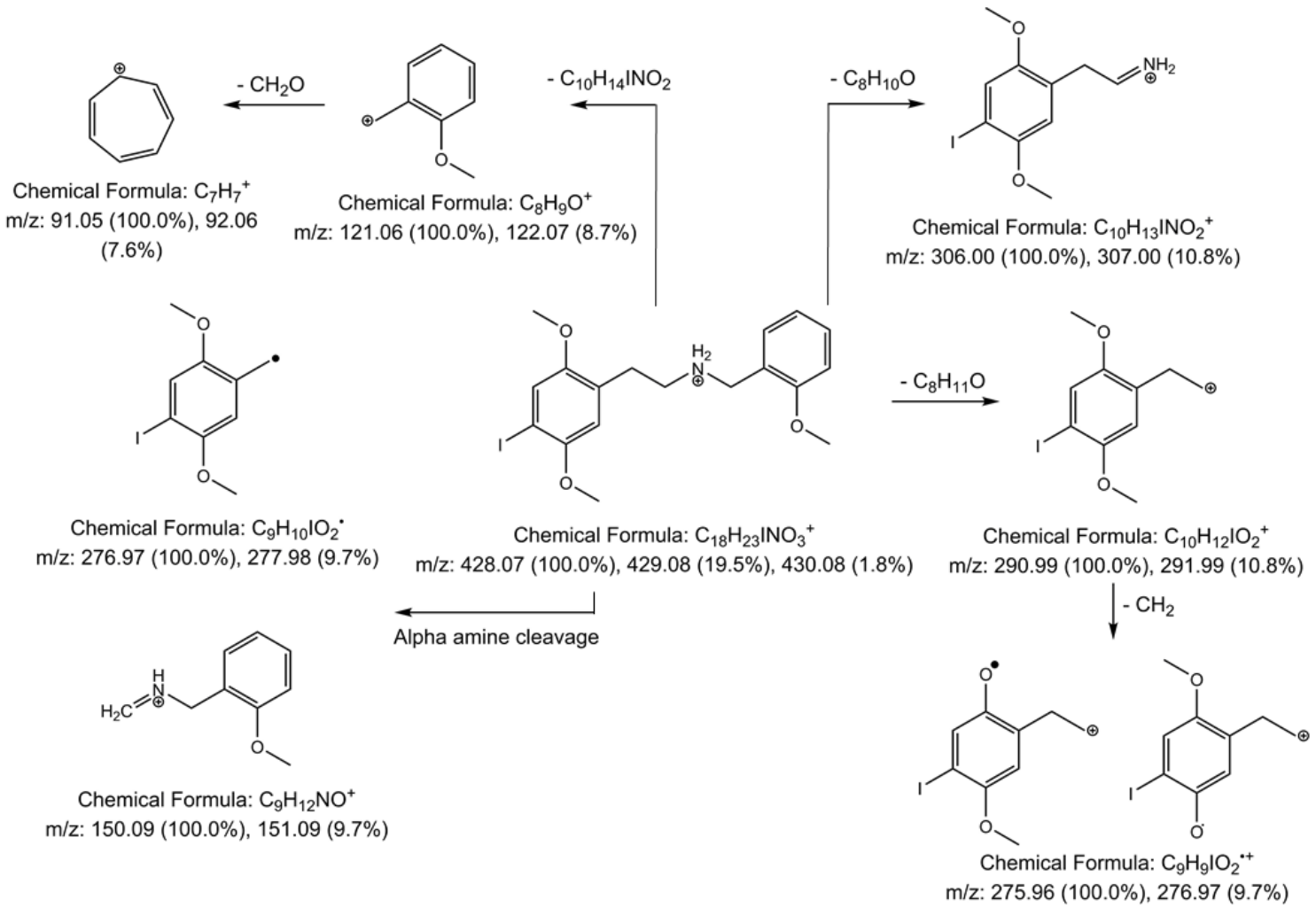

Figure 31 – GC-MS fragmentation pathway of **54**

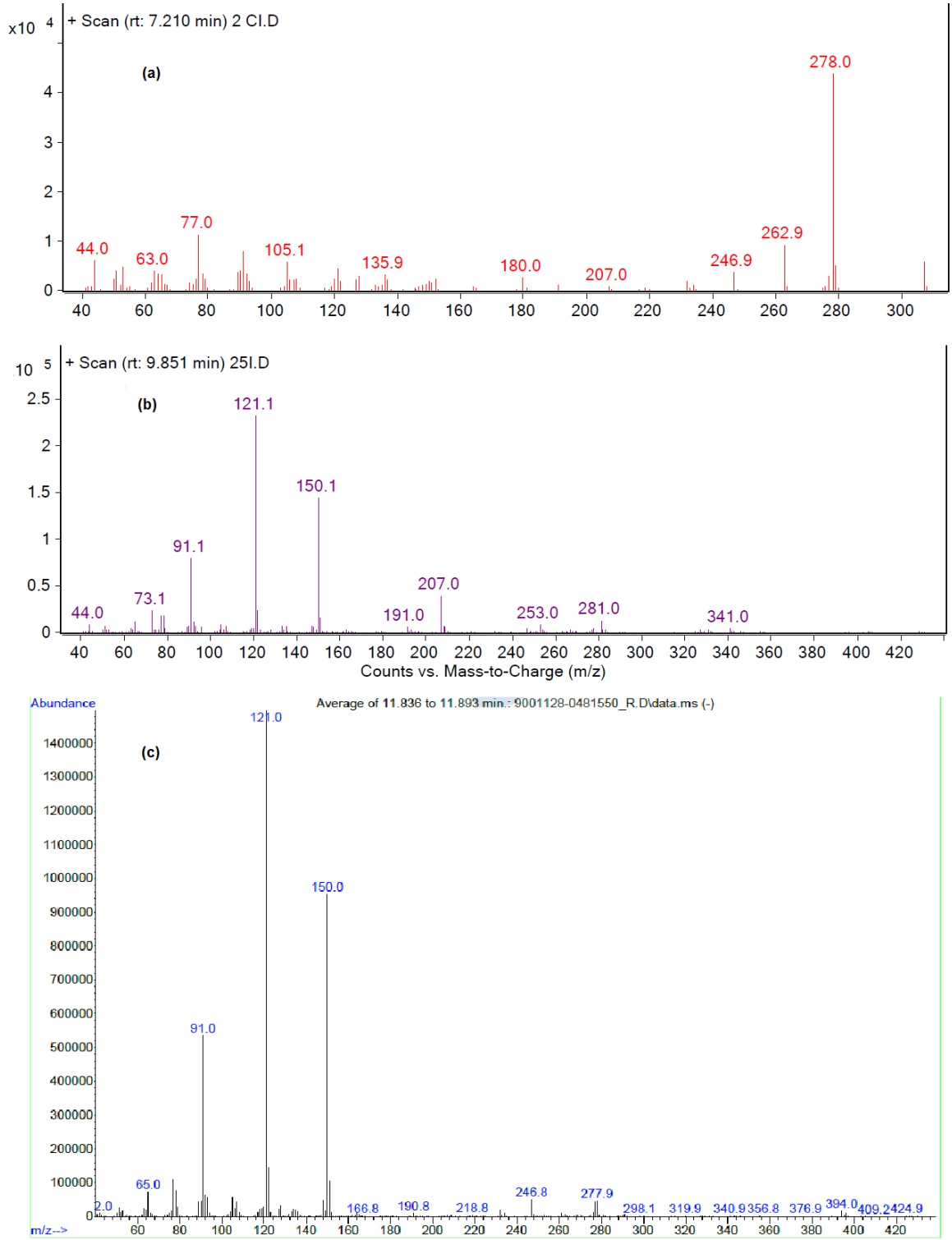

Figure 32 - GC-MS spectra of **47** (a), **54** (b) and Cayman Chemicals' **54** (c)

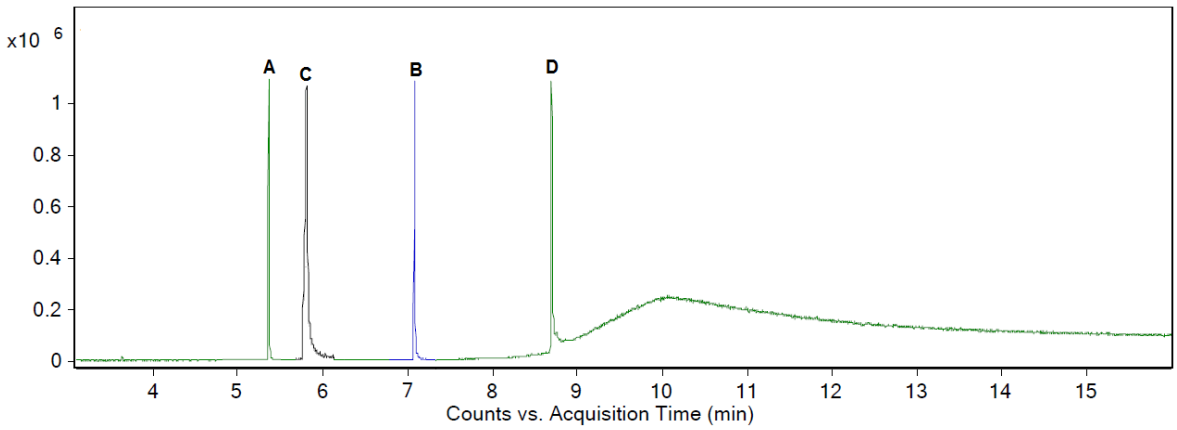

Figure 33 – Chromatogram of 25F-NBOMe (**53**, D) with subsequent starting materials

When looking at retention times between each reaction step, observing purity of the final NBOMe is possible as each compound has a different retention time. For example with 25F-NBOMe, there were three subsequent reactions with the retention times (Figure 33) being 5.368 min (**42,** A), 7.065 min (**43**, B), 5.802 min (**44**, C) and 8.692 min (**53**, D).

When looking at the derivatives of NBOMe's, the same fragmentation pattern occurs. Therefore, there are two ways to differentiate between them being retention times and isotopic ratios. The size of the halogen affects the retention times as the smallest compound being the 25F-NBOMe elutes at 8.692 min and progressively increases to 9.225 min (25C), 9.506 min (25B) and 9.851 min (25I). When looking at isotopic ratios and abundancy (%), ^{19}fluorine and ^{127}iodine is 100 %, ^{35}chlorine 75 % and ^{37}chlorine is 25 %, ^{79}bromine 50 % and ^{81}bromine 50 %. The mass spectra of compounds possessing chlorine and bromine will therefore be different due to M+2 peaks being observed in a 3:1 or 1:1 ratio respectively. The fluorine and iodine can be differentiated by the m/z, as some peaks will have a difference of m/z=100 due to the mass difference of the halogens.

3.13.1 NBOMe calibration analysis

Eight analogues of NBOMe's were all injected into the GC-MS and ran individually (1 mg mL^{-1}) to determine retention times (R_t) before being run as a mixture. Table 13 shows the retention times of the individual runs.

Table 13 - GC retention times for eight NBOMe analogues

	NBOMe	Retention times (R_t)
A	25F	8.629
B	25H	8.710
C	25D	8.862
D	25E	9.052
E	25C	9.369
F	25B	9.818
G	25I	10.426
H	25N	10.614

As there are no co-eluting peaks, method validation was performed using SIM mode with eicosane as an internal standard (R_t – 7.234 min). SIM mode was used as the base peak for all the NBOMe's was m/z 121. By using this method, it reduces the concentration required to obtain sharp peaks. Figure 34 displays a chromatogram of the NBOMe mixture at a concentration of 20 µg mL^{-1}. Street samples typically ranging from 300 µg – 1 mg. Therefore, by minimising the concentration of the analyte, an accurate concentration can be generated from a street sample. But as street samples are not necessarily 100% pure, and the dangers which can arise from consumption, a lower limit of detection (LOD) and limit of quantification (LOQ) would increase the accuracy of the drug concentration within the street sample.

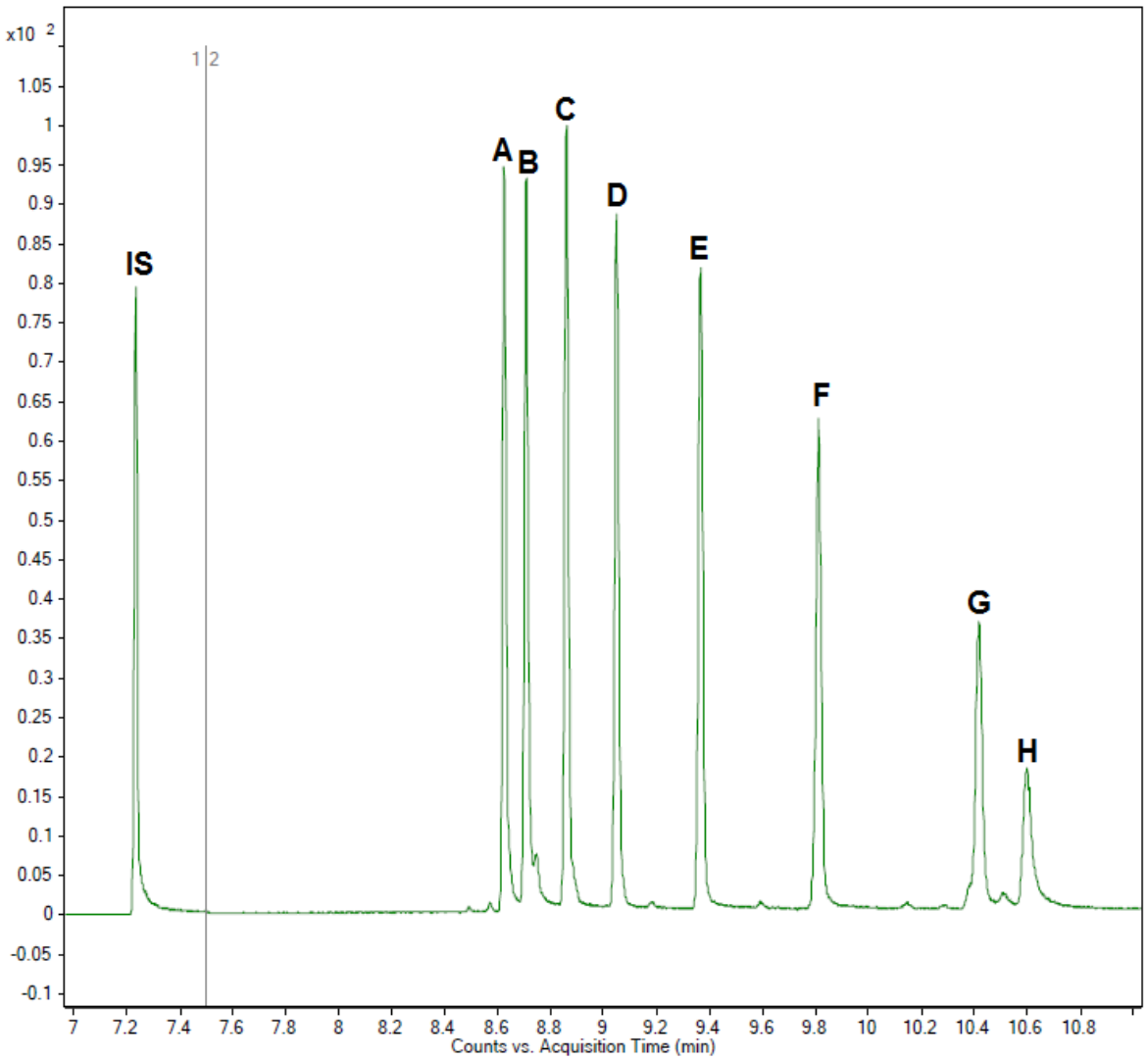

Figure 34 – GC-MS validation chromatogram of an 8 NBOMe mixture (IS = eicosane)

The developed method was validated individually for a mixture of the NBOMe derivatives. All correlation coefficients are above an acceptable level (>0.99) for the compounds, with limits of detection (LOD) and limits of quantification (LOQ) values shown in Table 14. LOD values range between 6.20 – 10.75 μg mL^{-1} and LOQ values ranging from 18.77 – 32.57 μg mL^{-1}. All, but 25H-NBOMe, relative standard deviation percentages fall below an acceptable 4% and can also be seen in Table 14.

What these results enable is the ability to accurately measure the concentration of NBOMe's within a mixture. At present, this is only applicable for a powdered sample. However, most cases of NBOMe's are found within a blotter. Further work details this GC-MS method being applied to the detection of NBOMe's within a spiked blotter, 3.13.2.

Table 14 - Validation values for the NBOMe's including LOD, LOQ and %RSD for all calibration standards

NBOMe	R_t (mins)	r^2	LOD (μg mL^{-1})	LOQ (μg mL^{-1})	Precision (%RSD) n=6				
					10 μg mL^{-1}	15 μg mL^{-1}	20 μg mL^{-1}	25 μg mL^{-1}	30 μg mL^{-1}
25F	8.63	0.995	7.36	22.29	3.30	0.42	1.07	1.14	1.29
25H	8.71	0.995	6.20	18.77	3.55	7.30	4.62	6.48	7.66
25D	8.86	0.995	6.81	20.63	3.39	1.29	1.75	2.30	2.97
25E	9.05	0.995	7.69	23.32	0.64	1.18	1.60	2.10	2.73
25C	9.37	0.993	7.68	23.27	0.69	1.24	1.70	2.26	2.97
25B	9.82	0.995	6.67	20.21	0.54	1.08	1.53	2.05	2.70
25I	10.43	0.994	8.90	26.97	0.36	0.76	1.13	1.55	2.09
25N	10.61	0.992	10.75	32.57	0.13	0.41	0.72	1.09	1.52

3.13.2 Street sample analysis

25C, 25B and 25I are the most commonly found substances from the range of NBOMe's in blotters, so street samples were prepared (as individuals) and tests followed using the blotter dry and after extraction.

Using the dried blotters, presumptive colour testing (Marquis and Liebermann's) and ATR-FTIR analysis provided limited results. During the colour test it was found that due to the high acidity of the testing solutions, this interfered with the colour output (Table 15). The bee patterned blotter had a yellow and black print (Figure 35) which leached into the well, and in some cases turned the solution brown after being left for more than 15 mins. With ATR-FTIR analysis, a spectrum was recorded for both types of impregnated blotters as well as a blotter with no impregnation as a control. An example of ATR-FTIR analysis is shown in Figure 36 with spectrums of the unadulterated blotting paper (A), 25C-NBOMe (B) and the blotter adulterated with 25C-NBOMe (C). When compared, no change could be seen due to the sensitivity with this technique when using microgram scale. Therefore, qualitative analysis is possible using the blotters but the variant is what kind of print is on the paper. As the patterned paper used was white, black and yellow, the correct colours upon the addition of the presumptive testing solution was only visible on the white area with the yellow and black leaching either into the solution or the remainder of the blotter after 5 mins.

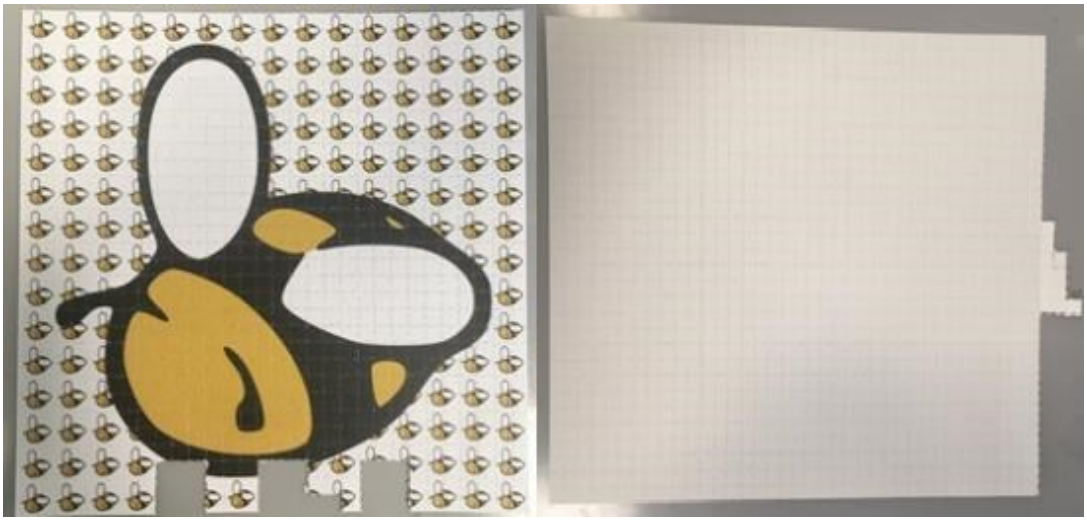

Figure 35 – Blotting paper used for street sample analysis

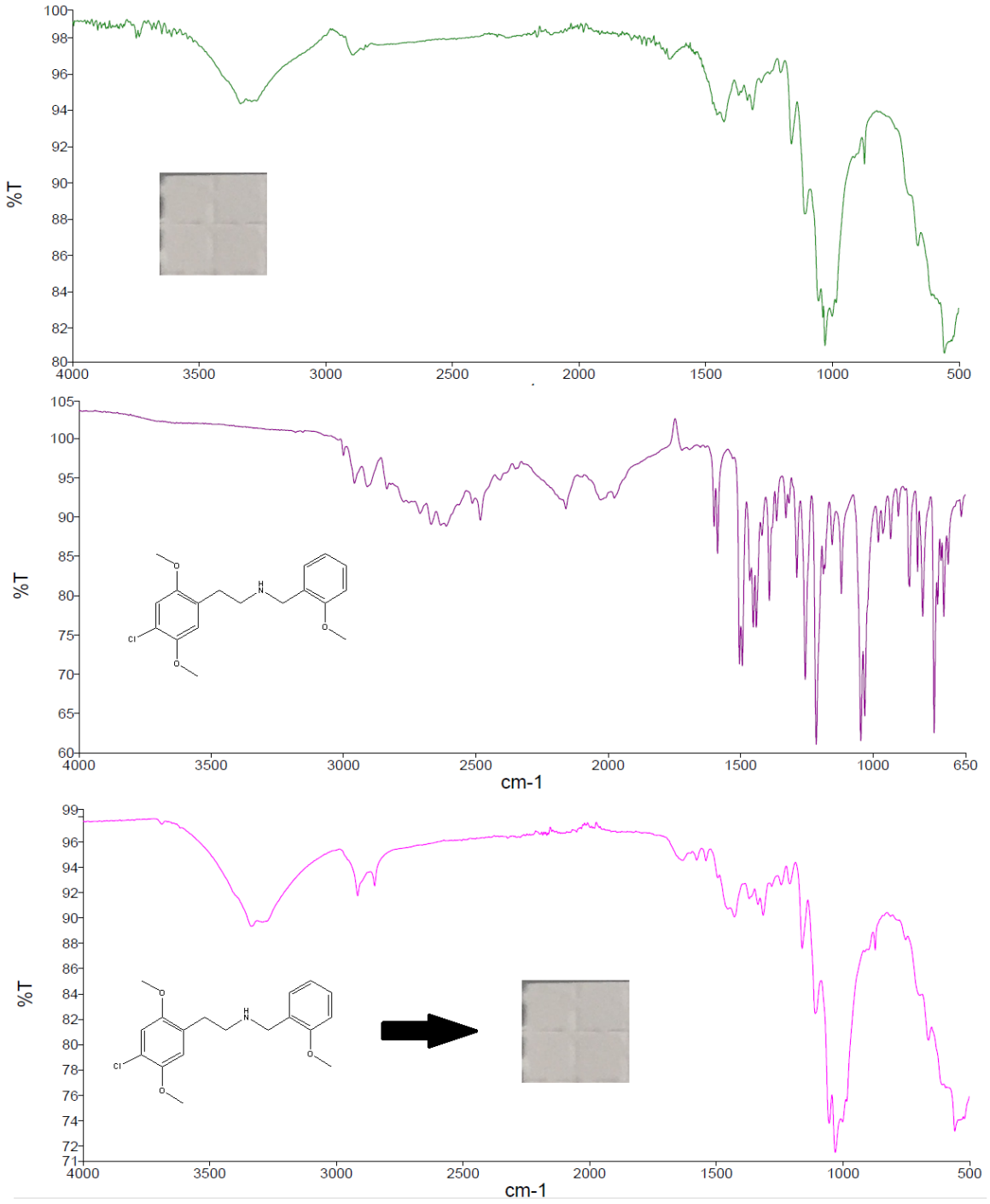

Figure 36 – ATR-FTIR spectra of an unadulterated blotter (A), 25C-NBOMe (B) and a blotter adulterated with 25C-NBOMe.

Table 15 - Presumptive colour test of impregnated blotters

		Marquis		Liebermann's	
		Immediate colour change	Colour change after 5 mins	Immediate colour change	Colour change after 30 mins
25C-NBOMe	Control	Peach	Peach	Dark green	Yellow
	Blotter (plain)	Yellow blotter, yellow solution	Brown blotter, brown solution	Green blotter, clear solution	Yellow blotter, clear solution
	Blotter (bee)	Brown solution	Brown solution	Yellow solution	Yellow solution, brown leaching from blotter
25B-NBOMe	Control	Yellow	Yellow	Purple	Clear with purple ring
	Blotter (plain)	Yellow blotter	Yellow blotter	Slight yellow solution	Slight yellow solution
	Blotter (bee)	Red blotter	Red solution from leaching	Yellow blotter	Yellow solution from leaching
25I-NBOMe	Control	Green	Green	Brown	Brown/yellow
	Blotter (plain)	Green blotter, green solution	Green blotter, green solution	Brown blotter	Bown blotter, orange leaching from blotter
	Blotter (bee)	Green blotter, green solution	Green blotter, green solution	Brown blotter	Bown blotter, orange leaching from blotter

After extraction, presumptive colour testing (Marquis and Liebermann's) and GC-MS analysis provided both qualitative and quantitative results. With the presumptive colour testing results (Table 16), this showed the correct colour changes with each drug; the colour output was transparent but due to the lower concentrations this was expected.

Table 16 - Presumptive colour test output after extraction

		Marquis		Liebermann's	
		Immediate colour change	Colour change after 5 mins	Immediate colour change	Colour change after 15 mins
25C-NBOMe	Control	Peach	Peach	Dark green	Yellow
	Blotter (plain)	Faint yellow	Clear	Clear	Clear
	Blotter (bee)	Faint peach	Clear	Clear	Clear
25B-NBOMe	Control	Yellow	Yellow	Purple	Clear with purple ring
	Blotter (plain)	Yellow	Yellow	Purple	Clear with purple ring
	Blotter (bee)	Yellow	Yellow	Purple	Clear with purple ring
25I-NBOMe	Control	Green	Green	Brown	Brown/yellow
	Blotter (plain)	Green	Green	Brown	Brown
	Blotter (bee)	Green	Green	Brown	Brown/yellow

Upon extraction and dilution to the suitable concentration range, which fit within the calibration plot, GC-MS analysis provided both qualitative and quantitative results. A separate run of 300 µg mL^{-1} 25B-NBOMe, 500 µg mL^{-1} 25C-NBOMe and 800 µg mL^{-1} 25I-NBOMe with eicosane (250 µg mL^{-1}) was run against the extracted solutions to compare the extraction method performance against the output from the calibration plot (Table 17). The dilution stocks from each blotter set was concentrated *in vacuo* and diluted with 1 mL MeOH to be the absolute extraction concentration.

Table 17 – Average mass recovered after blotter extraction

		R_t (mins)	Mass recovered from dilutions (%)	Precision (%RSD) n=9	Mass recovered against control (%)	Precision (%RSD) n=3
25C-NBOMe	Blotter (plain)	9.359	80	10.09	33	15.67
	Blotter (bee)	9.361	65	17.12	25	29.88
25B-NBOMe	Blotter (plain)	9.808	49	7.38	19	7.29
	Blotter (bee)	9.805	38	10.24	13	3.93
25I-NBOMe	Blotter (plain)	10.406	81	3.98	19	3.55
	Blotter (bee)	10.408	63	34.64	10	2.81

Extraction from the plain blotting paper was higher in all three drugs for both the diluted and concentrated. This suggests there is a possibility of the drug interacting with the ink or the kind of paper used, as the plain blotting paper looked more porous which could lead to an increase in extraction rates. Examples are shown in Figure 37 of the chromatograms of 25C-NBOMe blotters. The plain patterned blotter (A) in the chromatogram shown extracted 410 µg (82 %), whereas the bee patterned blotter (B) extracted 348 µg (70 %)

Extension of the validation of NBOMe's has enabled an accurate and precise method to analyse NBOMe's within a street sample. After performing analytical techniques of the raw samples, this concluded that it is not possible to determine what is present within a blotter. Therefore, samples which have been spiked with an NBOMe derivative must be extracted, with MeOH, before analysis. The described post extraction techniques can be used both qualitative and quantitatively.

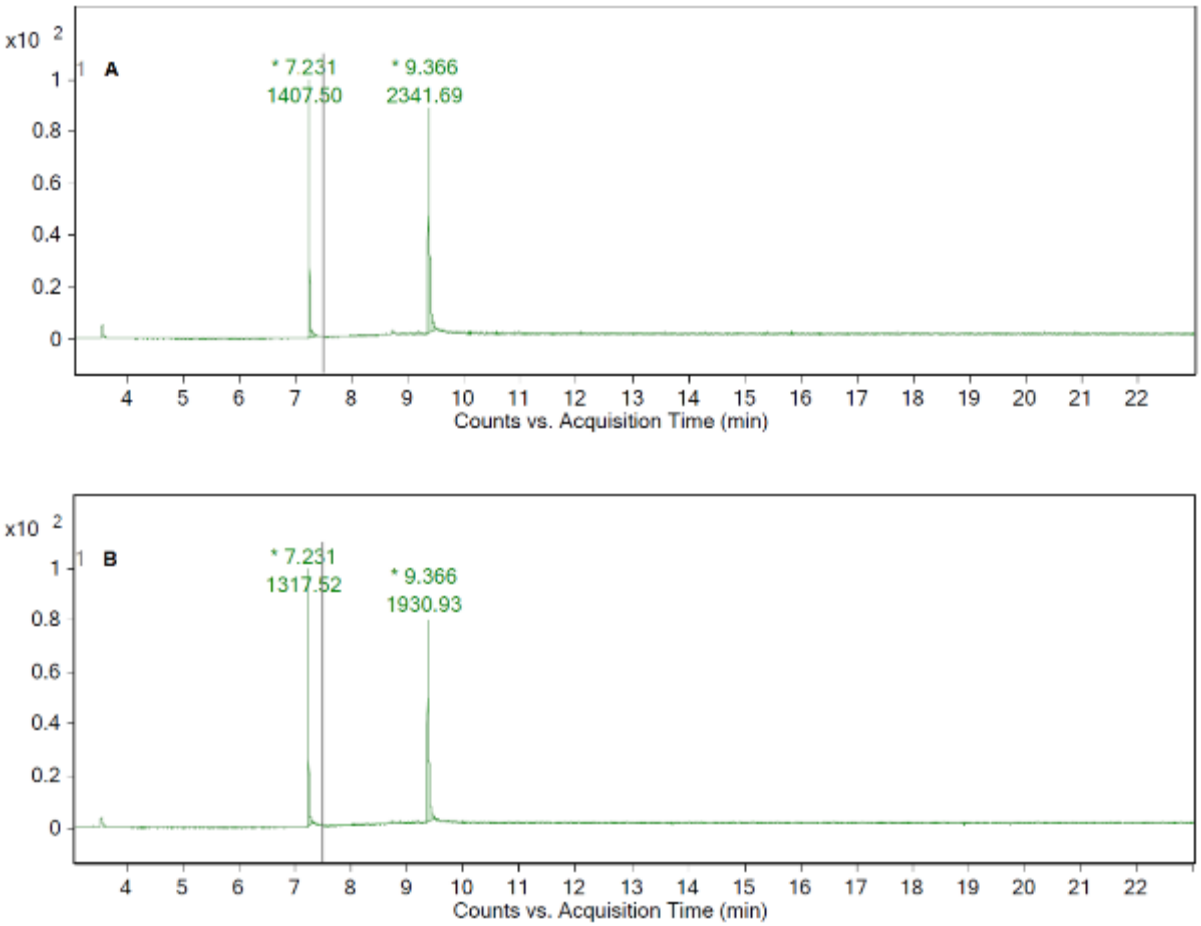

Figure 37 – GC-MS chromatograms of the extraction of 25C-NBOMe from a plain patterned blotter (A) and a bee patterned blotter (B).

4 Chapter 4 - Hyperpolarisation

4.1 Introduction

Hyperpolarisation techniques have been increasingly useful to overcome the sensitivity issues involved with NMR and MRI. Methods involving hyperpolarized magnetic resonance spectroscopy (MRS) have been successful for ^{1}H,[98] ^{13}C,[147] ^{15}N[148] and ^{19}F[149] detection. The current techniques include dynamic nuclear polarisation (DNP),[150] spin exchange optical pumping (SEOP)[151] and *para*hydrogen-induced polarisation (PHIP).[92] An example of an advance in hyperpolarised MR imaging utilises SEOP to create hyperpolarised xenon and helium gas to image lung space to visualise lung diseases such as cystic fibrosis.[152] Using this technique, all 23 branches of the lungs can be imaged which contrasts with computerised tomography, which can image the first six only. A further example utilises DNP to obtain images of prostate cancer. This approach uses ^{13}C-labelled pyruvate,[153] which is metabolised through the Kreb's cycle to acetyl CoA. Hyperpolarised pyruvate is used as a biomarker to acquire ^{13}C images of the colon in order to provide images of this tissue to better inform diagnosis.

The focus of this chapter is the employment of the non-hydrogenative form of PHIP, SABRE.[102] SABRE does not require the molecule of interest to be directly hydrogenated to facilitate polarisation transfer, unlike PHIP that does. The source of polarisation in SABRE is *para*hydrogen, a spin isomer of di-hydrogen. *Para*hydrogen is a nuclear singlet and has a total spin of zero and so is not visible in an NMR experiment. However, by breaking the symmetry of *para*hydrogen, such as at a metal centre (typically iridium) through the formation of hydrides, the polarised state becomes unlocked and can be transferred to other spin-1/2 nuclei through J-coupling that has been established between *para*hydrogen-derived hydrides and the spin-1/2 nuclei of ligands bound *trans* to them. Both the *para*hydrogen-derived hydrides and ligands freely exchange at the metal centre, enabling polarisation to be built up in the bulk. This creates a pool of hyperpolarised free-ligand, which can be interrogated using radio-frequency pulses to obtain the representative, significantly enhanced, NMR spectrum.

This powerful analysis technique can be used in forensic applications. In the last two years, derivatives of fentanyl[99] (**77**) and benzylpiperazines[100] (**81**) (Figure 38 and

Figure 39 respectively), have both been polarised. It is noteworthy that these fentanyl and BZP derivatives have been modified to include a pyridyl function, in order to create a ligation point to the metal centre. This interaction is needed to facilitate polarisation transfer from *para*hydrogen derived hydrides to the derivatives highlighted via the established *J*-coupling.

Current methods of analysis of fentanyl analogues include Raman spectroscopy, immunoassays, LC-MS/MS and low-field NMR in conjunction with high-field NMR. Raman spectroscopy has been utilized in combination with density-functional theory (DFT) towards detection of trace samples. Surface-enhanced Raman spectroscopy proved to give an enhancement factor of $\geq 1.6\times10^5$, which was endowed by proximity to silver or gold nanoparticles.[154] Immunoassay has also been investigated as a technique for the detection of fentalogues, but none of the ELISA (Enzyme-Linked ImmunoSorbent Assay) kits evaluated proved to have sufficient cross-reactivity towards the *N*-acyl and piperidine-modified fentalogues studied.[155] LC-MS/MS has been utilized to detect 24 fentanyl derivatives and metabolites in whole blood in under 14 min screening time with a LOD of 0.05 ng mL^{-1} and lower limit of quantification (LLOQ) of 0.1 ng mL^{-1}.[156] Developments in fentanyl analysis has been shown by Elbardisy *et al.*[157] where an electrochemical approach was taken. A combination of LC-MS with a dual-diode array and electrochemical (amperometric) detector achieved simultaneous detection of heroin, fentanyl and 10 fentalogues. However, with a LOD of 0.41 µg mL^{-1} and a LOQ of 1.39 µg mL^{-1}, this technique is not as sensitive as that shown by Strayer *et al.*[156]

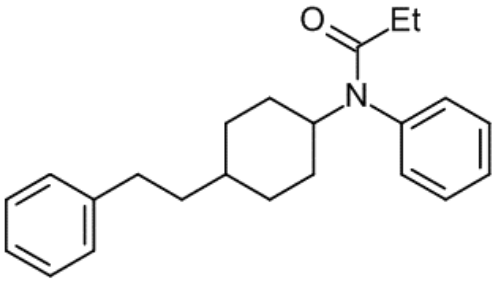

77

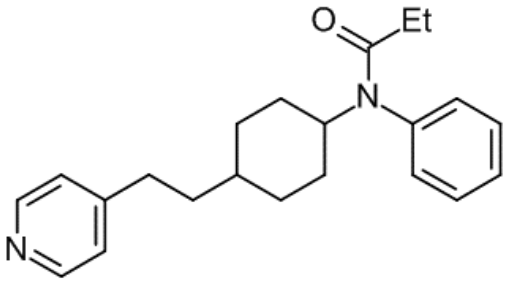

78

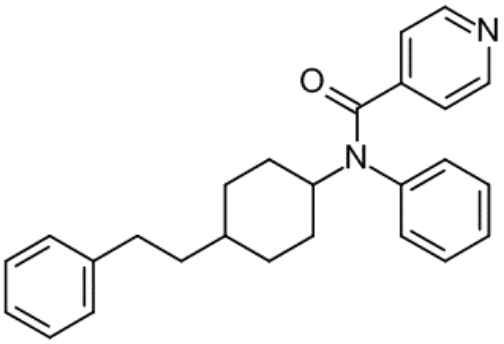

79

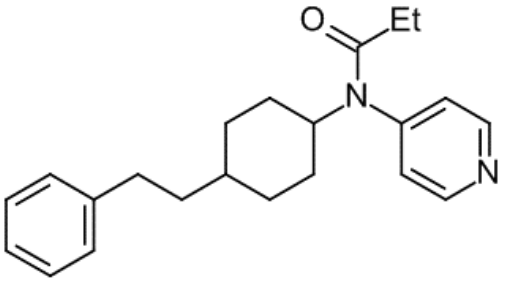

80

Figure 38 – Fentanyl (**77**) and the pyridyl-fentanyl analogues prepared by Robertson *et al.*[99] for hyperpolarisation studies; *N*-phenyl-*N*-(1-(2-(pyridin-4-yl)ethyl)piperidin-4-yl)propionamide (**78**), *N*-(1-phenethylpiperidin-4-yl)-*N*-phenylisonicotinamide (**79**), *N*-(1-phenethylpiperidin-4-yl)-*N*-pyridylpropionamide (**80**)

Gilbert *et al.*[158] highlighted that GC-MS and presumptive testing can be employed for detecting, and discriminating between different fentalogues. GC-MS (SIM mode) was used to differentiate 18 fentalogues, five controlled substances and four adulterants. The sensitivity of this technique yielded a LOD of 0.034 μg mL^{-1} and LOQ of 0.01 μg mL^{-1}. Along with this, presumptive testing with Scott's, Marquis and Eosin Y provided rapid results (5 mins) to determine whether fentanyl was present within a sample.

Furthermore, low-field (62 MHz) NMR spectroscopy has been used to differentiate 65 fentalogues in conjunction with quantum mechanical spin system analysis of spectra acquired at a frequency of 600 MHz to produce comparison spectra. Low-field NMR was selected in this instance due to the cost saving attributes it possesses (smaller

footprint, no need for cryogens, cheaper instrument cost) over high-field instrumentation.[159]

Robertson *et al.*[99] sought to employ a method of detection, due to the low-threshold for overdose, of fentalogues within a heroin matrix (97 % w/w). SABRE was chosen as it would be able to detect a fentalogue within a single scan, thus saving instrument time whilst significantly increasing the signal intensity observed. Enhancements of 50-fold, 168-fold and 38-fold were reported for the *ortho*-pyridyl protons of **78**, **79** and **80** respectively. **78** was selected to be tested within a matrix of heroin (ratio 97:3; heroin:**78**), with the *ortho*- hydrogen being enhanced by 47-fold initially, although this subsequently fell to 24-fold in further polarisation experiments.

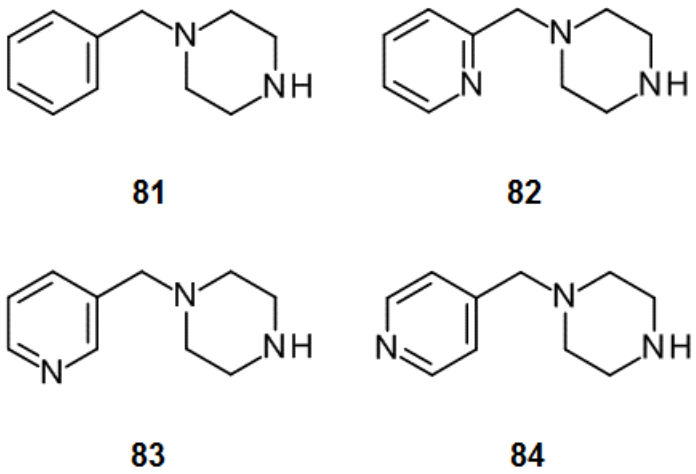

Figure 39 - Benzylpiperazine (**81**) and the pyridyl-BZP analogues (PMP) prepared by Tennant et al.[100] for hyperpolarisation studies; 1-(2-pyridylmethyl)piperazine (**82,** 2-PMP), 1-(3-pyridylmethyl)piperazine (**83,** 3-PMP), 1-(4-pyridylmethyl)piperazine (**84,** 4-PMP)

Tennant *et al.*[100] reported that the pyridyl-BZP analogues (Figure 39) do not all have the same enhancement values. Enhancements for the signal of the *ortho*-pyridyl protons differ in that 2-PMP (**82**) yields a negligible enhancement, 3-PMP (**83**) an enhancement of eightfold and 4-PMP (**84**) an enhancement of 313-fold. This highlights the problems faced with pyridyl isomers binding with the catalyst due to steric hindrance. For **82**-**84**, steric hindrance increases in the order **82**>**83**>**84**. In the case of **82**, steric hindrance was reported to completely hinder binding to the metal centre, thus preventing polarisation transfer. Again, hindrance problems are evident for **83** as reflected in the low enhancement, however, optimisation of the magnetic field utilised

for polarisation transfer could improve these further.[100] Similar to the fentalogues, this study focussed on the *para*-isomer of PMP including the polarisation on the hydrochloride salt (4-PMP.3HCl). Traditionally, SABRE requires the analyte to be a free-base so the nitrogen can ligate to the metal centre. Therefore, attempts to polarise the salt using the same methodology did not result in polarisation transfer.[100] Overcoming this issue by the addition of triethylamine (TEA) *in-situ* results in successful polarisation, with the addition of 3 eq. of TEA producing an enhancement of 300-fold for the *ortho*-pyridyl protons.

When looking at the biological aspects of SABRE, what has to be considered is forming a heterogeneous catalyst as well as the safe removal of the spent catalyst. Such work has been investigated by Goodson *et al.* who took [Ir(IMes)(COD)][PF_6] (IMes = 1,3-*bis*(2,4,6-trimethylphenyl)imidazole-2-ylidene, COD = cyclooctadiene) and tethered it to a commercially available polymer microbead functionalised with 4-dimethylaminopyridine (Figure 40). [160, 161]

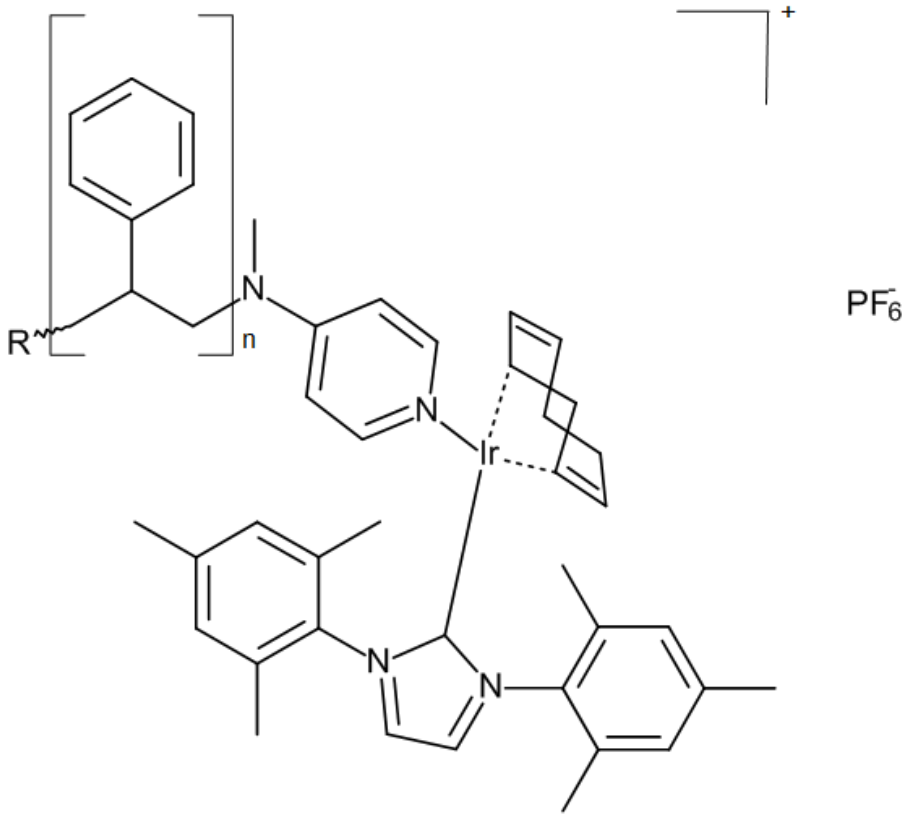

Figure 40 - Structure of heterogeneously solid supported SABRE catalyst synthesised by Goodson and co-workers. R = polymer microbead.[160]

This complex was used to polarise pyridine in CD_3OD, resulting in three signals being found with the enhancements ranging from threefold to fivefold (*ortho*-hydrogen gave the strongest enhancement). It was also found that extraction of the supernatant liquid produced no SABRE-based polarisation transfer. Thus, the catalyst remained firmly bound to the support during polarisation transfer, which is important for the SABRE approach towards the delivery of hyperpolarisable bolus, as the normally used catalyst [Ir(IMes)(COD)Cl] has been shown to be toxic.[97]

Methanol is the typical solvent used in polarisation, but as methanol is not biologically compatible, alternatives have been investigated. The use of ethanol/water mixtures have been used to good effect with the polarisation of nicotinamide (amide of vitamin B_3). Nicotinamide polarised by [Ir(IMes)(COD)Cl] in a ratio of 16:1 yielded a 70-fold enhancement for the proton *α* to both the ring nitrogen and the amide functional group.[162] By using a 50:50 mixture of D_2O:d_6-ethanol an enhancement of 105-fold was achieved. Nicotinamide can be polarised in neat water, however, the preparation has to be altered. This can be achieved by activating the SABRE catalyst and nicotinamide in neat ethanol, followed by removal of the solvent and reconstituting in D_2O. Water soluble catalysts have been prepared and tested,[96] with [Ir(IMes)(MeCN)(pr)$(H)_2$(*m*tppms)BF_4] having an enhancement of 71-fold in CD_3OD, similar to the enhancement obtained in a 30% mixture of ethanol-water mixture. Therefore, when looking at polarising the compounds in this study, steps have been made for future biological uses.

Due to the increase in signal-to-noise ratios over the years, SABRE as a technique has been vastly improved. The analyte can now be detected at far lower concentrations than NMR. However, these concentrations will have to be lower if they are to be used safely within the body. NBOMe's become dangerous exceeding a dose of 1 mg, whereas the current masses used contain 3 – 5 mg. How these drugs will react in the body is still unknown but this is a step in the right direction.

4.2 Results and discussion

The catalyst used throughout this study was [Ir(COD)(IMes)Cl] (**85**, Figure 41) and all experiments were performed at 4 molar equivalents constituted in CD_3OD. This was due to the investigation focussing on determining if SABRE polarisation transfer to the NBOMe ligands was possible, following interrogation by NMR methods.

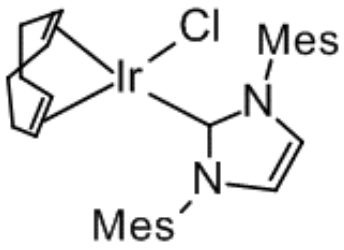

85

Figure 41 - Structure of the iridium catalyst used in hyperpolarisation experiments.

The catalyst chosen is highlighted by Mewis[94] as being the first carbene complex to be used in conjunction with SABRE and was first utilised in 2011.[95] It focused on the use of IMes to form the complex (**85**), which following activation by hydrogen in the presence of pyridine (py) gave $[Ir(IMes)(H)_2(py)_3]Cl$ (py = pyridine). Thus, it was structurally analogous to the mono-phosphine complexes reported previously, as both utilise electron rich ligands.[163] Comparison of $[Ir(IMes)(H)_2(py)_3]Cl$ (**86**) and $[Ir(PCy_3)(H)_2(py)_3]Cl$ (**87**) (Figure 42) as SABRE catalysts led to the observation that the former enhanced the *meta* ^1H signal of pyridine in CD_3OD by 266-fold (Polarisation, P = 0.4%), whilst the latter only achieved 18-fold (P = 0.03%). Therefore, the inclusion of the more electron-donating NHC ligand in the polarisation transfer catalyst led to a significant improvement in the observed enhancement.[94]

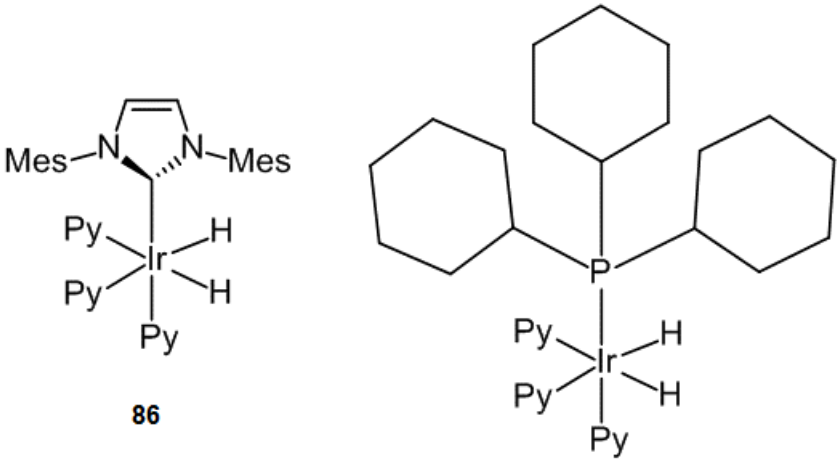

Figure 42 - Chemical structures of $[Ir(IMes)(H)_2(py)_3]Cl$ (**86**) and $[Ir(PCy_3)(H)_2(py)_3]Cl$ (**87**) as studied by Cowley *et al.*[95] to ascertain the effect of the carbine / phosphine ligand on the ^1H polarisation of pyridine.

4.2.1 Hyperpolarisation of NPyr ligands using [Ir(IMes)(COD)Cl]

Hyperpolarisation studies begun with evaluating the ability of catalyst **85** to form efficient SABRE polarisation transfer catalysts with compounds **56** – **62**. Table 18 shows the enhancement of the *ortho*-pyridyl ^{1}H nuclei after polarisation transfer in earth's magnetic field (0.5 G, $0.5x10^{-4}$ T). The enhancements from highest to lowest for **49** – **55** were found to be Cl > NO_2 > Br > Et > F > I > Me.

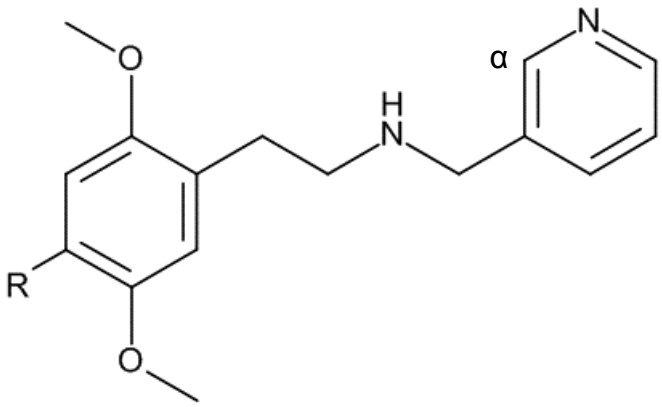

Table 18 - Enhancement values of NPyr compounds.

R	NPyr	^{1}H Enhancement of *o*-H_α in earth's magnetic field
Br	**56**	108
Cl	**57**	127
Me	**58**	25
Et	**59**	98
F	**60**	55
I	**61**	48
NO_2	**62**	113

56 was examined first with an enhancement being visible, indicating the formation of [Ir(H_2)(IMes)(**56**)$_3$]Cl when examined under SABRE. Evidence for the formation of [Ir(H_2)(IMes)(**56**)$_3$]Cl was obtained in that a single strong hydride signal was observed at −22.8 ppm, which suggests the complex is symmetrical in that the hydrides are chemically equivalent. Similar hydride shifts have been identified for analogous pyridyl complexes,[164] fentalogues[99] and BZP[100] complexes, all of which possessed chemically-equivalent hydride signals at ca. -23 ppm. Figure 43 shows the comparison of the thermal spectrum of **56** with the hyperpolarised spectra. When comparing **56** with the other halogenated NPyr's (**57**, **60**, **61**), there is a decrease in enhancement from the chloro- to the iodo-substituted NPyr's. This could be due to the increase in

molecular size of these compounds making it difficult for them to bind to the catalyst. High field NMR shows that three ligands bind to the iridium centre, therefore increasing the ligand size could implicate equatorial binding. However, if this was the case then **58** would have a larger enhancement than **61**.

As shown in Figure 43, the thermal spectrum is shown at x4 magnification relative to the hyperpolarised spectrum. The hyperpolarised spectrum shows an enhancement of 108-fold (the right hand side of Figure 43 displays the hydride peaks). As there is only one hydride peak, this would indicate that there is symmetrical binding to the catalyst. However, due to the activation process involved with the SABRE technique, the first shake with *para*hydrogen shows three peaks in the hydride region. The peaks shown at -12.5 ppm and -16.5 ppm is due to the hydrogenation of one of the double bonds of COD to octene. Subsequent spectra do not possesses these peaks as the COD moiety has been completely hydrogenated to octane. The hydrogenation of the COD ligand is a necessary step in the production of [Ir(H_2)(IMes)(**56**)$_3$]Cl from [Ir(IMes)(COD)Cl], the former being the fully activated form of the polarisation transfer catalyst.

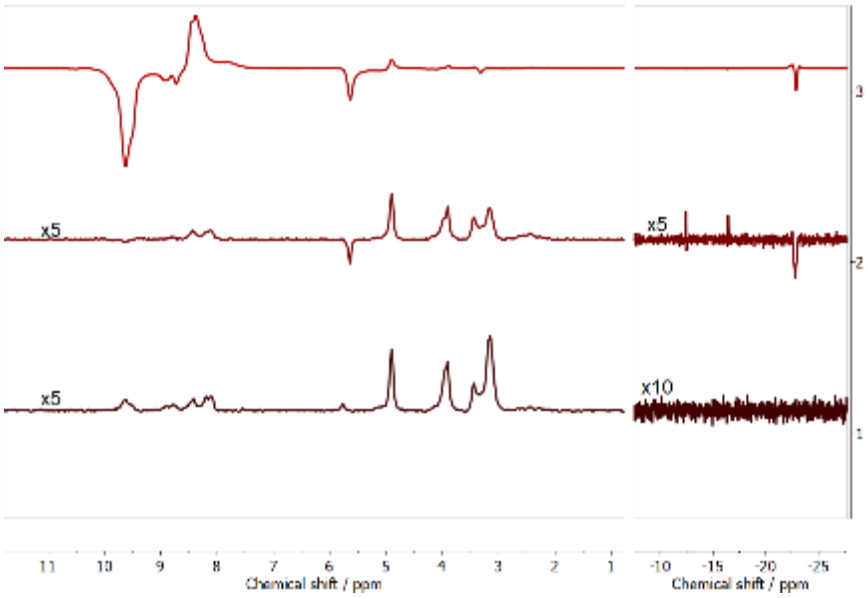

Figure 43 – ^{1}H NMR spectra of **56** in the presence of [Ir(IMes)(COD)Cl and *para*hydrogen at thermal equilibrium (bottom), after the first polarisation transfer at earth's magnetic field (middle) and subsequent polarisation transfer at earth's magnetic field (top).

At the start of the activation process (process shown in Scheme 28), the chloride in **85** can be easily displaced by **56** to give [Ir(IMes)(COD)(**56**)] (both complexes are square planar). The oxidative addition of *para*hydrogen to the metal centre causes a change in oxidation state from +1 to +3 along with hydrogenating one of the double bonds of COD i.e. the complex $[Ir(IMes)(CODH_2)(H)_2(\mathbf{56})_2]^+$ could be postulated. COD would then be fully hydrogenated to cyclooctane enabling the fully formed version of the catalyst $[Ir(IMes)(H)_2(\mathbf{56})_3]^+$. The signals are more deshielded for the hydrides when one of them is *trans* to an alkenic bond – this is the hydride at -12.5 ppm whereas the one at -16.5 ppm is most likely *trans* to NBOMe. This is why after the first shake, the peaks between 12 – 17 ppm are quickly replaced by the dominant symmetrical hydride at -22.8 ppm.

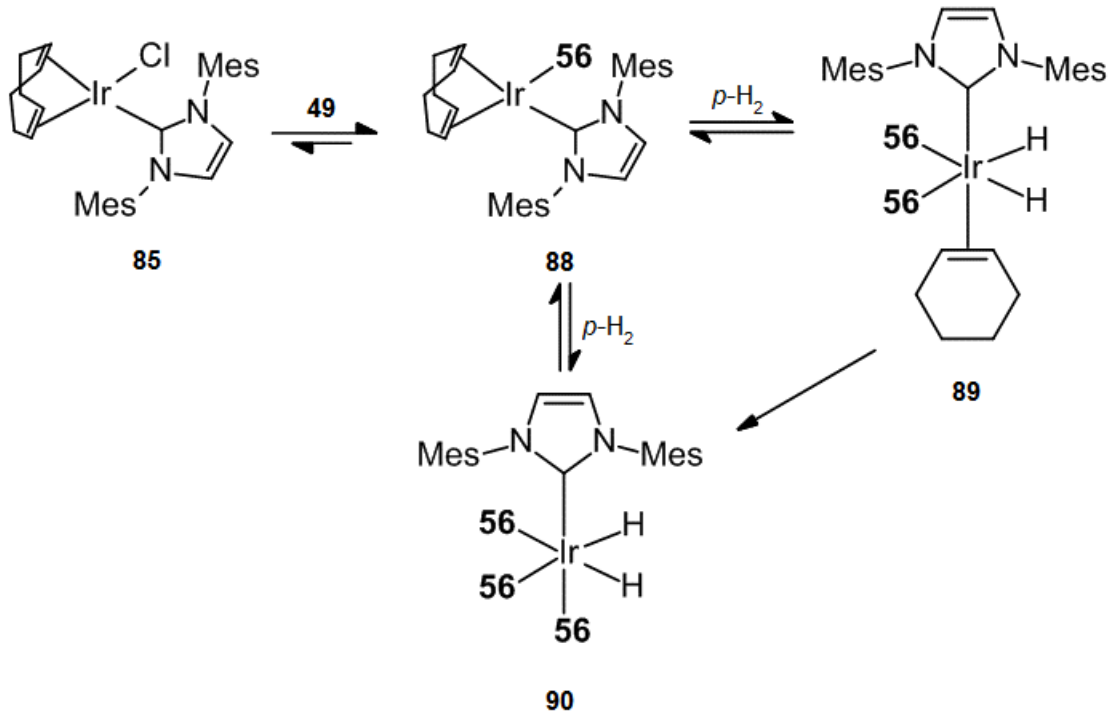

Scheme 28 – Iridium catalyst sequence during the first shake of SABRE polarisation

Upon the addition of hydrogen, the sample started to go colourless. The single hydride observed at -22.8 ppm indicates that symmetry is within the complex, similar chemical shifts have been reported for the hydride ligand for a range of different [Ir(NHC)(COD)Cl] complexes when pyridine is the ligand due to the formation of $[Ir(NHC)(pyridine)_3(H)_2]^+$.[164]

4.2.2 Hyperpolarisation of NPF ligands using [Ir(IMes)(COD)Cl]

The structure of the NPF's allow for both ^{1}H and ^{19}F SABRE polarisation, both of which were performed in this study. The enhancement values are given below in Table 19 (highest to lowest being F > Cl > NO_2 > Me > Br, Et > I). Hyperpolarisation transfer was conducted at earth's magnetic field for both studies to facilitate ease of comparison.

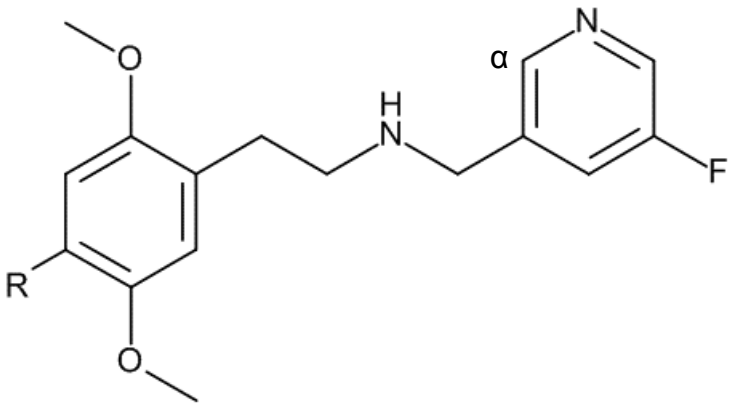

Table 19 - Enhancement values of NPF compounds.

R	NPF	^{1}H Enhancement of *o*-H_α in earth's magnetic field	^{19}F Enhancement of F on the pyridine ring in earth's magnetic field
Br	**63**	2	13
Cl	**64**	37	-
Me	**65**	4	-
Et	**66**	2	-
F	**67**	46	-
I	**68**	-	-
NO_2	**69**	23	-

As evidenced from Table 19, the enhancements were all significantly lower compared to the NPyr's. However, the marginal enhancements again provide evidence that these compounds can be polarised by SABRE. **67** gave the highest ^{1}H NMR enhancement of 46-fold for the *ortho*-pyridyl H_α (Figure 44). Conversely, there was no enhancement observed for **68** after multiple purges. The difference in the atomic radii of F (**67**) and I (**61**) may result in the former having greater accessibility for the metal centre (due to reduced sterics), despite the halogen being located far from the pyridyl nitrogen. If the halogenated compounds are considered, then enhancement increases in the order F (**67**) > Cl (**64**) > Br (**63**) > I (**69**). The 23-fold enhancement observed for **69**, however,

seems to not correlate with this trend; it would be expected that this group would produce an enhancement of effectively zero.

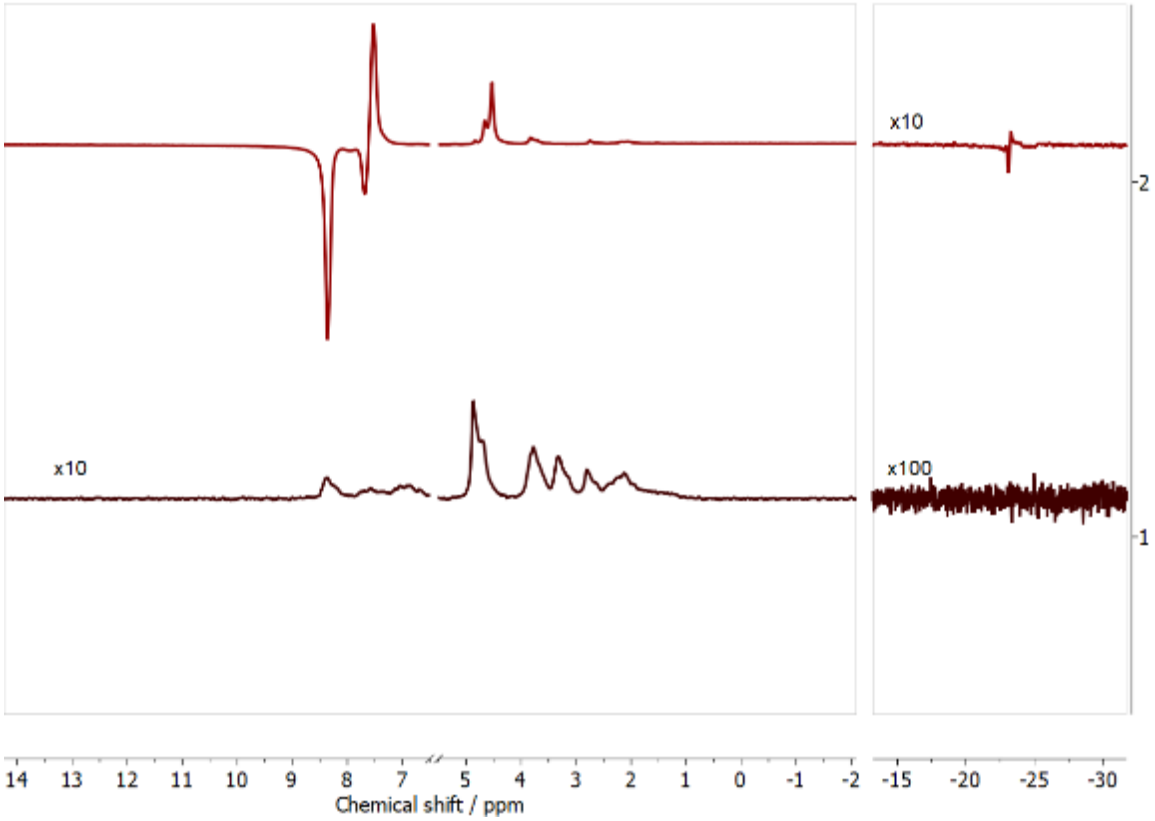

Figure 44 -^{1}H NMR spectra of **67** in the presence of [Ir(IMes)(COD)Cl and *para*hydrogen at thermal equilibrium (bottom) and after polarisation transfer at earth's magnetic field (top).

Olaru *et al.* recently showed that the polarization transfer of four equivalents of voriconazole (**91**, Figure 45) using **85** in the presence of *p*-H_2 in earth's magnetic field led to the pyrimidine ring protons being enhanced only two-fold. Compared with the other ligands studied, **91** possesses the greatest steric bulk, and so this could be the main factor for the low enhancement obtained. When the ratio of **91**/**85** was increased to 20:1, SABRE enhancement of the pyrimidine ring protons was not detectable, due to the polarisation reservoir being distributed over a greater number of proton spins.

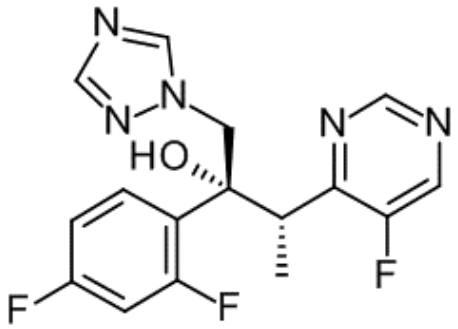

91

Figure 45 – Voriconazole (**91**) which was SABRE hyperpolarised by Olaru et al.[131]

Although steric bulk of the analyte molecules could be a cause for why enhancements are lower compared to those detailed in 4.2.1 there are a number of other factors including Shoolery's rule,[165] proton dilution, pK_a, electron effects and human error.[166] When comparing the general shape of the NBOMe's, these are linear which would indicate that there would be less stress binding to the iridium centre despite their general size. However, **91** has more of a triangular or wedge geometry, increasing the potential of steric clashing. Thus, a main factor as to why these enhancements are so low is due to the difference in molecular architectures compared to the NPyr compounds. Further studies could look at the relaxation times between all three sets of molecules to determine whether the fluoro- or methoxy-substituent is effecting the polarisation longevity of the *ortho*-hydrogens. Several groups have investigated the effect of T_1 on the longevity of the hyperpolarised signal. For example, the fentalogues **78**-**80** all possess pyridyl ^1H T_1 values of 2.1-3.5 s. In the space of 5-6 T_1s, the spin-lattice magnetisation is fully restored, thus meaning complete loss of hyperpolarisation. In the case of **78**-**80** this is ca. 18 s. Comparatively, the T_1 of pyridyl protons are much longer (*ca.* 12 s). Larger molecules tend to have shorter T_1 values due to increased molecular tumbling rates. This would most likely apply to the NPF compounds (**63 - 69**) investigated herein.

Following the addition of *p*-H_2, shaking for 10s and being placed in a spectrometer, a ^{19}F NMR spectrum was recorded of **70** (Figure 46). The ^{19}F nuclei were enhanced by 13-fold following polarisation transfer in earth's magnetic field, based on integral differences between the hyperpolarised spectrum and the spectrum at thermal

equilibrium. The signal-to-noise (S/N) differential between the thermal and polarised spectrum were enhanced 6-fold (evaluated by dividing the mean signal value by the standard deviation of the background noise).

It is beneficial to hyperpolarise the ^{19}F nuclei of molecules because there are no natural molecules within the body that contain fluorine. This is not true of ^{1}H, for which a large background signal is present in the body, meaning that large enhancements are required in order to successfully translate the technique to MRI, in order to collect MR images. In terms of ^{19}F imaging, there will be no background noise, making the signal easier to see.

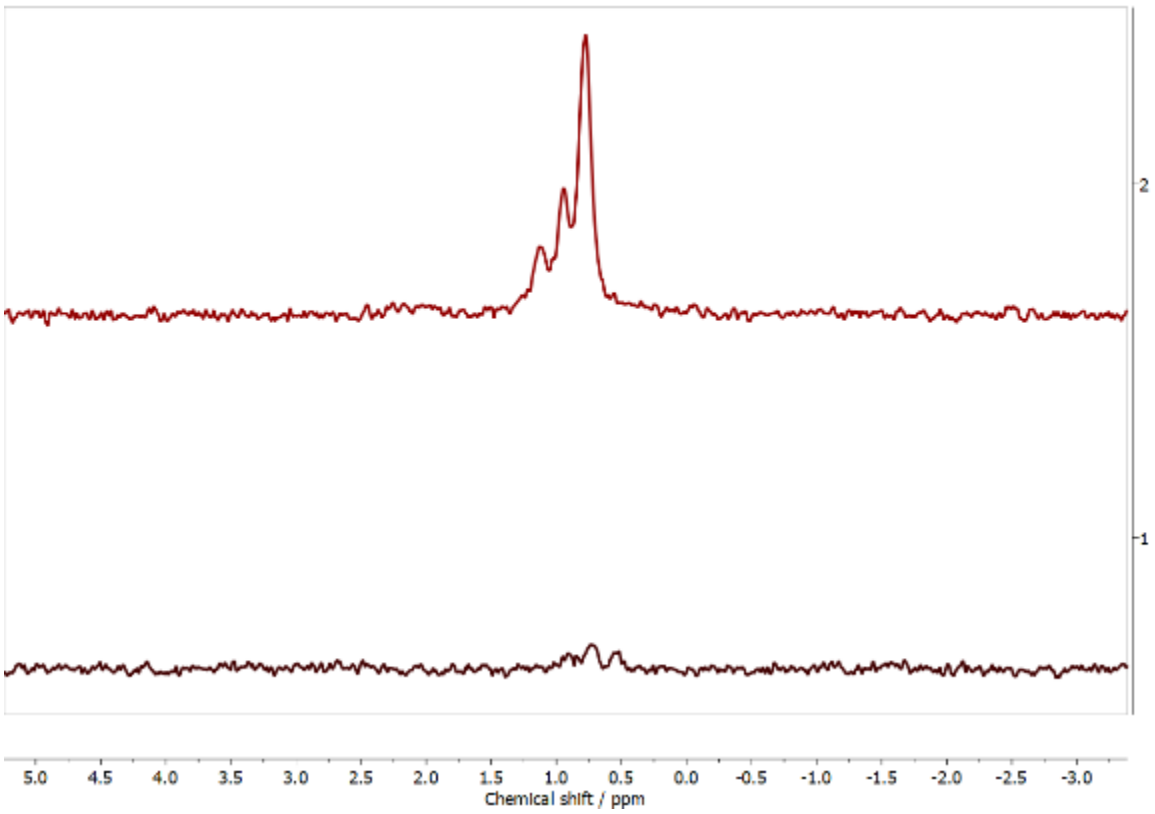

Figure 46 – ^{19}F NMR spectra of **56** in the presence of [Ir(IMes)(COD)Cl and *para*hydrogen at thermal equilibrium (bottom) and after polarisation transfer at earth's magnetic field (top).

Olaru *et al.*[131] reported successful ^{19}F polarized of the 19F nucleus on the pyrimidine ring. It possessed an enhancement of fivefold following polarisation transfer at earth's magnetic field and was observed as an anti-phase signal. However, no polarization

was observed for the other two ^{19}F nuclei, owing to insufficient J coupling to propagate polarization to these two nuclei. Despite the low enhancement observed, the T_1 of the polarized ^{19}F resonance is 5.15 s in a measurement field of 1.4 T. This is comparable to the T_1 observed for a ratio of 20:1 **91**/**85** at 11.74 T for the other substrates studied.[131] The anti-phase signal observed indicates asymmetrical binding to **85**, enforcing that steric hindrance would be a cause for the low enhancements. Compared to the symmetrical binding of **56**, which provided a slightly higher enhancement, the rigidity of a larger compound could be the cause of greater steric hindrance.

Olaru and co-workers also reported that although the results of the ^{19}F hyperpolarization studies are very promising and exhibit enhancement values high enough to enable high-resolution images (with the exception of **91**) to be recorded, they are two orders of magnitude lower than those obtained for ^{1}H. This is a remarkable decrease considering the high sensitivity of ^{19}F, which is very close to that of proton. In order to fully rationalize this difference, one must take into account the relaxation and exchange rates for the ligands analysed, as well as the dependence of the polarization transfer on the value of the magnetic field at which the transfer takes place.[131]

4.2.3 Hyperpolarisation of NPOMe ligands using [Ir(IMes)(COD)Cl]

Finally, the NPOMe class of compounds were investigated to see if they could be hyperpolarised by SABRE. The lack of ^{19}F nuclei in these compounds meant that the focus was on their respective ^{1}H polarisations, with focus being on the pyridyl ring as this point of ligation meant that J-coupling was maximised for polarisation transfer. With their similarities to the NBOMe's, it was expected that the NPOMe class would hyperpolarise similarly. The enhancement values for ligands **63**-**69** are given below in Table 20 (highest to lowest being Br > F > Et > NO_2 > Cl > I > Me).

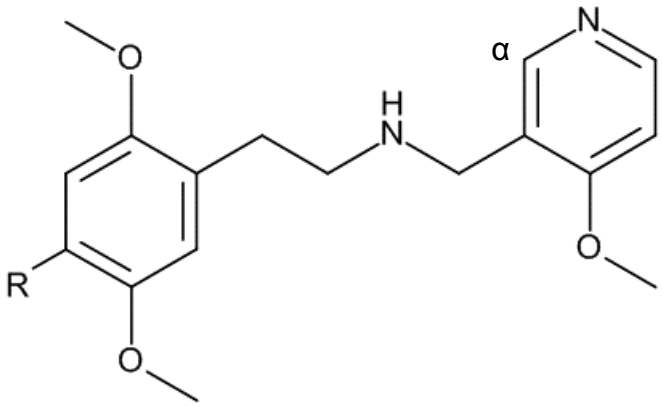

Table 20 - Enhancement values of NPOMe compounds.

R	NPOMe	^{1}H Enhancement of *o*-H_α in earth's magnetic field
Br	**70**	192
Cl	**71**	31
Me	**72**	3
Et	**73**	53
F	**74**	161
I	**75**	12
NO_2	**76**	38

Figure 47 displays the ^{1}H NMR spectra of **63**, following polarisation transfer or at thermal equilibrium. Following polarisation transfer at earth's magnetic field, the pyridyl *ortho*-protons were enhanced by 192-fold. This was the largest enhancement observed for all the compounds investigated. Furthermore, the value of enhancement is slightly higher than the fentanyl results obtained by Robertson *et al.* who reported an enhancement of 168-fold for the *ortho*-pyridyl protons of **79**.[99]

A single hydride peak is again observed at –23 ppm. During the first SABRE experiment with **70** (Figure 47) there are three hydride peaks seen, which simplifies to

only a single peak in subsequent spectra. Again, this is due to the COD being hydrogenated as was shown for the polarisation of **56**.

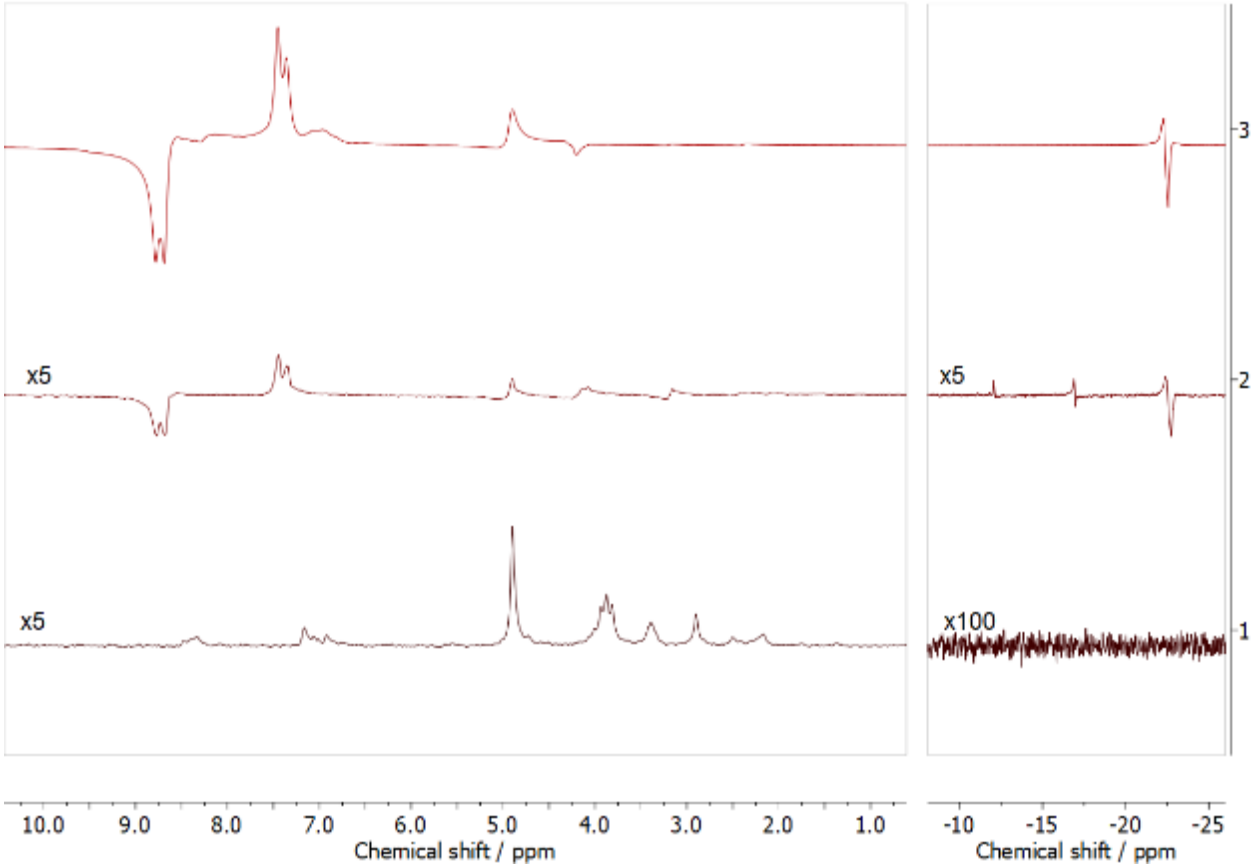

Figure 47 – ^{1}H NMR spectra of **70** in the presence of [Ir(IMes)(COD)Cl and *para*hydrogen at thermal equilibrium (bottom), after the first polarisation transfer at earth's magnetic field (middle) and subsequent polarisation transfer at earth's magnetic field (top).

As steric hindrance could be considered a common issue throughout the differing class of NBOMe derivatives, the A-values could be considered. As the A-values of these groups could be utilised to provide guidance relating to their steric properties. This is despite these values being associated with cyclohexane, and not phenyl rings. The order of these A-values (Table 21) generally coincide with the results presented herein, with the exception of iodine, indicating that steric hindrance within the phenyl group could be a factor.

Table 21 - A-Values of substituents on cyclohexane (average values)

Substituent	A-Value (kcal mol^{-1})
F	0.26[167, 168]
Br	0.38[167, 168]
I	0.46[167, 168]
Cl	0.48[167, 168]
NO_2	1.09[167, 168]
Me	1.70
Et	1.75
OMe	0.68[167, 168]

4.3 Conclusion

This chapter has detailed the evaluation of a range of NPyr's, NPF's and NPOMe's to from complexes with [Ir(IMes)(COD)Cl] (**85**) and *p*-H_2 to facilitate the successful polarisation transfer to both ^{1}H and ^{19}F nuclei. Positive ^{1}H enhancements were found for all molecules (excluding **68**) alongside the positive ^{19}F enhancement for **63**, indicating that these compounds can be hyperpolarised by SABRE. Furthermore, it indicates that these compounds could be used as potential MRI contrast agents, especially so for **63** due to the low / negligible ^{19}F background of the human body.

From the data, the trend that was observed at earth's magnetic field was that, in general, NPyr's > NPOMe's > NPF's in terms of enhancements (from the average calculated between the class). This trend, highlights that steric hindrance is a factor in terms of enhancement potential. Observing the general trends within each class, it is noted that Br > F > Cl > Nitro > Et > I > Me based on average enhancements of the three classes. Steric hindrance is a concern with respect to ligation, alongside the linear geometry of these compounds. Whilst there would be some rotation in the backbone of the compound, the bulkiness of the dimethoxy phenyl (including the R-group) would come into effect. The A-values of these groups could be utilised to provide guidance relating to their steric properties. As previously discussed, they generally coincide with the enhancements values given within the three different classes.

However, steric hindrance is not the only factor that contributes to enhancement potential. One of the factors could be due to the ligands pK_a. There is no literature values for the ligands discussed, so predicted values were obtained. Throughout the three classes, the pK_a values are between 8 and 9 whereas pyridine has a pK_a of 5.23. This entails the Ir-N(ligand) bond length would be shorter than when pyridine is bound. Shorter bond lengths would suggest there would be an increase in steric clashing. However, as the estimated pK_a's are similar, there is clear differentiation between each series within the enhancement data. This highlights that the ligands' pK_a is an unlikely factor in terms of the ease of which it can be polarised by SABRE.

Proton dilution is an effect where it is assumed that polarisation transfer is equal, and takes account of the number of protons that could be polarised. This is a suitable theory for the ligands mentioned as the environments differ between each class. The NPyr's have four protons, NPF's have three protons and one fluorine and the NPOMe's have three protons. Where proton dilution could come into effect here is with the NPyr and NPF series as the polarisation transfer to the pyridyl groups are shared between four regions, whereas the NPOMe series has three. There will be an increase from 25% to 33% respectively. This could be a reason as to why the highest enhancements came from the NPOMe series.

However, Mewis and co-workers researched the effect on random error when performing SABRE experiments.[94] These factors included the shaking technique, the time taken to insert the Young's tube into the NMR spectrometer and the time taken to initiate data collection using a software package. They followed up with saying the enhancement values here are more susceptible to error due to the significant changes in magnetic field during transfer to the magnet when contrasted to performing the same experiment but shaking the tube in earth's magnetic field. A ±20% variation in enhancement values has been reported for the same sample when analyzed by different experimenters.

5 Final conclusion and future work

This study initially looked at the successful synthesis of phenethylamines and NBOMe's, by a range of synthetic techniques. By modifying the work up of the reduction reaction of the nitro-aldol to phenethylamine to include an acid–base wash, this significantly improved the purity of the compounds.

A validated GC-MS method was developed for the detection and separation of eight NBOMe (**49 - 55**) derivatives within 11 minutes. All eight NBOMe's were successfully separated with no co-eluting peaks and baseline resolution. LOD values ranged between 6.20 – 10.75 μg mL^{-1} and LOQ values ranged from 18.77 – 32.57 μg mL^{-1}, which is low enough to effectively quantify the concentration of NBOMe within a blotter.

25C-, 25B- and 25I-NBOMe were used, in separate instances, to simulate an impregnated blotter for analysis. ATR-FTIR and presumptive colour testing (Marquis and Leibermanns) could not be used confidently to identify the substances within the blotter. For ATR-FTIR, the amount of analyte was too low to be detected. For presumptive testing, the high acidity of the testing reagents tended to interact with the blotter paper, leading to leaching of the ink or staining on the blotter. Positive results were acquired after drug extraction of the blotters via GC-MS. There was a variation in success with the presumptive testing post extraction as 25C-NBOMe did not produce the colour output after extraction, but 25B- and 25I-NBOMe did. This was also the first documented case of Liebermann's reagent being used to identify NBOMe's, which can be applied in the case of the three NBOMe's mentioned as they all differ in colour change.

A library of 21 novel NBOMe derivatives were successfully synthesised, via reductive amination, with potential for being a replacement for PET imaging tracers. With all the characterisation completed, the data could be used as a presumptive library so that should these drugs emerge onto the black market, their detection and characterisation should be relatively facile. NBOMe derivatives possessing a pyridyl moiety (**56 – 76**), were subjected to SABRE. Hyperpolarised ^{1}H and ^{19}F NMR spectra were obtained. These compounds all displayed hyperpolarisation via SABRE, which could also be used as another rapid detection method, provided a facility were able to perform

SABRE-based experiments. **70** possessed the largest enhancement (192-fold) showing great promise in that it could replace the PET imaging agent cimbi-36 due to similarity in chemical structure.

For future work, this would include performing *in vivo* biological assays with 25B-NPOMe and 25I-NPOMe to show if there is an interaction with the 5-HT_{2A} receptor. These two compounds are pertinent, due to the similarity of their radio labelled counterparts cimbi-5 and cimbi-36. However, this could also include the studies of another member of the research group, Nicolas Gilbert (PhD).[169] This work focussed on the pyridyl derivatives of fentanyl, examples shown in Figure 38, which would also benefit from assay studies and bear structural similarity to the compounds synthesised herein.

Such studies have been performed with the NBOMe derivatives**,** thus direct comparison of binding affinities can be applied and assessed. However, before embarking on this study, computational studies should be performed initially, to minimise costs associated with the synthesis and biological assays. With the crystal structure of serotonin receptor 5-HT_{2A} being available, this could be prepared for docking and a faster method to determine which of the novel compounds would be the best fit. With the substitution of the methoxybenzyl for the methoxypyridyl group, an extra form of hydrogen bonding would be available, dependent on if there is a donating group provided on the protein backbone in close enough proximity. The presence of additional hydrogen bonding may increase binding affinity to the 5-HT_{2A} receptor. This could lead into a computational project solely focusing on differing series of pyridyl drug derivatives.

Hyperpolarisation of the pyridyl NBOMe's is the first step to potentially unlocking how the 5-HT_{2A} receptors function, however, further work is required for a biological compatible catalyst i.e. non-toxic and the ability to polarise the compound *in-vivo*. This could first be trialled by polarizing the samples with a biologically compatible solvent i.e. DMSO-d_6. If this was to obtain a positive response similar to/or better than that reported for MeOH-d_4, a solvent for intravenous administration could have been potentially found.

Due to only one ^{19}F SABRE experiment being performed, there is a lot of scope fluoro hyperpolarization. The enhancement value of **63** would need to be larger to be considered for biological purpose. The current enhancement provides proof-of-concept, as there are a number of ways to increase this value. Optimisation would include trialling different catalysts to perform polarisation transfer, utilisation of different solvents (with a focus on biological compatible solvents / mixtures), increasing the pressure of *p*-H_2 and altering the magnetic field in which polarisation is conducted. One method to consider would be the use of a ^{19}F SABRE in shield enables alignment transfer to heteronuclei (SHEATH) based experiment. These experiments utilise a micro-tesla field to conduct polarisation transfer in. Use of micro-tesla fields could improve polarisation transfer to ^{19}F when compared to earth's magnetic field, which was used for the SABRE studies detailed herein.

6 References

1. R. Heim, Dissertation, Freie Universität Berlin 2004.
2. D. A. Cahal, *Brit. Med. J.*, 1974, **1**, 70-72.
3. Legislation.gov, *Misuse of Drugs Act 1971*, https://www.legislation.gov.uk/ukpga/1971/38/, Accessed 4 March 2017, 2017.
4. U. Government, *Drug penalties*, https://www.gov.uk/penalties-drug-possession-dealing.
5. Legislation.gov, The National Archives, Editon edn., 2001.
6. Legislation.gov, The National Archives
Editon edn., 2005.
7. B. V. Dean, S. J. Stellpflug, A. M. Burnett and K. M. Engebretsen, *J. Med. Toxicol.*, 2013, **9**, 172-178.
8. M. E. Nelson, S. M. Bryant and S. E. Aks, *Disease a Month*, 2014, **60**, 110-132.
9. D. S. Theobald, G. Fritschi and H. H. Maurer, *J. Chromatogr. B Analyt. Technol. Biomed. Life Sci.*, 2007, **846**, 374-377.
10. D. d. Boer and I. Bosman, *Pharm. World. Sci.*, 2004, **26**, 110-113.
11. J. L. Poklis, S. A. Raso, K. N. Alford, A. Poklis and M. R. Peace, *J. Anal. Toxicol.*, 2015, **39**, 617-623.
12. D. E. Administration, *Federal register*, 2013, **78**, 68716.
13. S. J. Stellpflug, S. E. Kealey, C. B. Hegarty and G. C. Janis, *J. Med. Toxicol.*, 2014, **10**, 45-50.
14. D. Zuba and K. Sekuła, *Drug Test. Anal.*, 2013, **5**, 634-645.
15. D. Zuba, K. Sekula and A. Buczek, *Forensic Sci. Int.*, 2013, **227**, 7-14.
16. K. Sekuła and D. Zuba, *Rapid Commun. Mass Spectrom.*, 2013, **27**, 2081-2090.
17. T. S. Krebs and P. O. Johansen, *J. Psychopharmacol.*, 2012, **26**, 994-1002.
18. F. X. Vollenweider, M. F. I. Vollenweider-Scherpenhuyzen, A. Bäbler, H. Vogel and D. Hell, *Neuroreport*, 1998, **9**, 3897-3902.
19. K. H. Adams, E. S. Hansen, L. H. Pinborg, S. G. Hasselbalch, C. Svarer, S. Holm, T. G. Bolwig and G. M. Knudsen, *Int. J. Neuropsychopharmacol.*, 2005, **8**, 391-401.
20. F. A. Moreno, C. B. Wiegand, E. K. Taitano and P. L. Delgado, *J. Clin. Psychiatry*, 2006, **67**, 1735-1740.
21. P. Celada, V. M. Puig, M. Amargós-Bosch, A. Adell and F. Artigas, *J. Psychiatry Neurosci.*, 2004, **29**, 252.
22. R. L. Carhart-Harris, D. Erritzoe, T. Williams, J. M. Stone, L. J. Reed, A. Colasanti, R. J. Tyacke, R. Leech, A. L. Malizia and K. Murphy, *Proc. Natl. Acad. Sci.*, 2012, **109**, 2138-2143.
23. K. Okamoto, H. Imbe, A. Kimura, T. Donishi, Y. Tamai and E. Senba, *Neuroscience*, 2007, **147**, 1090-1102.
24. F. Nau Jr, B. Yu, D. Martin and C. D. Nichols, *PloS one*, 2013, **8**, e75426.
25. E. Hamel, *Cephalalgia*, 2007, **27**, 1293-1300.
26. R. A. Sewell, J. H. Halpern and H. G. Pope, *Neurology*, 2006, **66**, 1920-1922.
27. R. R. Griffiths, W. A. Richards, U. McCann and R. Jesse, *Psychopharmacology*, 2006, **187**, 268-283.
28. D. L. Nelson, V. L. Lucates, D. B. Wainscott and R. A. Glennon, *Naunyn-Schmiedeberg's Arch. Pharmacol.*, 1999, **359**, 1-6.
29. A. L. Halberstadt and M. A. Geyer, *Neuropharmacology*, 2014, **77**, 200-207.
30. A. T. Caspar, S. D. Brandt, A. E. Stoever, M. R. Meyer and H. H. Maurer, *J. Pharm. Biomed. Anal.*, 2017, **134**, 158-169.
31. J. Suzuki, M. A. Dekker, E. S. Valenti, F. A. Arbelo Cruz, A. M. Correa, J. L. Poklis and A. Poklis, *Psychosomatics*, 2015, **56**, 129-139.
32. M. R. Braden, J. C. Parrish, J. C. Naylor and D. E. Nichols, *Mol. Pharmacol.*, 2006, **70**, 1956-1964.

33. M. Hansen, University of Copenhagen, 2010.
34. M. E. Silva, R. Heim, A. Strasser, S. Elz and S. Dove, *J. Comput. Aided Mol. Des.*, 2011, **25**, 51-66.
35. C. Tirapegui, M. A. Toro-Sazo and B. K. Cassels, *J. Chil. Chem. Soc.*, 2014, **59**, 2625-2627.
36. C. J. Pimentel Barros, Z. Cardosa De Souza, J. J. Rufino De Freitas, P. B. Norberto Da Silva, G. C. Gadelha Militao, T. Goncalves Da Silva, J. C. Rufino Freitas and J. Rufino De Freitas Filho, *J. Chil. Chem. Soc.*, 2014, **59**, 2359-2362.
37. M. Hansen, K. Phonekeo, J. S. Paine, S. Leth-Petersen, M. Begtrup, H. Brauner-Osborne and J. L. Kristensen, *ACS Chem. Neurosci.*, 2014, **5**, 243-249.
38. G. Klopman and O. T. Macina, *J. Theor. Biol.*, 1985, **113**, 637-648.
39. M. Thakur, A. Thakur and P. V. Khadikar, *Bioorg. Med. Chem.*, 2004, **12**, 825-831.
40. K. Neuvonen, H. Neuvonen and F. Fülöp, *Bioorganic Med. Chem. Lett.*, 2006, **16**, 3495-3498.
41. M. R. Braden, Citeseer, 2007.
42. A. Ettrup, M. Hansen, M. A. Santini, J. Paine, N. Gillings, M. Palner, S. Lehel, M. M. Herth, J. Madsen and J. Kristensen, *European journal of nuclear medicine and molecular imaging*, 2011, **38**, 681-693.
43. A. Ettrup, M. Hansen, M. A. Santini, J. Paine, N. Gillings, M. Palner, S. Lehel, M. M. Herth, J. Madsen, J. Kristensen, M. Begtrup and G. M. Knudsen, *Eur. J. Nucl. Med. Mol. Imaging*, 2011, **38**, 681-693.
44. V. B. Kueppers and C. T. Cooke, *Forensic Sci. Int.*, 2015, **249**, e15-18.
45. D. B. Kitchen, H. Decornez, J. R. Furr and J. Bajorath, *Nat. Rev. Drug Discov.*, 2004, **3**, 935-949.
46. N. Brooijmans and I. D. Kuntz, *Annu. Rev. Biophys. Biomol. Struct.*, 2003, **32**, 335-373.
47. K.-Y. Tseng and M. Atzori, *Monoaminergic modulation of cortical excitability*, Springer, 2007.
48. J. Cheng, P. M. Giguère, O. K. Onajole, W. Lv, A. Gaisin, H. Gunosewoyo, C. M. Schmerberg, V. M. Pogorelov, R. M. Rodriguiz and G. Vistoli, *J. Med. Chem.*, 2015, **58**, 1992-2002.
49. V. Beliveau, M. Ganz, L. Feng, B. Ozenne, L. Højgaard, P. M. Fisher, C. Svarer, D. N. Greve and G. M. Knudsen, *J. Neurosci.*, 2017, **37**, 120-128.
50. E. A. Engleman, Z. A. Rodd, R. L. Bell and J. M. Murphy, *CNS Neurol. Disord. Drug Targets*, 2008, **7**, 454-467.
51. C. Wang, Y. Jiang, J. Ma, H. Wu, D. Wacker, V. Katritch, G. W. Han, W. Liu, X. P. Huang and E. Vardy, *Science*, 2013, **340**, 610-614.
52. D. Wacker, C. Wang, V. Katritch, G. W. Han, X. P. Huang, E. Vardy, J. D. McCorvy, Y. Jiang, M. Chu, F. Y. Siu, W. Liu, H. E. Xu, V. Cherezov, B. L. Roth and R. C. Stevens, *Science*, 2013, **340**, 615-619.
53. Y. Q. Wang, W. W. Lin, N. Wu, S. Y. Wang, M. Z. Chen, Z. H. Lin, X. Q. Xie and Z. W. Feng, *Acta Pharmacol. Sin.*, 2019, **40**, 1138-1156.
54. J. Z. Chen, J. Wang and X. Q. Xie, *J. Chem. Inf. Model.*, 2007, **47**, 1626-1637.
55. Z. Feng, M. H. Alqarni, P. Yang, Q. Tong, A. Chowdhury, L. Wang and X. Q. Xie, *J. Chem. Inf. Model.*, 2014, **54**, 2483-2499.
56. Z. Feng, S. Kochanek, D. Close, L. Wang, A. Srinivasan, A. A. Almehizia, P. Iyer, X. Q. Xie, P. A. Johnston and B. Gold, *J. Chem. Biol.*, 2015, **8**, 79-93.
57. Z. Feng, L. V. Pearce, X. Xu, X. Yang, P. Yang, P. M. Blumberg and X. Q. Xie, *J. Chem. Inf. Model.*, 2015, **55**, 572-588.
58. K. Pfleger, H. H. Maurer and A. Weber, *Mass spectral and GC data of drugs, poisons, pesticides, pollutants and their metabolites. Part 1: methods, tables, indexes*, Wiley-VCH, Weinheim, 2007.
59. Y. Boumrah, L. Humbert, M. Phanithavong, K. Khimeche, A. Dahmani and D. Allorge, *Drug. Test. Anal.*, 2016, **8**, 248-256.
60. A. T. Caspar, A. G. Helfer, J. A. Michely, V. Auwarter, S. D. Brandt, M. R. Meyer and H. H. Maurer, *Anal Bioanal Chem*, 2015, **407**, 6697-6719.

61. D. E. Nichols, S. P. Frescas, B. R. Chemel, K. S. Rehder, D. Zhong and A. H. Lewin, *Bioorg. Med. Chem.*, 2008, **16**, 6116-6123.
62. P. Nikolaou, I. Papoutsis, M. Stefanidou, C. Spiliopoulou and S. Athanaselis, *Drug Chem. Toxicol.*, 2015, **38**, 113-119.
63. L. K. Laskowski, F. Elbakoush, J. Calvo, G. Exantus-Bernard, J. Fong, J. L. Poklis, A. Poklis and L. S. Nelson, *J. Med. Toxicol.*, 2015, **11**, 237-241.
64. A. Al-Imam, *Iran. J. Psychiatry Behav. Sci.*, 2018, **12**.
65. H. M. Elbardisy, C. W. Foster, J. Marron, R. E. Mewis, O. B. Sutcliffe, T. S. Belal, W. Talaat, H. G. Daabees and C. E. Banks, *ACS Omega*, 2019, **4**, 14439-14450.
66. B. Duffau, C. Camargo, M. Kogan, E. Fuentes and B. K. Cassels, *J. Chromatogr. Sci.*, 2016, **54**, 1153-1158.
67. C. Kyriakou, E. Marinelli, P. Frati, A. Santurro, M. Afxentiou, S. Zaami and F. P. Busardo, *Eur. Rev. Med. Pharmacol. Sci.*, 2015, **19**, 3270-3281.
68. J. Coelho Neto, *Forensic. Sci. Int.*, 2015, **252**, 87-92.
69. K. G. Shanks, T. Sozio and G. S. Behonick, *J. Anal. Toxicol.*, 2015, **39**, 602-606.
70. A. M. d. Moreira, H. L. de Oliveira, J. F. Allochio Filho, D. H. A. Florez, M. M. C. Borges, V. Lacerda, W. Romão and K. B. Borges, *Trend Anal. Chem.*, 2019, **114**, 260-277.
71. R. D. Johnson, S. R. Botch-Jones, T. Flowers and C. A. Lewis, *J. Anal. Toxicol.*, 2014, **38**, 479-484.
72. N. Uchiyama, Y. Shimokawa, S. Matsuda, M. Kawamura, R. Kikura-Hanajiri and Y. Goda, *Forensic Toxicol.*, 2014, **32**, 105-115.
73. S. L. Hill, T. Doris, S. Gurung, S. Katebe, A. Lomas, M. Dunn, P. Blain and S. H. L. Thomas, *Clin. Toxicol.*, 2013, **51**, 487-492.
74. S. R. Rose, J. L. Poklis and A. Poklis, *Clin. Toxicol.*, 2013, **51**, 174-177.
75. J. L. Poklis, C. R. Nanco, M. M. Troendle, C. E. Wolf and A. Poklis, *Drug Test. Anal.*, 2014, **6**, 764-769.
76. J. L. Poklis, D. J. Clay and A. Poklis, *J. Anal. Toxicol.*, 2014, **38**, 113-121.
77. J. L. Poklis, K. G. Devers, E. F. Arbefeville, J. M. Pearson, E. Houston and A. Poklis, *Forensic Sci. Int.*, 2014, **234**, e14-e20.
78. K. Yoshida, K. Saka, K. Shintani-Ishida, H. Maeda, M. Nakajima, S. Hara, M. Ueno, K. Sasaki, H. Iwase and T. Sakamoto, *Forensic Toxicol.*, 2015, **33**, 396-401.
79. M. Andreasen, F., R. Telving, I. Rosendal, M. B. Eg, J. Hasselstrøm, B. and L. V. Andersen, *Forensic Sci. Int.*, 2015, **251**, e1-e8.
80. J. J. Kristofic, J. D. Chmiel, G. F. Jackson, S. P. Vorce, J. M. Holler, S. L. Robinson and T. Z. Bosy, *J. Anal. Chem.*, 2016, **40**, 466-472.
81. J. P. Walterscheid, G. T. Phillips, A. E. Lopez, M. L. Gonsoulin, H. H. Chen and L. A. Sanchez, *Am. J. Forensic Med. Pathol.*, 2014, **35**, 20-25.
82. J. L. Poklis, J. Charles, C. E. Wolf and A. Poklis, *Biomed. Chromatogr.*, 2013, **27**, 1794-1800.
83. K. B. Borges, E. F. Freire, I. Martins and M. de Siqueira, E. P. B., *Talanta*, 2009, **78**, 233-241.
84. L. Nováková and H. Vlčková, *Anal. Chim. Acta*, 2009, **656**, 8-35.
85. P. Nikolaou, A. M. Coffey, M. J. Barlow, M. S. Rosen, B. M. Goodson and E. Y. Chekmenev, *Anal. Chem.*, 2014, **86**, 8206-8212.
86. B. M. Goodson, N. Whiting, A. M. Coffey, P. Nikolaou, F. Shi, B. M. Gust, M. E. Gemeinhardt, R. V. Shchepin, J. G. Skinner and J. R. Birchall, *eMagRes*, 2007, 797-810.
87. M. L. Hirsch, N. Kalechofsky, A. Belzer, M. Rosay and J. G. Kempf, *J. Am. Chem. Soc.*, 2015, **137**, 8428-8434.
88. T. Walker and W. Happer, 1997.
89. J. H. Ardenkjær-Larsen, B. Fridlund, A. Gram, G. Hansson, L. Hansson, M. H. Lerche, R. Servin, M. Thaning and K. Golman, *Proc. Natl. Acad. Sci.*, 2003, **100**, 10158-10163.
90. G. Closs, in *Advances in Magnetic and Optical Resonance*, Elsevier, Editon edn., 1974, vol. 7, pp. 157-229.

91. K. H. Mok and P. J. Hore, *Methods*, 2004, **34**, 75-87.
92. C. R. Bowers and D. P. Weitekamp, *Phys. Rev. Lett.*, 1986, **57**, 2645-2648.
93. R. W. Adams, J. A. Aguilar, K. D. Atkinson, M. J. Cowley, P. I. Elliott, S. B. Duckett, G. G. Green, I. G. Khazal, J. López-Serrano and D. C. Williamson, *Science*, 2009, **323**, 1708-1711.
94. R. E. Mewis, *Magn. Reson. Chem.*, 2015, **53**, 789-800.
95. M. J. Cowley, R. W. Adams, K. D. Atkinson, M. C. Cockett, S. B. Duckett, G. G. Green, J. A. Lohman, R. Kerssebaum, D. Kilgour and R. E. Mewis, *J. Am. Chem. Soc.*, 2011, **133**, 6134-6137.
96. M. Fekete, C. Gibard, G. J. Dear, G. G. Green, A. J. Hooper, A. D. Roberts, F. Cisnetti and S. B. Duckett, *Dalton Trans.*, 2015, **44**, 7870-7880.
97. A. Manoharan, P. J. Rayner, W. Iali, M. J. Burns, V. H. Perry and S. B. Duckett, *ChemMedChem*, 2018, **13**, 352-359.
98. A. N. Pravdivtsev, A. V. Yurkovskaya, H. Zimmermann, H. M. Vieth and K. L. Ivanov, *RSC Advances*, 2015, **5**, 63615-63623.
99. T. B. R. Robertson, L. H. Antonides, N. Gilbert, S. L. Benjamin, S. K. Langley, L. J. Munro, O. B. Sutcliffe and R. E. Mewis, *ChemistryOpen*, 2019, **8**, 1375-1382.
100. T. Tennant, M. C. Hulme, T. B. R. Robertson, O. B. Sutcliffe and R. E. Mewis, *Magn. Reson. Chem.*, 2020.
101. K. D. Atkinson, M. J. Cowley, S. B. Duckett, P. I. P. Elliott, G. G. Green, J. Lopez-Serrano, I. G. Khazal and A. C. Whitwood, *Inorg. Chem.*, 2009, **48**, 663-670.
102. R. W. Adams, J. A. Aguilar, K. D. Atkinson, M. J. Cowley, P. I. P. Elliott, S. B. Duckett, G. G. R. Green, I. G. Khazal, J. Lopez-Serrano and W. D. C., *Science*, 2009, **323**, 1708-1711.
103. P. M. Richardson, A. J. Parrott, O. Semenova, A. Nordon, S. B. Duckett and M. E. Halse, *Analyst*, 2018, **143**, 3442-3450.
104. J. J. Vaquero and P. Kinahan, *Annu. Rev. Biomed. Eng.*, 2015, **17**, 385-414.
105. G. T. Gullberg, G. L. Zeng, F. L. Datz, P. E. Christian, C. H. Tung and H. T. Morgan, *Phys. Med. Biol.*, 1992, **37**, 507.
106. S. Geethanath and J. T. Vaughan, Jr., *J. Magn. Reson. Imaging*, 2019, **49**, e65-e77.
107. E. Kaplan, A. K. Prashanth, C. Brennan and L. Sirovich, *Optics and Photonics News*, 2000, **11**, 26.
108. T. C. Kwee, D. A. Torigian and A. Alavi, *J. Thorac. Imaging*, 2013, **28**, 1-10.
109. S. J. Finnema, V. Stepanov, A. Ettrup, R. Nakao, N. Amini, M. Svedberg, C. Lehmann, M. Hansen, G. M. Knudsen and C. Halldin, *Neuroimage.*, 2014, **84**, 342-353.
110. L. W. Fitzgerald, D. S. Conklin, C. M. Krause, A. P. Marshall, J. P. Patterson, D. P. Tran, G. Iyer, W. A. Kostich, B. L. Largent and P. R. Hartig, *J. Neurochem.*, 1999, **72**, 2127-2213.
111. A. Ettrup, M. Palner, N. Gillings, M. A. Santini, M. Hansen, B. R. Kornum, L. K. Rasmussen, K. Nagren, J. Madsen, M. Begtrup and G. M. Knudsen, *J. Nucl. Med.*, 2010, **51**, 1763-1770.
112. B. Biver, S. Goldman, A. Leuxen, M. Monclus, M. Forestini, J. Mendlewicz and F. Lotstra, *Eur. J. Nuc. Med.*, 1994, **21**, 937-946.
113. H. Ito, S. Nyberg, C. Halldin, C. Lundkvist and F. L., *J. Nucl. Med.*, 1998, **39**, 208-214.
114. L. H. Pinborg, K. H. Adams, S. Yndgaard, S. G. Hasselbalch, S. Holm, H. Kristiansen, O. B. Paulson and G. M. Knudsen, *J. Cereb. Blood. Flow Metab.*, 2004, **24**, 1037-1045.
115. D. Hoyer, J. P. Hannon and G. R. Martin, *Pharmacol. Biochem. Behav.*, 2002, **71**, 533-554.
116. B. J. Jones and T. P. Blackburn, *Pharmacol. Biochem. Behav.*, 2002, **71**.
117. N. M. Barnes and T. Sharp, *Neuropharmacology*, 1999, **38**, 1083-1152.
118. D. Hoyer, D. E. Clarke, J. R. Fozard, P. R. Hartig, G. R. Martin, E. J. Mylecharane, P. R. Saxena and P. P. A. Humphrey, *Pharmacol. Rev.*, 1994, **46**, 157-203.
119. F. G. Boess and I. L. Martin, *Neuropharmacology*, 1994, **33**, 275-317.
120. G. V. Williams, S. G. Rao and P. S. Goldman-Rakic, *J. Neurosci.*, 2002, **22**, 2843-2854.
121. J. A. Harvey, *Learn. Mem.*, 2003, **10**, 355-362.
122. J. E. Leyson, D. de Chaffoy de Courcelles, F. de Clerck, C. J. E. Niemegeers and J. M. Van nueton, *Neuropharmacology*, 1984, **23**, 1493-1501.

123. A. R. Blaazer, P. Smid and C. G. Kruse, *ChemMedChem*, 2008, **3**, 1299-1309.
124. R. Narendran, D. R. Hwang, M. Slifstein, Y. Hwang, Y. Huang, J. Ekelund, O. Guillin, E. Scher, D. Martinez and M. Laruelle, *J. Pharmacol. Exp. Ther.*, 2005, **315**, 80-90.
125. R. Narendran, S. Mason, C. Laymon, B. Lopresti, N. Velasquez, M. May, S. Kendro, D. Martinez, C. Mathis and G. Frankle, *J. Pharmacol. Exp. Ther.*, 2010, **371**.
126. D. Martinez and R. Narendran, in *Behavioral Neuroscience of Drug Addiction*, eds. D. W. Self and J. K. Staley Gottschalk, Springer Berlin Heidelberg, Berlin, Heidelberg, Editon edn., 2010, vol. 3, pp. 219-245.
127. A. Ettrup, S. Holm, M. Hansen, M. Wasim, M. A. Santini, M. Palner, J. Madsen, C. Svarer, J. L. Kristensen and G. M. Knudsen, *Mol. Imaging Biol.*, 2013, **15**, 376-383.
128. S. Purser, P. R. Moore, S. Swallow and V. Gouverneur, *Chem. Soc. Rev.*, 2008, **37**, 320-330.
129. *Rapid Testing Methods of Drugs of Abuse*, https://www.unodc.org/documents/scientific/Rapid_Testing_Methods_of_Drugs_of_Abuse_E.pdf.
130. O. Torres, M. Martin and E. Sola, *Organometallics*, 2009, **28**, 863-870.
131. A. M. Olaru, T. B. R. Robertson, J. S. Lewis, A. Anthony, W. Lali, R. E. Mewis and S. B. Duckett, *ChemistryOpen*, 2018, **7**, 97-105.
132. T. Kanamori, H. Inoue, Y. Iwata, Y. Ohmae and T. Kishi, *J. Anal. Toxicol.*, 2002, **26**, 61-66.
133. B. J. D. Wright, J. Hartung, F. Peng, R. Water, H. Liu, Q. Tan, T. Chou and S. J. Danishefsky, *J. Am. Chem. Soc.*, 2008, **130**, 16786-16790.
134. J. L. Bloomer, K. W. Stagliano and J. A. Gazzillo, *J. Org. Chem.*, 1993, **58**, 7906-7912.
135. A. Miyawaki, D. Kikuchi, M. Niki, Y. Manabe, M. Kanematsu, H. Yokoe, M. Yoshida and K. Shishido, *J. Org. Chem.*, 2012, **77**, 8231-8243.
136. H. Sharghi, M. Jokar, M. M. Doroodmand and R. Khalifeh, *Adv. Synth. Catal.*, 2010, **352**, 3031-3044.
137. Y. Saito, A. Mizokami, H. Tsurimoto, K. Izumi, M. Goto and K. Nakagawa-Goto, *Eur. J. Med. Chem.*, 2018, **157**, 1143-1152.
138. W. P. Roberts and C. L. Ebner, *J. Org. Chem.*, 1987, **52**, 2297-2299.
139. B. Wang, H. X. Sun, Z. H. Sun and G. Q. Lin, *Adv. Synth. Catal.*, 2009, **351**, 415-422.
140. A. T. Shulgin and D. C. Dyer, *J. Med. Chem.*, 1975, **18**, 1201-1204.
141. R. A. Glennon, R. Young, F. Benington and R. D. Morin, *J. Med. Chem.*, 1982, **25**, 1163-1168.
142. M. Hansen, K. Phonekeo, J. S. Paine, S. Leth-Petersen, M. Begtrup, H. Bräuner-Osborne and J. L. Kristensen, *ACS Chem. Neurosci.*, 2014, **5**, 243-249.
143. A. T. Shulgin and A. Shulgin, *PIHKAL - A Chemical Love Story*, Transform Press, USA, 1991.
144. Huang-Minlon, *J. Am. Chem. Soc.*, 1946, **68**, 2487-2488.
145. S. A. Kaliyaperumal, S. Banerjee and K. S. U, *Org. Biomol. Chem.*, 2014, **12**, 6105-6113.
146. J. W. Baker and H. B. Hopkins, *J. Chem. Soc.*, 1949, **0**, 1089-1097.
147. S. Siddiqui, S. Kadlecek, M. Pourfathi, Y. Xin, W. Mannherz, H. Hamedani, N. Drachman, K. Ruppert, J. Clapp and R. Rizi, *Adv. Drug Deliv. Rev.*, 2017, **113**, 3-23.
148. M. L. Truong, T. Theis, A. M. Coffey, R. V. Shchepin, K. W. Waddell, F. Shi, B. M. Goodson, W. S. Warren and E. Y. Chekmenev, *J. Phys. Chem. C Nanomater Interfaces*, 2015, **119**, 8786-8797.
149. R. V. Shchepin, B. M. Goodson, T. Theis, W. S. Warren and E. Y. Chekmenev, *ChemPhysChem*, 2017, **18**, 1961-1965.
150. A. Abragam and M. Goldman, *Rep. Prog. Phys.*, 1978, **41**, 395-467.
151. N. D. Bhaskar, W. Happer and T. McClellend, *Phys. Rev. Lett.*, 1982, **49**, 25-28.
152. L. L. Walkup and J. C. Woods, *NMR Biomed.*, 2014, **27**, 1429-1438.
153. J. M. Lupo, A. P. Chen, M. L. Zierhut, R. A. Bok, C. H. Cunningham, J. Kurhanewicz, D. B. Vigneron and S. J. Nelson, *Magn. Reson. Imaging*, 2010, **28**, 153-162.
154. J. Leonard, A. Haddad, O. Green, R. L. Birke, T. Kubic, A. Kocak and J. R. Lombardi, *J. Raman Spectrosc.*, 2017, **48**, 1323-1329.
155. M. Schackmuth and S. Kerrigan, *Forensic Toxicol.*, 2018, **37**, 231-237.

156. K. E. Strayer, H. M. Antonides, M. P. Juhascik, R. Daniulaityte and I. E. Sizemore, *ACS Omega*, 2018, **3**, 514-523.
157. H. M. Elbardisy, C. W. Foster, L. Cumba, L. H. Antonides, N. Gilbert, C. J. Schofield, T. S. Belal, W. Talaat, O. B. Sutcliffe, H. G. Daabees and C. E. Banks, *Anal. Methods*, 2019, **11**, 1053-1063.
158. N. Gilbert, L. H. Antonides, C. J. Schofield, A. Costello, B. Kilkelly, A. R. Cain, P. R. V. Dalziel, K. Horner, R. E. Mewis and O. B. Sutcliffe, *Drug Test. Anal.*, 2020.
159. J. Duffy, A. Urbas, M. Niemitz, K. Lippa and I. Marginean, *Anal. Chim. Acta.*, 2019, **1049**, 161-169.
160. F. Shi, A. M. Coffey, K. W. Waddell, E. Y. Chekmenev and B. M. Goodson, *Angew Chem. Int. Ed. Engl.*, 2014, **53**, 7495-7498.
161. T. Theis, M. L. Truong, A. M. Coffey, R. V. Shchepin, K. W. Waddell, F. Shi, B. M. Goodson, W. S. Warren and E. Y. Chekmenev, *J. Am. Chem. Soc.*, 2015, **137**, 1404-1407.
162. R. E. Mewis, K. D. Atkinson, M. J. Cowley, S. B. Duckett, G. G. Green, R. A. Green, L. A. Highton, D. Kilgour, L. S. Lloyd, J. A. Lohman and D. C. Williamson, *Magn. Reson. Chem.*, 2014, **52**, 358-369.
163. R. W. Adams, S. B. Duckett, R. A. Green, D. C. Williamson and G. G. Green, *J. Chem. Phys.*, 2009, **131**, 194505.
164. L. S. Lloyd, A. Asghar, M. J. Burns, A. Charlton, S. Coombes, M. J. Cowley, G. J. Dear, S. B. Duckett, G. R. Genov, G. G. Green, L. A. Highton, A. J. Hooper, M. Khan, I. G. Khazal, R. J. Lewis, R. E. Mewis, A. D. Roberts and A. J. Ruddleston, *Cat. Sci. Technol.*, 2014, **4**, 3544-3554.
165. J. N. Shoolery, *Prog. NMR Spec.*, 1995, **28**, 37-52.
166. R. E. Mewis, M. Fekete, G. G. Green, A. C. Whitwood and S. B. Duckett, *Chem. Commun. (Camb)*, 2015, **51**, 9857-9859.
167. F. R. Jenson, C. H. Bushweller and B. H. Beck, *J. Am. Chem. Soc.*, 1969, **91**.
168. H. J. Schneider and V. Hoppen, *J. Org. Chem.*, 1978, **43**.
169. N. Gilbert, Manchester Metropolitan University, 2021.